The Development, Validation and Application of Novel Preclinical Models for the Study of Barrett's Carcinogenesis

Matthew Read

MBBS, FRACS

Submitted in fulfillment of the requirements of the degree of

Doctor of Philosophy

April 2019

Division of Cancer Surgery

Surgical Oncology Research Laboratory

Peter MacCallum Cancer Centre, Melbourne, Victoria, Australia
&
The University of Melbourne, Victoria, Australia

ORCID iD: 0000-0001-7178-1973

Abstract

Oesophageal adenocarcinoma is an aggressive malignancy and is associated with extremely poor rates of survival. Its only known precursor is Barrett's oesophagus, which is a metaplasia that occurs in the lower oesophagus in response to gastro-oesophageal reflux. Despite a number of recent advances, such as the introduction of neoadjuvant therapy and minimally invasive techniques, there has only been a modest improvement in overall survival over the last few decades. One factor that has contributed to this is the limited availability of well-validated, clinically relevant models for research purposes. Therefore, the aim of this thesis, was to develop novel preclinical models for the study of Barrett's carcinogenesis.

Central to this thesis was the optimisation of the patient-derived tumour xenograft model. This is a model in which immunodeficient mice are used as hosts in order to culture pieces of human tumour. Once established, the model provides a perpetual source of tumour tissue. Unfortunately, they have been difficult to establish in oesophageal adenocarcinoma using conventional techniques. Through the use of a novel intramuscular transplantation technique, the efficiency of the model has been greatly improved. Validation has also confirmed that the majority of derived xenografts are representative of the original patient tumour. Importantly, however, validation also confirmed that a subset had undergone lymphomagenic transformation and were no longer representative of the original tumour.

Following on from the success of the intramuscular xenograft technique, the model was subsequently used as a source of tissue for the generation of much needed cell lines. Using small pieces of xenograft tissue, rather than single cell suspensions, a robust technique was established for the generation of cell lines. In doing so, a cell line was established that had both metastatic and non-metastatic clones, making it a valuable tool for cancer research. Finally, the intramuscular transplantation technique was also used to successfully culture both normal human oesophageal tissue and metaplastic tissue. Validation of this model also confirmed that the cultured tissue recapitulated the human disease process.

In addition to the development and validation of multiple novel models for the study of Barrett's carcinogenesis, this thesis also begins to explore how these models can be used to investigate clinically significant aspects of disease biology.

Declaration

This declaration certifies that:

i. This thesis comprises only my original work towards the PhD except where indicated.
ii. Due acknowledgement has been made in the text to all other material used.
iii. The thesis is fewer than 100,000 words, exclusive of tables, maps, bibliographies and appendices as approved by the Research Higher Degrees Committee.

Matthew Read

15th April 2019

Preface

i. I have conducted the majority of the work in this thesis and estimate my overall contribution to the thesis to be greater than 90%. I would especially like to acknowledgement the work performed by Dr David Liu in helping to validate both the patient-derived tumour xenograft model and a number of the xenograft-derived cell lines. I estimate my overall contribution to the thesis to be 90%.

ii. No part of this thesis has been submitted for the award of any other qualification or degree.

iii. Funding was received from The University of Melbourne and the Royal Australasian College of Surgeons.

Acknowledgements

I would like to acknowledge the vital contribution that my supervisors made in helping me to achieve this goal. Firstly, I would like to thank Professor Wayne Phillips, my principal supervisor, for keeping his faith in me, even when all seemed lost! I could not have made it this far without the support and guidance that you provided. You have certainly taught me how to start thinking like a scientist. I would also like to thank my co-supervisors Cuong Duong and Nicholas Clemons. Cuong, thanks for being a great role model and for introducing me to the concept of being both surgeon and scientist. You have invested a great deal of energy and effort into my career development over the years and for that I am truly grateful. Nick, thanks for your friendship and for being that first port of call. Thanks also for helping me transition into the laboratory. It certainly wasn't an easy journey for me, but the advice and support that you gave me made it all possible.

I also need to acknowledge my mentor, Professor Mark Shackleton, who helped me to realise the unique position that I am in as both a clinician and a scientist. Mark also taught me how to structure a research question, and the need to focus on clinically relevant issues.

I would also like to recognise the support that I received from my fellow students, in particular David Liu, Glen Guerra and Pia Bernardi. It was great to be able to share this research experience with like-minded clinicians. The camaraderie that we shared was amazing and the support that we provided each other was invaluable. It was also great to be around a group of people who understood the unique pressures of both surgical training and research.

I also need to recognise the significant contribution made by a number of collaborators, especially Professor Sheila Krishnadath. Sheila, I feel lucky to have you as both friend and mentor. It has been an inspiration to work alongside you and to be able to witness first-hand what it takes to succeed as both clinician and researcher. You have also provided me with invaluable input into my project and you helped shape the direction of my thesis. In addition, you have also introduced me to an amazing network of researchers from around the world, which will help me in my continued journey. I would also like to thank both Paul Burton and Andrew Taylor. Without the access to tissue that you provided I would not have been able to complete this work.

Most importantly, however, I need to thank my wife, Linda, and children Oliver, Lila and Freya from the bottom of my heart. I could not have come this far without the understanding, support, love and affection that you have all provided me throughout this journey. Whilst it has been a rewarding path to take, it has also been extremely challenging and has come with a great degree of sacrifice. Not only has it taken up valuable family time, but it has also meant that Linda has had to sacrifice a large part of her career as a midwife. For this, I am truly sorry and will be forever in your debt.

Publications

Read MD, Krishnadath KK, Clemons NJ, Phillips WA. Preclinical models for the study of Barrett's carcinogenesis. Ann N Y Acad Sci. 2018 Jul 5. doi: 10.1111/nyas.13916.

David S. Liu, Cuong P. Duong, Sue Haupt, Karen G. Montgomery, Colin M. House, Walid J. Azar, Helen B. Pearson, Oliver M. Fisher, **Matthew Read**, Glen R. Guerra, Ygal Haupt, Carleen Cullinane, Klas G. Wiman, Lars Abrahmsen, Wayne A. Phillips & Nicholas J. Clemons. Inhibiting the system xC/glutathione axis selectively targets cancers with mutant-p53 accumulation. Nature Communications 2017. DOI: 10.1038/NCOMMS14844.

Liu DS, Hoefnagel SJ, Fisher OM, Krishnadath KK, Montgomery KG, Busuttil RA, Colebatch AJ, **Read M**, Duong CP, Phillips WA, Clemons NJ. Novel metastatic models of esophageal adenocarcinoma derived from FLO-1 cells highlight the importance of E-cadherin in cancer metastasis. Oncotarget. 2016 Dec 13;7(50).

Liu DS, **Read M**, Cullinane C, et al. APR-246 potently inhibits tumour growth and overcomes chemoresistance in preclinical models of oesophageal adenocarcinoma. Gut 2015. DOI: 10.1136/gutjnl-2015-309770.

Read M, Liu D, Duong CP, Cullinane C, Murray W, Fennell C, Shortt J, Westerman D, Burton P, Clemons NJ, Phillips WA. Intra-muscular transplantation improves engraftment rates for esophageal patient-derived tumor xenografts. Annal of Surg Onc. DOI: 10.1245/s10434-015-4425-3.

Presentations

M. Read. Esophageal Stem Cells (Invited Talk). OESO, Geneva, 2017.

M. Read, A. Correia, S. Calpe, N. Clemons, D. Liu, W.A. Phillips, K.K. Krishnadath. Remodeling Barrett's Metaplasia in a Novel In Vivo Organoid Model. Digestive Diseases Week, Chicago, 2017.

M Read, A Correia, D Liu, D Straub, N Clemons, C Duong, K.K. Krishnadath & W Phillips. Reversing Barrett's Metaplasia in a Novel Organoid Model. Combined ANZGOSA / SUGGS Meeting, Sydney, 2016.

M. Read, Krishnadath KK, Liu DSH, Duong CP, Clemons NJ, Phillips WA*. A novel xenograft model of human Barrett's esophagus. Digestive Diseases Week, San Diego, 2016.

M Read, S Calpe, D Liu, D Straub, N Clemons, C Duong, K.K. Krishnadath & W Phillips. Targeting the BMP pathway in Barrett's carcinogenesis for molecular imaging & therapeutics. General Surgeons Australia, Annual Scientific Meeting, Cairns, 2015.

Matthew Read, David Liu, Nicholas Clemons, Christina Fennell, Cuong Duong & Wayne Phillips. A novel xenograft model for investigating Barrett's carcinogenesis. Australian Health and Medical Research Congress, Melbourne, Australia, 2014.

M Read, D Liu, MP Bernardi, C Duong, N Clemons, W Phillips. A novel preclinical model for the study of Barrett's oesophagus. Annual Scientific Congress of the Royal Australasian College of Surgeons, Singapore. 2014. Abstract published in ANZ Journal of Surgery. 2014; 84: 209.

Matthew Read, Nicholas Clemons, Wayne Phillips, Christina Fennell & Cuong Duong. An improved xenograft model for testing novel therapies in oesophageal adenocarcinoma. Annual Scientific Congress of the Royal Australasian College of Surgeons, Auckland. 2013. Abstract published in ANZ J. Surg. 2013; 83 (Suppl. 1) 98-104.

Matthew Read, Nicholas Clemons, Christina Fennell, Cuong Duong & Wayne Phillips. Patient derived tumour xenografts and the development of personalized medicine in oesophageal adenocarcinoma. Combined IsDEAS & ANZGOSA Meeting, Melbourne. 2013.

Read, M., Croagh, D., Clemons, N. J., Fennell, C., Duong, C., Phillips, W. A. Developing a novel in vivo tissue reconstitution system for the study of Barrett's oesophagus. 13th World Congress of the International Society for Diseases of the Esophagus, Venice, Italy (oral presentation). Abstract published in Diseases of the Esophagus. 2012; 25 (Supp.1): 57A

Posters

M. Read, S. Calpe, MC. Sancho-Serra, D. Straub, N. Clemons, D. Liu, W. Phillips, K.K. Krishnadath. Expression of Bone Morphogenic Protein (BMP4) in esophageal cancer is regulated by stroma-dependent Sonic Hedgehog Signals. Digestive Diseases Week, San Diego, 2016.

M. Read, S. Calpe, MC. Sancho-Serra, D. Straub, N. Clemons, D. Liu, W. Phillips, K.K. Krishnadath. The Function of the Tumor Microenvironment in Cancer Progression. Digestive Diseases Week, San Diego, 2016.

M. Read, S. Calpe, MC. Sancho-Serra, D. Straub, N. Clemons, D. Liu, W. Phillips, K.K. Krishnadath. Tumor-stroma crosstalk upregulates the in vivo expression of Bone Morphogenic Protein 4 (BMP4) in esophageal cancer. BMP Signaling in Cancer, Cambridge, 2016.

M. Read, S. Calpe, MC. Sancho-Serra, D. Straub, N. Clemons, D. Liu, W. Phillips, K.K. Krishnadath. Chemoresistance in a SMAD4 esophageal adenocarcinoma xenograft model is modulated by BMP4 inhibition. BMP Signaling in Cancer, Cambridge, 2016.

M Read, MP Bernardi, D Liu, C Fennell, R Ramsay, A Heriot, C Duong, W Phillips, N Clemons. Development of Esophageal and Anal Cancer Patient Derived Tumor Xenograft (PDTX) Models Using a Novel Implantation Technique. Digestive Diseases Week, Chicago, 2014. Abstract published in Gastroenterology. 2014; 146(5) Suppl. 1 S-695.

M Read, N Clemons, C Fennell, C Duong & W Phillips. An improved xenograft model for identifying a cancer stem cell population in oesophageal adenocarcinoma. Australian Gastroenterology Week, Melbourne. 2013. Abstract published in J Gastroenterol Hepatol. 2013; 28 (Suppl. 2) 11-18.

Matthew Read, Nicholas Clemons, Christina Fennell, Cuong Duong & Wayne Phillips. Improved Engraftment of Oesophageal Patient Derived Tumour Xenografts Using a Novel Intramuscular Technique. Australian Health and Medical Research Congress, Adelaide, Australia. 2012.

List of Tables

List of Figures

List of Abbreviations

AE1/AE3	Pan cytokeratin (CKs 1 to 8, 10, 14 to 16 and 19)
BMP4	Bone morphogenetic protein 4
BO	Barrett's oesophagus
BrdU	Bromodeoxyuridine
CAF	Cancer associated fibroblast
CD	Cluster of differentiation
CDX	Caudal-related homeobox transcription factor 2
CK	Cytokeratin
CSC	Cancer stem cell
CT	Computed Tomography
eGFP	Enhanced green fluorescent protein
EBV	Epstein-Barr virus
ELDA	Extreme limiting dilution assay
EMT	Epithelial-mesenchymal transition
EpCAM	Epithelial cell adhesion molecule
FACS	Fluorescence-activated cell sorting
FCS	Foetal calf serum
FFPE	Formalin-fixed paraffin-embedded
FITC	Fluorescein isothiocynate
GORD	Gastro-oesophageal reflux disease
H&E	Haematoxylin and eosin
HISC	Human intestinal stem cell
HLA	Human leukocyte antigen
IHC	Immunohistochemistry
IM	Intramuscular
Lgr5	Leucine-rich repeat-containing G-protein coupled receptor 5
MMR	Mismatch repair
NAF	Normal associated fibroblast

NIR	Near-infrared
NOD	Non-obese diabetic
NOD/SCID	Non-obese diabetic / severe combined immunodeficiency
NSG	NOD/SCID interleukin-2 receptor gamma chain knockout
OAC	Oesophageal adenocarcinoma
PDTX	Patient-derived tumour xenograft
PET	Positron-emission tomography
R0	Resection margin negative for tumour following microscopic assessment
SCC	Squamous cell carcinoma
SCJ	Squamocolumnar junction
SMG	Submucosal gland
STR	Short tandem repeat
TIC	Tumour initiating cell
TMA	Tissue microarray
TRG	Tumour regression grade

Chapter 1 Literature review

1.1 Overview

Oesophageal cancer is an extremely aggressive cancer and is associated with very poor survival. Worldwide, it is the eighth most common cancer and the sixth leading cause of cancer related death, posing a significant health burden (Ferlay, Shin, Bray, Forman, Mathers et al., 2010). There are two main subtypes of oesophageal caner; oesophageal squamous cell carcinoma (SCC) and oesophageal adenocarcinoma (OAC). Despite key differences with respect to risk factor profiles, tumour distribution and responses to therapy, both subtypes are treated in a similar fashion. Whilst the incidence of SCC predominates in developing countries, OAC has recently superseded SCC as the most common subtype in the developed world (Pohl & Welch, 2005). In order to fully understand this disease process, a clear knowledge of the structure, function and development of the normal human oesophagus is required.

1.2 The structure and function of the human oesophagus

The oesophagus is a muscular tube that forms the upper part of the gastrointestinal tract, connecting the oral cavity to the stomach (Sinnatamby, 2011). Embryologically, it is a foregut structure that is derived from the endoderm. From above, it is bordered by the cricopharyngeus muscle, which forms the upper oesophageal sphincter. Its function is to co-ordinate the swallow reflex and prevent the passage of ingested contents into the respiratory tract. From below, it is bordered by the lower oesophageal sphincter, which functions to protect the lower oesophagus from the reflux of gastric acid and bile. Throughout its course, the oesophagus traverses the neck and thoracic cavity before reaching the abdomen, where it joins the stomach at the gastroesophageal junction. Its main function is to facilitate the passage of ingested contents via a coordinated series of peristaltic contractions. This process requires a complex interaction between both the central nervous system and the myenteric plexus and involves both sensory and motor nerves (Paterson, 2006). At rest, the oesophagus is a flat structure, however, with the passage of a bolus, it is able to distend.

The wall of the oesophagus consists of four separate layers. The mucosa, consisting of a non-keratinised stratified squamous epithelium, forms the innermost layer. The main function of this epithelial layer is to protect the underlying tissues from the noxious effects of both gastroduodenal refluxate and ingested substances. This is achieved through the presence of an apical cell membrane and tight intercellular junctions (Orlando, 1998). It is also important to note, however, that from an embryological perspective, the oesophagus is initially lined by a pseudostratified layer of ciliated columnar epithelium before transitioning to a stratified squamous epithelium after the fourth month of gestation (Kuo & Urma, 2006). Regeneration of this epithelium occurs within its basal layer and newly formed cells migrate to the luminal surface over a period of approximately three weeks, becoming terminally differentiated. As the epithelium interdigitates with the underlying supportive connective tissue, a series of papillary regions are formed. Immediately below the basal layer, the mucosa also consists of a thin layer of supportive tissue, known as the lamina propria as well as the muscularis mucosa (Figure 1-1). The second layer consists of the submucosa, which contains a rich plexus of both blood vessels and nerves as well as submucosal glands (SMG), which are connected via ducts to the lumen. These glands produce both mucus and bicarbonate and have an important role in both lubricating the oesophagus and protecting it against the effect of acid refluxate (Orlando, 1998). The varied distribution of these glands is shown in Figure 1-2. Deep to this is the muscularis propria, consisting of an inner circular layer and an outer longitudinal layer that function together to produce a peristaltic wave. In the upper oesophagus, this layer is composed of striated muscle, whereas in the lower oesophagus, it is composed entirely of smooth muscle. The outer surface of the oesophagus consists only of an adventitial layer.

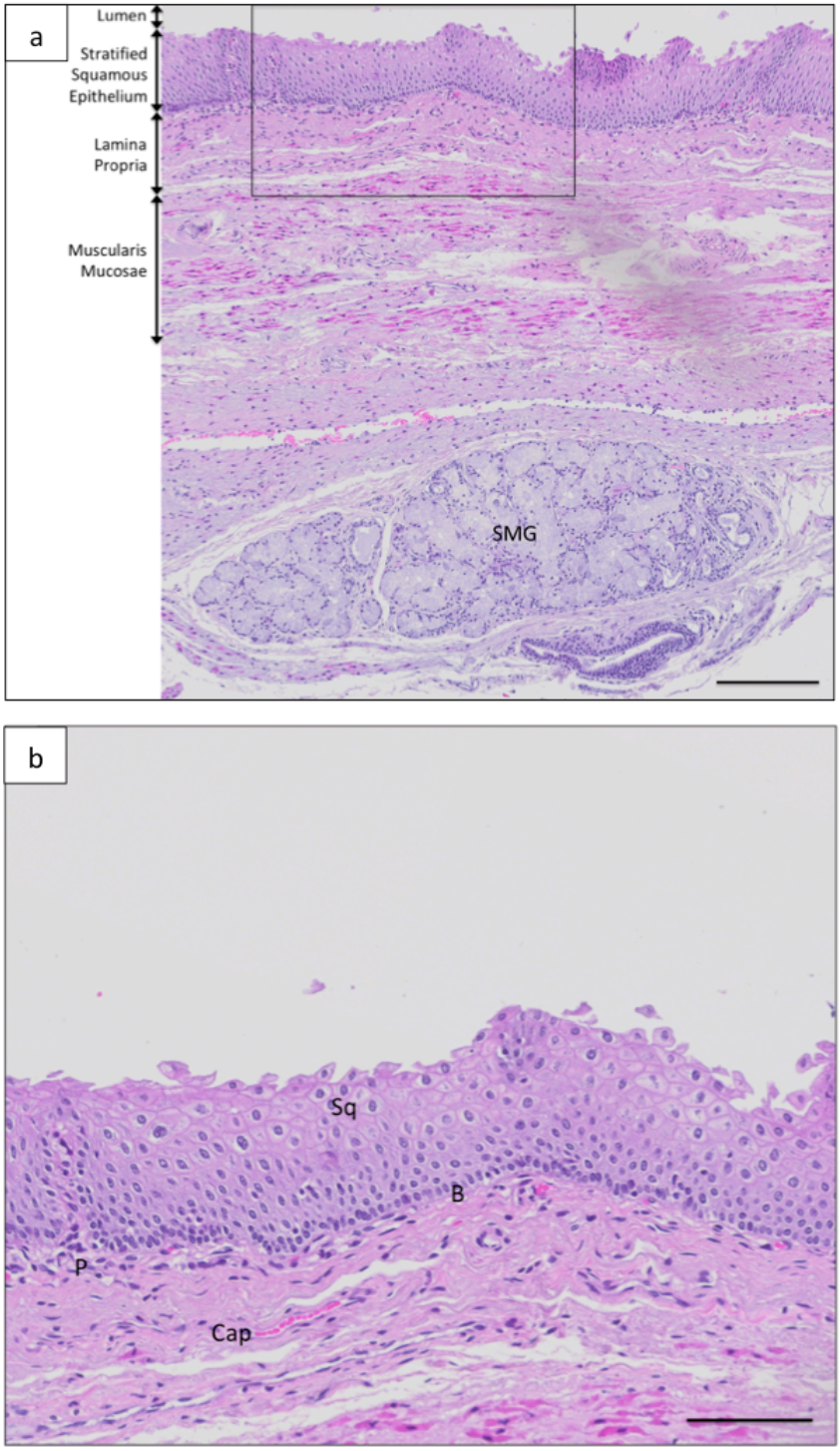

Figure 1-1 Structure of normal human oesophageal epithelium

A haematoxylin and eosin (H&E) section of normal human oesophagus demonstrating both mucosal and submucosal layers (a). Within the submucosa is a SMG. Scale bar represents 200µm. A magnified view of the region of interest demonstrating the features of the epithelial layer (b). Within this section is a papillary zone (P), a basal layer (B) and more differentiated squamous cells (Sq) in the suprabasal layers. Within the lamina propria there is a capillary (Cap). Scale bar represents 100µm.

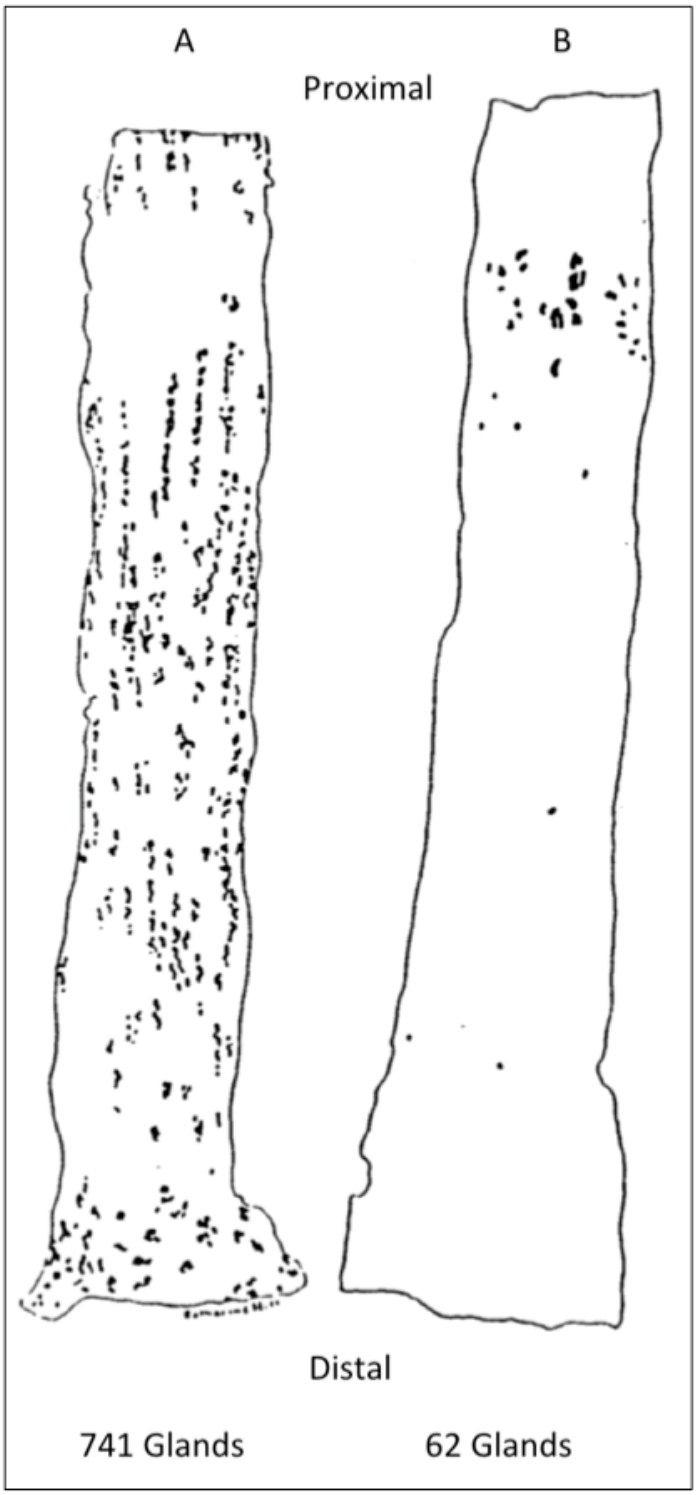

Figure 1-2 The distribution of submucosal glands within the human oesophagus

A diagram demonstrating the distribution of SMGs within two separate human oesophagi (A and B). Image from Goetsch E. The structure of the mammalian esophagus. Am J Anat 1910;10:34.

1.3 Pathophysiology of gastro-oesophageal reflux disease

There are a number of anti-reflux mechanisms that exist in order to protect the oesophagus. These include mechanisms that are both intrinsic and extrinsic to the oesophagus. Intrinsic factors include the lower oesophageal sphincter (LOS) with its associated high-pressure zone, the presence of both apical cell membranes and tight intercellular junctions that function together to create a protective epithelial layer as well as the secretion of both mucus and bicarbonate secretion from the SMGs. The LOS is one of the main contributors to the anti-reflux mechanism and is composed of specialised smooth muscle that has a high resting tone and is located within the wall of the distal oesophagus (Findlay & Maynard, 2019). Unlike other sphincters, such as the pylorus, the LOS is an anatomically discrete structure.

Extrinsic factors include the diaphragmatic sphincter, the presence of an intra-abdominal portion of oesophagus, the 'angle of His', and the phreno-oesophageal ligament (Sinnatamby, 2011). The diaphragmatic sphincter is formed by right crural fibres which wrap around the distal oesophagus as it passes into the abdominal cavity, acting like a pinchcock clamp. The phreno-oesophageal ligament is layer of fascia that connects the gastro-oesophageal junction to the diaphragm and is important in maintaining the 'angle of His' and an intra-abdominal length of oesophagus. The 'angle of His' is the acute angle formed between the distal oesophagus and the gastric cardia. Such an angulation contributes to anti-reflux mechanisms by creating a flap valve effect. An intra-abdominal portion of oesophagus is also mechanically advantageous as it exposes the distal oesophagus to the positive pressure of the abdomen, as opposed to the negative pressure of the thorax. This leads to compression of the distal oesophagus. Disruption to any of these mechanisms has the potential to lead to gastro-duodeno-oesophageal reflux.

The key noxious contents of gastro-duodeno-oesophageal reflux include acid, pepsin and bile. By disturbing the local pH-ion balance, acid has a direct injurious effect on the epithelium. It also acts indirectly by activating pepsin, a proteolytic enzyme, leading to an impaired mucosal barrier. In contrast, bile is able to pass directly into cells and disrupt cellular function by virtue of its lipophilic properties (Boeckxstaens & Rohof, 2014). All of these processes eventually lead to tissue injury and the ensuing inflammatory response.

The clinical entity describing the reflux of both gastric and duodenal secretions into the lower oesophagus is known as gastro-oesophageal reflux disease (GORD) and it is estimated to occur in up to 20% of the population (Boeckxstaens et al., 2014). The clinical sequalae of GORD can be varied. Short term exposure to refluxate typically results in oesophagitis. In contrast, chronic exposure can result in structural changes to the lower oesophagus, ranging from peptic stricture formation to the development of intestinal-type metaplasia known as Barrett's oesophagus (BO), which is thought to represent a protective mechanism (Yachimski, 2016).

1.4 Barrett's oesophagus

1.4.1 Definition and clinical significance

BO is the eponymous name describing the metaplasia that arises in the lower oesophagus in response to GORD. In this process the normal stratified squamous epithelium of the lower oesophagus is replaced by columnar epithelium (Wang & Souza, 2011) (Figure 1-3). It occurs in approximately 5% of the population and is clinically significant as it is the only known precursor lesion for OAC, conferring between a 30 to 100-fold increased risk (Streitz, 1994). This typically arises through a sequence of metaplasia followed by dysplasia. For patients with non-dysplastic BO, the rate of progression to either high grade dysplasia or OAC is between 1 to 3 / 1000 patients per year (Whiteman & Kendall, 2016). For those with low grade dysplasia, the rate has been reported to be as high as 13% per year (Whiteman et al., 2016).

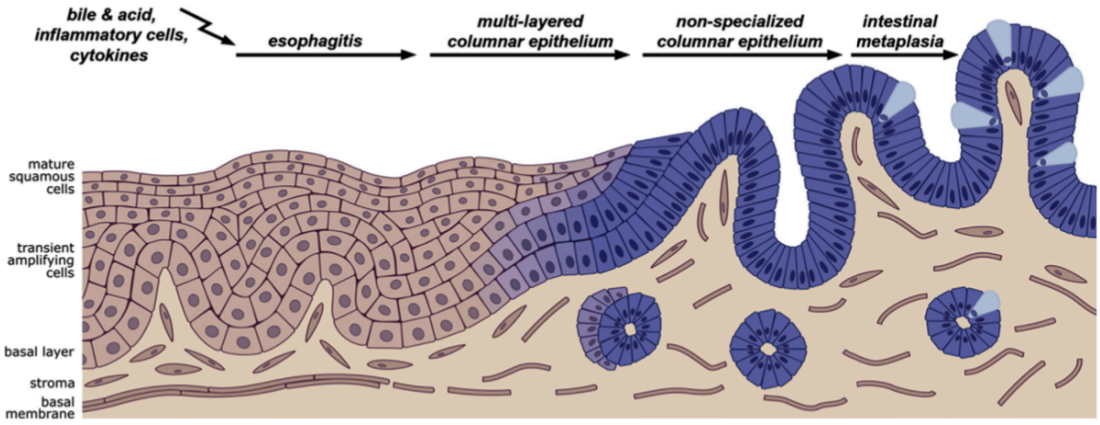

Figure 1-3 The development of BO

Barrett's metaplasia occurs in a stepwise fashion. In the initial phase GORD leads to inflammation in the lower oesophagus. This then triggers a process of metaplasia whereby the stratified squamous epithelium is replaced by columnar epithelium. Gradually specialised intestinal epithelium forms following the development of mucus producing goblet cells (light blue cells) (Krishnadath & Wang, 2015. Reproduced with permission.)

The diagnosis of BO requires an upper gastrointestinal endoscopic examination in order to detect the presence of a columnar-lined oesophagus extending more than 1cm proximal to the GOJ. Columnar-lined oesophageal mucosa appears salmon-pink in colour compared to the much paler appearance of stratified squamous epithelium (Figure 1-4). Unfortunately, high costs prohibit the use of upper gastrointestinal endoscopy as a diagnostic tool for screening purposes (Barbiere & Lyratzopoulos, 2009). However, this may change with the development of less invasive and more cost-effective detection modalities (Offman & Fitzgerald, 2017). Whilst there is no evidence for screening at a population level, a more targeted approach to screening may also be possible as researchers seek to better understand those at risk of BO through epidemiological studies (Thrift, Kendall, Pandeya, Vaughan, Whiteman et al., 2012). However, clinicians need to be cognizant of the fact that not all patients with either GORD or BO are symptomatic. In fact, the population prevalence of individuals with BO but without reflux symptoms is in the order of 1.2% (Ong, Lao-Sirieix, & Fitzgerald, 2010). This explains why a significant proportion of cases of OAC are diagnosed at an advanced stage and in patients who are not on surveillance programs (Cooper, Kou, & Chak, 2009; Keld & Ang, 2011).

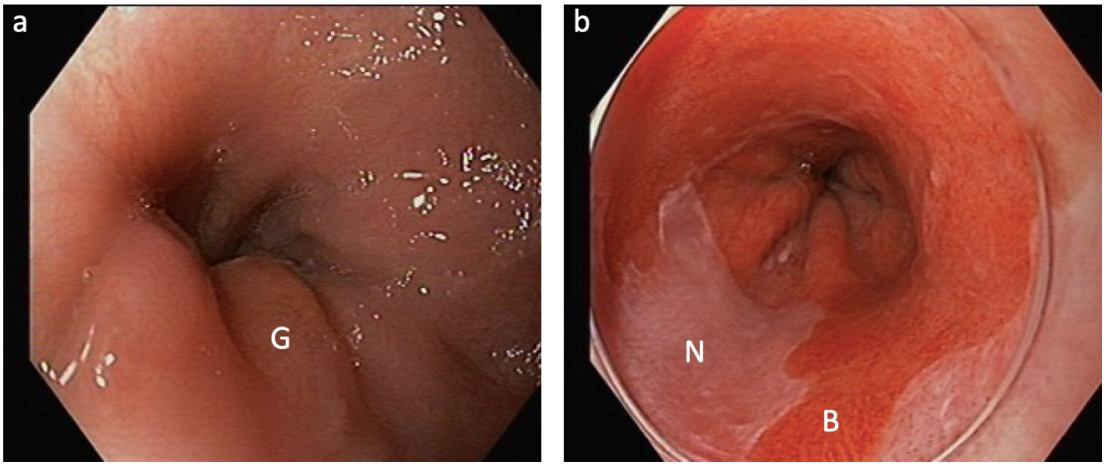

Figure 1-4 Endoscopic appearance of the lower oesophagus

Image 'a' demonstrates the normal appearance of the lower oesophagus. The top of the gastric folds (G) indicate the GOJ. Image 'b' demonstrates a segment of BO arising proximally from the GOJ. The salmon pink appearance of the Barrett's segment (B) is easily identified. This is in contrast to the pale appearance of the normal oesophageal epithelium (N). Images courtesy of Dr Bronte Holt, St Vincent's Hospital, Melbourne.

1.4.2 Current management

Once an endoscopic diagnosis of BO is made, confirmation is obtained via histological examination. According to both the Australian and American guidelines, this requires the presence of intestinal metaplasia, characterised by the presence of mucus secreting goblet cells (Whiteman et al., 2016). British guidelines, however, only require evidence of a columnar lined oesophagus (Tan, di Pietro, & Fitzgerald, 2017).

Once the presence of BO is confirmed, patients are stratified based on the length of the BO segment and the presence of dysplasia. The length of the BO segment is measured from the GOJ, to its most proximal extension. Australian guidelines state that patients with non-dysplastic BO should undergo surveillance, with the interval being determined by the length of the BO segment. Patients with short segments (< 3cm) should undergo endoscopic assessment every three to five years, whereas those with long segments (>3cm) should be assessed every two to three years. Patients with low-grade dysplasia, on the otherhand, should undergo endoscopic surveillance every six months irrespective of the length of the BO segment. If a diagnosis of high-grade dysplasia is made, patients should be referred to a tertiary centre for endoscopic treatment. (Whiteman, Appleyard, Bahin, Bobryshev, Bourke et al., 2015). Unfortunately, there are a number of issues with surveillance programs. Firstly, there is generally poor adherence to recommended guidelines. Secondly, there is a significant amount of sampling error and inter-observer variability associated with the detection of dysplastic foci. This is because the lesions are usually flat and indistinguishable from the surrounding metaplasia (Ong et al., 2010). In an attempt to overcome these difficulties and improve the endoscopic detection of both pre-malignant and malignant lesions, a consensus statement has recently been published by a number of leading endoscopists, stating that narrow band imaging with magnification should be used in conjunction with standard white light endoscopy to enhance the image during endoscopy (Chiu, Uedo, Singh, Gotoda, Ng et al., 2019). In an attempt to further stratify patients with dysplastic foci, researchers are focusing on the development of biomarkers that will aid in predicting those patients who are most likely to progress to OAC (Frankell, Jammula, Li, Contino, Killcoyne et al., 2019).

In patients diagnosed with dysplastic BO, confirmation is required by a second expert pathologist. For low grade dysplasia, management consists of either more intensive surveillance or endoscopic treatment. However, for high grade dysplasia, endoscopic

treatment must be offered. The main principles of endoscopic management involve resecting dysplastic foci and ablating remaining non-dysplastic segments. Patients undergoing endoscopic treatment are also required to undergo treatment for GORD. This is to enable the oesophageal epithelium to regenerate in the absence of reflux. This is usually achieved by either pharmacologically or surgically by means of fundoplication (Whiteman et al., 2016).

1.4.3 Current theories regarding the pathogenesis of BO

Current theories suggest that the development of BO is due to a complex interplay between environmental exposures, molecular genetics and cellular interactions. Unfortunately, the exact mechanisms responsible for the development of BO at both the cellular and molecular level are poorly understood. As a result, a number of different theories regarding the pathogenesis of BO exist, especially regarding Barrett's cell of origin. These theories are explored in the following sections.

1.4.3.1 Barrett's cell of origin

Given the embryological basis of oesophageal development, it seems highly plausible that the Barrett's cell of origin resides in a niche intrinsic to the oesophagus. For this to occur, cells native to the oesophagus must go through the process of either transdifferentiation or transcommitment. Transdifferentiation is the process whereby a phenotypic switch occurs between one differentiated cell type to another, typically involving cell types that were present during embryogenesis (Tosh & Slack, 2002). This theory, however, fails to explain the ability of Barrett's tissue to regenerate, as, by definition, differentiated cells lack the ability to self-renew (Shackleton, 2010). Transdifferentiation also fails to explain how separate clones within a segment of BO are able to expand, a phenomenon that has been reported to occur quite frequently (Evans & McDonald, 2016; Nicholson, Graham, Simpson, Humphries, Burch et al., 2012). However, both of these observations can be explained by the transcommitment model, as, in this model, the phenotypic switch occurs at the resident stem or progenitor cell level (Kapoor, Agrawal, & Mittal, 2015).

Within the human oesophagus, a number of potential stem cell niches exist, that could potentially harbour the Barrett's cell of origin. These include the interpapillary basal layer as well as the SMG and its associated duct (Nicholson et al., 2012; Seery & Watt, 2000). In support of this theory is the observation that human Barrett's mucosa occurs in continuity

with oesophageal gland ducts (Coad, Woodman, Warner, Barr, Wright et al., 2005). This theory is further supported by experimental work conducted using a canine model, which, like the human, also contain SMGs (Gillen, Keeling, Byrne, West, & Hennessy, 1988). In the study by Gillen et al. (1988), the effects of acid and bile on regenerating oesophageal mucosa was tested. Results revealed the formation of a columnar epithelium in response to acid and bile exposure in regions of the lower oesophagus that had been denuded. As the epithelium was denuded in such a fashion as to prevent the migration of cells from gastro-oesophageal junction and gastric cardia, the authors concluded that the columnar cells originated from a source intrinsic to the oesophagus. Like the human, the columnar epithelium was also found to be in continuity with SMGs. More recently, an in vitro study that generated organoids from porcine SMGs, demonstrated that SMGs had the potential to generate both squamous and ductal phenotypes (von Furstenberg, Li, Stolarchuk, Feder, Campbell et al., 2017).

A number of other purported theories suggest that the Barrett's cell of origin may in fact reside at the gastro-oesophageal junction. However, a key criticism of all of these theories, is that they are based on the findings from rodent models and not humans. As there are a number of differences between the rodent and human oesophagus, this makes it difficult to interpret findings from one species to another. Key differences include the absence of SMGs and the presence of a keratinised stratified squamous epithelial layer lining the oesophagus. The squamo-columnar junction is also located in the forestomach rather than the true GOJ (Read, Krishnadath, Clemons, & Phillips, 2018).

In a study by Wang et al. (2011), a p63 knockout mouse was used to model human BO. As p63 is essential for the development of all stratified epithelial tissues, its loss inhibits the transition from columnar to stratified squamous epithelium that occurs within the oesophagus during embryogenesis, resulting in a Barrett's like phenotype. However, a limitation of this model is that it is represents a defect of embryogenesis and not true metaplasia. Extrapolating the findings from this model, the authors then identified a population of residual embryonic cells at the squamocolumnar junction (SCJ) in both wild-type mice and human samples which they claim have the potential to repopulate the oesophagus following injury. However, these claims are not supported by any functional study.

Stem cells residing at the gastric cardia have also been implicated in the pathogenesis of BO. In a study by Quante et al. (2012), a transgenic mouse model was used that overexpressed

the inflammatory cytokine IL-1β in stratified squamous epithelia. This was selected in order to replicate the inflammatory response that occurs in GORD, one of the key risk factors for the development of BO. The development of metaplasia and adenocarcinoma was further enhanced by exposure to bile acids and nitrosamines. In this model, metaplasia and adenocarcinoma formation was localised to the SCJ and, through lineage tracing, was found to have originated from leucine-rich repeat-containing G-protein coupled receptor 5 ($Lgr5^+$) cells residing in the adjacent gastric cardia. These results suggest that gastric intestinal metaplasia is being modelled rather than BO.

More recently Jiang et al. (2017) published evidence of a multi-layered epithelium at the SCJ or transition zone in both mice and humans. These cells were found to be $p63^+Krt5^+Krt7^+$ and following ectopic expression of caudal-related homeobox transcription factor 2 (CDX2), transformed into a Barrett's like phenotype within the confines of the transitional zone. No effect was seen within normal squamous regions. However, a criticism of this study is that the ectopic expression of CDX2 could be considered to be an artificial effect. A similar result has also been reported in another study, whereby the intestinalisation of $p63^+Krt5^+$ cells was artificially induced following transfection with the CDX2 gene (Mari, Milano, Parikh, Straub, Everts et al., 2014).

An alternative theory is that circulating bone marrow progenitor cells contribute to the development of BO. In a study by Sarosi et al. (2008), female rats were irradiated with lethal dose of radiation and then rescued via a tail vein injection of bone marrow cells obtained from male rats. In order to induce metaplasia, rats then underwent an oesophagoduodenostomy. Subsequent analysis of both normal and metaplastic tissue confirmed the presence of Y chromosomes. Although the authors claim that these cells were contributing to the formation of metaplasia, it is more likely that they represent an inflammatory cell infiltrate.

1.4.3.2 Key molecular pathways

Three major pathways have been suggested to play a role in the development of BO (Clemons, Koh, & Phillips, 2014). The Notch and the caudal-related homeobox transcription factor (CDX) pathways are important regulators of intestinal differentiation. They have been shown to be upregulated after bile and acid exposure in squamous cells and to drive upregulation of intestinal and BO specific genes, such as mucin2 and cytokeratin (CK) 20

(Clemons, Koh, et al., 2014). As such, it is not surprising that they are aberrantly expressed in BO tissues. Surprisingly, however, overexpression of CDX2 in the mouse oesophagus under the cytokeratin 14 (CK14) promoter failed to induce columnar metaplasia, suggesting that CDX2 alone is insufficient to induce columnar metaplasia (Kong, Crissey, Funakoshi, Kreindler, & Lynch, 2011).

The Sonic Hedgehog (Shh) pathway and its downstream effectors bone morphogenetic protein 4 (BMP4) and SOX9 have been gaining recent interest as putative drivers of metaplasia. Shh signalling is also an important pathway for gut development (Krishnadath, 2007). Shh signalling is mediated by two membrane-bound receptors: patched (Ptch) and smoothened (Smo). Binding to Patch1 leads to activation of a cytoplasmic protein complex containing Gli transcription factors and to the activation of pathway targets such as BMP4 and SOX9 (Wang, Clemons, Miyashita, Dupuy, Zhang et al., 2010). Both Shh (Wang et al., 2010) and BMP4 (Milano, van Baal, Buttar, Rygiel, de Kort et al., 2007; van Baal, Milana, Rygiel, Sondermeijer, Spek et al., 2008) are highly expressed in BO. Bile and acid have been shown to activate expression of Shh in epithelial cells, both *in vitro* and *in vivo* (Sun, Wang, Gai, Song, Jia et al., 2015; Wang et al., 2010). This epithelial Shh acts in a paracrine manner on mesenchymal cells and induces BMP4 secretion (Wang et al., 2010). Interestingly, epithelial cells also secrete BMP4 after direct contact to acid and bile salts (Zhou, Sun, Wang, Wang, Wang et al., 2009). Both mesenchymal-derived and epithelial-derived BMP4 acts on epithelial cells, as shown by the high expression of BMP4 targets such as ID2 in the epithelia of BO (van Baal, Milana, et al., 2008; van Baal, Rygiel, Milano, Anderson, Bergman et al., 2008). An important set of *in vitro* and *in vivo* experiments evaluated the significance of BMP4 signalling on epithelial cells in the development of BO. Exposure to BMP4 induced striking morphological changes on squamous epithelial cells and a shift in the cytokeratin expression pattern, in which the expression of CK10 and CK13 decreased and that of CK7 and CK20 was upregulated (Milano et al., 2007). RNA analysis of BMP4-treated squamous cells confirmed their transformation into a columnar type of cells, but not an increase in the expression of intestinal epithelial markers. Similarly, ectopic expression of BMP4 in the mouse oesophagus under the control of the CK14 promoter induced columnar differentiation but did not lead to intestinal metaplasia (Mari et al., 2014). It was only when CDX2 was also overexpressed in squamous cells, that BMP4 stimulation could induce the expression of both columnar and intestinal genes (Mari et al., 2014). Further, chromatin immunoprecipitation experiments on human BO cells, confirmed, at the molecular level, that both CDX2 and phosphorylated

SMAD (the transcription factor for BMP4) bind to the mucin 2 gene promoter. Importantly, using a surgical mouse model of BO the exact sequence in which these markers appear during the development of non-intestinal to intestinal metaplasia were identified (Mari et al., 2014). In this model it was shown that activation of the BMP4/pSMAD pathway is an early event, whereas CDX2 and MUC2 expression appear late during the development of intestinal metaplasia. Together, these experiments have therefore demonstrated an important role of the BMP4/CDX2 pathway in the development of columnar and intestinal metaplasia, rendering this pathway highly attractive as a therapeutic target for Barrett's metaplasia.

1.5 Oesophageal adenocarcinoma

1.5.1 Background

In Australia, the current 5-year survival rate for OAC is approximately 16%, which is only a modest improvement from the level of 10% that was recorded 25 years ago (Cancer Council Victoria, 2011). This is despite extensive research efforts and changes to clinical management over this period. Such changes have included improvements to endoscopic technologies to better identify early cancers, staging techniques, endoscopic resection, the introduction of neoadjuvant therapy, the development of less invasive surgical techniques, the establishment of centralised cancer services and the improved management of post-operative complications (Kleinberg, 2013; Rouvelas & Lagergren, 2010; van Hagen, Hulshof, van Lanschot, Steyerberg, van Berge Henegouwen et al., 2012; Zehetner, DeMeester, Hagen, Ayazi, Augustin et al., 2011).

The incidence of OAC has also risen more than six-fold over the last four decades, which is more than any other solid cancer over that same period (Pohl et al., 2005). Through population-based studies, obesity and GORD have been identified as two of the strongest risk factors for the development of OAC (Thrift, Pandeya, & Whiteman, 2012). It is widely accepted that the rising prevalence of these risk factors is contributing to the steep rise in incidence seen in OAC.

1.5.2 Clinical presentation and management

The majority of patients that present with OAC have either advanced locoregional or metastatic disease. These patients typically present with dysphagia. However, they may also present with iron deficiency anaemia secondary to a bleeding tumour. Only approximately 25% of patients present with localised disease with fewer than 15% being detected via Barrett's surveillance programs (Rubenstein & Shaheen, 2015).

.

The current management of OAC varies according to the stage of disease, patient fitness and institutional practices. The treatment of early cancers that are confined to either the mucosa or superficial sub-mucosa are typically based on endoscopic approaches, such as either endoscopic mucosal resection (EMR) or endoscopic submucosal dissection (ESD) (Rubenstein et al., 2015). The 5-year survival rate for patients who present in this early stage has been

reported to be as high as 90% (Keld et al., 2011). For patients with locally advanced disease, treatment consists of either neoadjuvant chemotherapy (combination of cytotoxic and antimetabolite agents) or chemoradiotherapy followed by surgery with curative intent. This is based on the results from three seminal publications. These include the MAGIC trial, the CROSS study and, more recently, the FLOT study (Al-Batran, Hofheinz, Pauligk, Kopp, Haag et al., 2016; Cunningham, Allum, Stenning, Thompson, Van de Velde et al., 2006; van Hagen et al., 2012). In the MAGIC trial, which compared the combination of peri-operative chemotherapy in the form of epirubicin, cisplatin and fluorouracil (ECF) in combination with surgery versus surgery alone for resectable gastroesophageal cancers, results revealed a 5-year survival of 36 percent in the combined chemotherapy and surgery group versus 23 percent in the surgery alone group (Cunningham et al., 2006). In the CROSS study, the added effect of radiotherapy was assessed. This resulted in improved R0 resection rates and a 5-year survival of 49.4 months in the group receiving chemoradiotherapy in conjunction with surgery versus 24 months for the group that received surgery alone (van Hagen et al., 2012). More recently, the combination of perioperative docetaxel, oxaliplatin, leucovorin and fluorouracil (FLOT) was compared to perioperative ECF (Al-Batran et al., 2016). Results revealed that higher proportions of patients treated with perioperative FLOT achieved a complete pathological response compared to those treated with ECF (16% vs 6%; p=0.02). Unfortunately, the majority of patients present with disease in its later stages with between 50 to 60% having distant metastasis at the time of diagnosis (Howlader, Noone, Krapcho, Garshell, Miller et al., 2015; Tejani & Burtness, 2012). For these patients, palliation is the only option. This consists of various combinations of chemotherapy, radiotherapy, endoscopic stenting and comfort measures (Rubenstein et al., 2015).

1.5.3 Current theories regarding the pathogenesis of oesophageal adenocarcinoma

Given that the 5-year survival rate for patients with OAC that are treated with curative intent is less than 45% (Weaver, Ross-Innes, & Fitzgerald, 2014), alternative treatment strategies are urgently needed. As the hallmark features of OAC are its rising incidence, late presentation and resistance to treatment, research efforts should focus on risk factor modification, improved screening to enable earlier detection and the development of improved treatment options. However, in order to identify novel therapeutic targets, a greater understanding of both the genetic and cellular events involved in the pathogenesis of OAC is required. Such

knowledge may even help to better identify patients who need more intensive treatment and surveillance.

1.5.3.1 Key genetic events

A number of key discoveries into the genetic landscape of both BO and OAC have been identified through the use of genome-wide analyses in two recently published studies (Nones, Waddell, Wayte, Patch, Bailey et al., 2014; Weaver, Ross-Innes, Shannon, Lynch, Forshew et al., 2014). In the study by Nones et al. (2014) a combination of whole-genome sequencing, single-nucleotide polymorphism arrays and copy number analyses revealed that catastrophic genomic events were frequent in OAC. This was reportedly due to a recently discovered process known chromothripsis (Zhang, Spektor, Cornils, Francis, Jackson et al., 2015), which was found to have occurred in 32% of cases. In this process, a limited number of chromosomes become fragmented before reforming haphazardly, thereby creating multiple mutations within a single cell cycle. This process, previously unrecognised in OAC, explains the mechanism behind the marked heterogeneity seen in OAC. This theory can also be used to explain the rapid genomic evolution the occurs in OAC as well as the broad range of oncogenes that it encompasses.

In the study by Weaver et al. (2014), OAC samples from a cohort of 112 patients were sequenced in order to determine commonly mutated genes. In an attempt to determine the order of mutations in the Barrett's carcinogenesis sequence, samples were also sequenced from a separate cohort of patients with BO from two separate disease points. These included non-dysplastic BO and BO with associated high-grade dysplasia. One of the key findings of this study was that the majority of recurrently mutated genes were found to be present in only a small proportion of patients. Surprisingly, the most frequently mutated genes identified in the OAC cohort were also found to be present at a similar frequency in the non-dysplastic BO samples. Of these mutations, the only ones that were found to have occurred in a disease stage specific manner were p53 and SMAD4, with the p53 mutation marking the transition from non-dysplastic BO to BO with high-grade dysplasia, and SMAD4 marking the transition between high-grade dysplasia and early OAC. Unfortunately, the utility of SMAD4 as a biomarker is limited, as it was only found to be present in 13% of OAC samples.

1.5.3.2 Model of cancer cell propagation

Disease recurrence is one of the main factors contributing to the high mortality rate associated with OAC. This is due to the presence of residual cancer cells with tumorigenic potential. In the case of OAC, it is unknown if all cells have this potential or only a small sub-population. If it is only a small sub-population, it is likely that OAC follows the cancer stem cell (CSC) model. Conversely, if all cells have equal tumorigenic potential, then it seems likely that OAC follows the model of clonal evolution. Although not a defining feature, CSCs have also been shown to exhibit chemoresistance properties, as demonstrated by the cluster of differentiation (CD) 133+ population of cells within glioblastoma (Liu, Yuan, Zeng, Tunici, Ng et al., 2006). Possible explanations for this include enhanced DNA damage repair mechanisms, impaired apoptosis and more efficient drug efflux (Dean, Fojo, & Bates, 2005; Grotenhuis, Wijnhoven, & van Lanschot, 2012). Being able to identify such a population within OAC may help in the development of more targeted therapies.

Based on the fact that CSC populations have already been identified in a number of other solid cancers, including breast, brain and colon cancer (Grotenhuis et al., 2012), research efforts have focused on identifying a CSC population within OAC. As a result, a range of candidate markers have already been tested. These have included CD24, CD29, CD34, CD44, CD133, CD166, EpCAM, β -catenin, Musashi-1, leucine-rich-repeat-containing G-protein-coupled receptor 5 (Lgr5) and the $\alpha6^{bri}/CD71^{dim}$ cell population (Becker, Huang, & Mashimo, 2010; Bobryshev, Freeman, Botelho, Tran, Levert-Mignon et al., 2010; Grotenhuis, Dinjens, Wijnhoven, Sonneveld, Sacchetti et al., 2010; Zhao, Quaroni, & Casson, 2012). Despite these efforts, a true CSC population within OAC is yet to be identified.

However, before further research is undertaken in this area, initial research efforts should focus on trying to identify the model of cancer cell propagation that OAC follows. Only if the frequency of tumour initiating cell (TIC) within OAC is found to be low, should efforts be made to identify a potential CSC population.

1.6 Preclinical models for the study of Barrett's carcinogenesis

Despite recent advances in the management of both BO and OAC over the last few decades, there has only been an incremental improvement with respect to the overall survival rate for this disease (Cancer Council Victoria, 2011). For there to be a significant improvement in survival rates, novel treatments need to be developed. However, the limited availability of suitable preclinical models has proven to be a significant barrier to progress (Liu, Duong, Phillips, & Clemons, 2016). Two common models currently used in cancer research include the cancer cell line and the xenograft model (Hidalgo, Amant, Biankin, Budinska, Byrne et al., 2014; Mullard, 2018).

Cancer cell lines are typically established following the digestion of pieces of primary tumour followed by an extended period of *in vitro* culture. By definition, they are clonal populations of cells and lack the heterogeneity that is typical of most cancers (Mullard, 2018). Despite this limitation, cancer cell lines are an extremely versatile and commonly used model. They enable a high throughput of invitro assays, ranging from drug screens to mechanistic studies. Unfortunately, a robust technique for the establishment of cell lines has not been established. This is of particular concern in OAC, as there are only six bona fide cell lines derived from Barrett's associated adenocarcinomas (Boonstra, Tilanus, & Dinjens, 2015).

Another commonly used preclinical cancer model is the xenograft model. Traditionally, these have been generated following the injection of established cancer cell lines into immunodeficient mice (Dodbiba, Teichman, Fleet, Thai, Sun et al., 2013b). However, more recently, the patient-derived tumour xenograft (PDTX) model has gained popularity (Hidalgo et al., 2014). In this model, tissue pieces are transplanted into an immunodeficient host. Following successful engraftment, tumours are then serially passaged through multiple generations until multiple cohorts are established. They are thought to be superior to conventional cell line models as they better recapitulate tumour heterogeneity and contain elements of human stroma (Hidalgo et al., 2014). There are many potential applications of the PDTX model, however, they are most commonly used for drug target validation (Tentler, Tan, Weekes, Jimeno, Leong et al., 2012). However, like the cell line model, PDTXs have also proven difficult to establish in OAC (J. J. Boonstra, R. van Marion, H. J. Douben, J. S. Lanchbury, K. M. Timms et al., 2012; de Both, Wijnhoven, Sleddens, Tilanus, & Dinjens, 2001; Dodbiba, Teichman, Fleet, Thai, Starmans et al., 2015; Dodbiba et al., 2013b).

A number of preclinical models have also been developed for the study of BO. The following published review highlights the progress that has been made in the development of these models as well as their key applications and limitations.

Ann. N.Y. Acad. Sci. ISSN 0077-8923

ANNALS OF THE NEW YORK ACADEMY OF SCIENCES
Special Issue: *Global Perspectives on Esophageal Diseases*
CONCISE REVIEW

Preclinical models for the study of Barrett's carcinogenesis

Matthew D. Read,[1] Kausilia K. Krishnadath,[2] Nicholas J. Clemons,[3,4] and Wayne A. Phillips[3,4]

[1]Cancer Biology and Surgical Oncology Laboratory, Peter MacCallum Cancer Centre, Melbourne, Victoria, Australia. [2]Department of Gastroenterology and Hepatology, Academic Medical Center, Amsterdam, the Netherlands. [3]Division of Cancer Research, Peter MacCallum Cancer Centre, Melbourne, Victoria, Australia. [4]Sir Peter MacCallum Department of Oncology, University of Melbourne, Melbourne, Victoria, Australia

Address for correspondence: Matthew D. Read, Cancer Biology and Surgical Oncology Laboratory, Peter MacCallum Cancer Centre, 305 Grattan Street, Melbourne, VIC 3000, Australia. mattread80@gmail.com

Barrett's esophagus (BE) is clinically significant, as it is the only known precursor lesion for esophageal adenocarcinoma. To develop improved therapies for the treatment of BE, a greater understanding of the disease process at the molecular genetic level is needed. However, achieving a greater understanding will require improved preclinical models so that the disease process can be more closely studied and novel therapies can be tested. Our concise review highlights progress in the development of preclinical models for the study of BE and identifies the most suitable model in which to test novel therapies.

Keywords: Barrett's esophagus; reflux models; transgenic models; organoid; preclinical model; animal models

Introduction

Barrett's esophagus (BE) is the eponym describing the metaplastic process that occurs in the lower esophagus in response to gastroesophageal reflux (GER). BE is clinically significant because it is the only known precursor lesion for esophageal adenocarcinoma (EAC), a cancer with an extremely poor prognosis and an incidence that has risen more than sixfold over the last four decades.[1] Unfortunately, the exact mechanisms responsible for both the initiation of BE and its progression to EAC are poorly understood, and this has led to several key controversies in the field. One of the main controversies surrounds the location and identity of the Barrett's cell of origin.[2,3] Current theories include cells that are native to the esophagus (squamous cells, ductal cells, and submucosal gland cells), cells located at the squamocolumnar junction (SCJ) (transitional basal cells and embryonic stem cells), cells from the proximal stomach (gastric cardia), and even bone marrow-derived cells.[4] Another controversy, closely entwined with the Barrett's cell of origin, is whether BE forms through a process of transdifferentiation (transformation of one differentiated cell type to another) or transcommitment (reprogramming at the stem or progenitor cell level).[3] Several controversies regarding the pathogenesis of Barrett's carcinogenesis also exist at the molecular genetic level. Examples include the component of refluxate responsible for the initiation of the metaplastic process,[5] as well as the sequence of mutations and epigenetic changes required for neoplastic progression.[6,7]

Current treatments for BE consist of endoscopically resecting or ablating metaplastic segments using a combination of either endoscopic submucosal dissection, endoscopic mucosal resection, or radiofrequency ablation.[8] These treatments aim to denude portions of the esophagus, which in the absence of the GER, undergo repair with neosquamous epithelium.[8] Unfortunately, these techniques can lead to both recurrent Barrett's[9] and buried Barrett's,[10] making ongoing surveillance and treatment challenging. These techniques can also lead to complications, such as perforation, stricture formation, and bleeding. In a recent systematic review, assessing the safety of endoscopic treatments for both BE and early EAC, the rates of perforation, stricture formation, and bleeding were 33.5%, 7.5%, and 1.3%, respectively.[11] There is currently no pharmacotherapy that targets the molecular drivers of

doi: 10.1111/nyas.13916

BE, either for the prevention or treatment of the disease.

To develop improved therapies to treat BE, a greater understanding of the disease processes at the molecular genetic level is required. However, for therapeutic development to occur, improved preclinical models are required for mechanistic studies and testing of novel therapies.[12] The ideal model for the study of Barrett's carcinogenesis should be manipulable, reproducible, and three-dimensional and should allow for environmental exposures. As BE is likely due to a complex interaction between different cell types,[13] the ideal model should include a full complement of epithelial, stromal, and inflammatory cells.[14] The epithelial component should include cells from the esophagus (including submucosal glands and ductal cells), stomach, and gastroesophageal junction. Through such an approach, all potential sources of the BE cell of origin should be included. The ideal model also needs to undergo strict validation to confirm that it recapitulates the human disease process and can model the progression from the BE cell of origin to columnar epithelia to adenocarcinoma (AC). Our review highlights the progress made in the development of preclinical models for the study of BE.

Methodology

A PubMed search was performed for publication dates from January 1950 to March 2018 using a combination of the following terms: Barrett's esophagus, preclinical model, reflux model, animal model, transgenic model, cell line, organotypic model, and organoid model. Articles were limited to those published in English. A manual search of citations for relevant articles was also performed. Both original articles and review articles were included.

In vivo models

While a number of key discoveries have been published from a range of different preclinical models of BE, there have also been a number of conflicting results. These conflicting results were observed because there is no single preclinical model that offers the ideal system with which to study Barrett's carcinogenesis.[15] While attempts have been made to develop an *in vivo* Barrett's model from several different species, research efforts have mainly focused on murine and canine models. To generate both the Barrett's phenotype and EAC within these animal models, a number of modifications have been attempted. These include the surgical induction of different types of reflux, genetic modification, and exposure to different forms of exogenous carcinogens.[16–19]

Research in this field was originally focused on reflux esophagitis and the columnar lined esophagus (CLE). During this early period, several studies were performed using canine models to investigate the effects of various refluxates on the esophagus. An advantage of this model is that both the canine and human esophagi contain submucosal glands.[15] In a landmark study by Bremner *et al.*, dogs were randomized to one of three groups following stripping of the lower esophageal mucosa. These included a surgically induced reflux group, a gastric hypersecretion group, and a control group.[20] The results indicated that neo-epithelialization occurred via a columnar epithelium in the reflux group, whereas a squamous epithelium predominated in those animals with a competent lower esophageal sphincter. From these results, the authors concluded that the CLE is an acquired condition formed from the migration of columnar cells from either a gastric or a junctional origin. In 1988, Gillen *et al.* published a similar study to that performed by Bremner *et al.*[21] However, in that study using a canine model, the lower esophageal mucosa was denuded in a certain manner to create a squamous barrier to any migrating gastric or junctional cells. Similar to Bremner, the authors observed the formation of a columnar epithelium in the presence of acid reflux, both on its own and in combination with bile (but not bile on its own). From these results, they also concluded that BE is an acquired condition. However, unlike Bremner, the authors concluded that the columnar cells originate from a source intrinsic to the esophagus, such as the submucosal gland. These results were further supported by canine studies conducted by Li *et al.,* who concluded that the regenerating epithelium was in continuity with the ducts of the esophageal glands.[22]

Two of the seminal studies assessing the effect of refluxate composition on the esophagus were Ferguson *et al.* in 1950[23] and Redo *et al.* in 1959.[24] Ferguson *et al.* demonstrated that either the combination of acid and pepsin or bile on its own is capable of causing esophagitis. However, when the lower esophagus is perfused with acid on its own, no effect is seen. In the study by Redo *et al.*,

canine esophagi were perfused with different types of refluxate over a seven-and-a-half-hour period. The refluxates included gastric juice, hydrochloric acid, pepsin, and bile, which were collected from a patient with a duodenal fistula. The results were consistent with those obtained by Ferguson *et al.*, suggesting that acid–pepsin activity is responsible for ulceration of the esophagus. However, in this study, no effect was seen with bile reflux. These results contradicted earlier observations made by Barrett regarding the destructive effects of bile. In his 1954 paper, Barrett described the severe esophagitis experienced by one patient following a total gastrectomy and esophagoduodenostomy.[25]

To further investigate the effects of reflux composition on the development of esophagitis, Levrat *et al.* devised a surgically induced reflux model in the rat.[16] This study followed on from previous work investigating reflux esophagitis in the rat following total gastrectomy.[26,27] In Levrat *et al.*'s study, six different types of anastomosis were fashioned to induce different types of reflux. These consisted of an esophagojejunostomy with different combinations of gastrectomy and pancreaticobiliary diversion. The different approaches enabled the study of gastric, biliary, and pancreatic secretions both in isolation and combination. The results suggested that bile was the key injurious factor and that gastric secretions alone had little effect. Despite key anatomical and histological differences between the murine and human esophagus, such as the presence of a keratinized squamous epithelium within the esophagus, an SCJ located within the forestomach, and the absence of esophageal submucosal glands (ESMGs),[15] this paper served to popularize the murine model and formed the basis from which several later surgical reflux models were generated.[28–35]

Once the association between the CLE and EAC became apparent, research shifted from investigating reflux esophagitis to the more clinically important metaplasia–dysplasia–carcinoma sequence. Given the complexities involved in such a disease process and its long natural time course, researchers have gone to great efforts to generate a suitable animal model. Potential advantages of animal models include the ability to adjust for the known risk factors, such as sex and obesity.[15] These models also have the ability to mount an inflammatory response, which is likely to be one of the key early steps in the pathogenesis of BE.[36] Such a model could allow investigation into each of the various stages of the malignant transformation and provide the opportunity to test both preventative and treatment strategies in a controlled fashion.[37] Unfortunately, despite many attempts over the last two to three decades, the ideal animal model to study Barrett's carcinogenesis has not been identified. This is largely due to animals rarely developing a natural BE phenotype.[15] In fact, there have only been three reported cases of animals developing spontaneous BE, two of which were in dogs[38,39] and one in a baboon.[40] Of the two cases reported in dogs, one also progressed to EAC.[38] Despite both the dog and baboon developing BE spontaneously, they failed to become popular as preclinical models because they are resource intensive and can take up to 30 months to develop BE[41] and 60 months to develop EAC.[15]

Despite its limitations, the bulk of the research has been conducted using the surgically induced reflux murine model to determine if both BE and EAC will develop under augmented conditions. In early studies, the added effect of carcinogen administration was tested in combination with the surgical induction of reflux.[19,42–44] The results from these studies revealed that reflux on its own could induce esophagitis, metaplasia, and cancer formation. However, the rates increased with carcinogen exposure. Clark *et al.*[19] reported that esophagitis occurred in 97%, metaplasia in 10%, dysplasia in 8%, and cancer in 3% of the cases. However, unlike humans, the cancers were squamous cell carcinomas and not ACs. When combined with carcinogen exposure, these rates increased to 99% for esophagitis, 13% for metaplasia, and 57% for carcinoma. In this setting, both squamous cell carcinomas and ACs developed at a ratio of approximately two to one. The requirement for carcinogen exposure to produce ACs of the distal esophagus was challenged in later studies.[45–47] Fein *et al.* reported AC formation without the need for carcinogen.[47] In this series, all animals exposed to duodenal reflux demonstrated evidence of severe esophagitis, 87% had evidence of a columnar lined distal esophagus, and 48% had AC of the anastomotic site. Goldstein *et al.* also reported AC formation in the absence of carcinogen. In their study, a higher rate of AC formation (73%) was achieved simply by correcting the iron deficiency anemia that occurs following the surgical induction of reflux.[46] This rate was not affected by the

administration of carcinogen, which promoted the formation of squamous cell carcinomas instead.

To extrapolate the results from animal models to the human disease process, it is essential that models undergo rigorous validation.[30] Unfortunately, the results from multiple studies aiming to validate the surgically induced reflux model have varied, leaving two fundamental issues unresolved. The first issue is whether the CLE seen within the model is truly metaplastic or simply is the migration of epithelial cells from below the anastomosis. The research supporting the metaplasia hypothesis has provided evidence that the CLE within the model shares similar morphology, mucin profile, and markers of differentiation (CK7, CK20, Das-1, villin, and pS2/TFF1) to BE.[48] Further studies have also been performed comparing the trefoil factor (TFF) gene expression profile between the CLE and jejunum distal to the anastomosis, as TFF has previously been validated as a marker capable of discriminating between BE and small intestine.[49] The results revealed a statistically significant higher expression of TFF-1 and TFF-2 within the CLE compared with that in the jejunum.[34] Gronnier *et al.* later confirmed these results.[30] However, they also identified Brunner's glands within the columnar lined esophageal segment. Because these glands normally reside within the submucosa of the first part of the duodenum, this raised the possibility that duodenal tissue may have been mechanically introduced into the distal esophagus, suggesting that both mechanisms may be occurring.[30] Buskens *et al.* also suggested that the ectopic glandular tissue could be implanted into the esophageal submucosa following an anastomosis, leading to AC formation.[37]

The second unresolved issue is whether the ACs that develop within the model are representative of those seen in humans. With respect to the histology and invasive potential of these tumors, most studies have reported the development of well-differentiated mucinous tumors at the level of the anastomosis.[35,37,50] Microscopically, these tumors appear to originate from the submucosa and extend to the external surface, lacking any mucosal involvement. They also exhibit a benign phenotype with no evidence of either local or distant dissemination.[37,50] This phenotype is in vast contrast to most human ACs, which display varying degrees of differentiation, arise from the mucosa, and frequently metastasize.[48] In contrast to these findings, Su *et al.* reported that 12 out of 14 cases of the EAC in their series demonstrated evidence of invasion into muscle, adventitia, and adjacent organs, although these findings were not readily apparent in the published images.[48] Gronnier *et al.* also described the presence of distant lung and liver metastases from their series in previously unreported data detailed in a letter to the editor.[51] In an attempt to validate these tumors at the molecular level, Su *et al.* demonstrated that the immunohistochemical expression of tumor markers p53 and COX2 within the reflux-induced ACs was comparable to that of human controls.[48] In contrast, Buskens *et al.* reported that p53 immunohistochemistry was not associated with malignant transformation within the model.[37]

Transgenic models

Although the exact mechanisms responsible for the development of BE and its subsequent progression to EAC remain unknown, it is likely that the disease involves a complex interplay between molecular and genetic events, cellular interactions, and environmental exposures. Given these complexities, numerous genes and signaling pathways have been implicated in its pathogenesis. Examples include genes involved in intestinal differentiation, such as the homeobox genes CDX1 and CDX2, and signaling pathways involved in both esophageal embryogenesis and intestinal development, including bone morphogenetic protein 4, sonic hedgehog (Shh), Notch, and WNT.[18,52,53] With the advent of the genetically engineered mouse models, a unique opportunity was presented to test the functional effect of individual genetic alterations in a controlled setting.

Unfortunately, despite initial optimism, genetically engineered mouse models still have significant limitations. First, these models still possess all the same limitations of mouse models that have previously been discussed. Second, the anticipated phenotype is not always achieved.[54] This is especially relevant for complex disease processes, such as Barrett's carcinogenesis, where multiple factors are involved in disease pathogenesis. In this instance, the addition of reflux may be required to generate the desired phenotype, as demonstrated by Fein *et al.*[55] Both factors make it difficult to interpret the results and relate them to the human disease process.

Despite these shortcomings, several key studies have attempted to investigate the fundamental questions related to the pathogenesis of BE using

transgenic models. Such areas include the cell of origin of BE and the role of inflammation and signaling pathways in the pathogenesis of BE.

In a study by Quante *et al.*, a transgenic mouse model was used to assess the effect of esophageal inflammation on the Barrett's carcinogenesis sequence.[17] In this model, interleukin (IL)-1β, a proinflammatory cytokine upstream of IL-6 and TNF-α, was overexpressed. This led to a Barrett's-like metaplasia at the SCJ, representative of the human disease. Through lineage tracing experiments, the authors also concluded that the metaplasia was due to the migration of $Lgr5^+$ cells from the gastric cardia.[17]

Another signaling pathway implicated in the pathogenesis of BE is the Hedgehog pathway, which drives the development of the CLE during embryogenesis.[36] To test if the reactivation of this pathway is sufficient to induce a columnar phenotype in the adult esophagus, Wang *et al.* used a conditional Shh transgenic model.[18] Following transduction, esophageal epithelial cells were cocultured with fibroblasts within an *ex-vivo* transplantable culture system. While Shh expression failed to generate an overt columnar epithelium in this model, it did lead to the expression of the columnar markers cytokeratin 8/18 and Sox9.

In a study addressing the cell of origin of BE, Wang *et al.* elected to use the p63-deficient mouse in an attempt to model the damage caused by reflux.[56] As p63 is required for the self-renewal of stem cells within stratified epithelium, these mice fail to generate stratified epithelial tissues and can only survive *in utero*. By assessing the embryonic tissue, the authors claimed that these mice generated Barrett's-like metaplasia, consistent with the human disease and that the columnar cells originate from residual embryonic cells located at the SCJ.[56] However, a criticism of this study is that the authors were simply studying a defect of embryogenesis rather than true metaplasia and that their conclusions may not be valid. More recently, however, Jiang *et al.* have challenged these findings.[57] Jiang *et al.* were the first group to identify a transitional zone at the SCJ in both humans and mice. This transitional zone is characterized by basal cells that express both squamous (p63, KRT5) and columnar (KRT7) markers and suprabasal cells that only express columnar markers. Lineage tracing confirmed that these KRT7 positive suprabasal cells originated from the basal layer of the transitional epithelium. Using a mouse model that was genetically engineered to express the intestinal transcription factor CDX2, this transitional zone was shown to expand. This led to a gradual decrease in squamous markers and an increase in columnar markers, typical of the human disease process.

Genetically engineered mouse models have also been combined with surgically induced reflux models in an attempt to investigate the role of both candidate genes and environmental exposures within a controlled system. However, it was precedent on the successful generation of the reflux model within the mouse. The first report of such a model was in 1999 by Fein *et al.*[55] In this study, a total gastrectomy was performed in conjunction with an esophagojejunostomy on the wild type, p53 gene knockout or APC-mutated mice. The results revealed that both p53 loss and APC-mutation were associated with the formation of a CLE, whereas only p53 loss was associated with progression to AC. Xu *et al.* later conducted further work assessing the feasibility of the surgically induced reflux model in mice.[58] In that study, the authors reported an extremely low operative mortality rate of only 7.5%. Consistent with earlier studies conducted in rats, both CLEs and carcinomas were evident. The carcinomas were predominantly either squamous or adenosquamous, and their rate of formation increased significantly with additional carcinogen administration. Raggi *et al.* also conducted similar work assessing the suitability of the mouse model.[33] However, they reported a much higher incidence of AC formation without the need for carcinogen. Given the steep learning curve and difficulties associated with operating on small animals,[33] an alternative technique has been developed that employs micromagnets to induce fistula formation.[59]

In vitro models

In vitro models are tools in which cells are cultured and studied outside of their native environment. To study BE, cells are typically derived from either the normal esophagus or regions of BE. However, as cells derived from freshly digested tissue tend to have a finite life span, the majority of research has focused on cells that have been immortalized. The successful culture of cells also requires the establishment of an artificial environment that attempts to recreate the *in vivo* conditions. Examples include

the simple two-dimensional culture of cells on plastic to more complex coculture systems that recreate a three-dimensional environment. More recently, organoid models have gained popularity in the field of Barrett's carcinogenesis.

Cell lines

In addition to established cancer cell lines, a number of immortalized epithelial cell lines have been generated from both normal esophageal tissue and BE, creating the potential to study multiple stages of the metaplasia-carcinoma sequence in the *in vitro* setting. The first such cell line, HET-1A, was developed in 1991.[60] In this study, normal esophageal tissue was collected at autopsy and cultured under serum-free conditions using an explant technique. Epithelial cells were then immortalized following transfection with viral genes (simian virus 40 large T-antigen).[60] An alternative technique for cell immortalization is via the expression of hTERT, the catalytic subunit of telomerase.[61] hTERT acts to maintain the lengths of the telomeres, which are protective structures at the end of chromosomes. Under normal conditions, telomeres undergo shortening with each cell division and, once a critical length is reached, trigger a permanent cell cycle arrest.[61] Using this technique, numerous normal esophageal and Barrett's cell lines have been created.[15,61] As an extension of the simple *in vitro* culture of established cell lines, numerous studies have augmented the culture conditions through the addition of both acid and bile salts.[62,63] While there are no standardized culture conditions, the addition of acid and bile salts has been demonstrated to induce BE-specific molecules.[62]

Unfortunately, established cell lines are clonal, and the identity of their progenitor cell is unknown, limiting their use in the study of Barrett's carcinogenesis.[15] In theory, for a cell line to be of value in the study of Barrett's carcinogenesis, it needs to be derived from the Barrett's cell of origin, which could include any number of sources, such as squamous cells, ductal cells, cells from the ESMG, transitional cells, or gastric cardia cells.[4]

As the stroma has been reported to play a crucial role in the pathogenesis of BE,[18] *in vitro* assays based purely on epithelial cell lines may also be ignoring key interactions with the microenvironment. In an attempt to overcome this limitation, the more complex organotypic model was developed.

Organotypic models

The organotypic assay was originally published in 1983 and was developed to better recapitulate the *in vivo* conditions of epithelial cells. Through the use of a collagen basal layer and an air–liquid interface, it was demonstrated that cultured skin keratinocytes could form a three-dimensional polarized epithelium both *in vitro* and *in vivo* using a transplantable culture system.[64] However, it took another 20 years before a group led by Rustgi adapted this model for the study of esophageal epithelium.[65] In this study, the model was modified to include the seeding of fibroblasts within the collagen matrix before it was subsequently used to assess the effect of epidermal growth factor receptor overexpression on epithelial homeostasis. Over the course of the following decade, Rustgi authored numerous other studies based on this model, including both methodological and mechanistic studies.[12,66–70] Using this model, researchers have attempted to investigate the factors related to the pathogenesis of the columnar metaplasia seen in BE. These factors include signaling pathways and transcription factors, such as WNT and COX2,[71] CDX1 and c-MYC,[69] in addition to the role of acid exposure.[12] Although these studies reported an upregulation of intestinal markers and varying degrees of mucin production, an overt Barrett's phenotype, consisting of a single layer of columnar cells, was not achieved. The organotypic model has also been used as a tool to promote the *in vitro* differentiation of intestinal stem cells.[72] This characteristic is thought to be the result of enhanced oxygen delivery to the cells and occurs because the thin film of media used within the model provides only a minimal barrier for gas diffusion.[73]

In addition to the culture of normal keratinocytes, the organotypic model can also be used to culture cancer cells. To investigate the role of the stroma on the invasiveness of EAC, Underwood *et al.* cultured the established cancer cell lines Flo-1 and OE33 in combination with either normal or cancer-associated fibroblasts.[74] The results from this study revealed an increase in tumor cell invasion in the presence of cancer-associated fibroblasts, partly due to the matricellular protein periostin.

Organoid models

Organoids are complex structures that resemble their tissue of origin and are grown *in vitro* from individual stem cells.[75] Sato *et al.* first described the

Table 1. Preclinical models of Barrett's carcinogenesis

Model	Advantages	Disadvantages
In vivo		

Murine	– Cost
	– Manipulable
	  – Reflux model
	  – Transgenic model
	  – Environmental exposure
	– Ability to test the functional effect of different genes and exposures in a controlled setting
		– Fails to demonstrate a natural BE phenotype without significant manipulation
		– Key anatomic and histologic differences with respect to the human (absence of ESMG, presence of a keratinized squamous epithelium, and SCJ located in the forestomach)
		– Expected phenotype is not always achieved
		– Tumors tend to demonstrate a phenotype different from that of human tumors (benign appearance, submucosal, increased rate of ESCC, mucinous, and fail to metastasize)
		– Technically difficult to generate surgically induced reflux models

Canine	– Presence of ESMG – Reported to develop a natural BE and EAC phenotype – Can be combined with a surgically induced reflux model	– Large animal and requires significant resources – Length of time to develop BE and EAC (up to 5 years) – Unable to be genetically manipulated
In vitro		
Cell lines	– Cost – Reproducibility	– Lack other essential cellular elements (e.g., stromal and inflammatory cells) – Two dimensional – Lack heterogeneity – Typically require established or immortalized cell lines
Organotypic	– Three dimensional – Can assess the effect of cell interactions – Manipulable	– Lacks other essential cellular elements (e.g., stromal and inflammatory cells) – Unable to generate a true BE phenotype
Organoid	– Reproducible – Three dimensional – Ongoing tissue resource	– Lacks other essential cellular elements (e.g., stromal and inflammatory cells) – Unable to culture human squamous organoids

ESMG, esophageal submucosal gland; SCJ, squamocolumnar junction; BE, Barrett's esophagus; EAC, esophageal adenocarcinoma; ESCC, esophageal squamous cell carcinoma.

model in their seminal paper entitled "Long-term expansion of epithelial organoids from human colon, adenoma, AC, and Barrett's epithelium."[76] The key to the development of this model was the identification of the essential factors required for stem cell maintenance. These factors include R-spondin (WNT agonist), Noggin (BMP inhibitor), epidermal growth factor, and Matrigel to recreate the laminin-rich crypt microenvironment.[76]

The great power of this model is that it can reconstitute a complete Barrett's phenotype from individual stem cells obtained from fresh biopsies, negating the use of established cell lines for preclinical studies. As organoids provide an ongoing tissue resource, there is also great potential to establish organoid biobanks for sharing of resources among researchers and replication of results. Compared with cell lines, organoids also provide a much better model of the molecular and genetic diversity seen within the human disease. Unfortunately, while squamous organoids derived from the murine esophagus have been readily cultured using this model,[76,77] researchers have failed to develop a reproducible technique for the culture of squamous organoids derived from the human esophagus. However, encouragingly, researchers have recently optimized the generation of squamous organoids from the porcine ESMG.[78] Given the histological similarities with the human esophagus, efforts should now be made to generate squamous organoids from the human esophagus using similar techniques.

Summary

This review highlights the range of preclinical models that have been used for the study of Barrett's carcinogenesis (summarized in Table 1). It also

identifies a number of key discoveries that have been made using these model systems. While the recently developed organoid models show great promise, it is clear that the ideal model for the study of Barrett's carcinogenesis is lacking. Thus, the choice of model system needs to be tailored to the hypothesis being investigated. Researchers may even find it prudent to use multiple models when answering a research question. For example, the organoid model may be used as a screening tool to assess potential compounds before progressing to animal models and, if successful, further progressing into clinical trials. Hopefully, such an approach will lead to improved patient outcomes.

Acknowledgments

N.J.C. is supported by a Fellowship (MCRF16002) from the Department of Health and Human Services acting through the Victorian Cancer Agency.

Competing interests

The authors declare no competing interests.

References

1. Pohl, H. & H.G. Welch. 2005. The role of overdiagnosis and reclassification in the marked increase of esophageal adenocarcinoma incidence. *J. Natl. Cancer Inst.* **97:** 142–146.
2. McDonald, S.A., D. Lavery, N.A. Wright, *et al.* 2015. Barrett oesophagus: lessons on its origins from the lesion itself. *Nat. Rev. Gastroenterol. Hepatol.* **12:** 50–60.
3. Souza, R.F. & S.J. Spechler. 2018. Oesophagus: a new candidate for the progenitor cell of Barrett metaplasia. *Nat. Rev. Gastroenterol. Hepatol.* **15:** 7–8.
4. Souza, R.F. 2016. From reflux esophagitis to esophageal adenocarcinoma. *Dig. Dis.* **34:** 483–490.
5. McQuaid, K.R., L. Laine, M.B. Fennerty, *et al.* 2011. Systematic review: the role of bile acids in the pathogenesis of gastro-oesophageal reflux disease and related neoplasia. *Aliment. Pharmacol. Ther.* **34:** 146–165.
6. Maag, J.L.V., O.M. Fisher, A. Levert-Mignon, *et al.* 2017. Novel aberrations uncovered in Barrett's esophagus and esophageal adenocarcinoma using whole transcriptome sequencing. *Mol. Cancer Res.* **15:** 1558–1569.
7. Weaver, J.M., C.S. Ross-Innes, N. Shannon, *et al.* 2014. Ordering of mutations in preinvasive disease stages of esophageal carcinogenesis. *Nat. Genet.* **46:** 837–843.
8. Phillips, W.A., R.V. Lord, D.J. Nancarrow, *et al.* 2011. Barrett's esophagus. *J. Gastroenterol. Hepatol.* **26:** 639–648.
9. Cameron, G.R., P.V. Desmond, C.S. Jayasekera, *et al.* 2016. Recurrent intestinal metaplasia at the gastroesophageal junction following endoscopic eradication of dysplastic Barrett's esophagus may not be benign. *Endosc. Int. Open* **4:** E849–E858.
10. Bartel, M.J., A. Srivastava, S. Gordon, *et al.* 2018. Subsquamous intestinal metaplasia is common in treatment-naive Barrett's esophagus. *Gastrointest. Endosc.* **87:** 67–74.
11. Desai, M., S. Saligram, N. Gupta, *et al.* 2017. Efficacy and safety outcomes of multimodal endoscopic eradication therapy in Barrett's esophagus-related neoplasia: a systematic review and pooled analysis. *Gastrointest. Endosc.* **85:** 482–495.e4.
12. Kosoff, R.E., K.L. Gardiner, L.M. Merlo, *et al.* 2012. Development and characterization of an organotypic model of Barrett's esophagus. *J. Cell Physiol.* **227:** 2654–2659.
13. Krishnadath, K.K. & K.K. Wang. 2015. Molecular pathogenesis of Barrett esophagus: current evidence. *Gastroenterol. Clin. North Am.* **44:** 233–247.
14. Kapoor, H., D.K. Agrawal & S.K. Mittal. 2015. Barrett's esophagus: recent insights into pathogenesis and cellular ontogeny. *Transl. Res.* **166:** 28–40.
15. Garman, K.S., R.C. Orlando & X. Chen. 2012. Review: experimental models for Barrett's esophagus and esophageal adenocarcinoma. *Am. J. Physiol. Gastrointest. Liver Physiol.* **302:** G1231–G1243.
16. Levrat, M., R. Lambert & G. Kirshbaum. 1962. Esophagitis produced by reflux of duodenal contents in rats. *Am. J. Dig. Dis.* **7:** 564–573.
17. Quante, M., G. Bhagat, J.A. Abrams, *et al.* 2012. Bile acid and inflammation activate gastric cardia stem cells in a mouse model of Barrett-like metaplasia. *Cancer Cell* **21:** 36–51.
18. Wang, D.H., N.J. Clemons, T. Miyashita, *et al.* 2010. Aberrant epithelial–mesenchymal Hedgehog signaling characterizes Barrett's metaplasia. *Gastroenterology* **138:** 1810–1822.
19. Clark, G.W., T.C. Smyrk, S.S. Mirvish, *et al.* 1994. Effect of gastroduodenal juice and dietary fat on the development of Barrett's esophagus and esophageal neoplasia: an experimental rat model. *Ann. Surg. Oncol.* **1:** 252–261.
20. Bremner, C.G., V.P. Lynch & F.H. Ellis, Jr. 1970. Barrett's esophagus: congenital or acquired? An experimental study of esophageal mucosal regeneration in the dog. *Surgery* **68:** 209–216.
21. Gillen, P., P. Keeling, P.J. Byrne, *et al.* 1988. Experimental columnar metaplasia in the canine oesophagus. *Br. J. Surg.* **75:** 113–115.
22. Li, H., T.N. Walsh, G. O'Dowd, *et al.* 1994. Mechanisms of columnar metaplasia and squamous regeneration in experimental Barrett's esophagus. *Surgery* **115:** 176–181.
23. Ferguson, D.J., E. Sanchez-Palomera, Y. Sako, *et al.* 1950. Studies on experimental esophagitis. *Surgery* **28:** 1022–1039.
24. Redo, S.F., W.A. Barnes & A.O. De La Sierra. 1959. Perfusion of the canine esophagus with secretions of the upper gastrointestinal tract. *Ann. Surg.* **149:** 556–564.
25. Barrett, N.R. 1954. Hiatus hernia. A review of some controversial points. *Br. J. Surg.* **42:** 231–244.
26. Balfour, D.C., G.M. Higgins & K.A. Woods. 1950. A factor in neutralized human gastric juice which prolongs survival of gastrectomized rats. *Proc. Staff Meet. Mayo Clin.* **25:** 434–441.
27. Helsingen, N., Jr. 1960. Oesophagitis following total gastrectomy in rats. II. Development of oesophagitis in relation to type of reconstruction. *Acta Chirurg. Scand.* **119:** 230–245.

28. Pham, T.H., R.M. Genta, S.J. Spechler, *et al.* 2014. Development and characterization of a surgical mouse model of reflux esophagitis and Barrett's esophagus. *J. Gastrointest. Surg.* **18:** 234–240; discussion 240-241.
29. Miyashita, T., H. Tajima, F.A. Shah, *et al.* 2014. Impact of inflammation–metaplasia–adenocarcinoma sequence and inflammatory microenvironment in esophageal carcinogenesis using surgical rat models. *Ann. Surg. Oncol.* **21:** 2012–2019.
30. Gronnier, C., E. Bruyere, G. Piessen, *et al.* 2013. Operatively induced chronic reflux in rats: a suitable model for studying esophageal carcinogenesis? *Surgery* **154:** 955–967.
31. Gibson, M.K., A.H. Zaidi, J.M. Davison, *et al.* 2013. Prevention of Barrett esophagus and esophageal adenocarcinoma by smoothened inhibitor in a rat model of gastroesophageal reflux disease. *Ann. Surg.* **258:** 82–88.
32. Fujimura, T., K. Oyama, S. Sasaki, *et al.* 2011. Inflammation-related carcinogenesis and prevention in esophageal adenocarcinoma using rat duodenoesophageal reflux models. *Cancers* **3:** 3206–3224.
33. Raggi, M., R. Langer, M. Feith, *et al.* 2010. Successful evaluation of a new animal model using mice for esophageal adenocarcinoma. *Langenbecks Arch. Surg.* **395:** 347–350.
34. Oh, D.S., S.R. DeMeester, C.M. Dunst, *et al.* 2009. Validation of a rodent model of Barrett's esophagus using quantitative gene expression profiling. *Surg. Endosc.* **23:** 1346–1352.
35. Li, Y. & R.C.G. Martin, 2nd. 2007. Reflux injury of esophageal mucosa: experimental studies in animal models of esophagitis, Barrett's esophagus and esophageal adenocarcinoma. *Dis. Esophagus* **20:** 372–378.
36. Wang, D.H. & R.F. Souza. 2011. Biology of Barrett's esophagus and esophageal adenocarcinoma. *Gastrointest. Endosc. Clin. North Am.* **21:** 25–38.
37. Buskens, C.J., J.B. Hulscher, T.M. van Gulik, *et al.* 2006. Histopathologic evaluation of an animal model for Barrett's esophagus and adenocarcinoma of the distal esophagus. *J. Surg. Res.* **135:** 337–344.
38. Chambers, J.K., T. Saito, K. Fukushima, *et al.* 2017. Adenocarcinoma of Barrett's esophagus in a dog. *J. Toxicol. Pathol.* **30:** 239–243.
39. Gibson, C.J., N.M. Parry, R.M. Jakowski, *et al.* 2010. Adenomatous polyp with intestinal metaplasia of the esophagus (Barrett esophagus) in a dog. *Vet. Pathol.* **47:** 116–119.
40. Rubio, C.A., J.R. Nilsson, M. Owston & E.J. Dick, Jr. 2012. The length of the Barrett's mucosa in baboons, revisited. *Anticancer Res.* **32:** 3115–3118.
41. Kapoor, H., K.R. Lohani, T.H. Lee, *et al.* 2015. Animal models of Barrett's esophagus and esophageal adenocarcinoma—past, present, and future. *Clin. Transl. Sci.* **8:** 841–847.
42. Pera, M., A. Cardesa, J.A. Bombi, *et al.* 1989. Influence of esophagojejunostomy on the induction of adenocarcinoma of the distal esophagus in Sprague–Dawley rats by subcutaneous injection of 2,6-dimethylnitrosomorpholine. *Cancer Res.* **49:** 6803–6808.
43. Attwood, S.E., T.C. Smyrk, T.R. DeMeester, *et al.* 1992. Duodenoesophageal reflux and the development of esophageal adenocarcinoma in rats. *Surgery* **111:** 503–510.
44. Pera, M., V.F. Trastek, H.A. Carpenter, *et al.* 1993. Influence of pancreatic and biliary reflux on the development of esophageal carcinoma. *Ann. Thorac. Surg.* **55:** 1386–1392; discussion 1392–1393.
45. Miwa, K., H. Sahara, M. Segawa, *et al.* 1996. Reflux of duodenal or gastro-duodenal contents induces esophageal carcinoma in rats. *Int. J. Cancer* **67:** 269–274.
46. Goldstein, S.R., G.Y. Yang, S.K. Curtis, *et al.* 1997. Development of esophageal metaplasia and adenocarcinoma in a rat surgical model without the use of a carcinogen. *Carcinogenesis* **18:** 2265–2270.
47. Fein, M., J.H. Peters, P. Chandrasoma, *et al.* 1998. Duodenoesophageal reflux induces esophageal adenocarcinoma without exogenous carcinogen. *J. Gastrointest. Surg.* **2:** 260–268.
48. Su, Y., X. Chen, M. Klein, *et al.* 2004. Phenotype of columnar-lined esophagus in rats with esophagogastroduodenal anastomosis: similarity to human Barrett's esophagus. *Lab. Invest.* **84:** 753–765.
49. Warson, C., J.H. Van De Bovenkamp, A.M. Korteland-Van Male, *et al.* 2002. Barrett's esophagus is characterized by expression of gastric-type mucins (MUC5AC, MUC6) and TFF peptides (TFF1 and TFF2), but the risk of carcinoma development may be indicated by the intestinal-type mucin, MUC2. *Hum. Pathol.* **33:** 660–668.
50. Oberg, S., R.V. Lord, J.H. Peters, *et al.* 2000. Is adenocarcinoma following esophagoduodenostomy without carcinogen in the rat reflux-induced? *J. Surg. Res.* **91:** 111–117.
51. Gronnier, C., G. Piessen, E. Leteurtre, *et al.* 2015. Suitability of surgically induced chronic reflux in rats for studying esophageal carcinogenesis. *Ann. Surg.* **261:** e140–e141.
52. Clemons, N.J. 2014. Advances in understanding the pathogenesis of Barrett's esophagus. *Discov. Med.* **17:** 7–14.
53. Milano, F., J.W. van Baal, N.S. Buttar, *et al.* 2007. Bone morphogenetic protein 4 expressed in esophagitis induces a columnar phenotype in esophageal squamous cells. *Gastroenterology* **132:** 2412–2421.
54. Lin, J.H. 2008. Applications and limitations of genetically modified mouse models in drug discovery and development. *Curr. Drug Metab.* **9:** 419–438.
55. Fein, M., J.H. Peters, N. Baril, *et al.* 1999. Loss of function of Trp53, but not Apc, leads to the development of esophageal adenocarcinoma in mice with jejunoesophageal reflux. *J. Surg. Res.* **83:** 48–55.
56. Wang, X., H. Ouyang, Y. Yamamoto, *et al.* 2011. Residual embryonic cells as precursors of a Barrett's-like metaplasia. *Cell* **145:** 1023–1035.
57. Jiang, M., H. Li, Y. Zhang, *et al.* 2017. Transitional basal cells at the squamous–columnar junction generate Barrett's oesophagus. *Nature* **550:** 529–533.
58. Xu, X., J. LoCicero, 3rd, E. Macri, *et al.* 2000. Barrett's esophagus and associated adenocarcinoma in a mouse surgical model. *J. Surg. Res.* **88:** 120–124.
59. DeMars, C.J. & N. Buttar. 2011. Novel *in-vivo* models of reflux injury and Barrett's esophagus. *Gastroenterology* **140:** S–75.
60. Stoner, G.D., M.E. Kaighn, R.R. Reddel, *et al.* 1991. Establishment and characterization of SV40 T-antigen immortalized human esophageal epithelial cells. *Cancer Res.* **51:** 365–371.
61. Harada, H., H. Nakagawa, K. Oyama, *et al.* 2003. Telomerase induces immortalization of human esophageal keratinocytes without p16INK4a inactivation. *Mol. Cancer Res.* **1:** 729–738.

62. Bus, P., P.D. Siersema & J.W. van Baal. 2012. Cell culture models for studying the development of Barrett's esophagus: a systematic review. *Cell. Oncol.* **35:** 149–161.
63. Bajpai, M., J. Liu, X. Geng, *et al.* 2008. Repeated exposure to acid and bile selectively induces colonic phenotype expression in a heterogeneous Barrett's epithelial cell line. *Lab. Invest.* **88:** 643–651.
64. Fusenig, N.E., D. Breitkreutz, R.T. Dzarlieva, *et al.* 1983. Growth and differentiation characteristics of transformed keratinocytes from mouse and human skin *in vitro* and *in vivo*. *J. Invest. Dermatol.* **81:** 168s–175s.
65. Andl, C.D., T. Mizushima, H. Nakagawa, *et al.* 2003. Epidermal growth factor receptor mediates increased cell proliferation, migration, and aggregation in esophageal keratinocytes *in vitro* and *in vivo*. *J. Biol. Chem.* **278:** 1824–1830.
66. Okawa, T., C.Z. Michaylira, J. Kalabis, *et al.* 2007. The functional interplay between EGFR overexpression, hTERT activation, and p53 mutation in esophageal epithelial cells with activation of stromal fibroblasts induces tumor development, invasion, and differentiation. *Genes Dev.* **21:** 2788–2803.
67. Oyama, K., T. Okawa, H. Nakagawa, *et al.* 2007. AKT induces senescence in primary esophageal epithelial cells but is permissive for differentiation as revealed in organotypic culture. *Oncogene* **26:** 2353–2364.
68. Kalabis, J., K. Oyama, T. Okawa, *et al.* 2008. A subpopulation of mouse esophageal basal cells has properties of stem cells with the capacity for self-renewal and lineage specification. *J. Clin. Invest.* **118:** 3860–3869.
69. Stairs, D.B., H. Nakagawa, A. Klein-Szanto, *et al.* 2008. Cdx1 and c-Myc foster the initiation of transdifferentiation of the normal esophageal squamous epithelium toward Barrett's esophagus. *PLoS One* **3:** e3534.
70. Kalabis, J., G.S. Wong, M.E. Vega, *et al.* 2012. Isolation and characterization of mouse and human esophageal epithelial cells in 3D organotypic culture. *Nat. Protoc.* **7:** 235–246.
71. Kong, J., M.A. Crissey, D.B. Stairs, *et al.* 2011. Cox2 and β-catenin/T-cell factor signaling intestinalize human esophageal keratinocytes when cultured under organotypic conditions. *Neoplasia* **13:** 792–805.
72. Wang, X., Y. Yamamoto, L.H. Wilson, *et al.* 2015. Cloning and variation of ground state intestinal stem cells. *Nature* **522:** 173–178.
73. Nossol, C., A.K. Diesing, N. Walk, *et al.* 2011. Air–liquid interface cultures enhance the oxygen supply and trigger the structural and functional differentiation of intestinal porcine epithelial cells (IPEC). *Histochem. Cell Biol.* **136:** 103–115.
74. Underwood, T.J., A.L. Hayden, M. Derouet, *et al.* 2015. Cancer-associated fibroblasts predict poor outcome and promote periostin-dependent invasion in oesophageal adenocarcinoma. *J. Pathol.* **235:** 466–477.
75. Sato, T. & H. Clevers. 2013. Growing self-organizing mini-guts from a single intestinal stem cell: mechanism and applications. *Science* **340:** 1190–1194.
76. Sato, T., D.E. Stange, M. Ferrante, *et al.* 2011. Long-term expansion of epithelial organoids from human colon, adenoma, adenocarcinoma, and Barrett's epithelium. *Gastroenterology* **141:** 1762–1772.
77. DeWard, A.D., J. Cramer & E. Lagasse. 2014. Cellular heterogeneity in the mouse esophagus implicates the presence of a nonquiescent epithelial stem cell population. *Cell Rep.* **9:** 701–711.
78. von Furstenberg, R.J., J. Li, C. Stolarchuk, *et al.* 2017. Porcine esophageal submucosal gland culture model shows capacity for proliferation and differentiation. *Cell. Mol. Gastroenterol. Hepatol.* **4:** 385–404.

In summary, OAC is devastating malignancy and is associated with a significant health burden. Whilst some progress has been made over recent years in regard to improving patient outcomes, the survival rates are still poor. It is clear that a greater understanding of the factors responsible for the both initiation of BO and its progression to OAC are required for continued improvements to be made. However, a key barrier to research has been the paucity of well-validated preclinical models that recapitulate the human disease process. The main aim of this thesis is to both develop and validate additional preclinical models for the study of Barrett's carcinogenesis, in the hope that this will enable a greater understanding of disease biology and lead to improved treatment options. Central to this is the optimisation of the PDTX model, a model that is used extensively in cancer research, as well as exploring many of the potential applications the PDTX model offers.

Chapter 2 Materials and methods

2.1 Materials

2.1.1 Mice

Severe combined immunodeficiency (SCID), Non-obese diabetic / severe combined immunodeficiency (NOD SCID) and NOD/SCID interleukin-2 receptor gamma chain knockout (NSG) mice were all used for the primary establishment of PDTX. Only NSG mice were used for cell injection xenografts. Mice were obtained from either the Animal Resource Centre (Canning Vale, Western Australia), the Walter & Eliza Hall Institute (Melbourne, Victoria) or bred internally at The Peter MacCallum Cancer Centre (Melbourne, Victoria). The Animal Experimentation Ethics Committee at The Peter MacCallum Cancer Centre approved all animal studies. Mice were housed in filter cages and received standard pellet feed and water whilst being kept on a 12-hour day / 12-hour night cycle.

2.1.2 Human Tissue

The Human Research Ethics Committee at The Peter MacCallum Cancer Centre provided the initial approval for the collection of human tissue for research purposes. Following this, both the St Vincent's Hospital in Melbourne and Cabrini Hospital in Malvern were recruited as additional tissue collection sites. This required the approval from the research ethics committee at both sites following the submission of an amended human research ethics committee (HREC) form, site specific assessment (SSA) form, patient information and consent form (PICF) and research collaborative agreement. The PICF has been included in appendix 1.

Table 2-1 General chemicals and reagents

Reagent	Description / Supplier
0.9% NaCl	Pfizer, NSW, Australia
5-fluorouracil	Hospira, Victoria, Australia
Alcian blue stain (1% w/v Alcian blue, 8GX in 3% v/v acetic acid, pH 2.5)	Sigma-Aldrich, St. Louis, MI, USA
Anaesthetic solution (normal saline with ketamine (10mg/mL) and xylazine (2mg/mL))	
Fluorescence-activated cell sorting (FACS) Blocking Buffer (PBS-/- supplemented with 2% BSA and 2% FCS)	
5% w/v skim milk, 0.1% v/v Tween 20 in Tris-buffered saline)	
Bromo-2'-deoxyuridine (BrdU)	Sigma-Aldrich
Bovine Serum Albumin (BSA)	Sigma-Aldrich
Calcein / cell dissociation solution	Thermo Fisher Scientific, Waltham, MA, USA
Chlorhexidine gluconate (2% v/v/) / isopropyl alcohol (70% v/v)	Perrigo, WA, Australia
Cisplatin	Hospira
Collagenase A	Roche Diagnostics, Mannheim, Germany
Dispase II	Roche Diagnostics
Dimethyl sulfoxide (DMSO)	Sigma-Aldrich
DNeasy Blood and Tissue Kit	Qiagen, Hilden, Germany

Reagent	Description / Supplier
Dulbecco's Modified Eagle Media (DMEM)	Life Technologies, Victoria, Australia
EpiGRO™ (basal medium supplemented with L-glutamine (6mM), EpiFactor P (0.40%), Epinephrine (1.0µM), rh TGF-a (0.5ng/mL), hydrocortisone hemisuccinate (100ng/mL), rh Insulin (5µg/mL) & Apo-Transferrin (5µg/mL))	Merck Millipore, Burlington, MA, USA
Epilife™ (Serum free basal medium with propriety supplements formulated for the culture of keratinocytes)	Invitrogen, Carlsbad, CA, USA
Foetal calf serum (FCS)	Gibco, Dublin, Ireland
Fluorodeoxyglucose [^{18}F]FDG	Provided by the Nuclear Medicine department at PMCC
Freezing solution (FCS + 10% DMSO)	
Gentamicin	Sigma-Aldrich
Hanks buffered salt solution without CaCl2 or MgCl2 (HBSS -/-)	Thermo Fisher Scientific, Waltham, MA, USA
Human intestinal stem cell (HISC) medium (DMEM/F12 supplemented with 1xB27, recombinant R-spondin (500ng/mL), recombinant Noggin (100ng/mL), recombinant bFGF (10ng/mL), recombinant EGF 20ng/mL) and nicotinamide)	Gibco ()

Reagent	Description / Supplier
Isofluorane	AbbVie, NSW, Australia
Ketamine	Parnell Laboratories, NSW, Australia
Labelling buffer (PBS-/- supplemented with 2% BSA)	
Luciferase / enhanced green fluorescent protein (eGFP) vector	Gift from the Shackleton Laboratory
Luciferin	Promega, Madison, WI, USA
Matrigel® (354234)	BD Biosciences, Franklin Lakes, NJ, USA
MCDB 153	Sigma-Aldrich
Normal buffered formalin (NBF)	Perrigo
Nuclear fast red (0.1% Nuclear fast red in 5% w/v aluminium sulphate)	
Tissue dissociation solution (HBSS supplemented with 6mg/ml Dispase II and 3 mg/ml of Collagenase A)	
OPSITE Spray	Smith & Nephew, Victoria, Australia
Penicillin	Gibco
Phosphatase Inhibitor (PhosphoSTOP)	Roche
Protease Inhibitor (Complete ULTRA)	Roche
Dulbeco's phosphate buffered solution without $CaCl_2$ or $MgCl_2$ (PBS -/-)	Gibco
PBS++ (PBS-/- supplemented with penicillin 200 U/ml & streptomycin 200 µg/ml)	
PBS+++ (PBS-/- supplemented with penicillin 12 µg/ml, gentamicin 160 µg/ml & fluconazole 600ng/ml)	

Reagent	Description / Supplier
Propidium Iodide	Thermo Fisher Scientific
Western Blot Rinsing Buffer (0.1% v/v Tween 20 in Tris-buffered saline)	
RIPA Buffer (1 mmol/L EDTA; 1% v/v NP40; 0.5% w/v sodium deoxycholate; 0.1% v/v SDS; 50 mmol/L sodium fluoride; 1 mmol/L sodium pyrophosphate in PBS)	Sigma-Aldrich
RPMI 1640	Life Technologies
Sequebrene	Sigma-Aldrich
Skim milk (5% w/v)	Fonterra, Victoria, Australia
Soybean Trypsin Inhibitor (0.5mg/ml)	Life Technologies
Streptomycin	Bayer, Leverkusen, Germany
Trypsin 0.05%	Gibco
Trypsin 0.25%-EDTA	Life Technologies
Tris-buffered saline	BDH, Poole, UK
Tween 20 (0.1% v/v)	Bio-Rad, Hercules, CA, USA
Xylazine	Bayer

Table 2-2 Antibodies used for immunohistochemical analyses

Antibody	Cat. No.	Concentration	Supplier
AE1/AE3	NCL-L	1:200	Leica Biosystems, Victoria, Australia
Anti-BrdU	347580	1:100	BD Transduction Laboratories, Franklin Lakes, NJ, USA
Anti-human mitochondrial antibody	MAB1273	1:500	Merck Millipore, Billerica, MA, USA
CD20	760-2531	0.3μg/ml	Ventana Roche, Tucson, AZ, USA
CD45	M0701	1:200	DakoCytomation, Glostrup, Denmark
CDX2	235R-16	1:200	Cell Marque, Rocklin, CA, USA
Cleaved caspase-3	9661S	1:300	Cell Signaling Technology, Danvers, MA, USA
CK5	305R-16	1:50	Cell Marque
CK7	POV-TL 12/30	1:50	DakoCytomation
CK19	RCK108	1:100	DakoCytomation
HMW	334M-85	1:200	Cell Marque
Ki67	790-4286	2μg/ml	Ventana Roche
MLH1	NCL-L	1:50	Leica Biosystems
MUC2	15334	1:50	Santa Cruz Biotech
MUC5AC	MRQ-18	1:100	Cell Marque
p40	AC13066C	1:100	Biocare Medical, Pacheco, CA, USA
p63	m7317	1:100	DakoCytomation
PMS2	760-5094	1μg/ml	Ventana Roche

Table 2-3 Antibodies used for the FACS sorting of xenograft-derived cells

Antibody	Cat. No.	Concentration	Supplier
Human EpCAM/TROP1 - Fluorescein isothiocynate (FITC)	AB9601F	1:5	R&D Systems, Minneapolis, MN, USA
Human leukocyte antigen (HLA) - FITC	BD 555552	1:5	BD Transduction Laboratories
Mouse IgG2B – FITC (EpCAM isotype control)	IC0041F	1:5	R&D Systems
Mouse IgG1 – FITC (HLA isotype control)	BD 555909	1:50	BD Transduction Laboratories

Table 2-4 Antibodies used for indirect immunofluorescence

Antibody	Origin	Dilution	Clone	Supplier
Primary				
DAPI		1:1,000	D1306	Thermo Fisher Scientific
CD44	Rabbit	1:100	157107	Abcam, Cambridge, MA, USA
CD133	Rabbit	1:100	OAAI00379	Aviva Systems Biologicals, San Diego, CA, USA
Lgr5	Rabbit	1:100	75732	Abcam
Secondary				
488 IgG (green)	Donkey	1:1000	A21206	Invitrogen, Waltham, MA, USA
594 IgG (red)	Donkey	1:1000	A21207	Invitrogen

Table 2-5 Antibodies used for the western blot analysis of xenograft-derived cells

Antibody	Origin	Clone	Supplier
Anti E-cadherin	Rabbit	EP700Y	Abcam
Anti N-cadherin	Mouse	32/N-Cadherin	BD Transduction Laboratories
Anti-GAPDH	Mouse	6C5	Abcam
Anti-Vimentin	Rabbit	R28	Cell Signaling Technology
Anti-rabbit	Swine	P0217	Dako
Anti-mouse	Goat	P0447	Dako

Table 2-6 Equipment for mice preparation and experiments

Description	Supplier
Scales	
Ear clippers	
Heat pad	
LACRI-LUBE®	Allergan, NSW, Australia
0.5mL 29-gauge insulin syringe	

Table 2-7 Equipment and surgical instruments

Category	Contents
Sterile set-up	• Sterile gloves • Tray • Gauze • Forceps • Drape
Sutures	• 3/0 vicryl on a reverse cutting needle • 4/0 vicryl rapide on a reverse cutting needle • 5/0 prolene on a reverse cutting needle
Instruments	• Needle holders • Plain or Debakey forceps • Adson forceps • Iris scissors • Baby Metzenbaum scissors • Scalpel blade holder • Scalpel blade

Table 2-8 Special equipment for tissue processing and both in vivo and in vitro cell culture

Description	Supplier
Amicon Ultra 15 (Cat. No. UFC900308)	Merck Millipore
Hat chamber culture system (Cat. No. 30268)	Renner KG, Dannstadt, Germany
McIlwain tissue chopper	Mickle laboratory Engineering, Surrey, UK
ProGrip™ mesh	Medtronic, Dublin, Ireland
T25 collagen coated cell culture flask (Cat No. 354534)	BD Transduction Laboratories
Terasaki plate	BD Transduction Laboratories

Table 2-9 Description and culture conditions of established cell lines

Cell line	Type	Media
HET-1A (Stoner, Kaighn, Reddel, Resau, Bowman et al., 1991)	Immortalised cell line derived from normal oesophageal squamous epithelium	MCDB 153
BAR-T (Jaiswal, Morales, Feagins, Gandia, Zhang et al., 2007)	Immortalised cell line derived from BO	MCDB 153
OE33 (Rockett, Larkin, Darnton, Morris, & Matthews, 1997)	Commercially available OAC cell line	DMEM supplemented with 10% FCS

2.2 Methods

2.2.1 Mechanical and enzymatic digestion of primary tumour

Primary tissue was both mechanically and enzymatically digested as previously described (Clemons, Do, Fennell, Deb, Fellowes et al., 2014). Following dissection from a surgical specimen, tumour tissue was placed in PBS^{+++} and kept on ice until further processing. Under aseptic conditions and within the confines of a cell culture hood, tumour tissue was placed on a petri dish and chopped into a slurry using a number 23 scalpel blade. The slurry was then incubated overnight in 6mg/ml of Dispase II. Following this, the suspension was centrifuged at 1,500 rpm and the pellet re-suspended in pre-warmed 0.25% trypsin-EDTA solution for 5 minutes at room temperature. The trypsin solution was then neutralised using 0.5mg/ml of soybean trypsin inhibitor and the suspension passed through a 70µm cell strainer. The filtrate was then centrifuged at 1,500 rpm and the pellet re-suspended in DMEM supplemented with 20%FCS. The cell solution was then plated and cultured at 37°C and 5% oxygen. Media was changed three times per week.

2.2.2 Positron-emission tomography Imaging

For assessment of [^{18}F]FDG positron-emission tomography (PET) avidity, mice bearing first generation xenografts were first anesthetized using isofluorane and then imaged using the Philips Mosaic small animal PET scanner, 90 minutes after receiving 14.8 MBq of [^{18}F]FDG via unilateral tail vein injection.

2.2.3 Mechanical and enzymatic digestion of patient-derived tumour xenografts

Viable xenograft tissue was digested using a modification of the Civenni technique (Civenni, Walter, Kobert, Mihic-Probst, Zipser et al., 2011). Xenografts were initially chopped into small pieces using a scalpel and then passed through a mechanical tissue chopper multiple times in order to yield a fine slurry. After processing, the slurry was collected in PBS^{++}, briefly vortexed and then centrifuged at 1,500 rpm for five minutes. Following aspiration of the supernatant, the cell slurry was then re-suspended in tissue dissociation solution at a concentration of 10ml per gram of tissue. This was then placed in a 37°C water bath for 45 minutes, with tituration every 5 minutes. After 45 minutes of enzymatic dissociation, the entire solution was centrifuged at 1,500 rpm for 5 minutes. The supernatant was then aspirated, and the cell

pellet resuspended in RPMI supplemented with 10% FCS in order to neutralize the tissue dissociation solution. After vortexing, the suspension was then passed through a 40µm cell strainer in order to yield a single cell solution.

2.2.4 Sphere formation assay

Cells were collected in Eppendorf tubes following FACS sorting. Eppendorf tubes were then centrifuged at 1500 r.p.m. for 5 minutes. Following this, the supernatant was aspirated and cell pellets resuspended in 25µL of Matrigel. The Matrigel / cell suspension was then seeded into individual wells of a 48 well plate and the Matrigel then allowed to polymerise at 37^{o}C for ten minutes. Following polymerization, 250uL of HISC media was then added to each well.

2.2.5 eGFP transduction of established cell lines

Established cell lines are lifted and split into a six-well tissue culture plate at a seeding density of 2×10^{5} cells per well. Once the cells were approximately 50% confluent, the old media was aspirated and the cells washed with PBS-/-. 500µl of eGFP/luciferase lentivirus, 250 µl of media and 0.75µl of sequebrene were then added to each well. The plate was then gently rocked to ensure an even distribution of virus and linker molecule. A spin inoculation was subsequently performed by placing the multi-well plate in a centrifuge at 2500 rpm for 30 minutes at 30^{o}C. The cells were then incubated for 12 hours before the media was changed. Following a period of passaging, the cells were lifted and filtered using a 40µm filter in order to form a single cell suspension. These cells were then sorted via FACS based on GFP expression. Matched non-transduced cells were used as an isotype control.

2.2.6 FACS sorting of both freshly isolated xenograft derived cells and cultured cells

FACS sorting of both freshly isolated xenograft cells and established xenograft derived cell lines was performed using the BD FACSAria II System. Sorting was performed based on the expression of epithelial cell adhesion molecules (EpCAM), human leucocyte antigen (HLA) and eGFP expression. Details of the antibodies used for FACS are provided in Table 2-3. Following the formation of a single cell suspension, cells were resuspended in blocking buffer and incubated for 20 minutes at 4^{o}C. A cell count was then performed, and cells resuspended in labelling buffer at a concentration of 10^{6} cells/10µl. Primary antibodies, including isotype

controls, were applied for one hour and incubated at 4°C on a rotating mixer. Cells were then washed twice with labelling buffer. Unstained cells were kept aside for calibration and viability testing using PI at a concentration of 1:200. For sorting based on eGFP expression, matched non-transduced cells were used as controls. The following table details both of the primary antibodies that were used including concentrations and isotype controls. Cells were then sorted on the basis of viability and either FITC or eGFP expression.

2.2.7 Cytospin preparation

Following FACS sorting, single cells were collected into Eppendorf tubes. Following collection, the final volume of FACS buffer was adjusted in order to yield a final concentration of 5×10^5 cells per ml. Slides were then labelled and 200µl of cell solution added to each of the cytospin chambers. Slides were then centrifuged at 250 r.p.m. for ten minutes. Cytospin preparations were then immediately fixed in acetone for ten minutes before being allowed to air dry. Slides were then stored at -30°C prior to being stained.

2.2.8 Immunohistochemical assessment

Immunohistochemical analysis was used to assess for the presence of human cells through the use of an antibody that reacts with human mitochondria. These were performed on cytospin preparations in addition to formalin-fixed paraffin-embedded (FFPE) sections of PDTX and cell injection xenografts. For FFPE samples the tissue was sectioned into 4µm slices and baked onto superfrost plus slides at 60°C for one hour. FFPE sections were then dewaxed using xylene and then rehydrated in ethanol. Antigen retrieval was then performed by boiling the slides for three minutes at a temperature of 125°C within a pressure cooker. Slides were then cooled in tap water before being blocked using the Dako peroxidase blocking system for five minutes. After washing with Tris-Buffered Saline with 0.1% Tween 20 (TBST), slides were then blocked using 10% BSA for one hour. The primary antibody was then applied and left to incubate for one hour at room temperature or overnight at 4°C. A secondary antibody, conjugated with HRP, was then applied and incubated for 45 minutes at room temperature. DAB staining was then performed, and the slides washed with water. Following antibody incubation, slides were washed three times with TBST.

Immunohistochemical (IHC) staining against the proteins CDX2, MUC5AC, AE1/AE3, HMW, p63, CK5, p40, MLH1, PMS2 and CD45 was performed by the Department of Pathology at the Peter MacCallum Cancer Centre using an automated staining machine. All IHC staining was performed in conjunction with positive and negative controls. Details of the antibodies used for IHC analyses are provided in Table 2-2.

2.2.9 Alcian blue staining

Tissue sections were stained with Alcian blue for 30 minutes at room temperature before being rinsed in distilled water for two minutes. Following this, sections were then counter stained with nuclear fast red for five minutes before being rinsed in distilled water. Sections were then dehydrated in 95% alcohol followed by two changes in absolute alcohol.

2.2.10 DNA extraction and sequencing

DNA was extracted from both FFPE and snap frozen tissue in addition to cells in culture using the DNeasy Blood and Tissue kit (QIAGEN) as per the manufacturer's protocol.

2.2.10.1 Targeted oncogene panel

Following DNA extraction, targeted sequencing across a panel of 48 known oncogenes (Table 2-10) was performed by the Department of Pathology at the Peter MacCallum Cancer Centre using the Illumina TruSeq Amplicon Cancer Panel (Illumina, San Diego, CA, USA) as previously described (Clemons, Do, et al., 2014) .

Table 2-10 Illumina TruSeq Amplicon Cancer Panel

Illumina TruSeq Amplicon Cancer Panel				
ABL1	EGFR	GNAS	MLH1	RET
AKT1	ERBB2	HNF1A	MPL	SMAD4
ALK	ERBB4	HRAS	NOTCH1	SMARCB1
APC	FBXW7	IDH1	NPM1	SMO
ATM	FGFR1	JAK2	NRAS	SRC
BRAF	FGFR2	JAK3	PDGFRA	STK11
CDH1	FGFR3	KDR	PIK3CA	TP53
CDKN2A	FLT3	KIT	PTEN	VHL
CSF1R	GNA11	KRAS	PTPN11	
CTNNB1	GNAQ	MET	RB1	

2.2.10.2 Short tandem repeat analysis

Following extraction, DNA was submitted for short tandem repeat (STR) genotyping to either the Australian Genome Research Facility using the PowerPlex 16HS System (Promega) or the Victorian Centre for Functional Genomics using the Promega GenePrint 10 System (Promega).

2.2.11 Tumorigenic assay

Established cell lines were resuspended in a 1:1 mixture of serum free media and Matrigel at a concentration of 5×10^6 cells per 100µl. After being anaesthetized with isoflurane, NOD-SCID IL-2Rg^{KO} (NSG) mice were then injected subcutaneously in the flank region with 5×10^6 cells. Mice were then closely monitored for tumor formation and culled according to guidelines once tumors reached the ethical limit of 1500 mm^3, as calculated by the formula (length × $width^2$)/2, or at any sign of discomfort or stress.

2.2.12 Determining the tumour initiating cell frequency in the oesophageal PDTX model through the use of an extreme limiting dilution assay

In order to determine the frequency of TIC within the PDTX model, an extreme limiting dilution assay (ELDA) was performed. This involved performing a series of tumorigenic assays consisting of differing number of cells per injection, ranging from 5×10^6 to single cells. Cell numbers per injection were established via serial dilution. However, for single cell injections, cells were collected via FACS, having been sorted based on EpCAM, into individual wells of a Terasaki plate. Individual cells were then resuspended in 100µl of serum free media and Matrigel in a 1:1 ratio. The cell suspension was then pipetted into a 29-gauge insulin syringe and kept on ice until subcutaneously injected into the flank of an NSG mouse. Mice were then closely monitored for tumor formation as previously described in section 2.2.11. Once tumours were established, a calculation of TIC frequency was performed using ELDA online calculator provided by the Walter and Eliza Hall Institute of Medical Research, Melbourne (http://bioinf.wehi.edu.au/software/elda/).

2.2.13 Assessment of metastatic burden

Mice harbouring cell injection xenografts formed by eGFP/luciferase-transduced cells were imaged using the Xenogen IVIS 100 Imaging System (Caliper Life Science, Hopkinton, MA, USA). Prior to imaging, mice were injected subcutaneously with 100µl of luciferin (20mg/ml) and subsequently anaesthetised using isoflurane for imaging. Mice were imaged using a 60 second exposure time. For *ex vivo* imaging, harvested organs and tumours underwent a five-minute exposure.

2.2.14 Western blot analysis

Cells were plated into a 10 cm tissue culture dishes cultured overnight. Cells were then lysed at 4°C in RIPA buffer containing both phosphatase and protease inhibitors. Protein concentrations were quantified against standard curves. Equivalent amounts of protein lysates were boiled and loaded into the wells of the SDS-PAGE gel. The gel was then run at 80 V for 20 minutes followed by 120 V for 60 minutes. Proteins were then transferred to PVDF membranes. Membranes were incubated for 1 h in blocking buffer and probed overnight at 4°C with the primary antibody. Blots were washed three times in rinsing buffer for five minutes each, followed by incubation with peroxidase-conjugated secondary antibody (Dako)

for 2 h at room temperature. Proteins were visualised by ECL Plus Western blotting substrate kit (Thermo Fisher Scientific). Blots were reprobed with anti-GAPDH antibodies to assess protein loading. Table 2-5 provides a summary of the antibodies used.

2.2.15 Migration assay

For the migration assay a number of different chemoattractants were used including serum free media, media containing 10% FCS and both normal associated fibroblast (NAF) and cancer associated fibroblast (CAF) concentrated conditioned media. Fibroblast conditioned media was established by culturing either NAFs or CAFs in DMEM with 10% FCS until they were 80% confluent. Fibroblasts were then serum starved for 24 hours. The conditioned serum free media was then collected and filtered through a 0.22µm. The conditioned media was then concentrated using the Amicon Ultra 15 centrifugal filter by spinning at 3,100g for 25 minutes. In this process 15ml of conditioned media was concentrated to a final volume of 600µl. Protein levels were then measured.

Established cell lines were cultured in T75 flasks until approximately 80% confluent. Cells were then washed twice with PBS -/- before being serum starved overnight at 37°C and 5% CO_2. Cells were then lifted and resuspended in serum free media. A cell count was then performed. Migration assays were then set up using the 96 well High Throughput Screening 8µm pore size apparatus (Corning Cat. No. 3374). Well inserts were then plated with 5×10^4 cells in 50µl of serum free media. The lower reservoirs were filled with 150µl of varying chemoattractants. Cells were then incubated for 24 hours. A standard curve of cell number to relative fluorescent unit was then established as per the manufacturer's protocol. Inserts were then washed once and receiver wells twice with PBS -/-. The insert tray was then placed into a separate receiver well containing 100µl of Calcein AM/CDS solution. Plates were then incubated for one hour at 37°C. Fluorescent readings were then recorded using the POLARStar OPTIMA multi-plate reader (BMG Labtech, Ortenberg, Germany) at an excitation wavelength of 485nm and emission wavelength of 520nm.

Chapter 3 Optimising the oesophageal patient-derived tumour xenograft model

3.1 Introduction

Xenograft models have proven to be valuable tools in the field of cancer research. Traditionally, xenografts have been created from the injection of established cell lines into immunodeficient host mice. As this model can be easily manipulated, it has proven to be a powerful tool for mechanistic studies. However, it does have limitations. With respect to OAC, there are only twelve widely available, bona fide cell lines and not all of these are tumorigenic (Liu, Duong, et al., 2016). Additionally, cell injection xenografts lack both the stromal elements and heterogeneity typically associated with OAC. One model that overcomes these limitations and is currently being used quite extensively in other cancers is the PDTX model.

In the PDTX model, fresh pieces of original patient tumour, denoted as F_0, are divided into approximately 1-2mm^3 and implanted into immunocompromised mice. Typically, a heterotopic transplantation site, such as the subcutaneous space is used. However, other sites, such as the renal capsule, have also been reported (Tentler et al., 2012). Following successful engraftment, denoted as F_1, the xenografts are then harvested, divided and implanted into a further cohort of immunocompromised mice. This is known as the expansion phase and is denoted F_x (where x refers to the generation or passage number). This process of serial transplantation continues indefinitely, or until the required numbers are reached for a specific experiment (Tentler et al., 2012) (Figure 3-1).

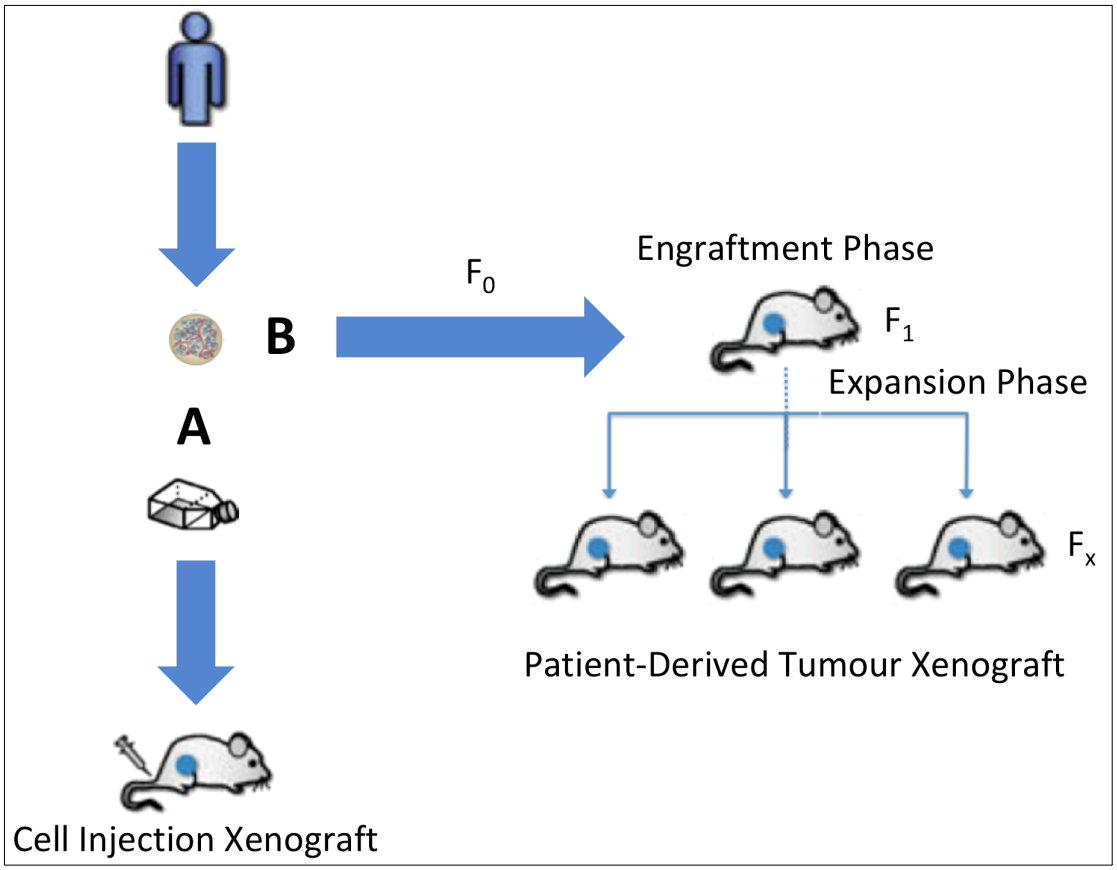

Figure 3-1 Xenograft models in cancer research

A diagrammatic representation of the two main types of xenograft models used in cancer research. On the left is the cell injection xenograft model (A). In this model, in vitro cell lines are established from patient tumours. These cell lines are then injected into an immunodeficient host mouse in order to form a xenograft. Alternatively, in the PDTX model (B), pieces of original patient tumour, rather than established cell lines, are implanted. Xenografts are then passaged multiple times in order to generate the required number of cohorts.

In order to verify that PDTX models recapitulate the human disease process they must undergo a strict process of validation (Decaudin, 2011). Validation requires a comparison between the characteristics of both the original patient tumour and the derived xenograft. Characterisation should consist of histopathological, IHC and molecular evaluation, as assessed by an expert pathologist. Genomic profiling is also recommended to ensure that genetic abnormalities present within the original tumour are also present within the preclinical model (Decaudin, 2011).

PDTXs are commonly used as preclinical tools to assess potential therapeutic responses. However, this relies on the PDTX model having a high predictive value. For this to occur, it must respond in a similar fashion to the original patient tumour. Unfortunately, there is no

way of validating the model's response to novel and untested treatments. In this situation, it needs to be assumed that the results seen in the preclinical setting will be translated to the clinical setting.

Another challenge that is especially relevant in the field of OAC involves modelling the marked genetic diversity that exists within the disease, as a significant proportion of OACs develop catastrophic chromosomal events (Nones et al., 2014). In order to overcome this limitation, repositories or 'biobanks' of PDTXs need to be established that incorporate a large range of mutations, especially those that are commonly mutated.

In addition to its role in biomarker discovery and drug target validation, well-characterized PDTX models can also be used for many other purposes. Examples include the study of metastasis, imaging assessments, angiogenesis and the identification of tumour initiating cells. Additionally, with the development of orthotopic models comes the opportunity to investigate the role of the microenvironment (Figure 3-2).

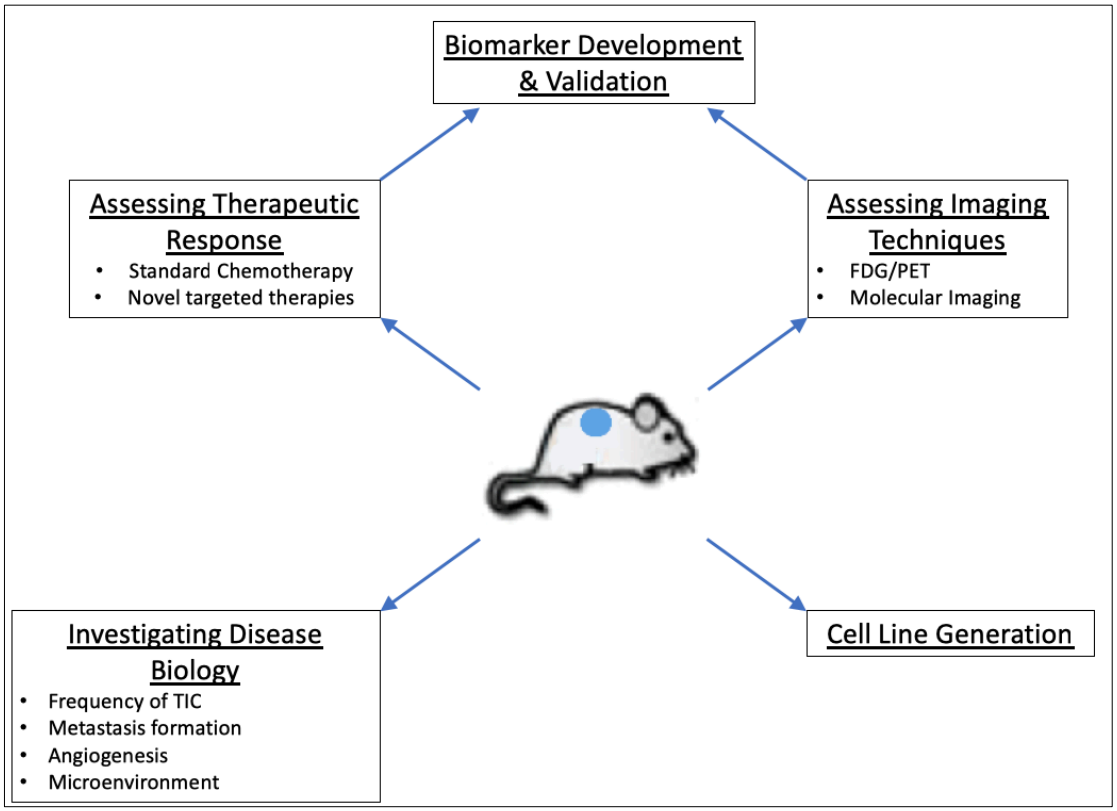

Figure 3-2 Applications of the PDTX model in cancer research

A diagrammatic representation of the multiple applications of the PDTX. One of the PDTX model's most popularized applications has been in the assessment of treatment responses and biomarker development. Other applications include the investigation of disease biology, the assessment of imaging techniques and the generation of additional cell lines.

Unfortunately, there has only been minimal success in generating PDTXs from OAC. Throughout the literature there have only been five studies that have reported the successful generation of PDTXs in OAC, with success rates ranging between 30 to 35% (J. J. Boonstra, R. van Marion, H. J. C. W. Douben, J. S. Lanchbury, K. M. Timms et al., 2012; de Both et al., 2001; Dodbiba, Teichman, Fleet, Thai, Sun et al., 2013a; El-Rifai, Harper, Cummings, Hyytinen, Frierson et al., 1998; Rumpel, Powell, & Moskaluk, 1999). This is in stark contrast to many other tumour types and serves to highlight the need for an improved PDTX model in OAC (Table 3-1). Therefore, the aim of this chapter is to improve the engraftment rate for oesophageal PDTXs.

Table 3-1 PDTX engraftment rates and cell line number across a range of different tumours.

Cancer	PDTX Engraftment Rate	No. of Commercially Available Cell Lines
PDA[a]	60%	20
Lung	95%	200
Breast	37%	84
Prostate	90%	17
Ovarian	95%	55
Colorectal	40%	60
Brain	96%	28
OAC[b]	35%	12

[a]PDA, pancreatic ductal adenocarcinoma; [b]OAC, oesophageal adenocarcinoma

("The European Collection of Authenticated Cell Cultures", 2019; Behrens, Walther, & Fichtner, 2017; Cunningham & You, 2015; Gazdar, Girard, Lockwood, Lam, & Minna, 2010; Lengyel, Burdette, Kenny, Matei, Pilrose et al., 2014; Tentler et al., 2012).

3.2 Intramuscular transplantation improves engraftment rates for oesophageal patient-derived tumor xenografts

Ann Surg Oncol
DOI 10.1245/s10434-015-4425-3

Annals of
SURGICAL ONCOLOGY
OFFICIAL JOURNAL OF THE SOCIETY OF SURGICAL ONCOLOGY

ORIGINAL ARTICLE – TRANSLATIONAL RESEARCH AND BIOMARKERS

Intramuscular Transplantation Improves Engraftment Rates for Esophageal Patient-Derived Tumor Xenografts

Matthew Read, MBBS[1,2], David Liu, MBBS, BMedSci[1,2], Cuong P. Duong, MBBS, FRACS, PhD[1,3], Carleen Cullinane, BSc(Hons), PhD[1,2], William K. Murray, MBBS, FRCPA, FRCPath[5], Christina M. Fennell, BBiomedSc(Hons)[1,2], Jake Shortt, BMedSc, MBChB, FRACP, FRCPA, PhD[2,6,7], David Westerman, MBBS, FRACP, FRCPA, FFSc[5,8], Paul Burton, MBBS, FRACS, PhD[9,10], Nicholas J. Clemons, BSc(Hons), PhD[1,2,4], and Wayne A. Phillips, BSc(Hons), PhD[1,2,3,4]

[1]Surgical Oncology Research Laboratory, Peter MacCallum Cancer Centre, Melbourne, VIC, Australia; [2]Sir Peter MacCallum Department of Oncology, University of Melbourne, Melbourne, VIC, Australia; [3]Division of Cancer Surgery, Peter MacCallum Cancer Centre, Melbourne, VIC, Australia; [4]Department of Surgery (St. Vincent's Hospital), University of Melbourne, Melbourne, VIC, Australia; [5]Department of Pathology, Peter MacCallum Cancer Centre, Melbourne, Australia; [6]School of Clinical Sciences at Monash Health, Melbourne, Australia; [7]Faculty of Medicine, Nursing & Health Sciences, Monash University, Melbourne, Australia; [8]University of Melbourne, Melbourne, Australia; [9]Monash University Centre for Obesity Research and Education, Alfred Hospital, Melbourne, Australia; [10]Cabrini Hospital, Melbourne, VIC, Australia

ABSTRACT

Background. Recently, there has been an increase in the availability of targeted molecular therapies for cancer treatment. The application of these approaches to esophageal cancer, however, has been hampered by the relative lack of appropriate models for preclinical testing. Patient-derived tumor xenograft (PDTX) models are gaining popularity for studying many cancers. Unfortunately, it has proven difficult to generate xenografts from esophageal cancer using these models. The purpose of this study was to improve the engraftment efficiency of esophageal PDTXs.

Methods. Fresh pieces of esophageal tumors obtained from endoscopic biopsies or resected specimens were collected from 23 patients. The tumors were then coated in Matrigel and transplanted in immunocompromised mice subcutaneously ($n = 6$) and/or using a novel implantation technique whereby the tumor is placed in a dorsal intramuscular pocket ($n = 18$). They are then monitored for engraftment.

Results. With the novel intramuscular technique, successful engraftment was achieved for all 18 patient tumors. Among these PDTXs, 13 recapitulated the original patient tumors with respect to degree of differentiation, molecular and genetic profiles, and chemotherapeutic response. Lymphomatous transformation was observed in the other five PDTXs. Successful engraftment was achieved for only one of six patient tumors using the classic subcutaneous approach.

Discussion. We achieved a much higher engraftment rate of PDTXs using our novel intramuscular transplant technique than has been reported in other published studies. It is hoped that this advancement will help expedite the development and testing of new therapies for esophageal cancer.

Esophageal cancer is currently the eighth most common cancer worldwide and has an extremely high case fatality rate.[1] Approximately 83 % of all cases occur in developing countries, where squamous cell carcinoma (SCC) is the main subtype.[2] In the developed world, esophageal adenocarcinoma poses the greater problem, as its incidence has

Nicholas J. Clemons and Wayne A. Phillips are co-senior authors.

Electronic supplementary material The online version of this article (doi:10.1245/s10434-015-4425-3) contains supplementary material, which is available to authorized users.

First Received: 27 November 2014

W. A. Phillips, BSc(Hons), PhD
e-mail: wayne.phillips@petermac.org

Published online: 18 February 2015

risen more than sixfold over the last four decades.[3] Currently, in the United States, only 17.5 % of all patients who present with esophageal cancer survive more than 5 years.[4] Alternative treatment strategies are needed to improve disease outcomes. Progress is being hampered by a lack of suitable preclinical models with which to study the disease and test new therapies.

One model that has shown great promise in the field of cancer research is the patient-derived tumor xenograft (PDTX), in which the patient's tumor tissue is grown and expanded in immunocompromised mice. As these models recapitulate the original patient tumors with respect to histology, molecular and genetic profiles, and therapeutic response, they are being increasingly used as preclinical models for drug target validation and biomarker identification.[5] PDTXs also have the capacity to provide a perpetual tissue bank, making them a valuable resource, particularly for esophageal cancer, where the collection of treatment-naive tissue is often limited to small endoscopic biopsies obtained prior to neoadjuvant therapy.[6] Unfortunately, there has been limited success in generating esophageal PDTXs, with success rates ranging between 30.0 and 38.5 %.[7–13]

Given the importance of the PDTX model to cancer research, refinements that lead to improvements in engraftment efficiencies are of great benefit.[14] One variable with the potential to improve engraftment efficiency is the transplantation site. Common sites for heterotopic transplantation include subcutaneous (SC) and renal subcapsular spaces.[5] We hypothesized that an intramuscular (IM) transplantation site might provide improved engraftment of PDTXs because of the well-vascularized transplant bed it provides.

MATERIALS AND METHODS

Mice

Scid, NOD *scid*, NOD-*scid* interleukin-2 (IL2) receptor gamma chain knockout (NSG), and athymic nude mice were obtained from either the Animal Resource Centre (Canning Vale, Western Australia), or the Walter & Eliza Hall Institute (Melbourne, Victoria), or they were bred internally at the Peter MacCallum Cancer Centre (Melbourne, Victoria). All mice were maintained and housed in the animal facility of the Peter MacCallum Cancer Centre. All experimental procedures involving animals were approved by the Peter MacCallum Cancer Centre Animal Experimental Ethics Committee and conducted in accordance with the National Health and Medical Research Council (NHMRC) Australian Code for the Care and Use of Animals for Scientific Purposes (8th edition, 2013).

Tissue Collection and Preparation

Patient tissue was collected from the Peter MacCallum Cancer Centre, the Cabrini Medical Centre, and other hospitals through the Victorian Cancer Biobank between March 2012 and June 2014. The collection and use of human tissue for this project was approved by the Ethics Committee of the Peter MacCallum Cancer Centre and carried out according to the NHMRC National Statement On Ethical Conduct in Human Research (2007).

After obtaining informed consent, fresh samples of either treatment-naive or posttreatment esophageal tumors were collected from patients' endoscopic biopsies or surgical resection specimens. They were placed in chilled phosphate-buffered saline (PBS) supplemented with penicillin 200 U/ml and streptomycin 200 µg/ml (PBS^{++}) and kept on ice. Samples were divided into approximately 2 mm^3 pieces, with any necrotic areas being discarded. Representative fragments were also snap frozen for DNA/RNA analysis or fixed in 10 % buffered formalin for histological evaluation. The remaining tumor pieces were placed in Matrigel (BD Biosciences, Franklin Lakes, NJ, USA) and kept on ice until implantation. All specimens were implanted within 90 min of collection.

Implantation and Monitoring

Mice were anesthetized via an intraperitoneal injection of 100 µl of anesthetic solution (ketamine 10 mg/ml and xylazine 2 mg/ml) per 10 g of body weight. The dorsum of the mouse was shaved and prepared with a 2 % (v/v) chlorhexidine gluconate/70 % (v/v) isopropyl alcohol solution. Under aseptic conditions, a 15-mm midline incision was made immediately caudal to the dorsal hump. Using blunt dissection, a skin flap was raised and the skin retracted laterally. For IM implantation, a superficial stay suture was placed in the dorsal musculature immediately caudal to the lowest rib using a 4/0 braided absorbable suture. After tenting the muscle fibers, an IM pocket was created using a combination of sharp and blunt dissection until it was just large enough to accommodate the tumor piece. The tumor piece coated in Matrigel was then placed in the IM pocket prior to suture closing (Fig. S1). For SC implantation, a tumor piece, similarly coated in Matrigel, was implanted under the raised skin flap. One or two separate transplantation sites were used per mouse. The skin was closed using 3/0 braided absorbable suture. Mice were closely monitored for tumor formation and culled according to guidelines once tumors reached the ethical limit of 1500 mm^3 as calculated by the formula (length × $width^2$)/2 or at any sign of discomfort and/or stress.

Harvesting and Processing of PDTXs

PDTXs were carefully resected to ensure that the muscle layer was dissected free. After débridement of any necrotic areas, the PDTX was divided into 2 mm^3 pieces and processed as per the original tissue. For cryopreservation, pieces were washed with PBS^{++} and then aliquoted into cryovials (up to two per cryovial) containing 1 ml of fetal calf serum containing 10 % (v/v) dimethylsulfoxide and frozen to −80 °C at approximately −1 °C/min.

Histology and Immunohistochemistry

Sections of formalin-fixed paraffin-embedded tissue from all of the original patient-derived tissues and the PDTXs were stained with hematoxylin and eosin (H&E). To confirm that the PDTXs were of human origin, immunohistochemistry was performed using an antibody against the human mitochondrial antigen, MAB1273 (1:500) (Merck Millipore, Billerica, MA, USA). CK7 (1:50) (POV-TL 12/30; DakoCytomation, Glostrup, Denmark) and CK19 (1:100) (RCK108; DakoCytomation) antibodies were used to confirm that adenocarcinomas were from the esophagus or the gastroesophageal junction.[15]

DNA Extraction and Sequencing

DNA from both the original patient sample and the PDTXs was extracted from freshly frozen pieces of tissue using the DNeasy Blood and Tissue kit (Qiagen, Hilden, Germany) as per the recommended protocol. Targeted sequencing across a panel of 48 known oncogenes was then performed using the Illumina TruSeq Amplicon Cancer Panel as previously described.[16]

Therapeutic Response

For assessment of the chemotherapeutic response, a single PDTX was divided and implanted into cohorts of up to 18 mice using the IM technique. Athymic nude mice were selected for this purpose because of the ease of tumor detection and better tolerance of the chemotherapy.[17,18] Once tumors reached a volume of 125 mm^3, the mice were randomized to receive either matched patient chemotherapy [5-fluorouracil (5FU)/cisplatin] or the vehicle (0.9 % NaCl) alone. Cisplatin (DBL) was suspended in 0.9 % (w/v) NaCl and administered at a dose of 4 mg/kg via intraperitoneal injection on a weekly basis for 3 weeks. 5FU (DBL) was suspended in 0.9 % NaCl and administered at 10 mg/kg via intraperitoneal injection on days 1 to 5 of a 14 day treatment cycle. This cycle was repeated twice. Given the rapid systemic absorption of both cisplatin and 5FU from the peritoneal cavity, the intraperitoneal route was chosen because of its ease of administration.[19,20]

RESULTS

Tumor samples from 23 patients were harvested from the esophagus, gastroesophageal junction (GEJ), or peritoneum (metastatic deposit from a primary GEJ tumor). They included both adenocarcinoma and SCC. One to four tumor pieces (mode = 2) from each patient were implanted. Samples from four patients were lost because of the premature death of the host mice during the first month (i.e., before a tumor could become established) and were excluded from further analysis. Of the remaining patients, samples implanted using the IM technique had a per-implant success rate of 65 % (24/37) and resulted in successful engraftment of at least one implant from each of the 18 patients with this method (Table 1). In comparison, the SC technique had a per-implant success rate of only 9 % (1/11) and was associated with successful engraftment ofjust one of the six (16 %) patients (Table 1).

All engrafted tissues were subjected to thorough histopathological analysis by an experienced histopathologist. All were demonstrated to be composed of human tissue, as demonstrated by staining with anti-human mitochondrial antibody (Fig. 1a). Of the 18 engrafted lines, 13 were confirmed to be of epithelial origin and to have maintained the same degree of differentiation (Fig. 1a) and expression of molecular markers (Fig. 1b) as their parent tumor. Thus, we were able to establish bona fide esophageal PDTXs from 13 of 18 patients (72 %) using the IM technique compared to just one from six patients using the SC method.

Of the five IM xenografts that failed to recapitulate their parent tumors, four were confirmed to be B cell lymphomas, and one was composed of a combination of both epithelial and lymphoid cells (Fig. S2a). These lymphomas stained strongly for Epstein-Barr virus (EBV) RNA (Fig. S2d), indicating that latent EBV may be the driver of this lymphomatous transformation. These five lymphoma lines were also reproducibly metastatic in the mice, with extranodal dissemination frequently noted in the lung, liver, and spleen (data not shown).

All of the validated esophageal PDTX lines have now been passaged up to seven times. We have also been able to reestablish four of the five esophageal PDTX lines following cryopreservation. All passages were performed in NSG mice except for the failed cryopreserved sample, which was implanted in NOD *scid* mice (Table 1).

Targeted sequencing of 48 known cancer-related genes revealed the model to be relatively stable genetically. From a single PDTX line (patient 1), the original tumor was compared to seven PDTXs across three consecutive

TABLE 1 Matched pathological features and engraftment results from implanted PDTXs

ID	Site	Type	Grade	Tissue source	Therapy prior to implantation		Technique[a]		Mouse strain	Engraftment after cryopreservation[a]
					CT	RT	IM	SC		
1	GEJ	AC	Poor	Resection	Y	N	1/4	0/2	SCID	2/2
2	GEJ	AC	Poor	Resection	Y	Y	1/2		SCID	2/2
3	GEJ	AC	Mod	Resection	Y	N		0/4	NOD SCID	
4	Esophagus	AC + NE	Mod	Biopsy	N	N	**2/2**		NSG	
5	Esophagus	AC	Mod–poor	Biopsy	N	N	1/2		NOD SCID	0/1
6	Esophagus	AC	In situ	Biopsy	N	N	1/2	0/1	NSG	
7	Esophagus	SCC	Mod	Biopsy	N	N	1/1		NSG	
8	Esophagus	AC	Mod	Biopsy	N	N	1/1		NSG	
9	Esophagus	AC	Mod	Biopsy	N	N	**1/1**[b]	0/1	NSG	
10	Esophagus	AC	Mod	Biopsy	N	N	2/2	1/2	NSG	1/1
11	Esophagus	SCC	Poor	Biopsy	N	N	2/2		NSG	
12	Esophagus	SCC	Mod	Resection	N	N	1/1		NSG	1/1
13	PM from GEJ	AC	Mod–poor	Resection	N	N	1/2		NSG	
14	Esophagus	AC	Poor	Resection	Y	N	**1/3**		NSG	
15	GEJ	AC	Mod	Biopsy	N	N	2/3		NSG	
16	Esophageal	AC	Poor	Resection	N	N	**1/2**[c]		NSG	
17	Esophageal	SCC	In situ	Biopsy	N	N	1/1	0/1	NSG	
18	Esophagus	AC	Mod	Biopsy	N	N	1/2		NSG	
19	Esophagus	AC + NE	Poor	Biopsy	Y	N	**3/4**		NSG	

Lymphomatous transformation within engrafted tumor is indicated in bold

PDTXs patient-derived tumor xenografts, *ID* patient identification number, *GEJ* gastroesophageal junction, *Mod* moderate, *PM* peritoneal metastasis, *AC* adenocarcinoma, *NE* neuroendocrine differentiation, *SCC* squamous cell carcinoma, *CT* chemotherapy, *RT* radiotherapy, *IM* intramuscular, *SC* subcutaneous, *Y* yes, *N* no, *no entry* not attempted

[a] Fractions indicate the number of successful engraftments divided by the total number of implants

[b] Transformation occurred at the second passage

[c] Mixed epithelial component

generations. Our results identified the presence of synonymous variants in five genes (*FGFR3*, *PDGFRA*, *EGFR*, *RET*, *PTEN*) and nonsynonymous variants in three genes (*HNF1A*, *TP53*, *STK11*) in the parent tumor. These were maintained in the original PDTX and subsequent passages, with the exception of one-second generation PDTX in which the *STK11* variant was not detected.

Importantly, we confirmed that the therapeutic responses observed in the patients are reproducible within the PDTX. For example, patient 11, who had a poorly differentiated SCC of the mid to lower esophagus, experienced a complete response to a combination of chemotherapy (5FU and cisplatin) and radiotherapy (50.4 Gy over 28 fractions). This complete response was mirrored in the matching PDTX (Fig. 2a). Similarly, patient 15, who underwent treatment for a moderately differentiated adenocarcinoma of the GEJ, demonstrated only a partial response to the combination of chemotherapy (5FU and cisplatin) and radiotherapy (50.4 Gy over 28 fractions), and this partial response was mirrored in the matching PDTX (Fig. 2b).

DISCUSSION

We report a methodology for improved establishment of PDTXs from esophageal tumors. Using this novel IM technique, we were able to establish esophageal PDTX lines from 13 of 18 patients. These results suggest that this IM transplantation technique is more robust than the standard SC approach for generating esophageal PDTXs. Given our early success using the IM technique and the importance placed on generating additional PDTX lines from the limited quantity of tissue available, the majority of specimens in our series were implanted using the IM technique. Hence, the numbers were too low for a direct comparison of the "take" rate between the IM and SC techniques. Nevertheless, given that the best reported engraftment rate across a range of esophageal PDTX studies is only 38.5 %,[7–13] the IM technique appears to be superior. Caution is needed when making such a comparison, however, as the small numbers mean that it is not possible to standardize for variables such as ischemia time and tumor viability.

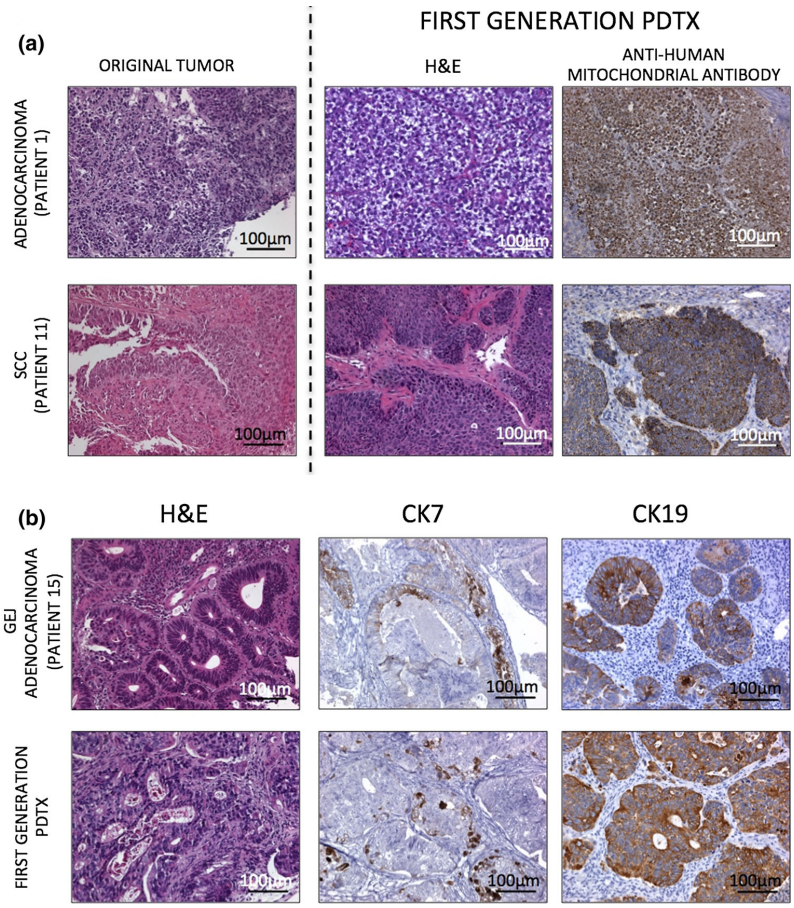

FIG. 1 Patient-derived tumor xenograft (PDTX) recapitulates the original patient tumor. **a** Hematoxylin and eosin (H & E) staining (of the original tumor and the PDTX) and immunohistochemistry using an anti-human mitochondrial antibody (PDTX only) of a poorly differentiated esophageal adenocarcinoma (patient 1, *top panels*) and an esophageal squamous cell carcinoma (patient 11, *bottom panels*). **b** H & E staining and immunohistochemistry using CK7 and CK19 antibodies in a gastroesophageal junctional adenocarcinoma (patient 15, *top panels*) and the corresponding PDTX (*bottom panels*)

We postulate that the improved "take" rate observed using the IM technique could possibly be attributed to the greater blood supply in the transplant bed. Evidence for this possibility can be extrapolated from a study of ectopic transplantation of ovarian tissue.[21] In that study, SC and IM transplantation sites were compared through a series of experiments involving xenografting normal rat ovarian tissue into nude mice. Results showed that the SC transplantation site exhibited pericyte loss and tissue damage, whereas the IM site maintained its vascularity and demonstrated tissue preservation.[21] It is also well established that there is greater autoregulatory control over blood flow in muscle tissue than in cutaneous tissue.[22] This control ensures that the temperature within the transplant bed remains relatively constant, protecting the tumor graft against hypothermic insult.

We confirmed that the esophageal PDTXs in our series are composed of human tissue and that they are representative of the original patient's tumor with respect to degree of differentiation and the molecular and genetic phenotypes. By assessing the response to standard chemotherapy, we have also produced evidence that the biology of the PDTX matches that of the original tumor. This finding highlights the potential power of well-validated PDTXs as preclinical tools for both biomarker validation and selection of second-line therapies.

The feasibility of cryopreserving esophageal PDTXs was also demonstrated in this study. This discovery has the potential to lead to significant reductions in the resources required to maintain perpetual PDTX biobanks. It also gives researchers the ability to share PDTX resources more readily with collaborators.

Researchers must also be cognizant of potential limitations when using PDTX models. Overall, 5 of the initial 18 established xenografts (26 %) underwent lymphomatous transformation. As it is not easy to distinguish poorly

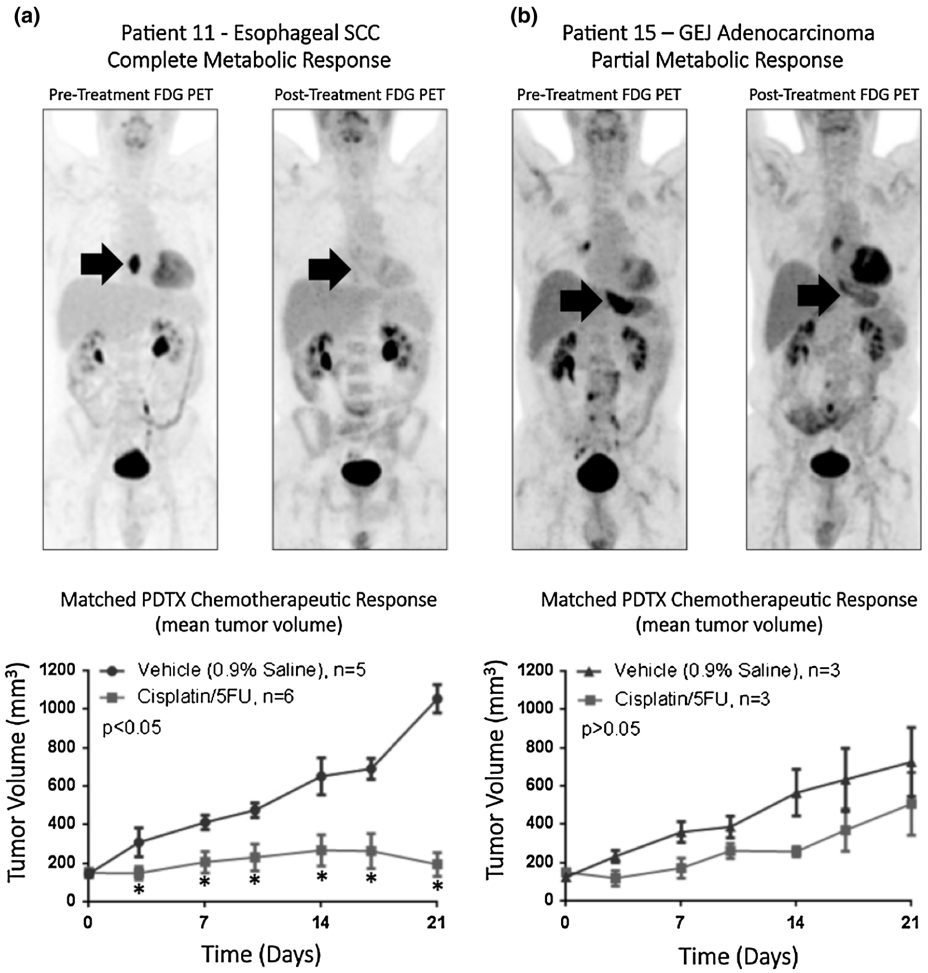

FIG. 2 Assessment of tumor biology. Pretreatment and posttreatment ^{18}F-fluorodeoxyglucose-positron emission tomography images and the growth curves for the respective PDTX with and without treatment with matched chemotherapy [cisplatin/5-fluouracil (5FU)] from representative patients who had either a complete metabolic response (**a**, patient 11) or a partial metabolic response (**b**, patient 15) to neoadjuvant treatment (cisplatin/5FU). Results are shown as the mean ± SEM. An unpaired t-test was performed on all data points using GraphPad Prism 5.0. $*p < 0.05$ for drug-treated tumors compared to vehicle-treated tumors at the same time point. *Arrows* indicate the sites of the primary tumors

differentiated carcinomas from lymphomas by histology alone, it is important that poorly differentiated PDTXs are tested for the expression of lymphoma markers. Indeed, the process of lymphomatous transformation in xenografts has only recently been reported,[7,23,24] and it can be as high as 68 %, as reported in one series.[24] It is most likely that the lymphomas arise through transformation of EBV-infected B cells that have been transplanted with the tumor tissue piece into a permissive environment. The situation is akin to the development of lymphomas in immunodeficient patients, putatively modeling an EBV-driven posttransplant lymphoproliferative disorder.[25] Given the high rate of EBV infection in the general population, it seems likely that this phenomenon has either been under-recognized or under-reported in the literature.

CONCLUSIONS

We have demonstrated that an IM transplant technique is associated with improved engraftment of esophageal

PDTXs. Given the importance of the PDTX as a preclinical tool, it is hoped that this refinement will lead to greater understanding of cancer biology and improved therapies.

ACKNOWLEDGMENT This work was supported by a NHMRC of Australia Centres for Research Excellence Grant (1040947). MR received the Thornell-Shore Memorial scholarship from the Royal Australasian College of Surgeons (RACS) and the Sir Thomas Naghten Fitzgerald scholarship from The University of Melbourne. DL received an NHMRC Australian Postgraduate Research award and Foundation for a Surgery Scholarship from the RACS. JS is supported by the Victorian Cancer Agency/Snowdome Foundation "Eva & Les Erdi Fellowship." Some tissue samples used in this Project were provided by the Victorian Cancer Biobank with appropriate ethics approval. The Victorian Cancer Biobank is supported by the Victorian Government, Australia.

DISCLOSURE None.

REFERENCES

1. Ferlay J, Shin HR, Bray F, Forman D, Mathers C, Parkin DM. Estimates of worldwide burden of cancer in 2008: GLOBOCAN 2008. *Int J Cancer.* 2010;127:2893–917.
2. Jemal A, Bray F, Center MM, Ferlay J, Ward E, Forman D. Global cancer statistics. *CA Cancer J Clin.* 2011;61:69–90.
3. Pohl H, Welch HG. The role of overdiagnosis and reclassification in the marked increase of esophageal adenocarcinoma incidence. *J Natl Cancer Inst.* 2005;97:142–6.
4. SEER Cancer Statistics Factsheets: Esophageal Cancer. Bethesda, MD: National Cancer Institute. Available: http://seer.cancer.gov/statfacts/html/esoph.html. Accessed 5 Nov 2014.
5. Tentler JJ, Tan AC, Weekes CD, et al. Patient-derived tumour xenografts as models for oncology drug development. *Nat Rev Clin Oncol.* 2012;9:338–50.
6. Boonstra JJ, Tilanus HW, Dinjens WNM. Translational research on esophageal adenocarcinoma: from cell line to clinic. *Dis Esophagus.* DOI: 10.1111/dote.12095.
7. Dodbiba L, Teichman J, Fleet A, et al. Primary esophageal and gastro-esophageal junction cancer xenograft models: clinicopathological features and engraftment. *Lab Invest.* 2013;93:397–407.
8. Rumpel CA, Powell SM, Moskaluk CA. Mapping of genetic deletions on the long arm of chromosome 4 in human esophageal adenocarcinomas. *Am J Pathol.* 1999;154:1329–34.
9. Boonstra JJ, van Marion R, Douben HJ, et al. Mapping of homozygous deletions in verified esophageal adenocarcinoma cell lines and xenografts. *Genes Chromosomes Cancer.* 2012;51:272–82.
10. De Both NJ, Wijnhoven BPL, Sleddens HFBM, Tilanus HW, Dinjens WNM. Establishment of cell lines from adenocarcinomas of the esophagus and gastric cardia growing in vivo and in vitro. *Virchows Arch.* 2001;438:451–6.
11. El-Rifai W, Harper JC, Cummings OW, Hyytinen ER, Frierson HF Jr, Knuutila S, Powell SM. Consistent genetic alterations in xenografts of proximal stomach and gastro-esophageal junction adenocarcinomas. *Cancer Res.* 1998;58:34–37.
12. Zhang J, Jiang D, Li X, et al. Establishment and characterization of esophageal squamous cell carcinoma patient-derived xenograft mouse models for preclinical drug discovery. *Lab Invest.* 2014;94:917–26.
13. Wang Z, Da Silva TG, Jin K, et al. Notch signaling drives stemness and tumorigenicity of esophageal adenocarcinoma. *Cancer Res.* 2014;74:6364–74.
14. Hidalgo M, Amant F, Biankin AV, et al. Patient-derived xenograft models: an emerging platform for translational cancer research. *Cancer Discov.* 2014;4:998–1013.
15. Taniere P, Borghi-Scoazec G, Saurin JC, et al. Cytokeratin expression in adenocarcinomas of the esophagogastric junction: a comparative study of adenocarcinomas of the distal esophagus and of the proximal stomach. *Am J Surg Pathol.* 2002;26:1213–21.
16. Clemons NJ, Do H, Fennell C, Deb S, Fellowes A, Dobrovic A, Phillips WA. Characterization of a novel tumorigenic esophageal adenocarcinoma cell line: OANC1. *Dig Dis Sci.* 2014;59:78–88.
17. Lieber J, Eicher C, Wenz J, Kirchner B, Warmann SW, Fuchs J, Armeanu-Ebinger S. The BH3 mimetic ABT-737 increases treatment efficiency of paclitaxel against hepatoblastoma. *BMC Cancer.* 2011;11:362.
18. Wunderlich M, Mizukawa B, Chou F, Sexton C, Shrestha M, Saunthararajah Y, Mulloy JC. AML cells are differentially sensitive to chemotherapy treatment in a human xenograft model. *Blood.* 2013;121:e90–7.
19. Johnsson A, Olsson C, Nygren O, Nilsson M, Seiving B, Cavallin-Stahl E. Pharmacokinetics and tissue distribution of cisplatin in nude mice: platinum levels and cisplatin-DNA adducts. *Cancer Chemother Pharmacol.* 1995;37:23–31.
20. Desgranges C, Razaka G, De Clercq E, Herdewijn P, Balzarini J, Drouillet F, Bricaud H. Effect of (E)-5-(2-bromovinyl)uracil on the catabolism and antitumor activity of 5-fluorouracil in rats and leukemic mice. *Cancer Res.* 1986;46:1094–101.
21. Israely T, Dafni H, Granot D, Nevo N, Tsafriri A, Neeman M. Vascular remodeling and angiogenesis in ectopic ovarian transplants: a crucial role of pericytes and vascular smooth muscle cells in maintenance of ovarian grafts. *Biol Reprod.* 2003;68:2055–64.
22. Braunwald E. Regulation of the circulation. *N Engl J Med.* 1974;290:1420–5.
23. John T, Yanagawa N, Kohler D, et al. Characterization of lymphomas developing in immunodeficient mice implanted with primary human non-small cell lung cancer. *J Thorac Oncol.* 2012;7:1101–8.
24. Chen K, Ahmed S, Adeyi O, Dick JE, Ghanekar A. Human solid tumor xenografts in immunodeficient mice are vulnerable to lymphomagenesis associated with Epstein-Barr virus. *PLoS One.* 2012;7:e39294.
25. Vockerodt M, Yap LF, Shannon-Lowe C, Curley H, Wei W, Vrzalikova K, Murray PG. The Epstein-Barr virus and the pathogenesis of lymphoma. *J Pathol.* DOI: 10.1002/path.4459.

3.2.1 Supplementary data

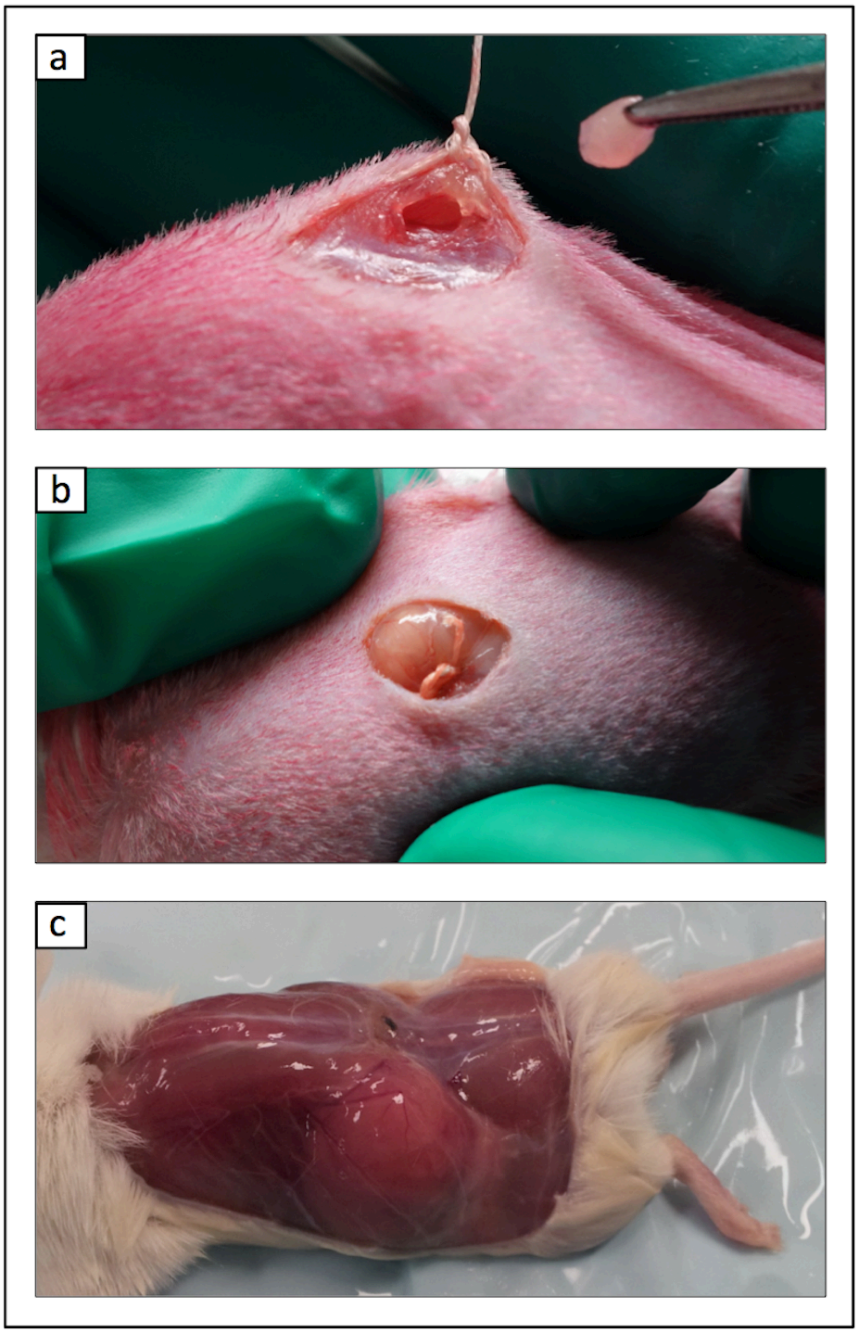

Figure 3-3 Supplementary Figure 1

Intramuscular (IM) implantation technique and PDTX formation. ***a*** *After placement of a stay suture, a small IM pocket is created on the dorsum of the mouse that is just large enough to accommodate the tumour piece.* ***b*** *After implantation, the IM pocket is sutured closed with the implant evident immediately below the outer muscle fibres.* ***c*** *Gross view of an IM PDTX at the time of harvest (Read, Liu, Duong, Cullinane, Murray et al., 2016. Reproduced with permission).*

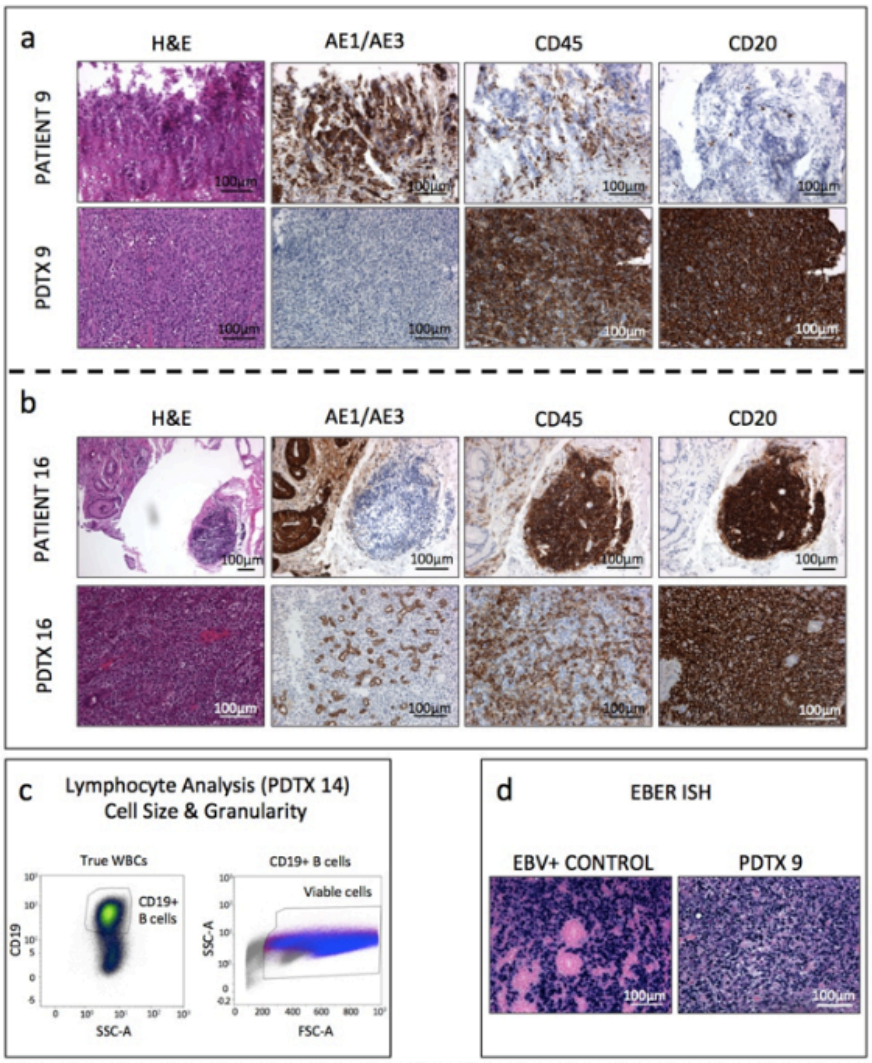

Figure 3-4 Supplementary Figure 2

*Identification and characterization of lymphomagenic transformation within a subset of established PDTXs. Immunohistochemistry using pan-cytokeratin AE1/AE3 (1:100) (NCL-L-AE1/AE3; Novocastra/Leica Microsystems, Newcastle, UK), CD20 (1:200) (M7055, DakoCytomation; Dako, Glostrup, Denmark), and CD45 (1:200) (M0701, DakoCytomation) antibodies on the original patient tumor and the corresponding PDTX. The PDTX of patient 9 (**a**) is negative for the pan-cytokeratin marker AE1/AE3 but positive for the common leukocyte antigen CD45 and the B-lymphocyte restricted antigen CD20, indicating that it is predominantly composed of human B cells. In comparison, the PDTX of patient 16 (**b**) exhibits a combination of epithelial cells (nests of AE1/AE3-positive cells) and lymphocytes. **c**Further analysis via flow cytometry was performed as previously described (Craig FE, Foon KA. Blood 2008;222:3941–67) of single cells derived from PDTX 14 and confirmed that the lymphoid cells were CD19+ B cells (left plot). The abnormal B-cell population was then gated and is depicted on the FSC vs. SSC plot in blue (right plot), indicating that these cells are also large. **d Right** In situ hybridization for the Epstein Barr virus (EBV) (blue staining) was performed on sections of formalin-fixed paraffin-embedded PDTX using the INFORM EBER Probe and ISH iVIEW Blue Detection Kit (Ventana/Roche, Tucson, AZ, USA) as per the manufacturer's protocol and counterstained with eosin (pink staining). **Left** EBV-positive nasopharyngeal carcinoma (positive control). Right Section from PDTX 9 (Read et al., 2016. Reproduced with permission).*

3.3 A detailed description of the IM transplantation technique

Tissue is obtained directly from a patient tumour (either from either a surgical resection specimen or endoscopic biopsy) in order to establish a first-generation PDTX. For passaging of PDTXs, tissue can be either freshly harvested or derived from a freshly thawed specimen. Following collection, tumour tissue is placed in normal saline and kept on ice. Within a laminar flow hood, tissue is then prepared for transplantation. Necrotic areas are debrided, and tumour tissue divided into 1 to 2 mm sized pieces (Figure 3-5). Pieces are then placed in Matrigel (50 µL/tumour piece) and keep on ice until transplantation.

Figure 3-5 Tissue pieces prior to transplant

A photo demonstrating the size of tumour pieces required for transplantation.

NSG mice are then anaesthetised via an intraperitoneal injection of anaesthetic solution (100µL/10g body weight). A small area is then shaved over the dorsum of each mouse. After being placed onto a sterile field, mice are then prepared with 2% chlorhexidine gluconate / 70% isopropyl alcohol. A small dorsal midline incision of approximately 15mm is then made using Metzembaum scissors at the level of the renal angle (immediately caudal to the dorsal hump) (Figure 3-6). Stay sutures are then placed in the skin to aid with retraction (3/0 undyed vicryl). On each side of the midline, a superficial suture is then placed into the dorsal musculature using 4/0 vicryl rapide. Muscle fibres are then tented by pulling up on the suture and a small incision made in the tented muscle fibres using Iris scissors. Using blunt dissection, a pocket is developed that is just large enough to accommodate a piece of tumour. Care is taken to remain inside the muscle and not enter the retroperitoneum. A tumour piece covered in Matrigel is then placed into the intramuscular pocket. The opening is then closed with a single interrupted suture using 4/0 vicryl rapide. The procedure is then repeated on the contralateral side if necessary. Skin is closed with 3/0 undyed vicryl using two to three interrupted sutures. Following closure, the wound is sprayed with OPSITE Spray.

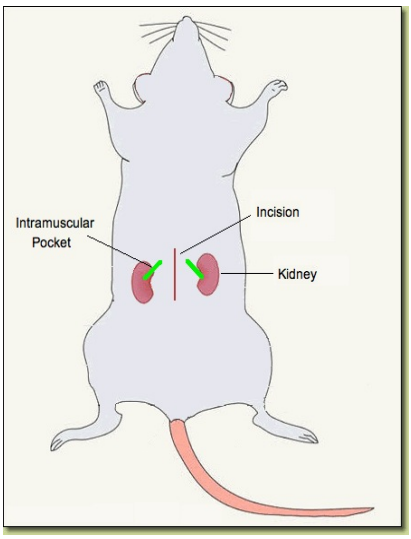

Figure 3-6 A Diagrammatic representation of the skin incision site

A 15mm dorsal skin incision is made at the level of the renal angle

Post transplantation, mice are housed on heat pads and monitored for any anaesthetic or procedure related complications. Antibiotic water (dilute stock solution to 1:100) is administered for five days post procedure. Mice are monitored weekly for signs of tumour development or distress. Care needs to be taken when assessing for tumour formation as tumours have the potential to invade the retroperitoneum (i.e. grow ventrally rather than dorsally).

Once tumour size reaches ethical limits, or mice display signs of suffering, mice are culled using CO_2 inhalation. After harvesting, PDTXs are debrided, with necrotic regions and host tissue being removed. PDTX tissue is allocated as per the following flow chart (Figure 3-7). For cryopreservation, PDTX tissue is divided into 1-2mm pieces. PDTX pieces are then placed into sterile cryo-tubes with 1mL of freezing solution (up to four PDTX pieces per tube). Cryo-tubes are then slowly cooled to -80^{o}C. before being placed in liquid nitrogen storage. Tissue is also kept for validation.

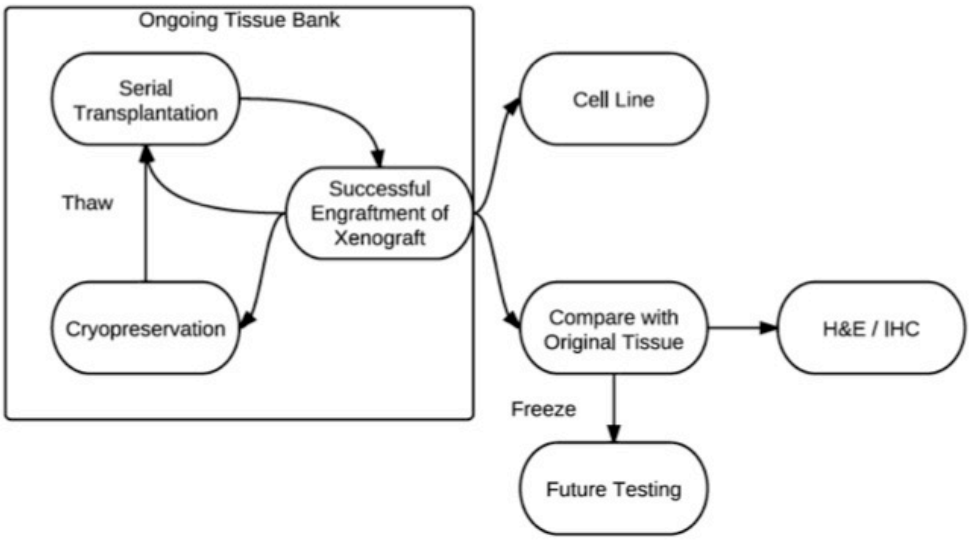

Figure 3-7 A flowchart demonstrating how successfully generated PDTXs are processed

Pieces of PDTXs can be used for serial passaging, cryopreservation and cell line generation. Tissue must also be kept for the purpose of validation. This typically involves both histopathological and IHC assessment as well as genomic analysis.

3.4 Establishment and validation of additional PDTX lines using the IM technique

Following the publication of the IM PDTX technique (Read et al., 2016), additional PDTXs were established. As a general rule, PDTX lines were maintained for at least four generations. In order to save on both costs and resources, PDTX lines were then cryopreserved and re-established when required. The details of the complete PDTX biobank are provided in the table below.

Table 3-2 The complete table of matched pathological features and engraftment results from implanted PDTXs

					Therapy prior to implantation		Technique			
ID	Site	Type	Grade	Tissue Source	CT	RT	IM	SC	Mouse Strain	Engraftment Post Cryopreservation
1	GOJ	AC	Poor	Resection	Y	N	1/4	0/2	SCID	2/2
2	GOJ	AC	Poor	Resection	Y	Y	1/2		SCID	2/2
3	GOJ	AC	Mod	Resection	Y	N		0/4	NOD SCID	
4	Oesophageal	AC + NE	Mod	Biopsy	N	N	2/2		NSG	2/2
5	Oesophageal	AC	Mod to Poor	Biopsy	N	N	1/2		NOD SCID	0/1
6	Oesophageal	AC	In-situ	Biopsy	N	N	1/2	0/1	NSG	
7	Oesophageal	SCC	Mod	Biopsy	N	N	1/1		NSG	
8	Oesophageal	AC	Mod	Biopsy	N	N	1/1		NSG	
9	Oesophageal	AC	Mod	Biopsy	N	N	1/1#	0/1	NSG	1/1
10	Oesophageal	AC	Mod	Biopsy	N	N	2/2	1/2	NSG	1/1
11	Oesophageal	SCC	Poor	Biopsy	N	N	2/2		NSG	1/1
12	Oesophageal	SCC	Mod	Resection	N	N	1/1		NSG	
13	PM from GOJ	AC	Mod to Poor	Resection	N	N	1/2		NSG	
14	Oesophageal	AC	Poor	Resection	Y	N	1/3		NSG	
15	GOJ	AC	Mod	Biopsy	N	N	2/3		NSG	
16	Oesophageal	AC	Poor	Resection	N	N	1/2*		NSG	
17	Oesophageal	SCC	In-situ	Biopsy	N	N	1/1	0/1	NSG	
18	Oesophageal	AC	Mod	Biopsy	N	N	1/2		NSG	
19	Oesophageal	AC + NE	Poor	Biopsy	Y	N	3/4		NSG	
20	**Oesophageal**	**AC**	**Poor**	**Biopsy**	**Y**	**N**	**1/2**		**NSG**	
21	**Oesophageal**	**AC**	**Mod**	**Biopsy**	**N**	**N**	**1/3**		**NSG**	
22	**Oesophageal**	**AC**	**Poor**	**Resection**	**N**	**N**	**2/2**		**NSG**	**1/1**
23	**Oesophageal**	**SCC**	**Poor**	**Biopsy**	**N**	**N**	**2/2**		**NSG**	
24	**Oesophageal**	**SCC**	**Poor**	**Biopsy**	**N**	**N**	**1/2**		**NSG**	

*Abbreviations: IM, intramuscular; SC, subcutaneous; GOJ, gastro-oesophageal junction; PM, peritoneal metastasis; AC, adenocarcinoma; NET, neuroendocrine tumour; SCC, squamous cell carcinoma; CT, chemotherapy; RT, radiotherapy; Y, yes; N, no; no entry, not attempted. Colours: Green, successful; Yellow, lymphomagenic transformation; Red, unsuccessful. * Mixed epithelial component # Transformation occurred at second passage. Entries in bold represent xenografts that were generated following the publication of the original series (Read et al., 2016).*

For the purpose of validation, a representative OAC (IS076, ID22) and oesophageal SCC (MA924, ID24) were selected from the PDTX biobank, for both H&E and IHC analysis. In order to improve the efficiency of IHC staining across multiple different PDTX lines, and to ensure uniform staining across all samples, a tissue microarray (TMA) was created. Details regarding the establishment of the PDTX TMA, including the layout of samples, is provided in Appendix 2. ID numbers correlate with those used in Table 3-2.

For the selected OAC line, IS076 (ID 22), IHC staining for the intestinal markers MUC5AC and CDX2 is shown. Results revealed the maintained degree of differentiation and expression of CDX2 and MUC5AC across both original patient tumour and derived PDTXs (Figure 3-8).

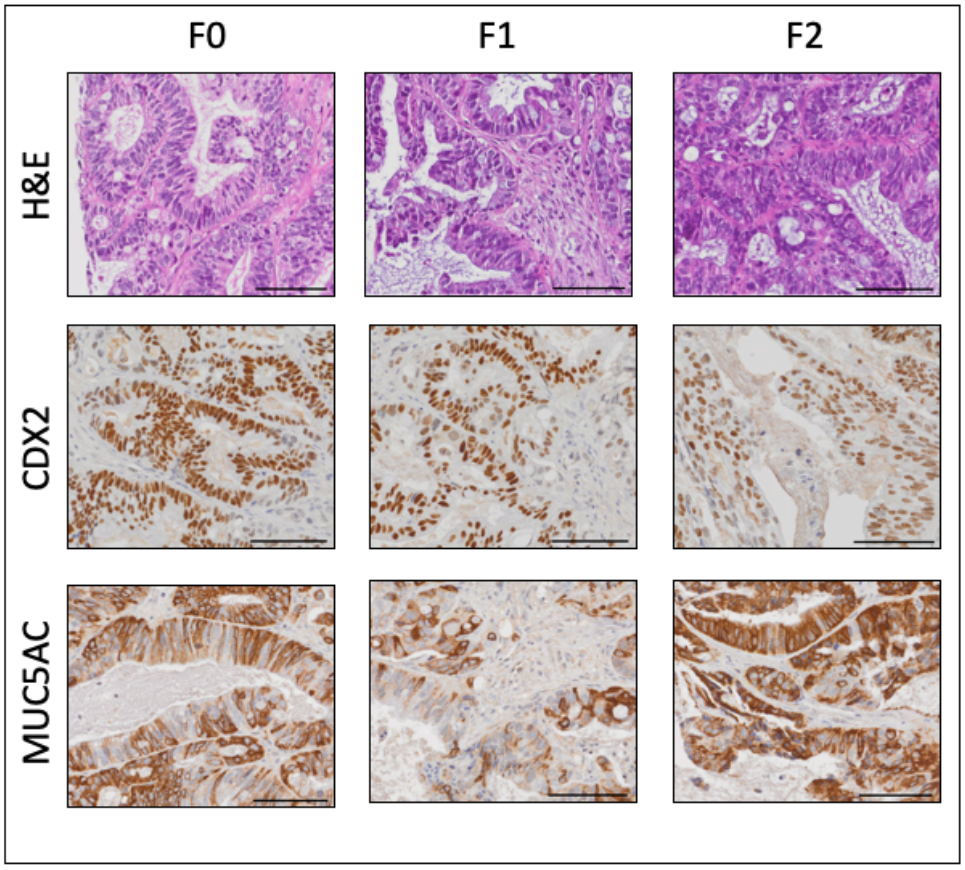

Figure 3-8 An analysis of tissue architecture and IHC profile from the original patient tumour & PDTX from the IS076 line

A comparison of tissue architecture and IHC profile across the original patient tumour and both first and second generations PDTXs for the IS076 line. IHC markers include the intestinal marker CDX2 and the upper gastrointestinal specific mucin MUC5AC. Scale bars represent 100µm.

For the selected SCC line, MA924 (ID 24), staining for the squamous markers p40, CK5, p63 and high molecular weight (HMW) cytokeratin is shown (Figure 3-9). Results revealed that the degree of differentiation and degree of keratinisation were maintained across the original patient tumour and both first and second generation PDTXs. In addition, IHC analysis confirmed the maintained expression of squamous markers P63, P40, CK5 and HMW.

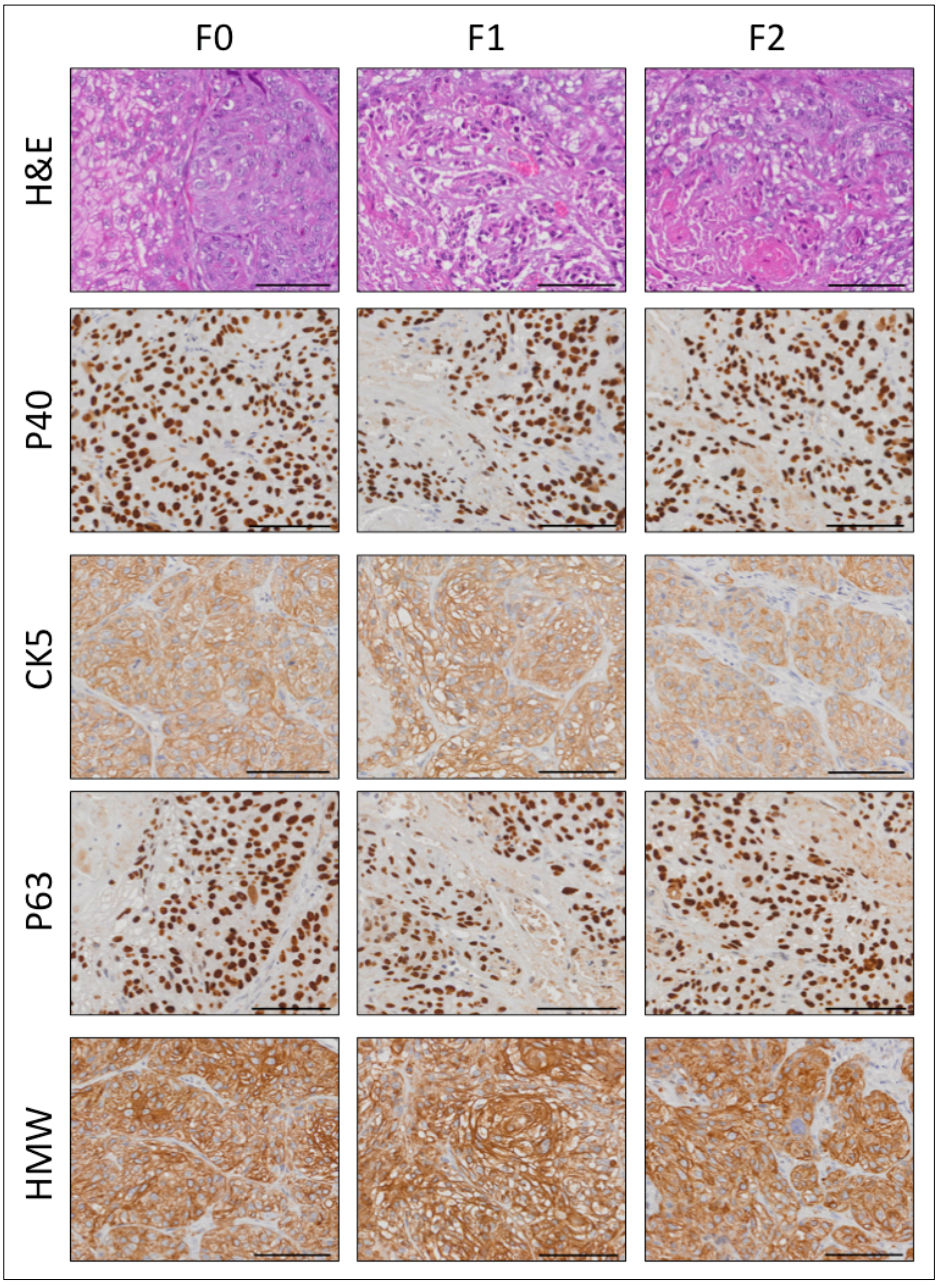

Figure 3-9 A comparison of tissue architecture and IHC profile between the original patient tumour and PDTX from the oesophageal SCC line MA924

H&E staining and a SCC specific immunohistochemistry panel consisting of p40, CK5, p63 and HMW of the original patient tumour (F0) and both first (F1) and second (F2) generations PDTXs of the oesophageal SCC line MA924. Scale bars represent 100µm.

3.5 Characterisation of PDTX lines that underwent lymphomagenic transformation

Validation of the PDTX model confirmed that approximately 20% (5/24) of engrafted xenografts had undergone lymphomagenic transformation. Such transformation was usually evident at time of necropsy, as mice typically developed splenomegaly with associated tumour formation (Figure 3-10).

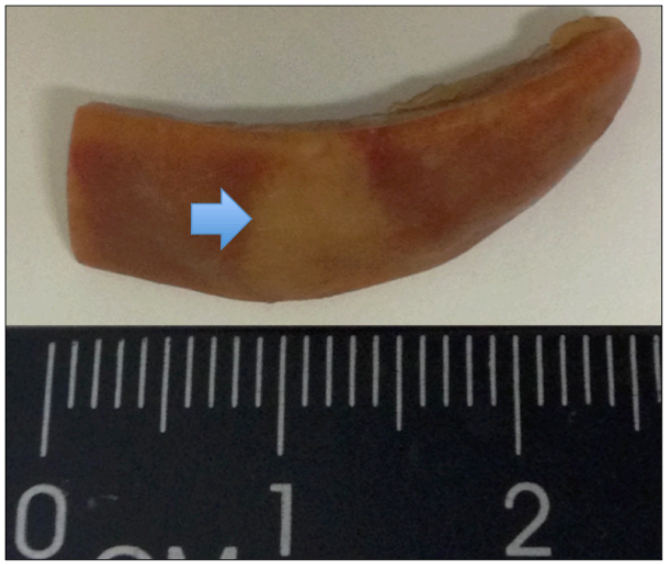

Figure 3-10 A spleen harvested from a mouse bearing an PDTX that had undergone lymphomagenic transformation

The spleen demonstrates evidence of splenomegaly. The arrow indicates the demarcation between splenic tissue and tumour.

In order to identify potential factors that may have contributed to this process, the clinical details and results of both IHC analyses and flow cytometric immunophenotyping of the relevant patients and PDTX lines were reviewed. The full clinical details of each of the patients are provided in appendix 3 (as per the previous section, ID numbers are provided which reference Table 3-2). However, an analysis of clinical details failed to identify a common causative factor, such as the subsequent development of a lymphoma in the patient or evidence of a lymphoproliferative carcinoma.

A histopathological and IHC analysis was performed on four of the PDTX lines suspected of undergoing lymphomagenic transformation, and their original patient tumours. IHC markers included the pan cytokeratin AE1/AE3, the common leukocyte antigen CD45 and the pan B-cell marker CD20 (Figure 3-11). In addition, in situ hybridisation for the Epstein Barr virus (EBV) was also performed on the PDTX line AN595 (ID9) (Figure 3-12). Analysis of original patient tumours revealed that they were all epithelial in origin, demonstrating strong staining for AE1/AE3. However, within the tumours there was also evidence of a lymphocytic infiltration, with both CD45 and CD20 positive cells being identified. Within two samples, entire aggregates were identified, consisting predominantly of CD20 positive B lymphocytes. In comparison, derived xenografts were characterised by a mass of undifferentiated tumour cells that were strongly positive for both CD45 and CD20, with very few AE1/AE3 positive epithelial cells being identified. Results from the in situ hybridization for the EBV within one of the PDTX lines revealed the virus to be present throughout the xenograft (Figure 3-12).

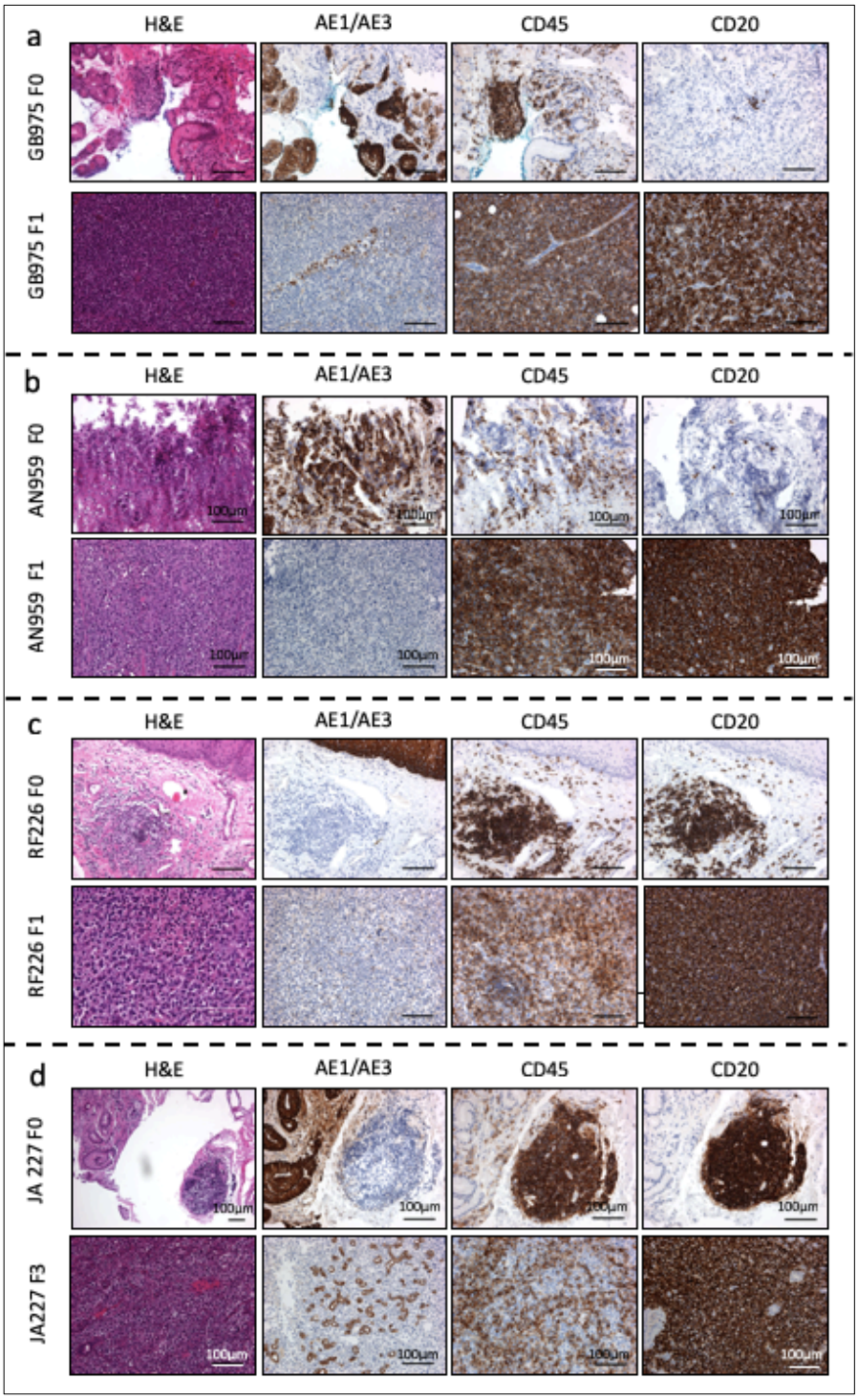

Figure 3-11 Histopathological and IHC analysis of PDTX lines suspected of undergoing lymphomagenic transformation

Hematoxylin and eosin (H&E) and IHC analysis using antibodies against AE1/AE3 (pan cytokeratin), CD45 (common leukocyte antigen) and CD20 (B-cell marker) on both the original patient tumours (F_0) and the corresponding PDTXs (F_1/F_3) of lines suspected of undergoing lymphomagenic transformation from four individual patients (a-d). Scale bars represent 100µm.

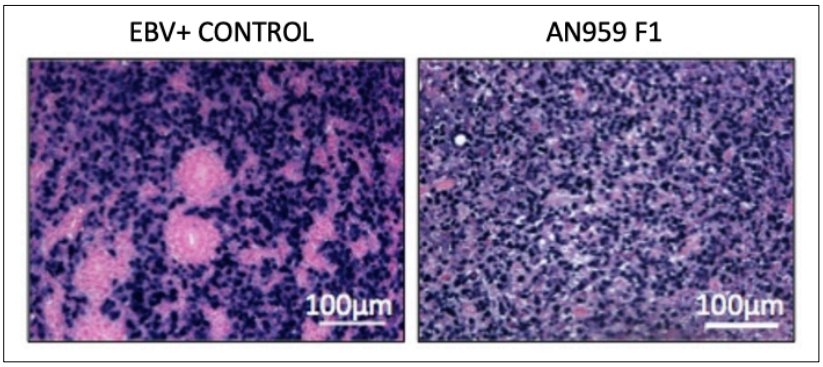

Figure 3-12 In situ hybridization for the Epstein Barr virus (EBV) within PDTX line AN959

In situ hybridization for the Epstein Barr virus (EBV) is indicated by dark blue staining. On the left is a positive control (EBV-positive nasopharyngeal carcinoma) and on the right is a FFPE section of a first-generation PDTX from the line AN959. Scale bars represent 100µm.

Flow cytometric immunophenotyping is a technique that is employed in order to diagnose haematological malignancies. This is achieved by identifying abnormal cell populations from within a sample based on a number of parameters. These parameters include cell size, granularity and cell surface marker expression. Analysis of three of the PDTX lines suspected of undergoing lymphomagenic transformation was performed using a panel of previously validated markers (Craig & Foon, 2008). These PDTX lines included GB975 (ID4), RF226 (ID14) and JA227 (ID16). The results revealed the consistent presence of an abnormal B-cell population. These cells tended to be large in size by light scatter properties and had exhibited evidence of light chain restriction. Such a clonal proliferation is diagnostic of a CD5 negative, B-cell non-Hodgkin lymphoma (Figure 3-13).

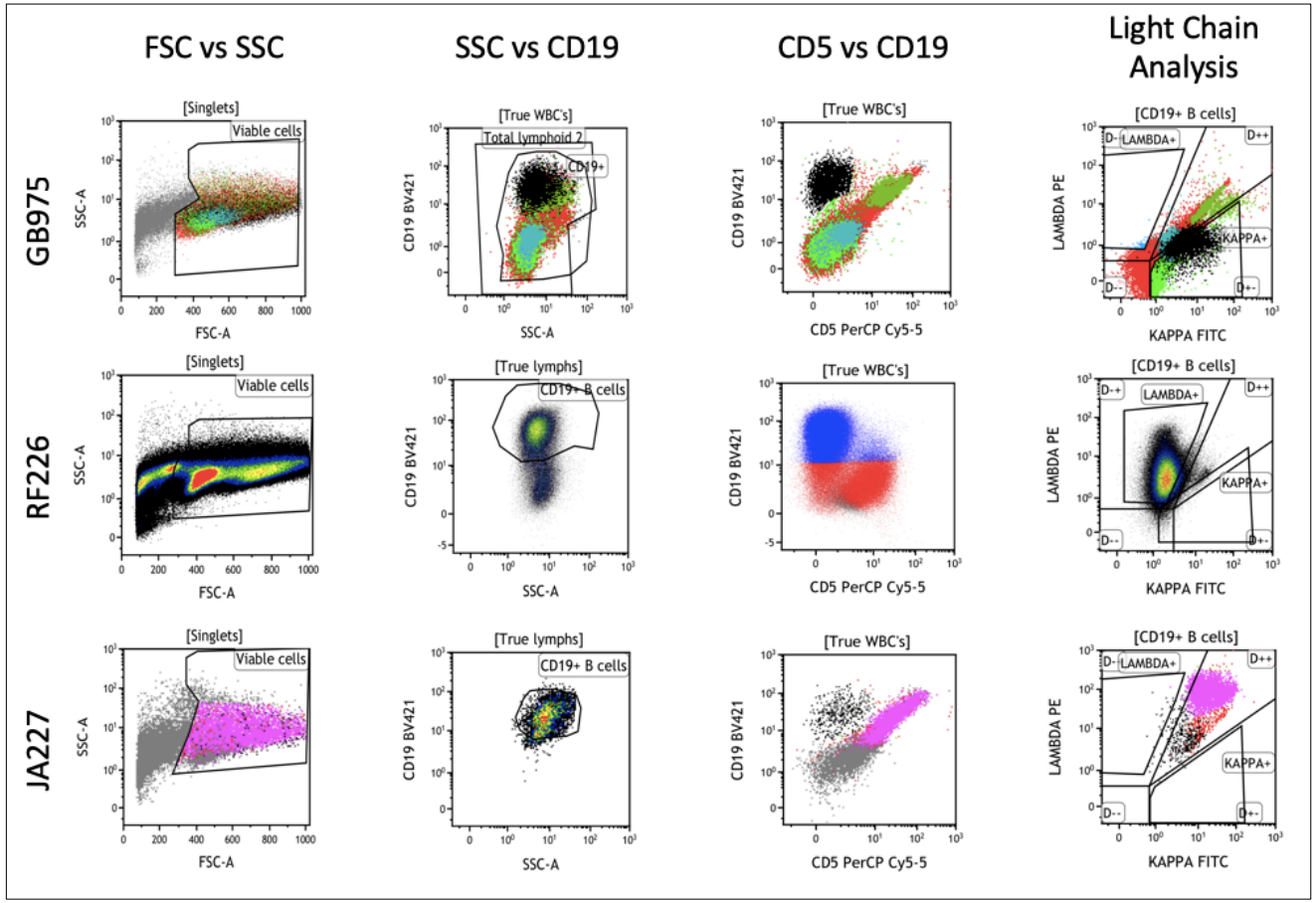

Figure 3-13 Flow cytometric analysis of PDTX lines suspected of undergoing lymphomagenic transformation

A representative panel of FACS plots used to determine the immunophenotype of the PDTX lines JA227, RF226 and GB975. Plots include forward (FSC) versus side scatter (SSC) profile as well as CD19, CD5 and light chain expression (kappa versus lambda).

3.5.1 Summary

IHC and flow cytometric analysis confirmed that approximately 20% (5/24) of the oesophageal cancer PDTX lines that were generated in this study, using the IM technique, had transformed into diffuse large B-cell lymphomas of human origin. However, it is important to note that this process is not unique to either oesophageal cancer or the IM transplantation technique, as there have been numerous other reports from PDTX series involving other cancer types of lymphomagenic transformation (Butler, Hou, Becker, Zanfagnin, Enderica-Gonzalez et al., 2017; Chen, Ahmed, Adeyi, Dick, & Ghanekar, 2012; John, Yanagawa, Kohler, Craddock, Bandarchi-Chamkhaleh et al., 2012). One study, involving the generation of prostate cancer PDTXs, even reported a lymphoma transformation rate of 80% (Wetterauer, Vlajnic, Schuler, Gsponer, Thalmann et al., 2015). These studies typically employed heterotopic transplantation sites such as the subcutaneous and intraperitoneal spaces.

In humans, the process of lymphomagenic transformation is commonly driven by the EBV infection of B cells (Vockerodt, Yap, Shannon-Lowe, Curley, Wei et al., 2015). Testing of one of the transformed PDTX in this series by in situ hybridisation confirmed the presence of EBV, suggesting that the virus may also play a role in transformation in the xenograft setting. This is consistent other studies that have investigated the same process (Butler et al., 2017; K. Chen et al., 2012). As EBV infected B cells are normally under the control of the immune system through the action of antigen-specific T lymphocytes, both of these studies concluded that the transformation is most likely related to the culture of EBV infected B cells in an immunodeficient setting (Landais, Saulquin, & Houssaint, 2005). Such a process is akin to the development of B-cell lymphomas post solid organ transplantation (Vockerodt et al., 2015). It may also explain why the rate of lymphomagenic transformation increases as the level of host immunity decreases (Choi, Lee, Kim, Sim, Kim et al., 2016). In the study by Choi et al. (2016), 15 gastric cancer PDTXs were established from a total of 62 different patient samples. Of these 15 PDTXs, six were established in nude mice (which are deficient in T cells), and nine in NSG mice (which are deficient in T, B and natural killer cells). In total, 5/15 of these PDTXs underwent lymphomagenic transformation, all of which occurred with NSG mice.

In an attempt to prevent lymphomagenic transformation from occurring, it is necessary to understand if the process occurs entirely in the host mouse or begins in the patient. Although

rare, primary lymphoepithelial carcinomas of the oesophagus are a recognised entity (Terada, 2013). More common, however, in the clinical setting, is the process of EBV driven lymphomagenic transformation. This typically occurs in immunocompromised patients, such as those with immunodeficiency disorders and in those receiving chemotherapy (Krishnan & Morgan, 2007). However, upon review of the clinical histories and pathologies of all of the patients in this series, there was no evidence that any of the patients had lymphomas prior to implantation nor did they subsequently develop lymphomas.

This phenomenon highlights an important limitation of the PDTX model and reinforces the need for strict validation. Simply confirming that PDTXs are of human origin and share the same genomic profile as the original patient is not sufficient. At a minimum, validation also needs to consist of both histopathological and IHC assessment, in order to confirm that the derived xenografts recapitulate the same degree of differentiation and molecular profile as the original tumour. Relying on histopathological assessment alone has limitations, especially in the setting of poorly differentiated tumours, as it can be difficult to distinguish epithelial from non-epithelial tumours in this setting. For this reason, an IHC analysis needs to be performed consisting of both epithelial and lymphoma markers. If transformation is suspected, confirmation can be achieved via a flow cytometric analysis in order to confirm clonality (Craig et al., 2008).

Researchers are also investigating techniques to prevent and even reverse this process once it has established. Having identified lymphomagenic transformation in their series of ovarian cancer xenografts, Butler et al. (2017) trialled the administration of an anti-CD20 antibody at the time of implantation, which decreased the rate of lymphomagenic transformation decreased from 11.1% (13/117) to 1.88% (3/160).

The discovery that oesophageal PDTXs are susceptible to lymphomagenic transformation has far reaching implications. Given that preclinical drug validation is currently the most common application of the PDTX model, failure to recognise transformed PDTX lines could have significant downstream effects. Clinical trials could either be commenced based on inaccurate preclinical data, or, more significantly, rejected when in fact the drug may have had a clinical effect. Such a scenario has previously occurred in the field of OAC when a series of commonly used cell lines were misidentified (Boonstra, van Marion, Beer, Lin, Chaves et al., 2010). In

this study, two mistakenly identified OAC cell lines were linked to over 100 publications and 11 US patents.

Whilst some researchers are slowly coming to the realisation that lymphomagenic transformation can occur, others have failed to be as diligent with PDTX validation. An example is seen in a study by Wang et al. (2014). In this study, oesophageal PDTX models were used to test the effect of Notch inhibition on tumour growth. Although the authors reported positive preclinical results, they did not perform an adequate validation of their model. They provided identical images of both the original patient tumour and PDTX, and subsequent images of the PDTX simply revealed evidence of a poorly differentiated carcinoma (Wang et al., 2014)(Figure 3-14).

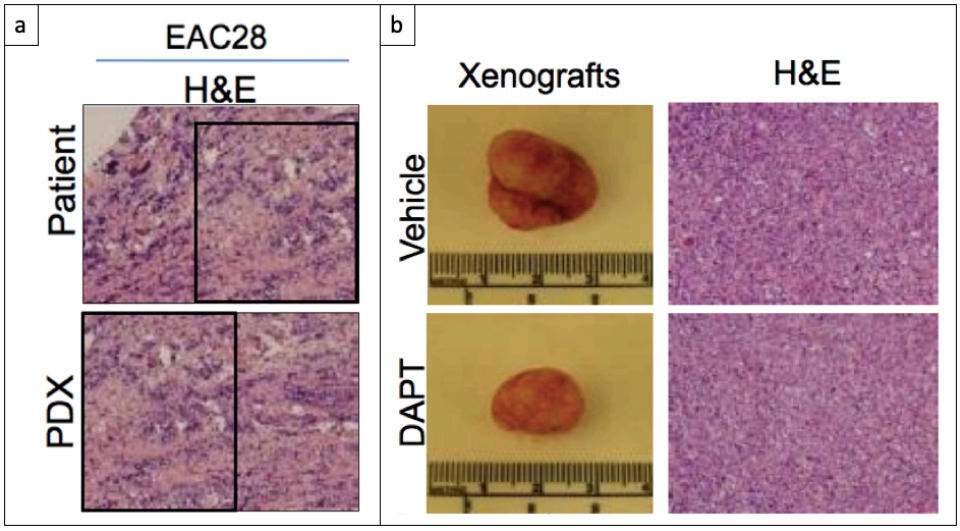

Figure 3-14 Poorly validated oesophageal PDTXs

H&E sections form both the original patient tumour and PDTX. Boxes outline regions of both primary tumour and PDTX that are an exact match (a). PDTXs treated with both vehicle and drug are shown in b. H&E sections form both drug and vehicle treated PDTXs reveal a poorly differentiated tumour with no clear epithelial component (b). Although the PDTXs shown in both a and b are all reportedly derived from the same line, they fail to demonstrate any similarities (Wang et al., 2014. Reproduced with permission).

3.6 Assessment of PET/FDG avidity within the PDTX model

3.6.1 Background

PET is a form of functional imaging that is commonly used in oncology. It provides an adjunct to the anatomical information gained from computed tomography (CT). It relies on the labelling of biologically important molecules with positron-emitting radionucleotides. Glucose is commonly used for this purpose in the form of fluorodeoxyglucose (FDG). This is based on the observation that tissue hypoxia within tumours leads to up regulation of the GLUT1 glucose transporter (Jadvar, Alavi, & Gambhir, 2009; Li, Du, Ma, Postel, & Civelek, 2014). This in turn leads to an increased amount of glucose entering the tumour cells. As the radionucleotide decays, radiation is emitted which is subsequently detected by a PET scanner.

In the field of oncology, PET is commonly used as a tool to detect metastatic disease. However, for reasons that are largely unknown, only certain tumour types are FDG avid. It is this FDG avidity which determines the clinical utility of the study. For example, it has been validated in oesophageal but not gastric cancer (Kelloff, Hoffman, Johnson, Scher, Siegel et al., 2005). In oesophageal cancer, FDG PET also has a role in measuring a tumour's metabolic response to neoadjuvant therapy. By comparing imaging pre and post neoadjuvant therapy, clinicians can determine if a tumour is a complete, partial or non-responder and alter treatment accordingly. A key limitation of FDG PET however, relates to the size of tumours that can be detected. Due to surrounding background activity, false-negatives are commonly found in lesions less than 7mm (Mahajan & Cook, 2016).

Given the important role that FDG PET plays in oesophageal cancer, the final form of validation of the PDTX model involved comparing the FDG PET avidity of the primary patient tumour to that of the derived xenograft. If these results correlate, it would provide further evidence that tumour biology is maintained between the original patient tumour and PDTX. It would also provide an additional preclinical tool for the development of molecular imaging studies.

3.6.2 Results

The results of FDG PET imaging from two separate first generation PDTX lines are shown below, alongside the matched results from the FDG PET imaging of the original patient tumours (Figure 3-15 & Figure 3-16). These lines include PL128 (ID18) & JB075 (ID19), both of which were derived from OAC. Identification (ID) numbers are also provided which reference back to Table 3-2. Unfortunately, validation of JB075 confirmed that it had undergone lymphomagenic transformation. In neither case did the FDG avidity correlate with the result seen in the patient.

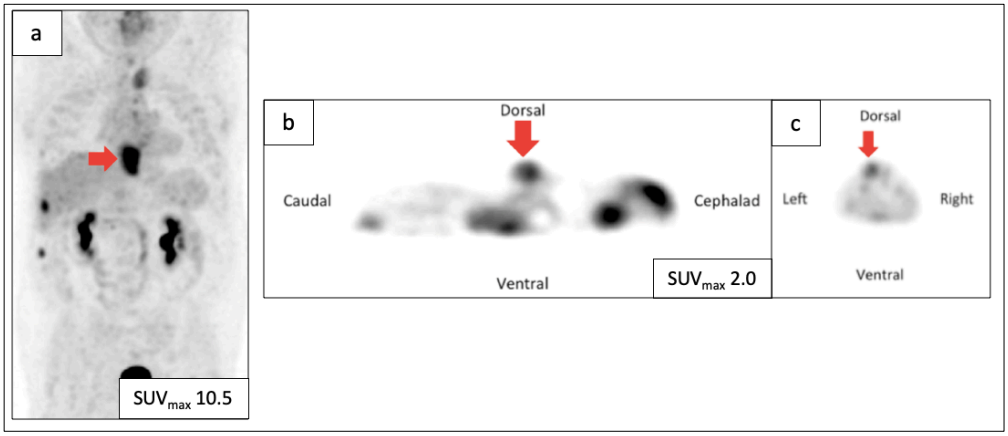

Figure 3-15 A comparison of FDG PET avidity between the original patient tumour and first-generation PDTX of the line PL128 (ID 18)

An FDG PET image from patient PL128 (ID 18) in coronal section at time of diagnosis (a). The corresponding FDG PET of the first-generation PDTX is shown in both sagittal (b) and transverse sections (c). Both original patient tumour and PDTX are identified by red arrows.

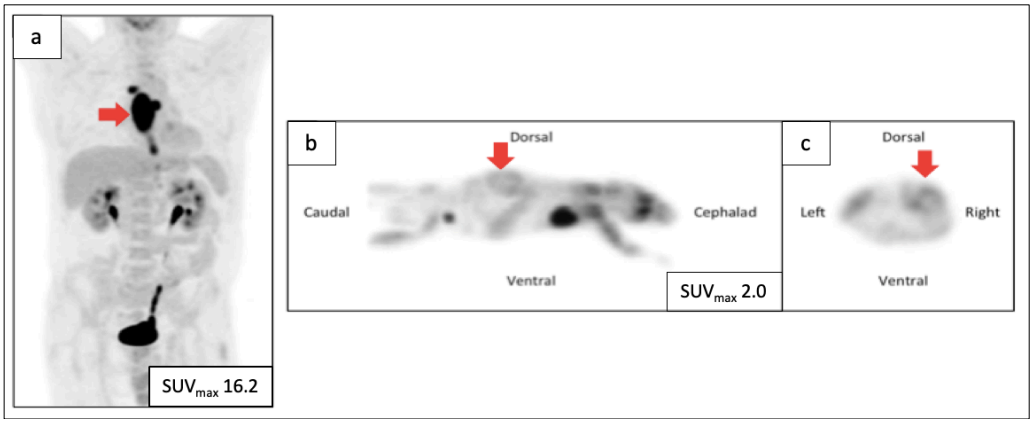

Figure 3-16 A comparison of FDG PET avidity between the original patient tumour and first-generation PDTX of the line JB075 (ID 19)

An FDG PET image from patient JB075 (ID 19) in coronal section at time of diagnosis (a). The corresponding FDG PET of the first-generation PDTX is shown in both sagittal (b) and transverse sections (c). Both original patient tumour and PDTX are identified by red arrows. This PDTX had undergone lymphomagenic transformation.

3.6.3 Summary

This is the first time that the FDG PET avidity of original patient tumours has been compared to first generation PDTXs in the setting of OAC. Unfortunately, whilst the PDTX demonstrated some degree of avidity, there was no clear correlation with patient results. These findings are consistent with other published series which assessed xenograft FDG PET from a range of other cancers (Apisarnthanarax, Alauddin, Mourtada, Ariga, Raju et al., 2006; Chen, Cheng, Walton, Wang, Ebi et al., 2012; Guerreschi, Scalbert, Qassemyar, Kluza, Ravasi et al., 2013; Moroz, Kochetkov, Cai, Wu, Shamis et al., 2011; Munk Jensen, Erichsen, Bjorkling, Madsen, Jensen et al., 2013). However, it should be noted that the majority of published studies are based on cell line derived xenografts and not PDTXs.

The poor correlation between the PDTX and the patient with respect to FDG PET imaging may be the result of an altered microenvironment. As the PDTX resides in a more vascular microenvironment compared to their native site, they could potentially be receiving a greater oxygen supply. This could have the potential to lead to a down regulation of the GLUT1 transporter.

3.7 Applications of the PDTX model

3.7.1 PDTXs as a preclinical tool for molecular imaging studies

As a proof of principle, an experiment was performed using a novel small molecular inhibitor labelled with a near-infrared (NIR) dye to determine the feasibility of imaging tumours *in vivo*. Such a technique forms the basis of 'firefly' or 'real-time image-guided surgery' and is currently being investigated in the treatment of brain, liver and prostate cancer (Cho, Jeon, Buch, Nag, Nasrallah et al., 2018; Contino, Eldridge, Secrier, Bower, Fels Elliott et al., 2016; Neuman, Eifler, Castanares, Chowdhury, Chen et al., 2015; Thursfield, Farrugia, Karahalios, & Giles, 2012; Tummers, Miller, Teraphongphom, van den Berg, Hasan et al., 2019). In this example, the selected molecule is an inhibitor of the BMP pathway and was chosen as there is evidence suggesting that activation of the BMP pathway is required for the development of both BO and OAC (Calpe, Correia, Sancho-Serra Mdel, & Krishnadath, 2016; Calpe, Wagner, El Khattabi, Rutten, Zimberlin et al., 2015; Clemons, Phillips, & Lord, 2013; Milano et al., 2007). In this experiment, mice harbouring PDTXs with high BMP expression were injected with a labelled inhibitor via intraperitoneal injection up to 24 hours prior to being imaged. Results revealed the accurate localisation of the tumour, as seen on both in vivo and ex vivo imaging (Figure 3-17). In OAC, such a technique could be used to indicate the extent of disease beyond the primary tumour. This could include the presence of involved lymph nodes or malignant infiltration into surrounding stroma. If successful, such an approach has the potential to have a huge impact in the surgical treatment of OAC, as it may lead to improved R0 resection margins and better local control.

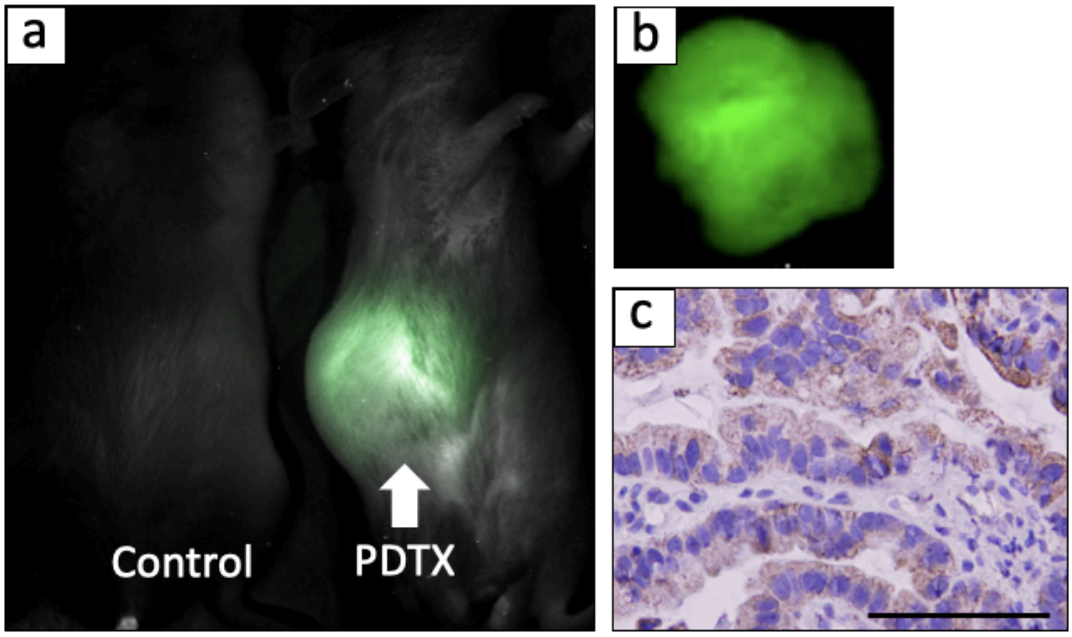

Figure 3-17 NIR imaging of an oesophageal PDTX with high BMP expression

A control mouse (non-tumour bearing) and mouse harboring an IM PDTX with high BMP expression were imaged 24 hours after the administration of a combined BMP2 and BMP4 inhibitor labelled with a NIR dye (100 mcg via intraperitoneal injection) (panel a). Ex vivo imaging is shown in panel b. A representative section of the PDTX is shown in panel c, demonstrating staining against BMP. Scale bar represents 100 μm.

3.7.2 Using PDTXs to investigate the frequency of tumour initiating cell within OAC

Some theories suggest that CSCs are responsible for disease recurrence and metastasis formation, as they tend to be resistant to both chemotherapy and radiotherapy owing to their quiescent state (Visvader & Lindeman, 2012). If OAC is demonstrated to follow a CSC model, successfully targeting these CSCs may lead to the development of novel therapeutic strategies and significant survival improvements. However, before trying to identify a specific OAC CSC population, the first step is to determine the frequency of tumour initiating cells from a range of different tumours. This will give some indication as to whether OAC follows a CSC model, in which only a minority of cells have tumorigenic potential or follows a clonal evolution model in which all cells share an equal tumorigenic potential. In order to assess this, a series of limiting dilution assays were performed across a range of different xenograft lines.

An Extreme Limiting Dilation Assay (ELDA) was performed using four separate OAC PDTX lines. This included one poorly differentiated PDTX line and three moderately differentiated PDTX lines. In total, 90 separate injections were performed resulting in the formation of 59 separate tumours (Table 3-3). The number of cells per injection ranged from 5,000,000 to a single cell. Results revealed a TIC frequency of 1/296 (CI of 1/496 to 1/177) for the poorly differentiated PDTX line and 1/1258 (CI 1/3166 to 1/499) for the three moderately differentiated PDTX lines. This was based on the aggregate results from all three moderately differentiated PDTX lines.

Table 3-3 Results of the limiting dilution assay

Grade	PDTX Line	Cells / Injection	Number of Tumours	Number of Injections
Poor	14582 (ID1)	10,000	4	4
		2,000	7	7
		1,000	9	11
		500	7	7
		250	7	7
		100	0	4
		10	0	4
		1	0	5
Mod	GB570 (ID15)	2,000,000	3	3
	PL128 (ID18)	100,000	0	3
		60,000	1	1
		50,000	0	3
		25,000	1	1
		15,000	0	1
		10,000	0	3
		1,000	1	3
	IS076 (ID22)	5,000,000	2	2
		160,000	3	3
		120,000	3	3
		40,000	3	3
		24,000	3	3
		10,000	3	3
		4,000	3	3
		1,000	2	3

In theory, given that these results suggest that the tumour initiating cell frequency within OAC represents a relatively rare population, it is possible that OAC follows the CSC model. However, whilst the CSC model requires that the tumour-initiating cell fraction represent a rare population, a strict threshold does not exist. Some studies have reported frequencies of CSCs ranging from <1% in acute myeloid leukaemia and liver cancer to 82% in acute lymphoblastic leukaemia (Rich, 2016). In order to confirm these findings, additional limiting dilution assays need to be performed across a larger number of PDTX lines. If OAC is proven to follow a CSC model, attempts should then be made to try and identify the specific CSC population. Once identified, these populations need to undergo functional testing in order to confirm their stemness. Such tests include tumorigenic and serial transplantation assays in order to assess for self-renewal and differentiation (Williams, Anderson, Santaguida, & Dylla, 2013).

3.8 Discussion

This chapter highlights the significant progress that has been made with respect to optimising the oesophageal cancer PDTX model, through the development of an IM transplantation technique (Read et al., 2016). By adopting such an approach, the successful engraftment rate of bona fide oesophageal PDTXs was approximately 78% (18/23). This is in contrast to a success rate of 16.6% (1/6) using the standard subcutaneous approach. Given the early success of the IM approach and the importance of generating PDTX models, the majority of samples were implanted using the IM technique, making it impossible to make a direct comparison between the two techniques. However, considering that the best reported engraftment rate in the literature is only 33% using the subcutaneous technique, the IM approach is clearly superior (de Both et al., 2001; Dodbiba et al., 2013b). Such a development is a significant advancement in the field of OAC, where a paucity of suitable preclinical models has hindered research (Liu, Duong, et al., 2016).

Another highlight in this chapter was the successful re-establishment of PDTXs post cryopreservation (Read et al., 2016), a methodology for which had not been previously described. Cryopreservation enables large repositories of PDTXs to be established, each with their unique mutational profile. This has important implications for cancers like OAC, which have extremely high mutational burdens and means that PDTXs only need to be re-established when their specific mutational profile is required to be tested. Other benefits include significant cost savings as well as the unnecessary passage of PDTXs. Cryopreservation also allows this precious resource to be more readily shared amongst researchers.

Another key finding in this chapter has been the importance of thorough validation, which is an essential step in ensuring that PDTXs recapitulate their original patient tumours and that results can be translated to the clinical setting. Validation should ensure that PDTXs maintain the same degree of differentiation, expression of molecular markers and mutational profile as the original patient tumour. If required, the response of PDTXs to standard chemotherapy should also be assessed.

However, a limitation of the PDTX model that needs to be highlighted is lymphomagenic transformation. Although previously recognised in the literature, the process was not widely reported. Publishing these findings has served to increase awareness of this process

throughout the research community, as evidenced through citations in a number of other papers (Choi et al., 2016; Dieter, Giessler, Kriegsmann, Dubash, Mohrmann et al., 2017; Kalavska, Kucerova, Schmidtova, Toro, Kozovska et al., 2018).

Optimising the PDTX model also has the potential to have marked impact on the preclinical development of novel therapies for oesophageal cancer, as seen from the preliminary results of BMP inhibition on a PDTX with high BMP expression. Another example of the this can be seen in a study by Liu et al. (Liu, Read, Cullinane, Azar, Fennell et al., 2015). In this study, the effect of a newly developed drug, APR-246 was assessed on a range of preclinical models of OAC. Included in this were PDTX lines obtained from the biobank established in this chapter. As APR-246 is purported to act by restoring the function of mutated p53 back to its wild-type function, PDTX lines both with and without p53 mutations were used. The use of PDTX models in this study directly contributed to the initiation of a clinical trial.

The IM transplantation technique has also been successfully applied to other cancer types. Examples include its use in the CASCADE program, which is a rapid autopsy program designed to obtain metastatic deposits from patients with breast, ovarian, melanoma and prostate cancer (Alsop, Thorne, Sandhu, Hamilton, Mintoff et al., 2016). Following collection, tissue is then either biobanked or xenografted. Other tumours types using the technique include both gastric cancer and anal SCC, which has led to the generation of the first anal SCC PDTX biobank (Bernardi, 2017).

The remainder of this thesis will explore multiple other novel applications of the PDTX model in the study of Barrett's carcinogenesis.

Chapter 4 The generation and validation of xenograft derived oesophageal cancer cell lines

4.1 Introduction

Preclinical models are essential tools in cancer research, as they enable the study of disease biology and also provide a means to screen novel therapies. Unfortunately, relevant models are lacking in the field of oesophageal cancer. This research barrier explains, in part, why there have been very little improvements to the overall survival for oesophageal cancer over the last few decades. Traditionally, cancer cell lines have been the most versatile and widely adopted preclinical model, as they are robust and enable the high throughput of experiments. Whilst there have been numerous publications describing the establishment and validation of SCC cell lines (Boonstra, van der Velden, Beerens, van Marion, Morita-Fujimura et al., 2007; Kuriya, Kitamura, Akaishi, Hirayama, Sekine et al., 1983; Nishihira, Hashimoto, Katayama, Mori, & Kuroki, 1993; Nishihira, Kasai, Mori, Watanabe, Kuriya et al., 1979; Shimada, Imamura, Wagata, Yamaguchi, & Tobe, 1992), there have been very few published adenocarcinoma cell lines. In fact, there have only been 12 bona fide OAC cell lines reported in the literature. These include FLO-1 (Hughes, Nambu, Soldes, Hamstra, Rehemtulla et al., 1997), KYAE-1 (Kan, Shimada, Sato, Maeda, Kawabe et al., 2001), SK-GT-4 (Altorki, Schwartz, Blundell, Davis, Kelsen et al., 1993), JROECLl9 (OE19) and JROECL33 (OE33) (Rockett et al., 1997), JH-EsoAd1 (Alvarez, Koorstra, Hong, Boonstra, Dinjens et al., 2008), OACM5.1 and OACP4CE (de Both et al., 2001), ESO26 and ESO51 (Boonstra et al., 2010), OANC1 (Clemons, Do, et al., 2014) and MFD-1 (Cowie, Garcia, Hayden, & Underwood, 2015; Garcia, Hayden, Cowie, Mellone, Derouet et al., 2015). Of these 12 cell lines, only six have been derived from patients with confirmed BO. The details of these cell lines are shown in Table 4-1.

Table 4-1 Details of the six bona fide OAC cell lines that originated from a region of BO

CELL LINE	YEAR CREATED	SITE OF PRIMARY	TISSUE SOURCE	DOCUMENTED BO	GRADE	TREATMENT NAÏVE
SK-GT-4 (Altorki et al., 1993)	1989	Distal Oesophagus	Primary Tumour	Yes	Well	Yes
OE-33 (Rockett et al., 1997)	1997	Distal Oesophagus	Primary Tumour	Yes	Poor	Not Stated
OACM5.1 (de Both et al., 2001)	2000	Distal Oesophagus	Lymph Node Metastasis	Yes	Not stated	
ESO51 (Boonstra et al., 2010)	2000	Distal Oesophagus	Primary Tumour	Yes	Not Stated	Not Stated
JH-Eso-Ad1 (Alvarez et al., 2008)	2008	Distal Oesophagus	Primary Tumour	Yes	Mod to Poor	Not Stated
OANC1 (Clemons, Do, et al., 2014)	2014	Distal Oesophagus	Primary Tumour	Yes	Mod	No

The discrepancy between the numbers of SCC versus adenocarcinoma cell lines may be due to the fact that, historically, SCC was the most common form of oesophageal cancer and this coincided with the period that the majority of cell lines were established. It has only been in recent years that OAC has taken over the incidence of SCC in the Western world (Pohl et al., 2005).

The limited availability of treatment naïve tissue has also hindered the development of oesophageal cancer cell lines. This has been particularly so since the introduction of neoadjuvant therapy, which has now become the standard of care for locally advanced oesophageal tumours. As resection specimens typically demonstrate some degree of therapeutic response, the viability of cells obtained from these sources is often reduced, leading to limited outgrowth of epithelial cells *in vitro*. Access to treatment naïve tissue has mainly been limited to small endoscopic biopsies obtained prior to treatment. Other issues to affect the *in vitro* growth of tumour cells include fibroblast outgrowth and the low adherence of freshly isolated tumour cells to plastic. Unfortunately, a robust technique for the establishment of cell lines has not been published, with most authors adopting differing methods and a 'trial and error' type approach.

It is also worth acknowledging that cell lines generated from tissue that has been treated with neoadjuvant therapy may not be representative of the original tumour, as neoadjuvant therapy has the potential to induce additional mutations within the tumour.

Current cell lines also fail to model two clinically relevant aspects of disease biology. The first is that they fail to model the genetic diversity observed in oesophageal cancer. At the genetic level, oesophageal cancer, especially adenocarcinoma, is a highly unstable disease and is characterised by marked intra and inter tumour genetic heterogeneity. A number of recently published studies using whole genome sequencing, have identified that this is due to the early loss of tumour suppressor genes, such as p53, which then lead to the rapid accumulation of catastrophic genetic events (Gregson, Bornschein, & Fitzgerald, 2016; Nones et al., 2014; Secrier, Li, de Silva, Eldridge, Contino et al., 2016). In order to recapitulate such a vast genetic landscape and provide clinically relevant preclinical models, many more cell lines are required. The second is that the majority of currently available cell lines fail to metastasise in the *in vivo* setting. This aspect of the disease is extremely important to model as it is leading cause of mortality for patients who present with the disease. Typically, locoregional disease can be treated with a combination of surgery and perioperative chemotherapy and/or chemoradiotherapy. However, once distant metastases have formed, treatment becomes

palliative. Unfortunately, the only cell line that exists that reproducibly metastasises is a subclone of the FLO-1 cell line that was successfully isolated and cultured by Liu et al (Liu, Hoefnagel, Fisher, Krishnadath, Montgomery et al., 2016). This cell line has been shown to be reproducibly metastatic when injected both subcutaneously and orthotopically.

The aim of this chapter, therefore, was to develop additional OAC cell lines. However, this is particularly challenging given the limited availability of treatment naïve OAC tissue. As a result, oesophageal SCC tissue is also used throughout this chapter in order to both develop and refine necessary techniques.

4.2 Results

Numerous techniques were trialled in an attempt to generate additional oesophageal cancer cell lines. These techniques involved using both primary tumour as well as the PDTX model as a source of tissue. A flow diagram outlining these techniques in addition to the range of steps performed in order to validate successfully derived cell lines is shown in Figure 4-1.

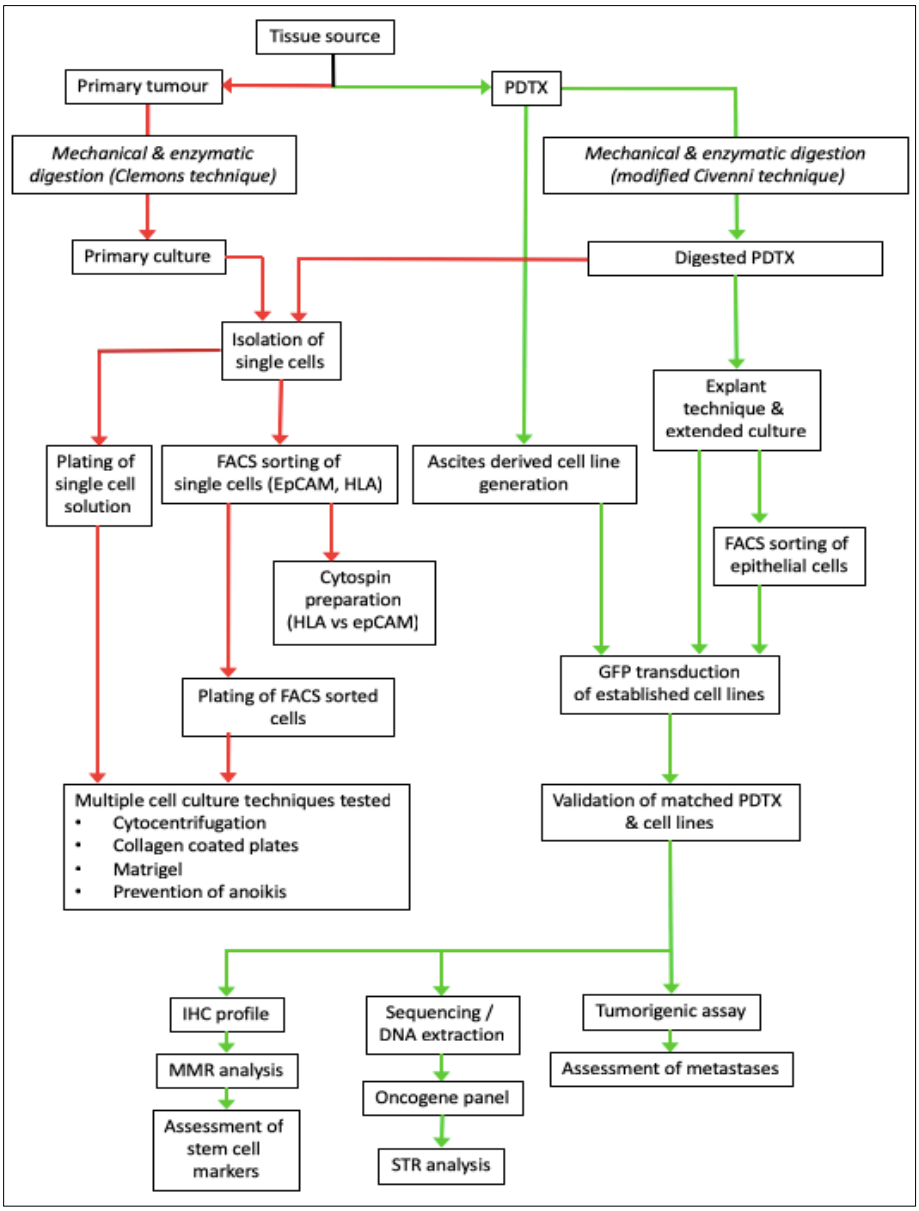

Figure 4-1 An outline of the techniques used for the generation and validation of addition cell lines.

Red lines outline failed techniques whilst green lines outline techniques that were associated with the successful generation of cell lines.

4.2.1 Attempted cell line generation from primary tumour tissue

Initial attempts at generating OAC cancer cell lines were performed using original patient tissue obtained from oesophageal resection specimens. In total, attempts were made at generating cell lines from four separate patient tumours. These tumours were mechanically and enzymatically digested, as described in section 2.2.1, and placed into culture. Short-term culture of these digested tumours revealed a large amount of floating cellular debris with only the occasional adherent cell. These adherent cells assumed a fibroblast-like morphology and failed to divide following extended culture. Despite repeated attempts using different media (EpiLife, EpiGro and RPMI with 20% FCS), different culture conditions (low oxygen) and culture surfaces (collagen and Matrigel); tumour cells could not be cultured.

4.2.2 Attempted cell line generation from patient-derived tumour xenograft tissue

Following these initial failures, attempts were then made at culturing cancer cells from PDTXs, as they enrich for viable tumour cells and provide a renewable source of tumour tissue, thereby allowing repeated attempts at cell line generation. In total, attempts were made to generate cell lines from ten separate PDTX lines. To digest xenograft tissue, a rapid digestion was performed using a combination of both dispase and collagenase over a 45-minute period at 37^{o}C. This method is a modification of the digestion technique published by Civenni et al. (2011) and is described in full in section 2.2.3. Following digestion, cells were filtered through a 40µm filter in order to produce a single cell suspension. Overall cell yield was further increased through the use of a commercially available mechanical tissue chopper, manufactured by McIlwain (Surrey, UK). This tissue chopper is specifically designed to prepare sections of tissue while at the same time minimising damage to cell structure. Despite trialling all of the same techniques that were used for the attempted generation of primary cell lines, including different types of media, a low oxygen environment and coated culture surfaces, xenograft derived tumour cells could not be cultured *in vitro*. The only cells that could be successfully cultured post digestion were fibroblast-like cells.

4.2.3 Attempted cell line generation from FACS sorted xenograft-derived cells

In an attempt to separate the epithelial from the stromal cells, digested PDTXs were sorted by flow cytometry. For this technique to be successful, a cell surface marker needed to be selected that is specific for human cells. The two cell surface markers that were assessed for this purpose were human leucocyte antigen (HLA) and human EpCAM. It was hypothesized that HLA would positively select for all human cells, including both epithelial and stromal cells, whereas EpCAM would only select for human epithelial cells. In order to test this, following FACS sorting, cytospin preparations of both HLA and EpCAM positive populations were assessed for the IHC expression of both human mitochondria and the pancytokeratin AE1:AE3 (Figure 4-2). Results revealed that whilst EpCAM and HLA were both able to positively sort for human cells, EpCAM was able to sort for a higher proportion of epithelial cells. Given this, EpCAM was adopted as the main cell surface marker for human epithelial cells.

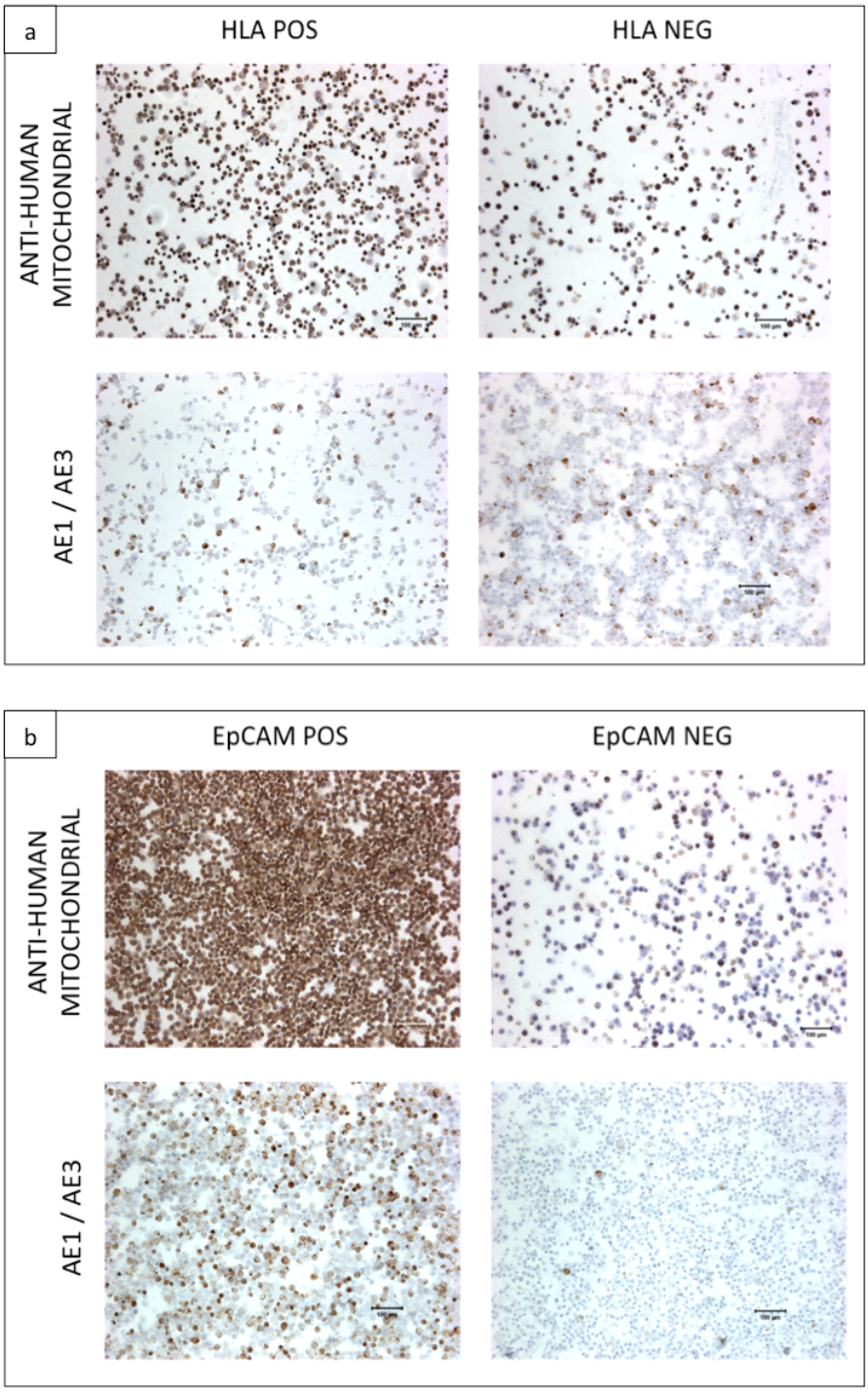

Figure 4-2 A comparison between FACS sorted xenograft derived cells based on HLA versus EpCAM surface markers

Cytospin preparations were generated following FACS sorting of xenograft derived cells based on either the HLA (panel a) or EpCAM (panel b). In order to determine the proportion of both human and epithelial cells within the sorted cells, cytospin slides were then stained for either human mitochondrial antibody or the pan cytokeratin AE1/AE3 and counter stained with DAB. Scale bars represent 100µm.

Unfortunately, FACS sorted EpCAM positive cells were still unable to be successfully cultured. This is despite twelve repeated attempts and trialling a number of additional techniques to encourage the growth of epithelial cells, including the use of HISC media designed to prevent anoikis (a form of programmed cell death that occurs once anchorage dependent cells are detached form the extra-cellular matrix) (Sato, Stange, Ferrante, Vries, Van Es et al., 2011). Other techniques included the centrifugation of cellular suspensions following sorting in order to facilitate the attachment of anchorage dependent cells to cell culture flasks and the use of sphere forming or stem cell assays in an attempt to enrich for cells with the potential for self-renewal. Centrifugation was performed at low g-force (250 r.p.m.) for 5 minutes using a swinging bucket rotor. Cells were then cultured at 37°C and 5% oxygen. Unfortunately, following these techniques, only cellular debris was evident.

4.2.4 Cell line generation using the explant technique

The next technique trialled was a modification of the explant technique of Giard et al. (1973). In this technique, xenografts underwent a process of mechanical dissociation followed by enzymatic digestion, as previously described in section 2.2.3. However, rather than passing the solution through a 40µm filter in order to yield solution comprised of single cells, the entire solution was centrifuged at 1,500 rpm for 5 minutes and the pellet (consisting of individual cells, cell clumps and small tissue pieces) re-suspended in RPMI supplemented with 20% FCS. This solution was then plated into a T75 flask. After plating, cell clumps and small tissue pieces soon became adherent, forming explants. These were left undisturbed for three days whilst being incubated at 37°C and 5% CO_2. Following this, half of the media was then refreshed, taking care not to dislodge any of the adherent explants.

Over a period of a few days, fibroblasts started to grow out from these explants. Following this, rounded tumour-like cells began growing on the bed of fibroblasts. Explants were then left in culture for periods of up to six-months. During this period, media was changed twice weekly and fibroblasts removed using a process of selective trypsinisation as they became confluent (typically once per week). During trypsinisation fibroblasts were found to lift after only a very short exposure to trypsin (approximately 30 seconds), whereas the tumour cells required a prolonged exposure (between 5 to 10 minutes). After a period of extended culture, regions of tumour cells began to form that were largely devoid of fibroblasts (Figure 4-3).

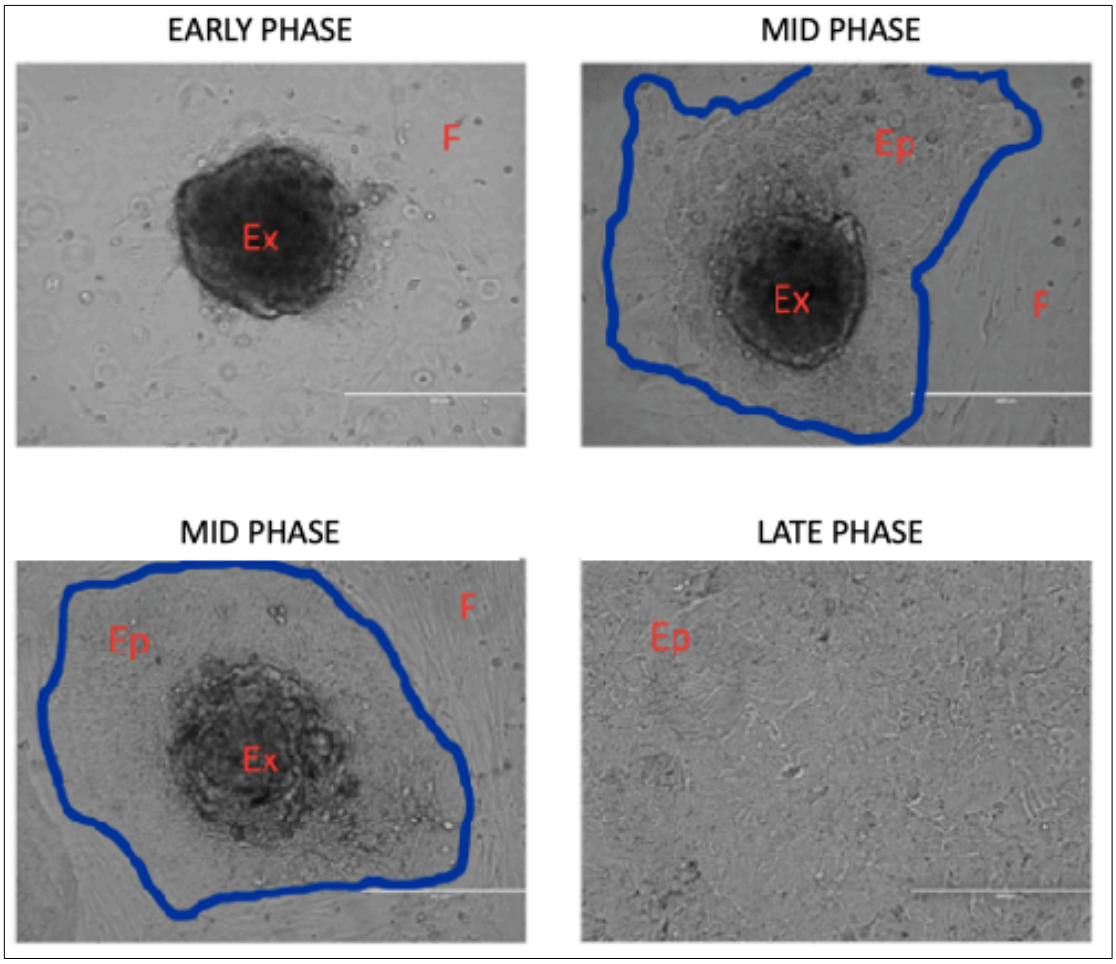

Figure 4-3 The evolution of an explant in culture

A series of images detailing the evolution of an explant (Ex) in culture. The explant was derived from the rapid digestion of an OAC PDTX and became adherent after only a few days. Soon after becoming adherent, fibroblasts (F) began to grow out. Over the following weeks (mid phase) the explant began to produce epithelial (Ep) cells which became adherent to the bed of fibroblasts. During a period of extended culture, media was changed twice weekly and fibroblasts gradually removed using repeated trypsinisation. Dominant clones began to emerge after two to three months (mid phase). After approximately six months, regions of tumour cells emerged that were largely devoid of fibroblasts (late phase). Blue line marks the demarcation between epithelial cells and fibroblasts. Scale bars represent 100µm.

In order to further enrich for tumour cells, regions of tumour cells were selectively passaged. Initially, this led to an outgrowth of both tumour cells and fibroblasts. However, by continuing the process of selective trypsinisation, a pure cancer cell line subsequently emerged (Figure 4-4).

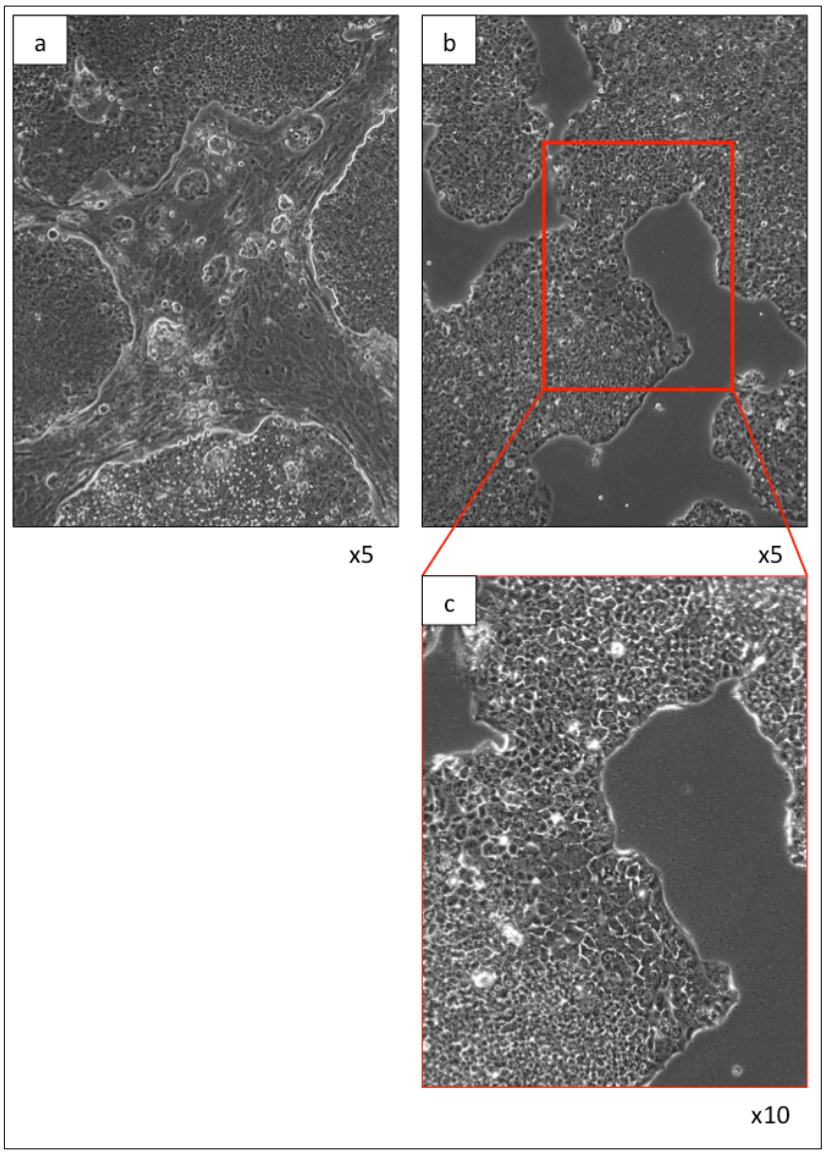

Figure 4-4 The establishment of a pure cancer cell line through the selective trypsinisation of fibroblasts.

Following passaging, multiple separate colonies of tumour cells would form, separated by fibroblasts (a). Compared to the epithelial cells, fibroblasts would detach after only a short exposure to trypsin. This allowed the fibroblasts to be selectively lifted whilst the epithelial cells remained adherent (b). A magnified view is shown demonstrating that all of the fibroblasts have been removed (c). This process was repeated up to twice weekly until a pure epithelial tumour line was established after approximately six months.

Following passaging, tumour cells were also enriched via FACS sorting using human specific EpCAM as a surface marker (Figure 4-5). As these cells had already adapted to *in vitro* conditions, ongoing culture post FACS sorting was easily achieved.

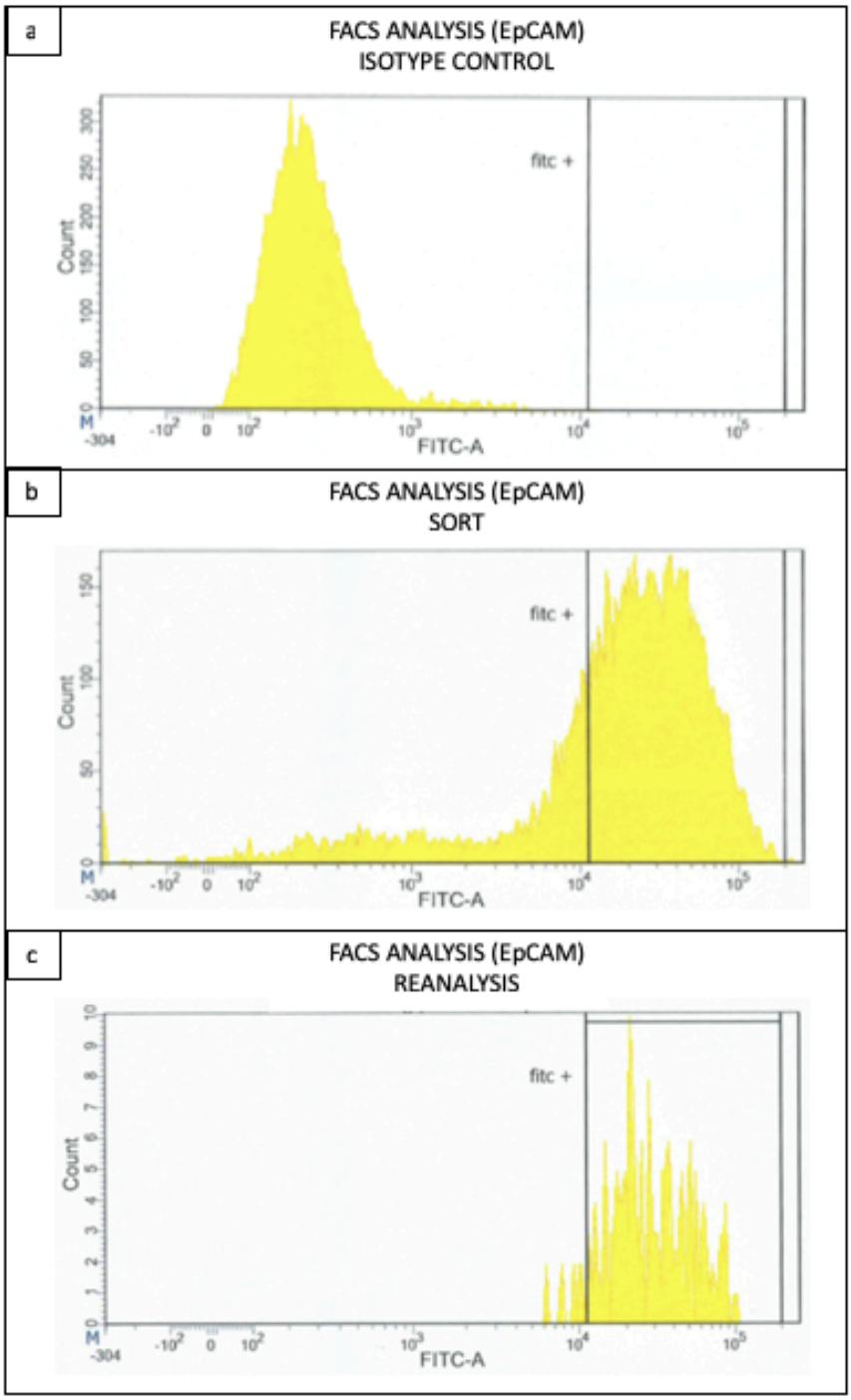

Figure 4-5 FACS sorting of explant generated cells based on EpCAM

A panel of histograms detailing the FACS sorting of explant derived cells originating from the OAC PDTX line IS076. Cells are labelled using an EpCAM antibody conjugated with FITC. An isotype control is initially used to identify a suitable threshold for the identification of EpCAM/FITC positive cells (a). Analysis of the sorted sample reveals a clear population of EpCAM/FITC positive cells (b). Reanalysis of the FITC positive sorted sample confirms that the sorted population is enriched for EpCAM/FITC positive cells (c).

4.2.5 Bona fide oesophageal PDTX-derived cell lines

The explant technique was successful in the generation of four matched xenograft-derived cell lines. These included two OAC lines (TB471 and IS076) and two oesophageal SCC lines (ST913 and MA924). Each xenograft derived cell line took on average six-months to develop a purified epithelial cell line that was devoid of fibroblasts and murine cells. During this period, cells were passaged twice weekly. In the following sections below, the clinical details from each original patient are detailed. ID numbers are also provided which reference back to Table 3-2.

4.2.5.1 TB471 (ID 21)

TB471 was a 66-year-old man who presented with a distal OAC arising from a segment of BO. This was on background of being anticoagulated for a history of mesenteric ischaemia. He presented with a six-month history of dysphagia and 12 kg loss of weight and was initially investigated with a barium swallow that revealed a distal oesophageal tumour. Endoscopy revealed the tumour to be at 34 cm from the incisors and near obstructing. Staging CT demonstrated a hiatus hernia with proximal oesophageal thickening. No nodal disease was evident; however, several pulmonary lesions were identified that were indeterminate in nature. FDG PET revealed an avid tumour of the distal oesophagus (SUV_{max} of 8) with no evidence of locoregional lymph node involvement or distant metastases. Following the insertion of a feeding jejunostomy the patient was commenced on neoadjuvant chemotherapy and radiotherapy as per the CROSS protocol (van Hagen et al., 2012). Repeat PET staging demonstrated a complete metabolic response. The patient then underwent an Ivor Lewis oesophagectomy and pathology revealed a complete response with a tumour regression grade (TRG) of 1 and with 0 out of 20 lymph nodes involved (Mandard, Dalibard, Mandard, Marnay, Henry-Amar et al., 1994). An area of BO was identified. In the follow-up period the patient subsequently developed both bone and adrenal metastases, which have been treated with a combination of resection and stereotactic ablative radiotherapy (SABR).

4.2.5.2 IS076 (ID 22)

IS076 was an 83-year-old man with synchronous oesophageal and colonic cancers. His past medical history consisted of atrial fibrillation (for which he was anticoagulated with warfarin), hypertension, GORD and hypercholesterolaemia. He initially presented with a two-month history of dysphagia, fatigue, loss of weight (4kg) and iron deficiency anaemia with haemoglobin of 68 g/L. Gastroscopy and colonoscopy revealed a large, ulcerating and partially obstructing distal oesophageal tumour in addition to a large, partially obstructing mass in the ascending colon. Histopathology revealed the oesophageal tumour to be a poorly differentiated adenocarcinoma and the colonic lesion to be a mucinous carcinoma. Staging FDG PET revealed intensely avid lesions within both the distal oesophagus (SUV_{max} of 11) and ascending colon (SUV_{max} of 17). Note was also made of a mesocolic lymph node that was possibly involved in addition to a likely right adrenal adenoma. No other distant metastases were identified. Given the patient's co-morbidities, the decision was made to proceed directly to surgery, as it was thought that he would not tolerate both chemotherapy and radiotherapy. He subsequently underwent a combined laparoscopic right hemicolectomy and laparoscopically assisted Ivor Lewis oesophagectomy. Histopathology confirmed that there was a 35mm poorly differentiated adenocarcinoma of the distal oesophagus and that the margins were clear. Six out of 30 lymph nodes were invaded with tumour giving an AJCC staging of T3N2. Pathology from the right colon revealed a T3N0 mucinous carcinoma. Immunohistochemistry for mismatch repair (MMR) proteins revealed a loss of expression of MLH1/PMS2 within the colonic tumour whereas the oesophageal tumour had a full expression, thereby demonstrating that the tumours were separate primaries.

4.2.5.3 ST913 (ID 23)

ST913 was a 51-year-old man who presented with a locally advanced SCC of the mid-oesophagus. This is on a background of gout, hypertension and hyperlipidaemia. He presented with a three-week history of worsening dysphagia to solids. He was initially investigated with a CT of the chest, which revealed a mid-oesophageal mass and an enlarged lymph node in the aorto-pulmonary window. Subsequent endoscopy revealed a partially obstructing mass situated between 26 to 31cm from the incisors. Biopsy confirmed this to be a SCC. Staging FDG PET revealed an intensely avid mid-oesophageal tumour with some low-grade uptake in one aorto-pulmonary lymph node. ST913 underwent neoadjuvant chemotherapy and radiotherapy as per the CROSS protocol. A feeding jejunostomy was placed to facilitate pre-operative nutrition. During the period of neoadjuvant treatment,

ST913 required an ICU admission for management of an altered conscious state that was thought to be due to a combination of hyper-osmolar non-ketotic coma and subdural haematoma. He subsequently recovered and a re-staging PET demonstrated that he had had a complete metabolic response. He proceeded to have a laparoscopically assisted Ivor Lewis oesophagectomy and histopathology confirmed a complete pathological response with associated trans-mural scar formation and 0 out of 10 lymph nodes involved.

4.2.5.4 MA924 (ID 24)

MA924 was a 77-year-old lady who presented with an oesophageal SCC. Her past medical history consisted of having a stroke secondary to carotid stenosis (which was treated with endarterectomy) and hypertension. She was a non-smoker. She initially presented with a two-month history of dysphagia and odynophagia and subsequent endoscopy demonstrated an oesophageal mass situated 30cm from the incisors. Biopsy revealed a SCC. Staging consisted on a FDG/PET and CT of the chest, abdomen and pelvis. FDG PET revealed an intensely avid lesion within the distal oesophagus over a length of approximately 4.2cm. Nodal disease was not evident. CT revealed a bulky tumour of the distal oesophagus with no distant metastases. Findings were consistent with a locally advanced SCC. MA924 underwent neoadjuvant therapy as per the CROSS protocol. Re-staging demonstrated evidence of a complete metabolic response, as the previous avidity within the distal oesophagus was no longer apparent. MA924 subsequently underwent preconditioning before having a laparoscopically assisted Ivor Lewis oesophagectomy. Histopathology demonstrated a complete pathological response with no residual SCC detected, consistent with the findings of her re-staging PET. In the initial post-operative period, MA924 noticed a perineal lesion, the biopsy of which confirmed SCC. This was initially treated with curettage. A subsequent formal excision did not reveal any residual tumour consistent with a TRG of 1. Two years post oesophagectomy, MA924 was progressing well and had no signs of disease recurrence.

4.2.6 Generation of the IS076 ascites-derived sub clone

Unique to the IS076 xenograft line is a metastatic sub clone. This was discovered at the second generation of passaging, when two mice harbouring tumours derived from one first generation xenograft developed widespread metastases whilst mice harbouring xenografts from the other first-generation xenograft remained free from metastases (Figure 4-6).

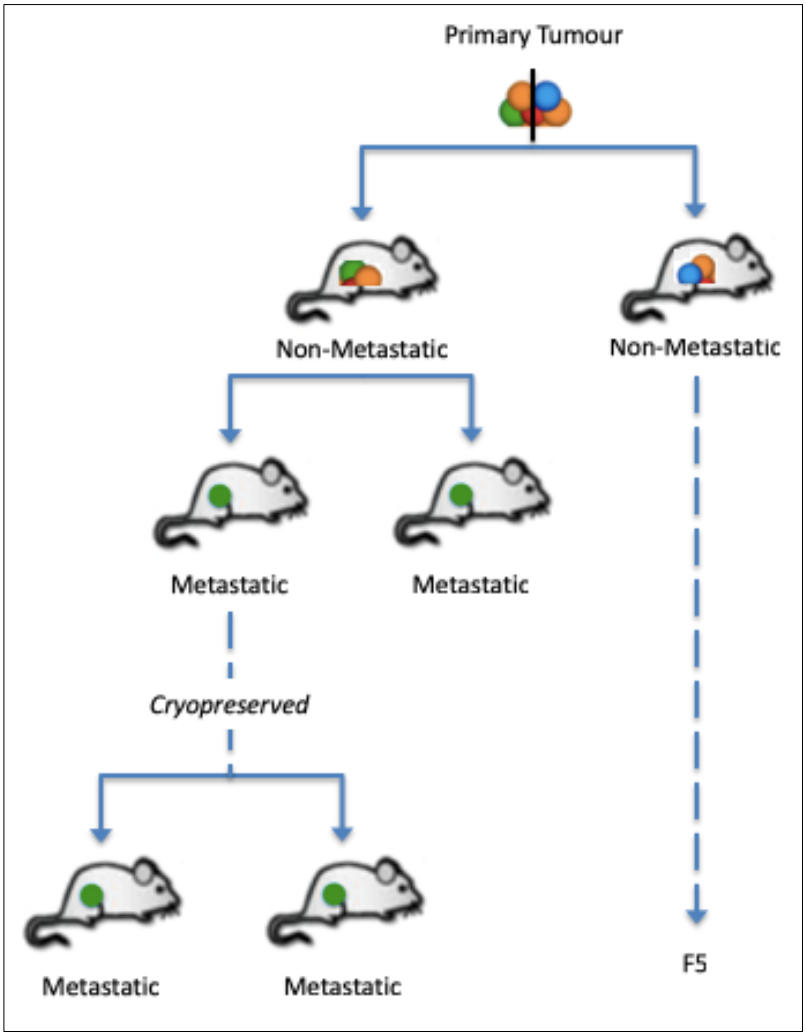

Figure 4-6 The evolution of both metastatic and non-metastatic IS076 sub clones

A phylogenetic tree detailing the evolution of both metastatic and non-metastatic clones from the IS076 PDTX line. The original patient tumour was divided and implanted intramuscularly into two mice. This led to the successful establishment of two separate PDTX lines. At the first passage, one line developed widespread metastases whilst the other line remained non-metastatic (up until the fifth generation of PDTX). The metastatic phenotype was maintained following a period of cryopreservation. The original patient tumour is represented by multiple different colours, each representing a different clone. The evolution of these clones through serial passaging is then shown, demonstrating one theory by which daughter xenografts can form with different phenotypes.

The metastases first became evident when mice developed rapid onset malignant ascites and required culling (Figure 4-7). In order to obtain a sterile sample of the malignant ascites, culled mice had their skin shaved and prepared with alcoholic iodine. Malignant ascites was then aspirated under aseptic conditions using a sterile 21-gauge needle attached to a 10ml syringe. The aspirate was then centrifuged and 1500 r.p.m. for 5 minutes and the pellet re-suspended in RPMI supplemented with 20% FCS and antibiotics (penicillin and streptomycin). The cell suspension was then plated into a T25 flask and left undisturbed for a period of 72 hours whilst being incubated at 37°C and 5% CO_2. Media was changed twice weekly over a period of six months. A cell line was successfully cultured using this technique and was termed IS076–A (for ascites). The original explant derived cell line was subsequently named IS076–P (for primary) in order to differentiate between the two sub clones. STR analysis confirmed that both IS076-A and IS076-P represent separate clones from the same original patient.

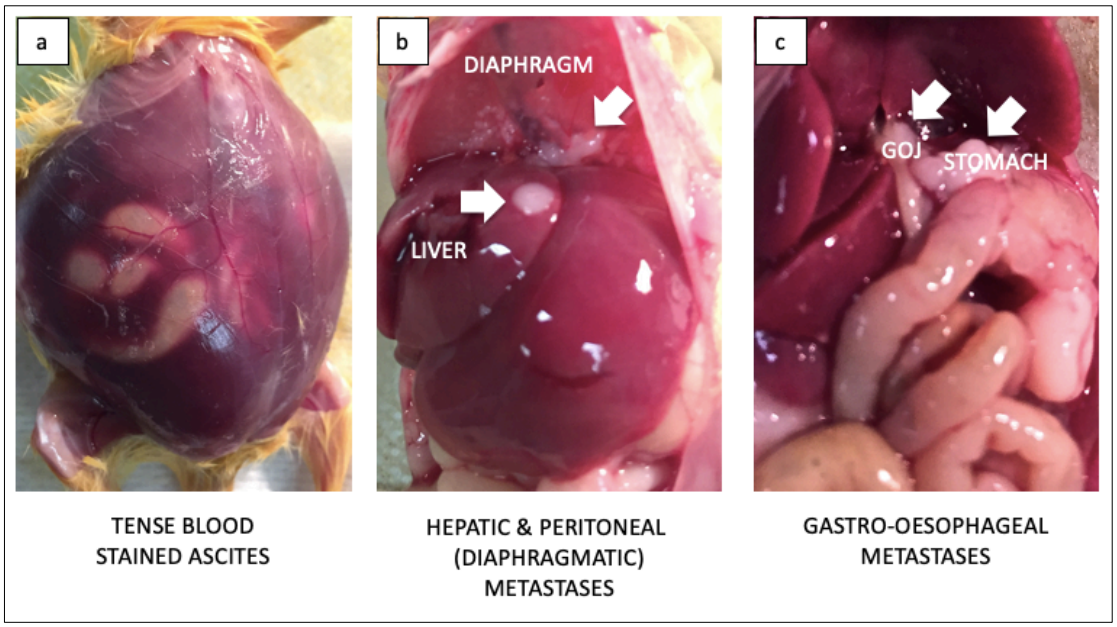

Figure 4-7 Evidence of metastasis formation within the PDTX model

Metastases from the IS076 metastatic sub clone were largely confined to the peritoneal cavity. At autopsy there was clear evidence of malignant, blood-stained ascites (a). There was also evidence of metastasis formation within the liver and surrounding diaphragmatic surface (b) as well as the gastro-oesophageal junction (c). Arrows indicate metastatic deposits.

Having separate metastatic and non-metastatic clones form the same patient presents a unique opportunity to study the metastatic process in OAC, especially given the limited availability of preclinical models that spontaneously metastasise. However, prior to using the models for the study of metastasis formation, it is essential that they undergo a thorough characterisation. Initial efforts to characterise these cell lines have involved performing both migration assays and western blots for known markers of epithelial to mesenchymal transition (EMT). Preliminary results demonstrated that the IS076-A was able to migrate much more readily in vitro compared to the IS076-P cell line. This effect was further heightened with the use of concentrated fibroblast conditioned media as the chemoattractant (Figure 4-8). This is in keeping with the preliminary results from a western blot analysis which revealed evidence of increased vimentin expression, a key regulator of EMT (Liu, Lin, Tang, & Wang, 2015), in the IS076-A cell line compared to the IS076-P cell line (Figure 4-9). However, given that these are only preliminary results, repeat experiments are required.

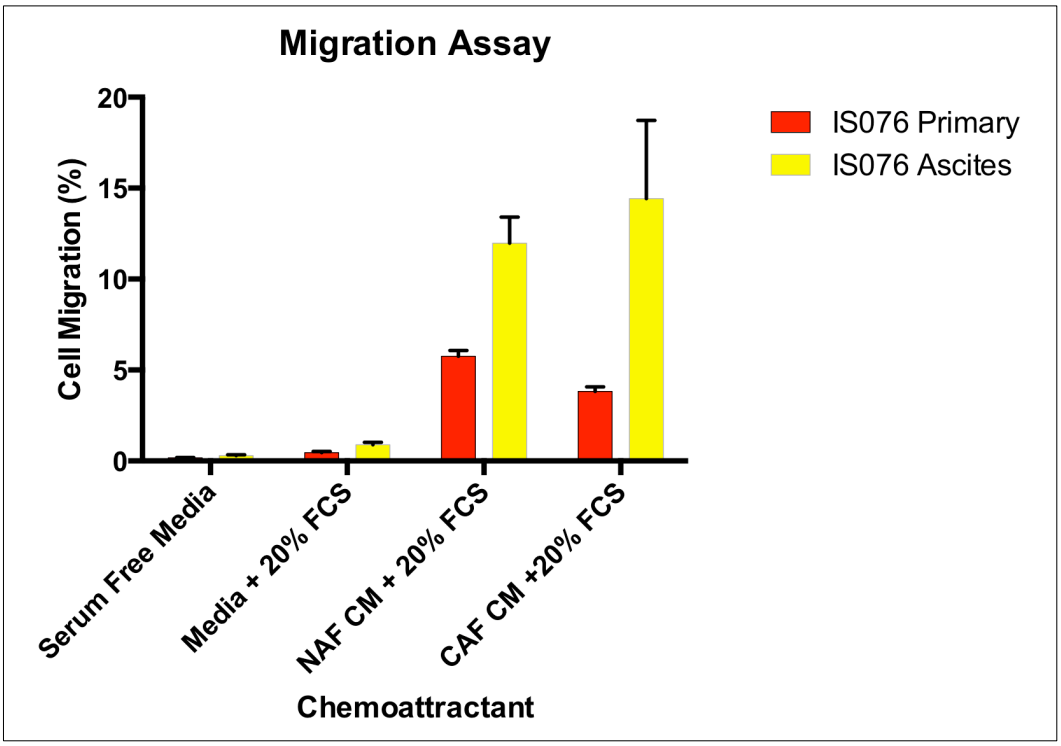

Figure 4-8 A comparison of cell lines IS076-A and IS076-P using an in vitro transwell migration assay

A transwell migration assay was used to assess the migratory ability of the metastatic (IS076-A) and non-metastatic (IS076-P) cell lines in vitro. 5×10^4 cells were pipetted into inserts containing an 8μm porous membrane. Lower chambers were filled with 150μl of varying chemoattractants (serum free media, media containing 20% FCS and both NAF and CAF conditioned media containing 20% FCS). Following 24 hours of incubation, the cells on the undersurface of the membrane were stained using calcein and imaged using a fluorescent reader. Cell numbers were determined from a standard curve of cell number to relative fluorescent unit. Cell migration is presented as a percentage based on the number of cells originally pipetted. Error bars = SEM, n=2.

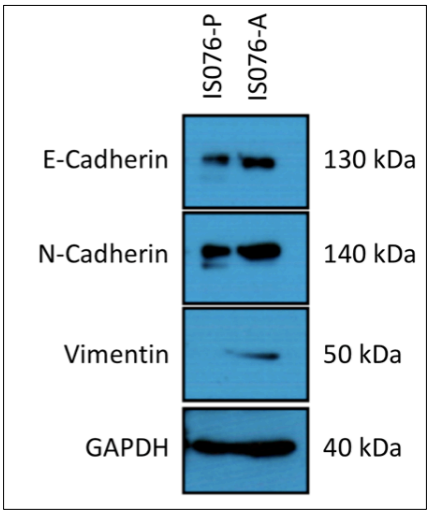

Figure 4-9 Western blot analyses of EMT

A western blots analysis comparing the EMT characteristics of cell lines IS076-A and IS076-P. Proteins are labelled alongside their associated densitometric analysis (normalised to GADPH).

4.2.7 *In vitro* morphology and growth characteristics

IS076-P, TB471, MA924 and ST913 all assumed an epithelial morphology *in vitro*. With the exception of the IS076-A cell line, they tended to form large cells that grew in colonies and were densely adherent, giving a cobblestone-like appearance (Figure 4-10). They initially grew as a monolayer, however, would start to grow in multiple layers once they became too dense. IS076-A, on the other hand, grew as smaller cells that were less adherent. Once established, cells became confluent every three to four days following a 1:4 split. All cell lines were initially cultured with RPMI supplemented with 20% FCS and antibiotics (penicillin and streptomycin). However, once established, media was transitioned to RPMI containing only 10% FCS and antibiotics.

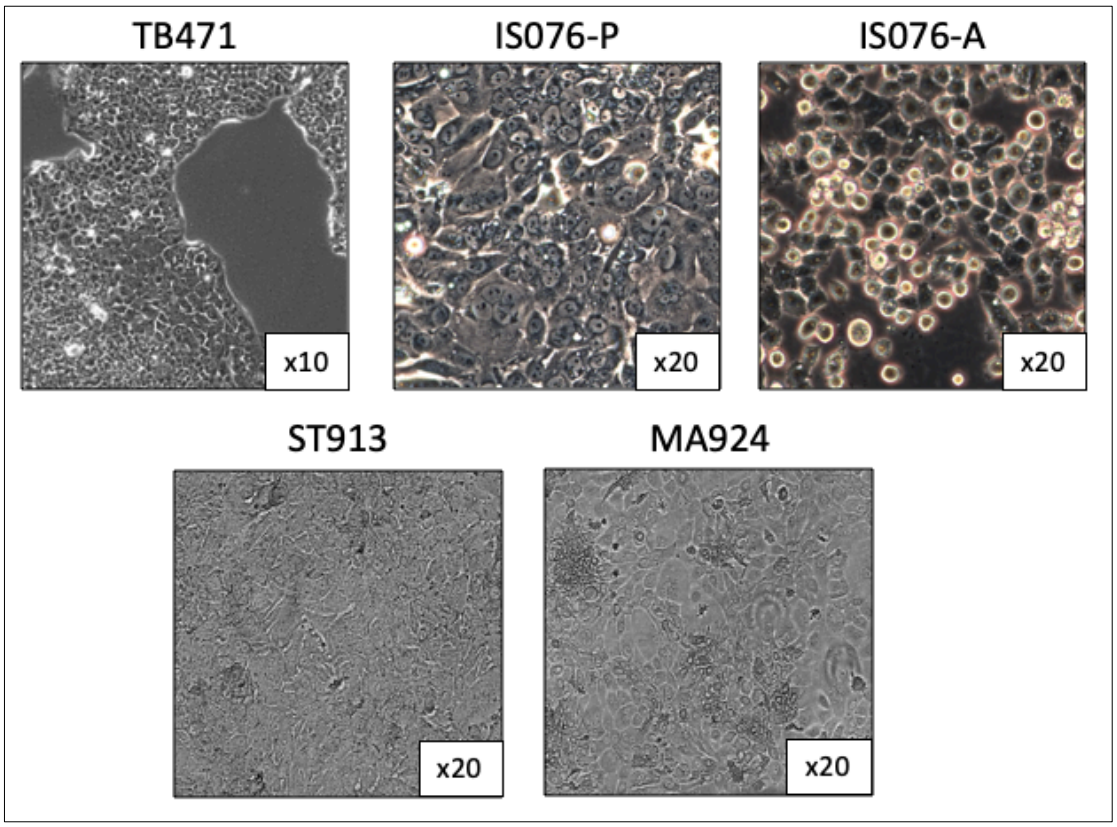

Figure 4-10 In vitro morphology of established xenograft-derived cell lines

The OAC lines TB471 and IS076-P both demonstrate a typical cobblestone appearance with cells growing closely together. In contrast, the IS076-A cells are much smaller and well-rounded in appearance. The SCC cell lines ST913 and MA924 both form a dense monolayer; however, the cells exhibit a more spindle-shaped appearance when compared to the adenocarcinoma cell lines.

4.2.8 Tumorigenic assay

Cell injection xenografts were successfully established from the OAC cell lines IS076-P, IS076-A and TB471 when injected subcutaneously into NSG mice. Whilst validation confirmed that tissue architecture was maintained between the original patient tumour and first-generation PDTX of IS076, the corresponding cell injection xenografts IS076-P and IS076-A failed to recapitulate the same degree of differentiation. However, IHC staining for the pancytokeratin AE1/AE3 demonstrated that both IS076-P and IS076-A cell injection xenografts were epithelial in origin (Figure 4-11).

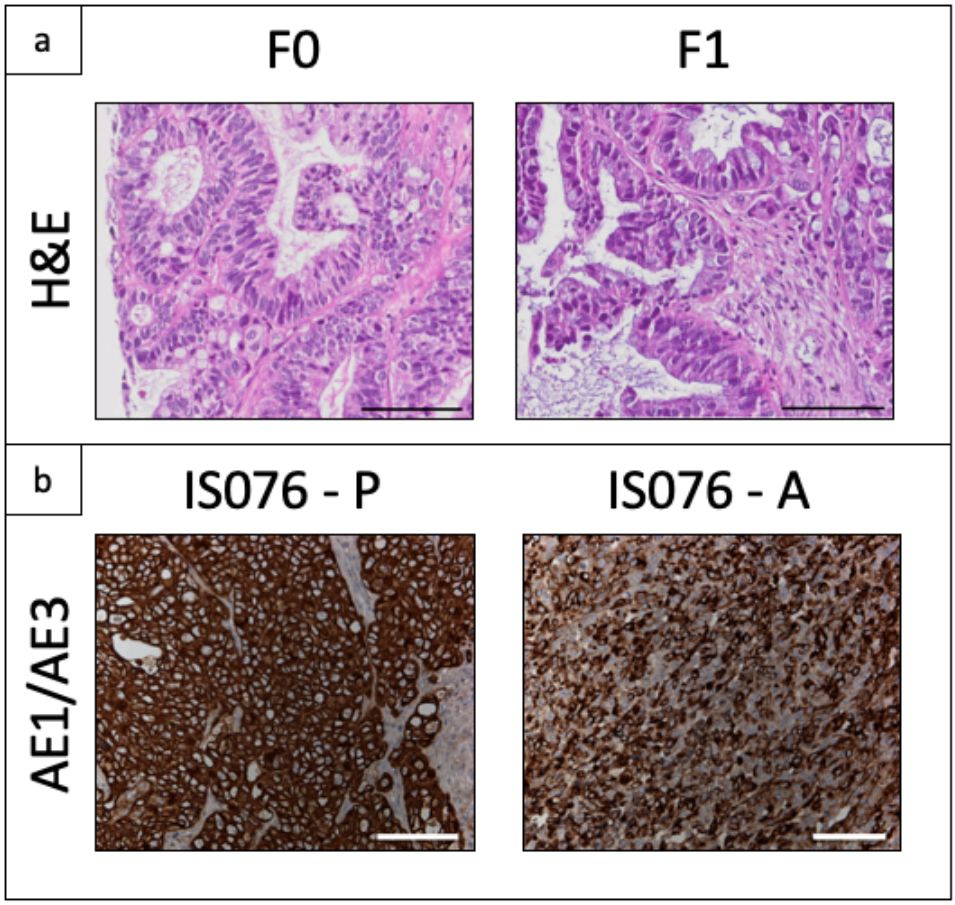

Figure 4-11 A comparison between the original patient tumour, first generation PDTX and cell injection xenografts of IS076

H&E staining of FFPE tissue comparing the original IS076 patient tumour to a first generation PDTX demonstrates maintenance of tissue architecture (a). IHC staining against the pan cytokeratin AE1/AE3 demonstrates that the cell injection xenografts derived from both IS076-P and IS076-A cell lines are epithelial in origin. Scale bars represent 100µm.

The TB471 cell injection xenograft, on the other hand, formed well-differentiated glandular structures that were filled with mucin (Figure 4-12). This was following 181 days of in vitro culture in order to establish a purified epithelial cell line and 98 days of in vivo culture following the injection of $5x10^6$ cell subcutaneously into an NSG mouse. This is consistent with the 226 days that it took to establish the first generation PDTX. This extended period of culture may be due to the fact the tumour was so well differentiated. In comparison, mice inoculated with the same amount of IS076 cells would form tumours much more rapidly, reaching ethical limits within 4 to 6 weeks.

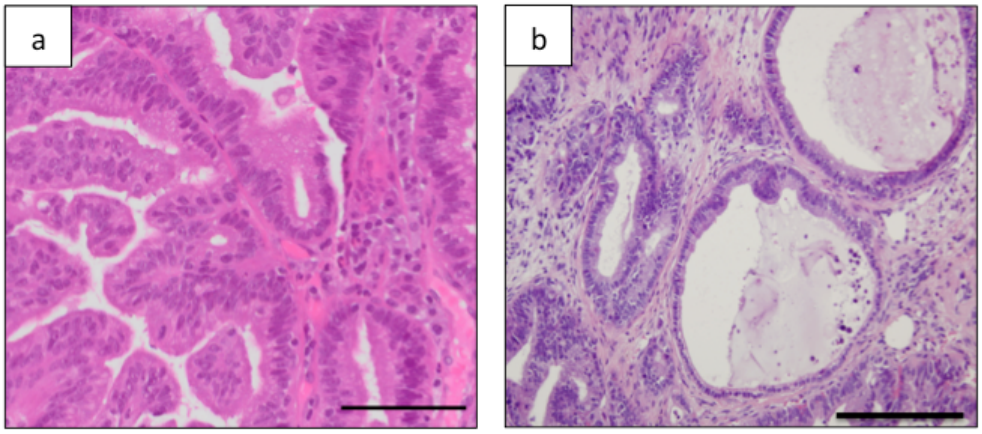

Figure 4-12 A comparison between the original patient tumour and cell injection xenograft of TB471

H&E staining of FFPE tissue comparing the original patient tumour TB471 (a) to a corresponding cell injection xenograft that had been in culture for eight weeks (b), demonstrating that tissue architecture is maintained. Both original tumour and cell injection xenograft display evidence of glandular formation and mucus production. Scale bars represent 100µm.

Given the metastatic tendency of the IS076 line, both the ascites and primary lines were transduced with eGFP / luciferase prior to injection, in order to assess for metastases. Results revealed that the IS076-A cell line maintained the metastatic phenotype of the parent PDTX and consistently formed metastases whilst the IS076-P cell line remained non-metastatic. Metastases predominately occurred in the liver, lung, gastroesophageal junction and omentum (Figure 4-13). Some mice also developed malignant ascites.

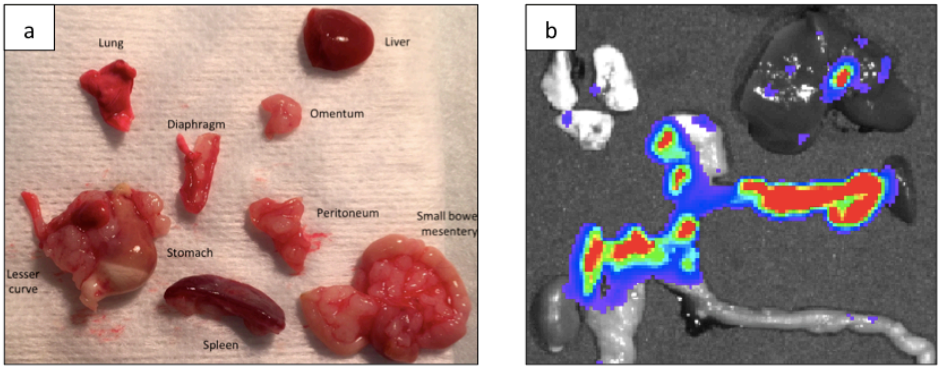

Figure 4-13 Assessing the metastatic burden from a cell injection xenograft derived from the IS076-A line

Individual organs have been displayed following the necropsy of a mouse harbouring a cell injection xenograft derived from the IS076-A cell line transduced with eGFP / luciferase (a). Ex vivo bioluminescence imaging confirms the presence of metastases (b).

4.2.9 Validation of xenograft-derived cell lines

STR analysis confirmed that all PDTXs and established cell lines originated from their corresponding original tumours and that no contamination had occurred (Table 4-2). Targeted sequencing using a panel of known oncogenes (Table 2-10) confirmed that the majority of mutations and variants are maintained across the range of PDTX and cell lines compared to the original patient tumour (Table 4-3). However, there is evidence that mutations can accumulate through the successive passage of xenografts, as seen with the acquisition of KRAS variants in the PDTXs of TB471, MA924 and ST913. Another example of accumulation is seen with the ST913 cell line that demonstrates evidence of a KIT variant that is not evident in the original tumour. There is also evidence that some cell lines fail to demonstrate all the mutations seen within the original patient tumour, such as in IS076-P with the loss of the CDKN2A mutation. This may be due to the fact that the cell line was derived from a clone lacking that mutation.

.

Table 4-2 STR analysis of original patient tumours (F0) and xenograft-derived cell lines

	STR locus															
	AMEL	CSF1PO	D13S317	D16S539	D18S51	D21S11	D3S1358	D5S818	D7S820	D8S1179	FGA	Penta D	Penta E	TH01	TPOX	vWA
IS076 F0	X,Y	10, 12	12, 14	12, 13	13, 16	30, 32.2	15, 16	11, 12	10, 11	12, 13	19, 20	11, 12	7, 8, 16	9, 9.3	8, 11	16, 18
IS076-P	X	10	14	12, 13	13	32.2	16	11	10, 11	12, 13	19, 20	12	8	9, 9.3	8, 11	16
IS076-A	X	10	14	13	13	32.2	15	11	10	12, 13	19, 20	12	8	9.3	11	16
TB471 F0	X, Y	11, 12	12, 13	12		28, 29		12	8, 9					9.3	8, 9	18, 19
TB471 CELL LINE	X	11	12	12		28, 29		12	9					9.3	8, 9	18, 19
MA924 F0	X	10, 13	12	10, 11		28		11, 12	8, 12					9	8	18, 19
MA924 CELL LINE	X	10, 13	12	10, 11		28		11, 12	8, 12					9	8	18, 19
ST913 F0	X, Y	10, 12	8, 11	9, 10		28, 31		12	9, 10					7, 9	8, 11	14, 19, 20
ST913 CELL LINE	X	10, 12	8, 11	10		28, 31		12	9, 10					7, 9	8, 11	14, 19, 20

Table 4-3 The mutation profiles of the original patient tumours (F0), PDTXs (Fx) and derived cell lines from IS076, TB471, MA924 and ST913

Sample ID	Gene	HGVSg	Consequences
IS076 F0	AKT1	chr14:g.105246462G>T	missense_variant
	TP53	chr17:g.7577142C>T	missense_variant
	CDKN2A	chr9:g.21971120G>A	stop_gained
IS076 F4	AKT1	chr14:g.105246462G>T	missense_variant
	TP53	chr17:g.7577142C>T	missense_variant
	CDKN2A	chr9:g.21971120G>A	stop_gained
CELL LINE IS076-P	AKT1	chr14:g.105246462G>T	missense_variant
	TP53	chr17:g.7577142C>T	missense_variant
TB417 FO	TP53	chr17:g.7578526C>A	missense_variant
TB417 F3	KRAS	chr12:g.25380344A>G	splice_region_variant,synonymous_variant
	TP53	chr17:g.7578526C>A	missense_variant
CELL LINE TB417	TP53	chr17:g.7578526C>A	missense_variant
MA924 F0	TP53	chr17:g.7578517G>A	missense_variant
	TP53	chr17:g.7577548C>T	missense_variant
MA924 F5	KRAS	chr12:g.25380344A>G	splice_region_variant,synonymous_variant
	TP53	chr17:g.7578517G>A	missense_variant
	TP53	chr17:g.7577548C>T	missense_variant
CELL LINE MA924	TP53	chr17:g.7578517G>A	missense_variant
	TP53	chr17:g.7577548C>T	missense_variant
ST913 FO	TP53	chr17:g.7578266T>A	missense_variant
ST913 F2	KRAS	chr12:g.25380344A>G	splice_region_variant,synonymous_variant
	TP53	chr17:g.7578266T>A	missense_variant
CELL LINE ST913	KIT	chr4:g.55599361G>C	splice_region_variant,intron_variant
	TP53	chr17:g.7578266T>A	missense_variant

HGSVg, genomic sequence variation.

Additional IHC staining was also performed on the IS076 lines to ensure that they were derived from the original patient's oesophageal cancer and not the synchronous colorectal cancer. This was performed using MLH1 and PMS2 in order to differentiate between the two tumours based on their microsatellite instability profile, as these proteins were the only ones to be differentially expressed between the two tumours (Table 4-4). Results revealed that both the metastatic and non-metastatic clones from the IS076 line PDTX both express the proteins MLH1 and PMS2, which were absent in the synchronous colorectal cancer (Figure 4-14).

Table 4-4 A comparison between the MMR protein expression of the original colon cancer versus the original OAC of patient IS076

COLON CANCER	OAC
MLH1 -	MLH1+
PMS2 -	PMS2+
MSH2+	MSH2+
MSH6+	MSH6+

protein not expressed; + protein expressed.

N.B. As the colonic cancer was unavailable for research purposes these results are based on the clinical pathology report.

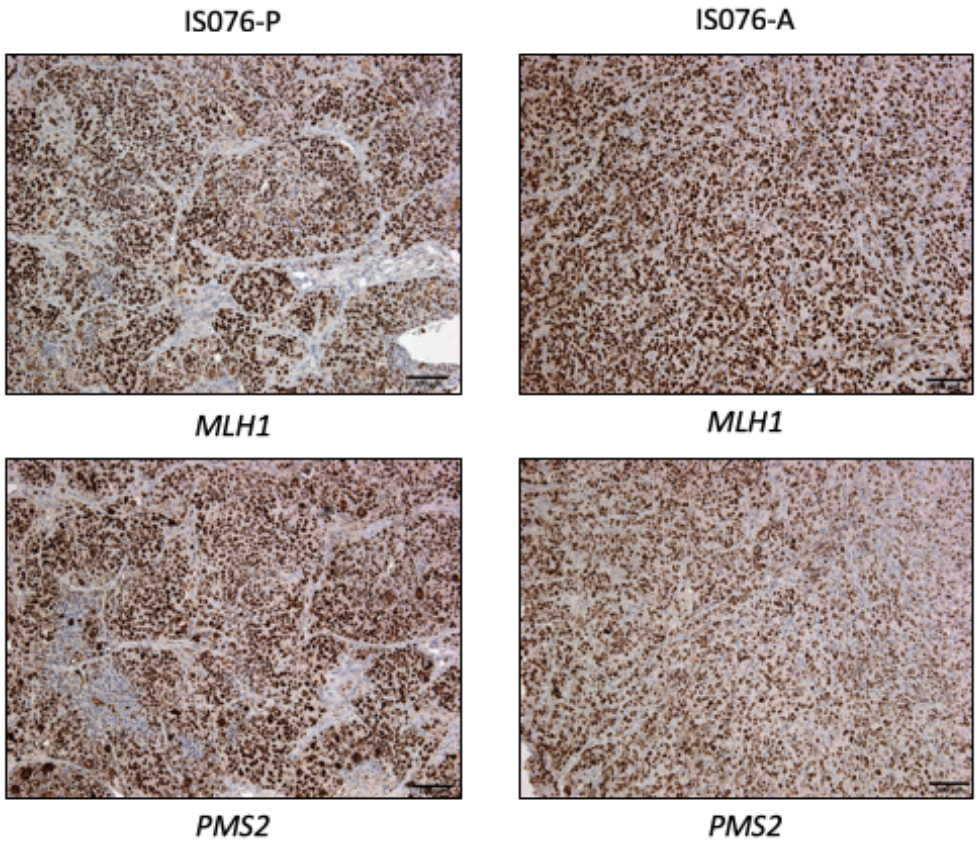

Figure 4-14 IHC profile of key MMR proteins within cell injection xenografts derived from cell lines IS076-A and IS076-P

The expression of both MLH1 and PMS2 within cell injection xenografts derived from both IS076-A and IS076-P matches the profile of the original OAC and not the synchronous colon cancer (image not shown). Scale bars represent 100µm.

4.2.10 In vitro assessment of putative stem cell markers

The cell line TB471 was also assessed *in vitro* for the presence of the putative CSC markers CD44, CD133 and Lgr5. The results from this analysis revealed a broad expression of both CD44 and Lgr5 across the entire cell population, with CD44 (Figure 4-15) being expressed almost uniformly amongst all of the cells whilst Lgr5 (Figure 4-16) was expressed by approximately 50% of the cells. In comparison, CD133 (Figure 4-17) appeared to be more specific, as it was expressed by only a minority of cells, in keeping with a potential CSC population (Kemper, Prasetyanti, De Lau, Rodermond, Clevers et al., 2012).

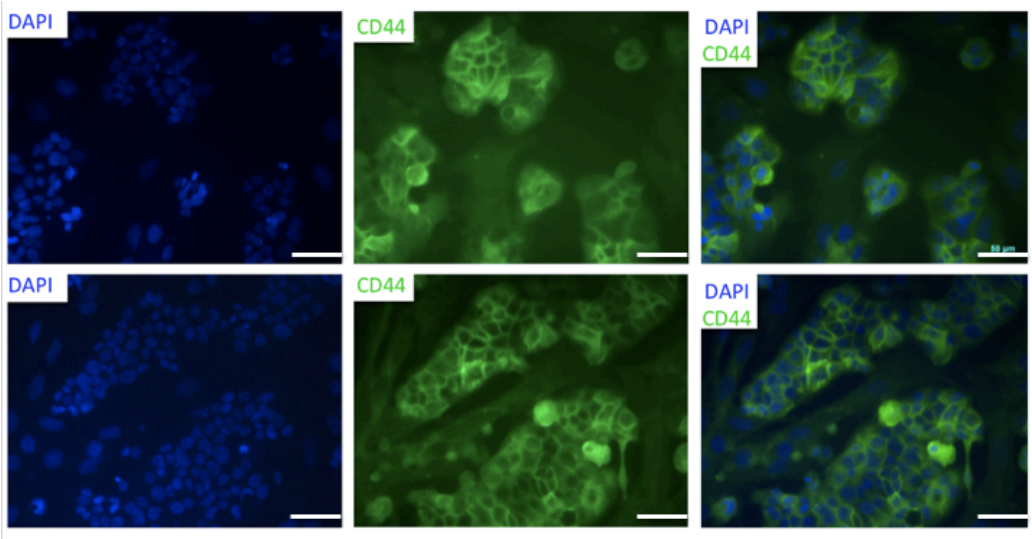

Figure 4-15 In vitro expression of the putative CSC marker CD44

Indirect immunofluorescence micrographs of the TB471 cell line following standard 2-dimensional in vitro culture. Nuclei have been stained with DAPI and are shown in blue. CD44 positive cells have been labelled using an anti-CD44 antibody and subsequently stained using a fluorescently labelled secondary antibody. Scale bars represent 50µm. Image courtesy of A. Farley, Pera Laboratory, The University of Melbourne.

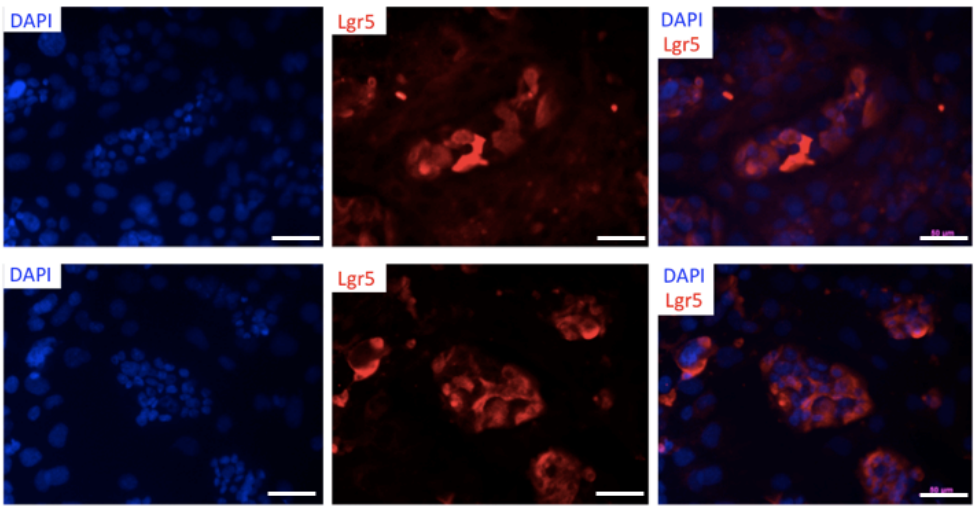

Figure 4-16 In vitro expression of the putative CSC marker Lgr5

Indirect immunofluorescence micrographs of the TB471 cell line following standard 2-dimensional in vitro culture. Nuclei have been stained with DAPI and are shown in blue. Lgr5 positive cells have been labelled using an anti-Lgr5 antibody and subsequently stained using a fluorescently labelled secondary antibody. Scale bars represent 50µm. Image courtesy of A. Farley, Pera Laboratory, The University of Melbourne.

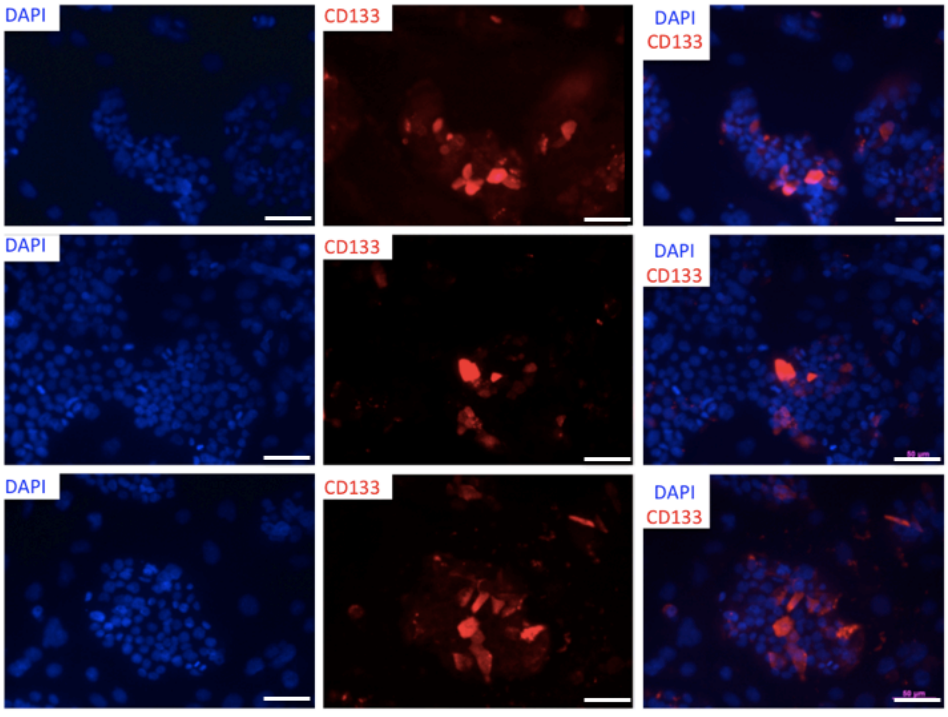

Figure 4-17 In vitro expression of the putative CSC marker CD133

Indirect immunofluorescence micrographs of the TB471 cell line following standard 2-dimensional in vitro culture. Nuclei have been stained with DAPI and are shown in blue. CD133 positive cells have been labelled using an anti-CD133 antibody and subsequently stained using a fluorescently labelled secondary antibody. Scale bars represent 50µm. Image courtesy of A. Farley, Pera Laboratory, The University of Melbourne.

4.2.11 Discovery of a lymphoma-derived cell line

One of the first cell lines to be successfully generated using the explant technique was derived from patient RF226. Unfortunately, as was highlighted in section 3.5, validation of this line confirmed that the PDTX from which it had originated had transformed into a human B-cell lymphoma whilst being cultured in an immunodeficient setting. As a result of this transformation, the RF226 cell line grew as spheres in suspension, in keeping with a lymphoma cell line (Figure 4-18). This is in contrast to the other oesophageal cancer cell lines that were generated, which were all attachment dependent. The cells within these spheres demonstrated rapid proliferation and a tendency to fuse with each other.

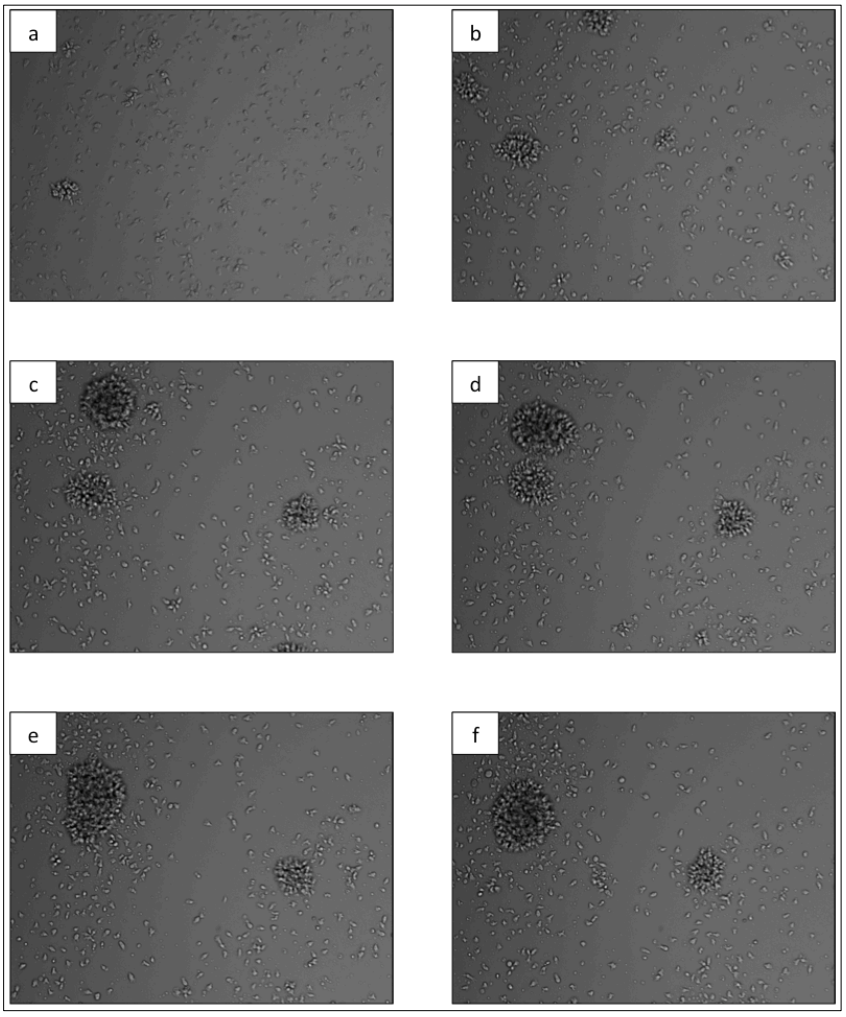

Figure 4-18 In vitro morphology of a lymphoma derived cell line

A sequence of time lapse images captured over a 12-hour period detailing the formation of spheres in a lymphoma derived cell line (panels a and b). Individual tumour cells initially divide and clump together in order to form small spheres. Once established, small spheres then fuse with other spheres in order to form larger spheres (images c to f).

4.2.12 Application of the cell line model for the preclinical assessment of a novel therapeutic target

One of the main applications of the cell line model is as a preclinical tool for the evaluation of novel therapeutic targets. As a proof of concept, the IS076-A cell line was used to test the effect of BMP inhibition in the management of OAC. This is based on evidence suggesting that activation of the BMP pathway is required for the development of both BO and OAC (Clemons et al., 2013; Milano et al., 2007). Through a collaboration with Professor Krishnadath, from the Academic Medical Center (AMC) in Amsterdam, a pilot experiment was performed in order to assess the effect of BMP inhibition in cell injection xenografts with high BMP expression, using newly generated anti-BMP llama-derived antibodies (Calpe et al., 2016; Calpe et al., 2015). The results from this experiment were extremely encouraging. When BMP inhibitors were administered as a single agent, tumour growth inhibition was similar that to that observed with standard chemotherapy. When both treatments were combined, this effect was further increased (Figure 4-19). In a subsequent experiment, the effect of BMP inhibition alone and in combination with cisplatin was also tested on a cell line lacking BMP expression. These results revealed that BMP inhibition had no effect on tumour growth (data not shown). However, in order to determine the significance of these preliminary findings, these experiments need to be repeated using additional models in order to determine if the results are reproducible. Complementing these in vivo studies, in vitro studies may also be required to determine the mechanisms responsible for any observed effects. These results may then form the basis of future clinical studies.

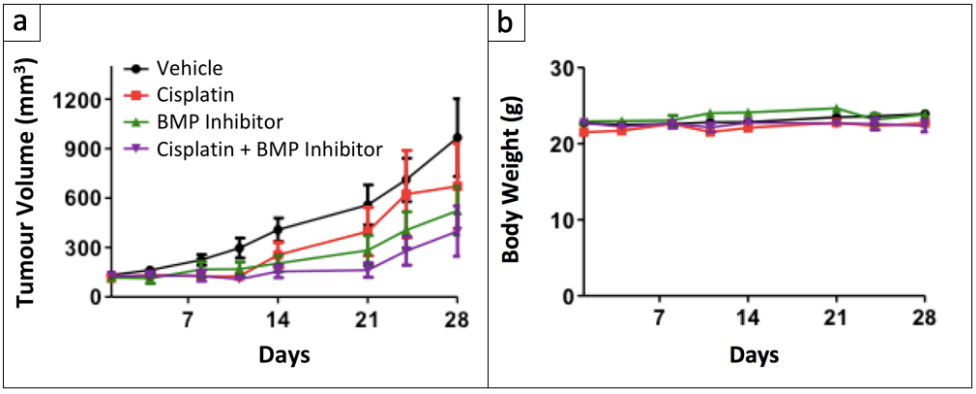

Figure 4-19 Assessing the effect of BMP 2 and 4 inhibition in combination with cisplatin on a PDTX with high BMP expression

Four separate cohorts of mice bearing cell injection xenografts (five per cohort) were established following the subcutaneous injection of 1×10^6 IS076-A cells. Once tumours reached a volume of 100mm^3 mice were randomised to receive either 2mg/kg of cisplatin weekly or 100 µg daily of combined BMP 2/4 inhibitor each via intraperitoneal injection. Tumour growth is shown in panel a and mean body weight as a surrogate marker of toxicity in panel b. Results represent a single experiment. Error bars = SEM.

4.2.13 Summary

In total, attempts at cell line generation were made using ten out of the 24 different patient lines (or their associated xenografts). These are summarised in Table 4-5. The first two attempts (ID 1 and ID 2) were based on the digestion of primary tissue and were both unsuccessful. Following this, multiple unsuccessful attempts were also made at establishing cell lines from FACS sorted xenograft derived cells (ID 8, 10 and 18). The remaining attempts were all based on the explant technique using PDTXs as the source of tissue (ID 14, 21, 22, 23 and 24). These attempts were all associated with the successful generation of cell lines. In the case of IDs 21, 23 and 24, these PDTXs were all derived from treatment naïve endoscopic biopsies at the time of diagnosis. Unfortunately, validation confirmed that ID 14 had undergone lymphomagenic transformation. Within this series, the selection of tissue for cell line generation (either primary tumour or PDTX) was simply determined based on tissue availability. The type of technique for the generation of an in vitro cell line continued to evolve until a cell line was successfully generated. Once the explant technique proved to be successful, all subsequent lines were derived using this technique. In total, cell line generation was attempted from ten different lines using the multiple different techniques previously described. The explant technique using PDTX tissue proved to be the most robust, with four of the five attempted lines yielding an epithelial cell line following validation.

Table 4-5 Attempted cell line generation and success rate for each individual patient line

					Therapy prior to implantation		Technique			Engraftment Post	Cell Line
ID	Site	Type	Grade	Tissue Source	CT	RT	IM	SC	Mouse Strain	Cryopreservation	Generated
1	GOJ	AC	Poor	Resection	Y	N	1/4	0/2	SCID	2/2	N
2	GOJ	AC	Poor	Resection	Y	Y	1/2		SCID	2/2	N
3	GOJ	AC	Mod	Resection	Y	N		0/4	NOD SCID		
4	Oesophageal	AC + NE	Mod	Biopsy	N	N	2/2		NSG	2/2	
5	Oesophageal	AC	Mod to Poor	Biopsy	N	N	1/2		NOD SCID	0/1	
6	Oesophageal	AC	In-situ	Biopsy	N	N	1/2	0/1	NSG		
7	Oesophageal	SCC	Mod	Biopsy	N	N	1/1		NSG		
8	Oesophageal	AC	Mod	Biopsy	N	N	1/1		NSG		N
9	Oesophageal	AC	Mod	Biopsy	N	N	1/1#	0/1	NSG	1/1	
10	Oesophageal	AC	Mod	Biopsy	N	N	2/2	1/2	NSG	1/1	N
11	Oesophageal	SCC	Poor	Biopsy	N	N	2/2		NSG	1/1	
12	Oesophageal	SCC	Mod	Resection	N	N	1/1		NSG		
13	PM from GOJ	AC	Mod to Poor	Resection	N	N	1/2		NSG		
14	Oesophageal	AC	Poor	Resection	Y	N	1/3		NSG		Y
15	GOJ	AC	Mod	Biopsy	N	N	2/3		NSG		
16	Oesophageal	AC	Poor	Resection	N	N	1/2*		NSG		
17	Oesophageal	SCC	In-situ	Biopsy	N	N	1/1	0/1	NSG		
18	Oesophageal	AC	Mod	Biopsy	N	N	1/2		NSG		N
19	Oesophageal	AC + NE	Poor	Biopsy	Y	N	3/4		NSG		
20	**Oesophageal**	**AC**	**Poor**	**Biopsy**	**Y**	**N**	**1/2**		**NSG**		
21	**Oesophageal**	**AC**	**Mod**	**Biopsy**	**N**	**N**	**1/3**		**NSG**		**Y**
22	**Oesophageal**	**AC**	**Poor**	**Resection**	**N**	**N**	**2/2**		**NSG**	**1/1**	**Y**
23	**Oesophageal**	**SCC**	**Poor**	**Biopsy**	**N**	**N**	**2/2**		**NSG**		**Y**
24	**Oesophageal**	**SCC**	**Poor**	**Biopsy**	**N**	**N**	**1/2**		**NSG**		**Y**

*Abbreviations: IM, intramuscular; SC, subcutaneous; GOJ, gastro-oesophageal junction; PM, peritoneal metastasis; AC, adenocarcinoma; NET, neuroendocrine tumour; SCC, squamous cell carcinoma; CT, chemotherapy; RT, radiotherapy; Y, yes; N, no; no entry, not attempted. Colours: Green, successful; Yellow, lymphomagenic transformation; Red, unsuccessful. * Mixed epithelial component # Transformation occurred at second passage. Entries in bold represent xenografts that were generated following the publication of the original series (Read et al., 2016).*

4.3 Discussion

Drawing on the success of the IM PDTX technique (Read et al., 2016), this chapter highlights the development of a robust technique for the establishment of xenograft-derived cell lines. This has culminated in the development of four matched PDTX and cell line models, one of which having both metastatic and non-metastatic clones. Such a development is a significant advancement, particularly in the field of OAC, which has been limited by a paucity of well-validated cell lines. The successful generation of cell lines in this series is based upon two key principles. The first is the use of the PDTX to enrich for viable tumour cells and provide a renewable source of tumour tissue. The second is the use of the explant technique. By providing an initial bed of fibroblasts, this technique appears to be much more robust and reproducible compared to the use of single cell suspensions. The explant technique itself has long been used in the development of cell lines (Giard et al., 1973).

Historically, OAC cell lines have been extremely difficult to generate. This is thought to be due to the limited availability of treatment naïve tissue, which is usually obtained at the time of diagnosis in the form of small endoscopic biopsies that contain varying amounts of viable tumour. For instance, biopsies taken from the centre of a tumour, may potentially contain necrotic tissue (as the centre of tumours are frequently necrotic). Biopsies taken from the periphery of the tumour also have the potential to contain surrounding non-malignant tissue. In both of these instances the proportion of viable tumour cells available for cell line generation is diminished. Obtaining tumour tissue from surgical resection specimens also has its limitation, as tumours have typically been treated with neoadjuvant therapy (chemotherapy +/- radiotherapy). As up to 82% of tumours have been reported to exhibit either a complete or partial response to neoadjuvant treatment (van Hagen et al., 2012), this can also have a significant effect on the proportion of viable tumour cells within a specimen. Within this series, three of the four patients from which cell lines were generated underwent a complete pathological response to neoadjuvant therapy. This highlights the importance of being able to use treatment naïve tissue for the generation of both PDTXs and subsequent cell lines. Given that IM PDTXs are more easily established from primary tissue than primary cell lines (14/19 vs 0/2), it seems logical to use the IM PDTX model to ensure the ongoing culture of tumour cells (Read et al., 2016). This may be due to the fact that the cells remain in an in vivo environment and do not have to adapt to the stress of in vitro culture. Drawing on the ability of the PDTX model to enrich for viable tumour cells, I have demonstrated that it is much

more efficient to produce cell lines from PDTX material than from primary tumour tissue. This finding is consistent with the generation of cancer cell lines from other cancers such as colorectal cancer (Dangles-Marie, Pocard, Richon, Weiswald, Assayag et al., 2007).

In this chapter, multiple different techniques for the generation of xenograft-derived cell lines were trialled. However, all of the techniques that were based on the generation of a single cell suspension were unsuccessful. This is likely due to the fact that epithelial cells are dependent on neighbouring cells, including the stroma. Trying to grow such cells in isolation requires highly augmented conditions. As such, the success of the explant technique may be related to the presence of fibroblasts. From observation, it was evident that tumour cells required a bed of fibroblasts in the early stages of culture to facilitate attachment. However, it is not clear from this study if this was due to secreted factors from the fibroblasts or a contact dependent phenomenon. It was only after an extended period of adaptation, of up to six months, that tumour cells were able to grow on their own.

Having matched PDTX and xenograft-derived cell lines provides an extremely powerful tool as it harnesses the strengths of both models. Compared to cell lines, which tend to be clonal, PDTX recapitulate the heterogeneity of the original tumour to a much greater degree. Early passage xenografts also maintain original stromal elements, which are known to play a key role in tumour biology (Tentler et al., 2012). However, cell lines have the advantage of being much more manipulable and conducive to mechanistic studies.

This study also provides an additional metastatic model, which is rare in the field of OAC. This is despite the fact that oesophageal cancer readily metastasises in the patient, and that the majority of deaths related to oesophageal cancer are due to metastatic disease. This may be due to a number of reasons. Firstly, tumour tissue collected for research purposes is usually collected from the primary tumour in patients being treated with curative intent as opposed to metastatic deposits, as those patients are typically being treated with palliative intent. Therefore, the tumour may not have evolved sufficiently to metastasise. Secondly, the metastatic potential of a cell line may be influenced by the microenvironment at the site of injection (typically subcutaneously). Finally, metastasis formation may be a function of time and may not occur (or be detectable) prior to mice needing to be culled for ethical considerations.

The only other truly metastatic cell line is a sub clone of FLO-1 (Liu, Hoefnagel, et al., 2016). Other metastatic models, such as that published by Gros et al. (2010), simply represent pseudo-metastatic models, as tumour cells are directly injected into the tail veins of mice and disseminate immediately. This enables metastases to form without cells having to undergo the initial process of EMT. Like Liu et al. (2016), we have been able to isolate a clone that has increased metastatic potential, and which demonstrates progression through EMT. Of particular note, the metastases that form recapitulate what we see in the patient, despite the heterotopic injection site. Metastases form in the liver, lung, peritoneal cavity and around the GOJ nodes. Having two clones from the same patient, one being reproducibly metastatic and the other not, provides a very powerful tool to investigate tumour biology with regards to metastasis formation.

This study also highlights the importance of validation of both PDTX and xenograft-derived cell lines, as one of the PDTXs from which a cell line was generated in this series had undergone lymphomagenic transformation. This is a phenomenon that we recently reported and has been reported to occur in up to 68% in some xenograft series (Read et al., 2016). This is of particular importance in the field of OAC, where the availability of suitable preclinical models is limited. Recent studies have also revealed that misidentification or contamination, especially when occurring at the source laboratory, can have significant downstream consequences (Alvarez et al., 2008). In the case of OAC, data from the use of misidentified cell lines has been used in over 100 publications and 11 patents and formed the basis of a number of clinical trials (Boonstra et al., 2010). Fortunately, validation of the remaining cell lines established in this study confirms that they are of epithelial origin and originate from their respective patients.

The diverse mutational profile that exists within OAC has proven to be a major barrier to research. In addition, OAC is characterised by both intra and inter-tumour heterogeneity. As a result, the few cell lines that are available to researchers fail to model the entire genetic landscape. It is therefore essential that we generate additional cells lines, each with their unique mutational profile, in order to better model this genetically diverse disease.

In summary, we have successfully generated and validated four additional esophageal cancer cell lines (two adenocarcinoma and two SCC) with matched PDTXs, creating powerful tools for cancer research. Of note, we have also generated corresponding metastatic and non-metastatic cell line clones from a single xenograft line. The combination of these models provides a significant advance to the types of preclinical models available for oesophageal cancer, in particular adenocarcinoma. It is hoped that these models will aid in the study of cancer biology and the development of novel treatments.

Chapter 5 The development & validation of preclinical models of both normal human oesophageal epithelium and BO

5.1 Introduction

Current evidence suggests that BO develops as a result of a complex interplay between molecular genetics, cellular interactions and environmental exposures (Krishnadath et al., 2015). Due to these complexities, researchers have been unable to develop the ideal model system with which to study the disease process (Nakagawa, Whelan, & Lynch, 2015). As previously stated, the ideal model system should produce a 3-dimensional epithelial layer, be both reproducible and manipulable, and allow for environmental exposures. Most importantly, however, it needs to contain all of the essential cellular elements required for the development of metaplasia (Read et al., 2018). This is extremely challenging given that the Barrett's cell of origin has not yet been identified (Rhee & Wang, 2018). Two models, however, have the potential to fulfil a number of these prerequisites.

The first is an *in vivo* tissue reconstitution system known as the hat chamber model. In this model, a culture system is implanted onto the dorsal fascia of an immunocompromised mouse (Figure 5-1). The hat chamber model was originally used for the study of epidermal regeneration (Maas-Szabowski, Fusenig, & Stark, 2005; Worst, Mackenzie, & Fusenig, 1982). It was later optimized for the study of oesophageal epithelium (Croagh, 2006). In theory, it enables the establishment of a 3-dimensional epithelial layer, is manipulable and allows for environmental exposures. In a series of experiments, epithelium was reconstituted from suspensions of oesophageal keratinocytes that were obtained from the digestion of fresh oesophageal tissue (Figure 5-2). Like the original human tissue, the reconstituted epithelium formed a three-dimensional stratified squamous epithelium that contained both basal, and papillary regions and expressed the same IHC profile. Staining against human mitochondria also confirmed that the tissue was of human origin (Figure 5-3). However, unlike the native tissue, the reconstituted epithelium also contained a keratinized layer. Whilst preliminary experiments demonstrated the model's feasibility, its application was limited due to issues with chamber fixation and cell containment, leading to an overall success rate of less than 20% (4/21).

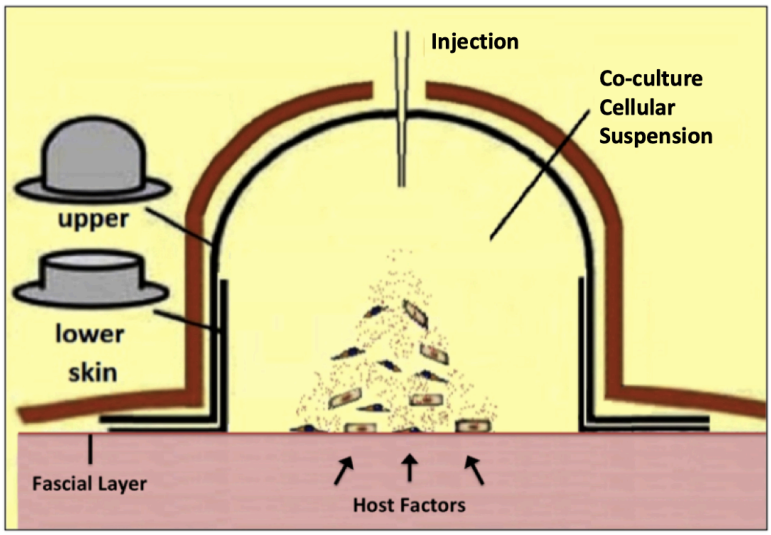

Figure 5-1 A diagrammatic representation of the silicone hat chamber model

The lower component is initially placed on the dorsal fascia of a mouse before the upper component (or hat) is fitted. The skin is then closed over the device leaving a small aperture to enable easy access via injection. Once positioned, a cellular suspension is then injected into the chamber.

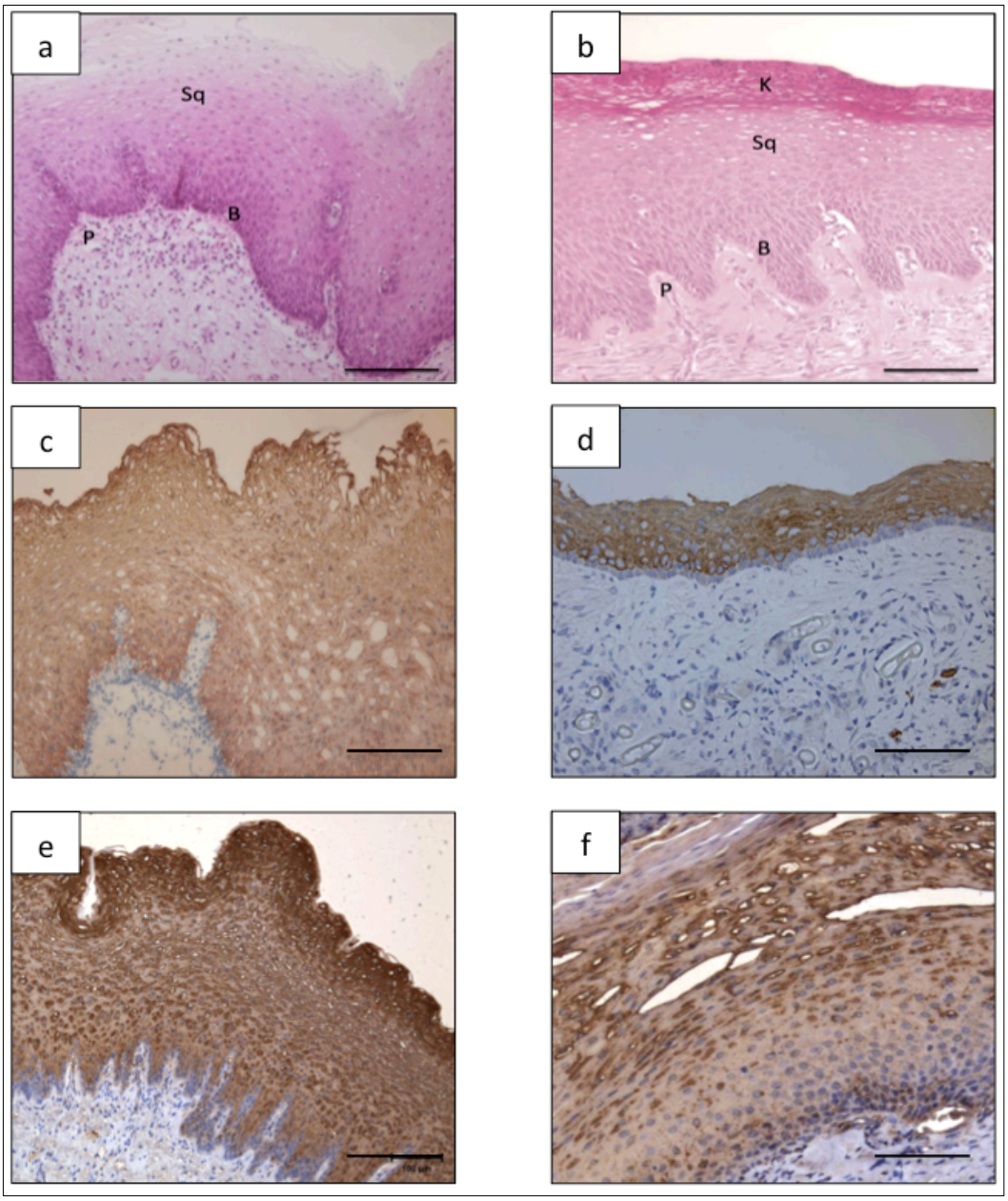

Figure 5-2 A comparison between normal human oesophageal squamous epithelium and epithelium cultured within the hat chamber system

H&E staining of normal human oesophageal squamous epithelium (a) versus squamous epithelium cultured within the hat chamber system (b). Both specimens consist of stratified squamous epithelium (Sq) comprised of both basal (B) and papillary (P) regions. The tissue cultured within the hat chamber also consists of a keratinised (K) layer. Epithelium cultured within the hat chamber also demonstrates similar IHC profiles for antibodies against both CK4 and involucrin, a marker of terminal differentiation. Image c represents staining against CK4 of normal human oesophageal squamous epithelium which is compared to epithelium cultured within the hat chamber in image d. Image e represents staining against involucrin of normal human oesophageal squamous epithelium compared to epithelium cultured within the hat chamber seen in image f. Scale bars represent 100µm (Modified from Croagh, 2006).

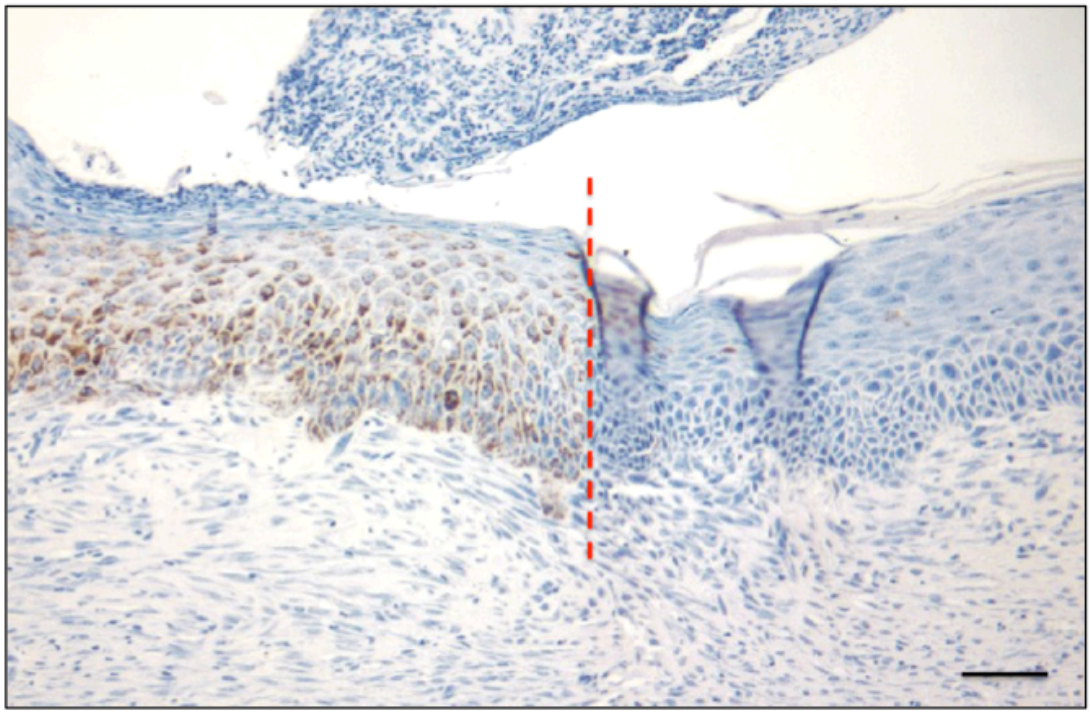

Figure 5-3 Epithelium cultured within the hat chamber system is of human origin

Staining against human mitochondria demonstrating the demarcation (represented by the dashed red line) between cultured human tissue (positive staining) versus host murine tissue (negative staining). Scale bar represents 100µm (Modified from Croagh, 2006).

Another model that has the potential to fulfil a number of the prerequisites of the 'ideal model' is the xenograft model. Although historically, the xenograft model has almost exclusively been used for the generation of tumour xenografts, it has also been used to culture normal human tissue. In an early example, Verstijen et al. (1988) implanted normal human colonic mucosa subcutaneously into nude mice and cultured it for up to five weeks in order to assess epithelial proliferation and differentiation. Results revealed the successful engraftment and ongoing culture of epithelial tissue, with the implanted tissue forming both crypt regions and more differentiated cystic structures lined by columnar epithelium (Figure 5-4). Given the similarities between colonic mucosa and BO, such as the presence of columnar epithelium and mucus producing goblet cells, this model provides a premise for a xenograft model of BO. The key advantage of using the xenograft model for the study of BO is that it has the potential to produce a 3-dimensional structure and does not rely on the digestion of tissue into single cells. Transplanted tissue pieces are also more likely to contain the full complement of cell types seen in the various stages of the development of BO such as squamous cells, columnar cells, goblet cells and stromal cells. Whole tissue pieces also have

the advantage of including cells from the different epithelial regions such as the luminal surface, basal layers, ducts and SMGs. As such, there is a greater chance that the Barrett's cell of origin will be contained within the model.

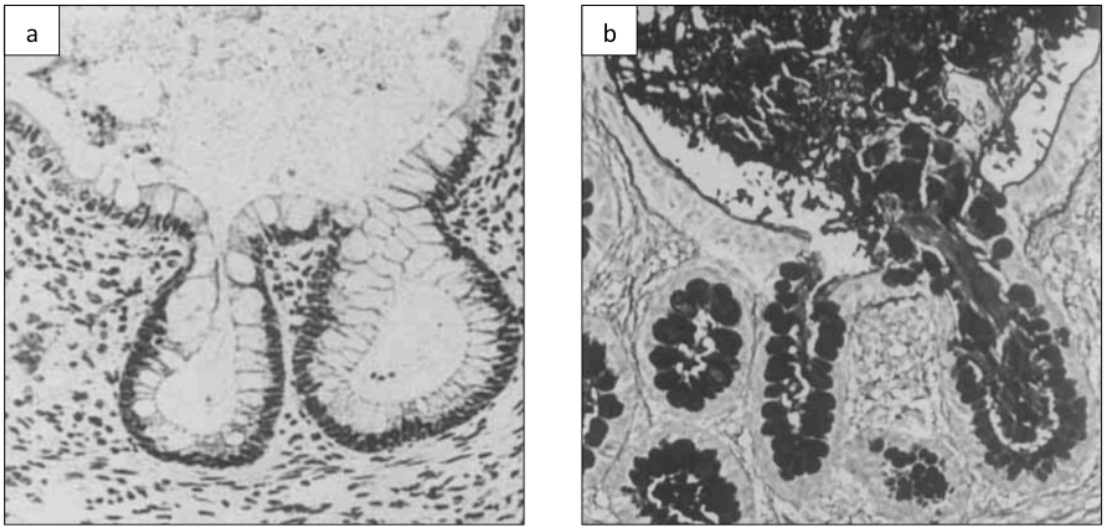

Figure 5-4 Normal human colonic xenografts two weeks post implantation.

Xenografts consist of both crypt regions and more differentiated cystic structures lined by columnar cells (a). HIDAB staining demonstrating the presence of mucus producing goblet cells (b) (Verstijnen et al., 1988. Image reproduced with permission).

The aim of this chapter was to develop an improved preclinical model that can culture both normal human oesophageal epithelium and BO. In order to achieve this the first objective was to optimise the hat chamber model by (1) improving chamber fixation and cell containment, and (2) demonstrating the successful generation of a Barrett's-like epithelium. The second objective was to draw on the success of the IM xenograft model by adapting the technique in order to generate xenografts of both normal human oesophageal mucosa and BO.

5.2 Results

5.2.1 Optimisation of the hat chamber culture system

In an attempt to improve the fixation of the hat chamber culture system to the dorsal fascia of the mouse, which was identified as major limitation in previous experiments performed by Croagh (2006), a piece of ProGrip™ mesh was secured to the base of the hat chamber system using a non-absorbable suture prior to implantation (Figure 5-5). A biological collagen mesh known as Permacol™ was also considered for this purpose, however, this was considered to be unsuitable as it does not permit tissue ingrowth.

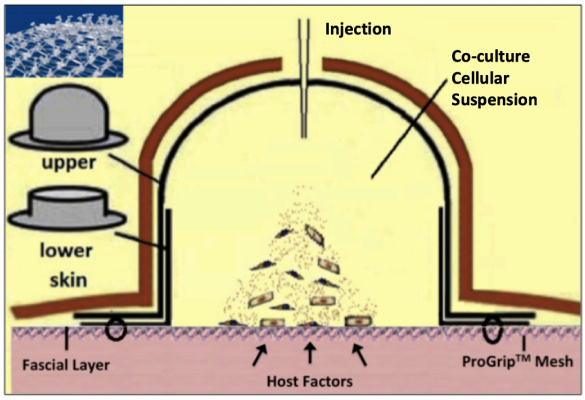

Figure 5-5 A diagrammatic representation of the modified silicone hat chamber model.

In order to facilitate better fixation, a piece of ProGrip™ polyester mesh (inset) was sutured to the lower component.

In order to implant the hat chamber culture system, immunodeficient mice were first anaesthetised and their dorsum prepared with alcoholic iodine. A dorsal incision was then made and stay sutures placed on the skin edges. Skin flaps were then raised in order to accommodate the culture system. The lower component of the culture system, with mesh attached, was then placed on the dorsal fascia of the mouse. A 100µl cellular suspension, consisting of either freshly isolated epithelial cells or cultured cells, was then delivered into the system before the upper component (hat) was fitted. The skin was then closed over the hat chamber system using absorbable suture. A small aperture was left in the wound in order to access the chamber. Mice were then recovered on a heat pad overnight and observed for any signs of suffering. Bile and gastric fluid were then injected into the culture system as required, in order to simulate the reflux of acid and bile into the lower oesophagus. Tissue cultured within the hat chamber was then harvested at predetermined time frame (typically four weeks) (Figure 5-6).

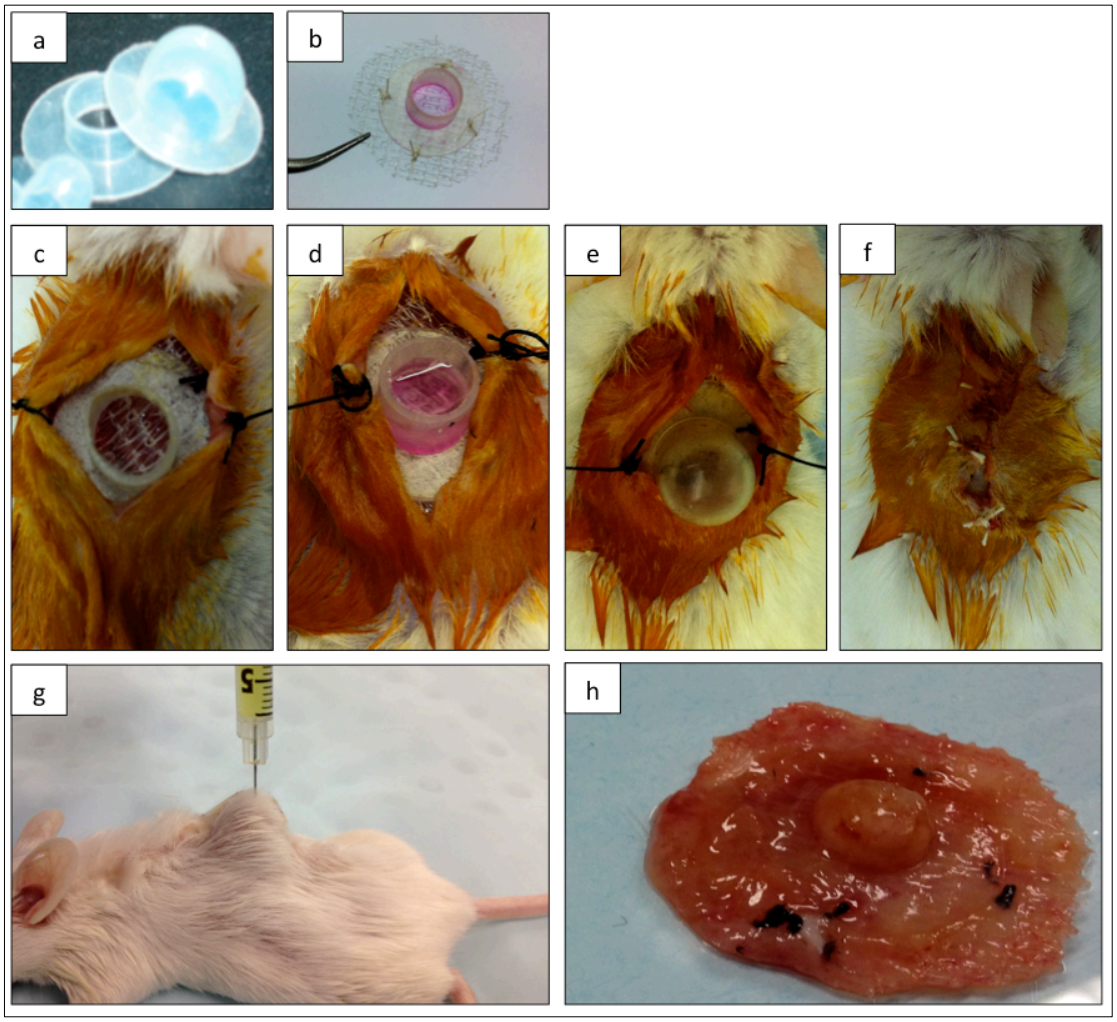

Figure 5-6 Methodology for the establishment and implantation of the modified hat chamber system

Both upper and lower components of the silicone hat chamber system can be seen in image a. Image b demonstrates the modified hat chamber system with the addition of a disc of ProGrip™ mesh to the base. In this image a layer of Matrigel has also been incorporated into the system prior to implantation. After placing stay sutures in the dorsal skin and raising skin flaps, the lower component (complete with mesh) is securely placed on the dorsal fascia of the host mouse (c). A cellular suspension is then delivered into the system (d) before the upper component is fitted (e). The skin is then closed over the hat chamber system leaving a small aperture for access (f). Bile and gastric fluid are then injected into the system as required (g). Cultured tissue is then harvested (h). In this image, tissue ingrowth into the ProGrip™ mesh is clearly evident.

In total, eight separate experiments were performed using the hat chamber culture system. Given that two mice were used per experiment, this equated to a total of 16 implantations. The addition of ProGrip^{TM} mesh to the chamber base plate successfully prevented chamber dislodgement. This was due to the complete incorporation of host tissue into the mesh, which created an extremely stable platform (Figure 5-7). Despite adequate chamber fixation, cell containment remained a problem. When cells were either injected or pipetted into the chamber in their associated media, the cell suspension soon dispersed below the chamber. This was prevented with the addition of Matrigel to the cell suspension at a ratio of 1:1, which, due to its viscosity, contained the cellular suspension within the chamber. In order to assess the effectiveness of this cellular containment; OE33 cells (an established oesophageal cancer cell line) were injected into the system. This led to the formation of a tumour xenograft completely within the confines of the chamber (Figure 5-7a). A similar appearance could also be observed from the culture of human oesophageal keratinocytes (Figure 5-7b). Unfortunately, an established epithelial structure could not be found within this specimen. It is hypothesized that this tissue growth may simply be the result of growth factors present within the Matrigel. In an attempt to further optimize the model, numerous other variables were tested without success. These included the strain of host mouse (*Scid* versus NOD-*scid*), cell number (3×10^5 vs 5×10^5), timing of cell injection, co-injection with fibroblasts as a form of feeder cell and the injection of freshly isolated versus cultured keratinocytes. Another variable that was tested was the effect of immediate cell inoculation versus after one week, as this would allow tissue ingrowth into the mesh at the base of the chamber. This could have the potential to further enable cell containment and provide a more vascularised environment for cell growth.

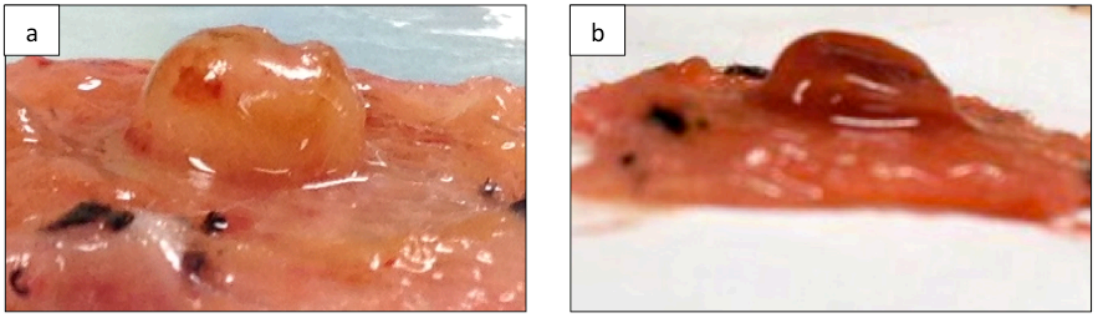

Figure 5-7 Tissue harvested from the chamber culture system

Tissue harvested from the hat chamber system following four weeks of culture. A cell injection xenograft derived from OE33 cells is seen in panel a. Tissue cultured from normal oesophageal keratinocytes seeded in Matrigel is seen in panel b. In both instances the ProGrip™ mesh has been completely incorporated with tissue.

5.2.2 The establishment of xenograft model capable of culturing both normal human oesophageal squamous epithelium and BO

The second aim of this chapter involved the development of a xenograft model capable of culturing both normal human oesophageal epithelium and BO. In order to achieve this, the IM transplantation technique was adopted. Firstly, tissue was obtained from either endoscopic biopsy or surgical resection specimen. In the case of surgical resection specimens, once they were received, they were opened longitudinally and carefully inspected for regions of normal epithelium, BO and OAC (Figure 5-8). This was either performed by an anatomical pathologist or by the surgical team in theatre. Pieces of epithelium, approximately $2mm^3$ is size, were then biopsied. Following collection, tissue pieces then underwent ex vivo imaging prior to transplantation (Figure 5-8).

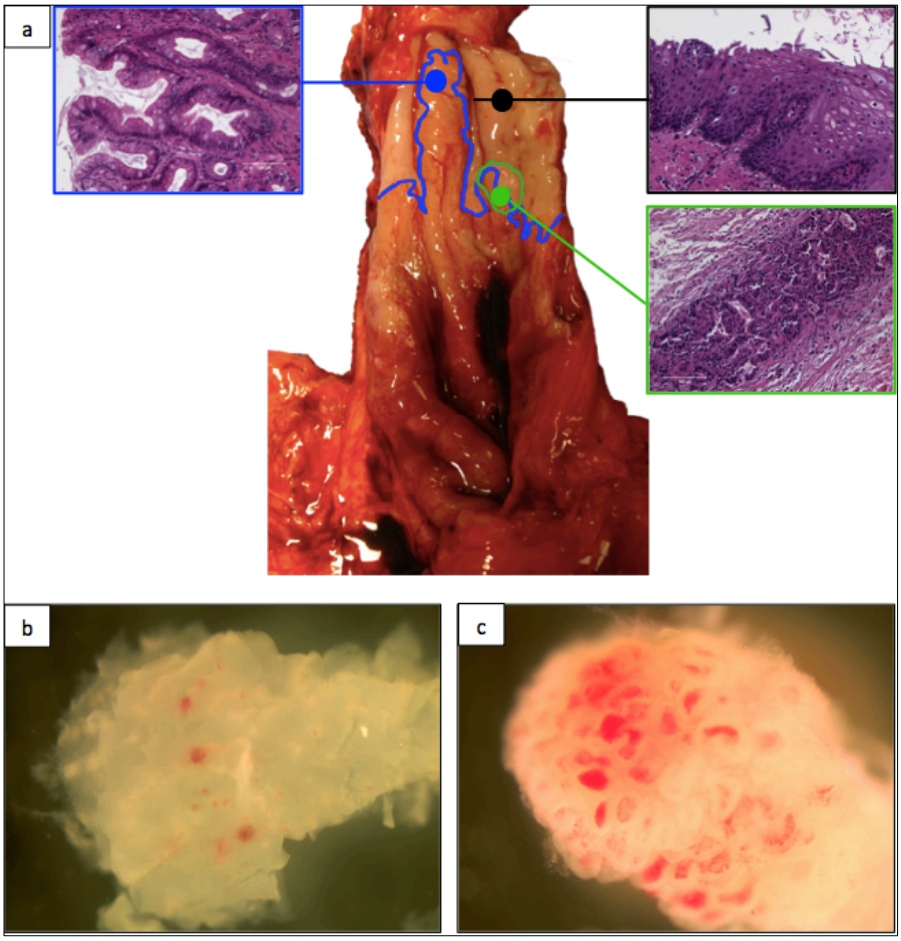

Figure 5-8 Identification of normal squamous epithelium, BO and OAC from a surgical resection specimen

A photo of a surgical resection specimen of the lower oesophagus and gastroesophageal junction that has been opened longitudinally (a) in order to demonstrate a region of BO (outlined in blue), normal squamous epithelium (black) and a corresponding adenocarcinoma (outlined in green). Representative H&E sections from all separate regions are shown alongside the main image. Scale bars represent 100µm. Representative pieces of both normal squamous epithelium (b) and BO (c) have then been sampled and imaged using a dissecting microscope in order to confirm their origin. Squamous epithelium is composed of flat sheets of epithelium whereas BO demonstrates a villous morphology.

Following collection, tissue was placed in Matrigel and kept on ice until transplanted. Tissue pieces were then transplanted as previously described in section 3.3. However, after closing the IM pocket, a non-absorbable 4/0 suture was then placed at the site of transplantation in order to help identify the site at time of retrieval. Xenografts were then cultured for periods of up to six months before being harvested (Figure 5-9).

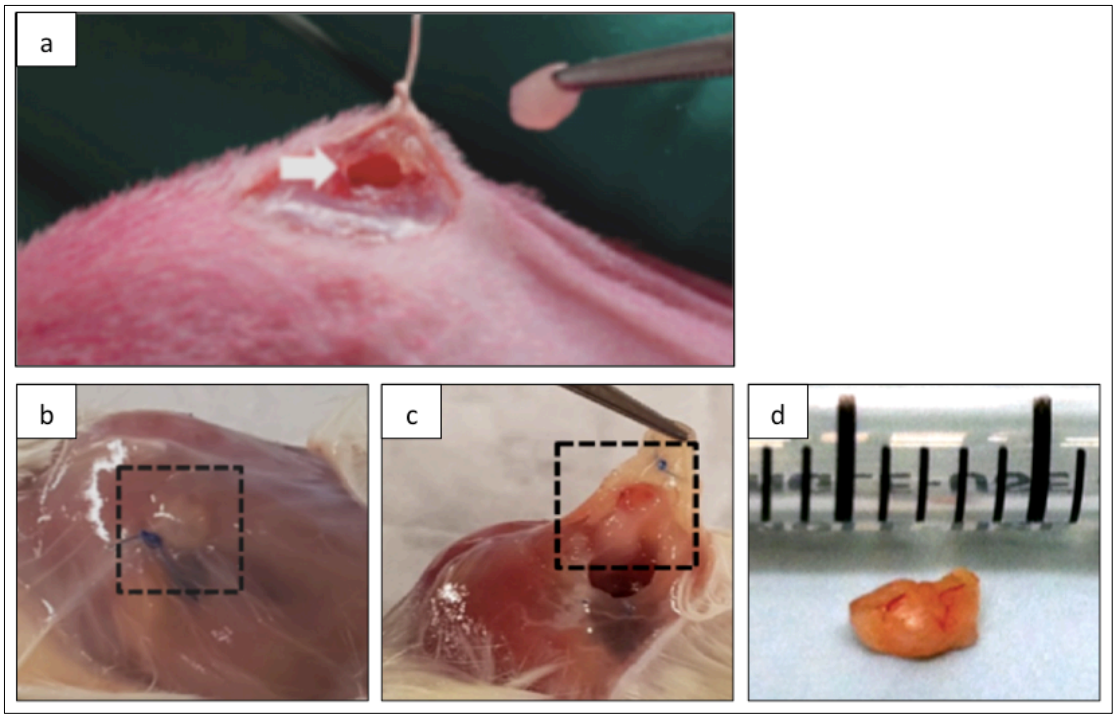

Figure 5-9 Establishment and harvesting of both normal oesophageal and BO xenografts

A small piece of epithelial tissue (obtained from either surgical resection specimen or endoscopic biopsy) is implanted into an IM pocket on the dorsum of a mouse in order to generate a xenograft (a). At a pre-determined time point (in this case three-months) the mouse is culled and the xenograft retrieved. The site of dissection is determined from a non-absorbable marking suture (region of interest in image b) and a muscle flap is raised revealing the xenograft (region of interest in image c). A xenograft of approximately two to three millimetres in dimension is dissected (d).

5.2.3 Results from the culture of normal oesophageal epithelium

In total, normal oesophageal epithelium was collected from four separate patients and implanted into a total of nine mice using the IM transplantation technique. Culture periods ranged from one to two months. Squamous xenografts were successfully harvested from six of the nine implanted specimens. All successfully generated xenografts were derived from oesophagectomy resection specimens, with normal tissue being harvested from the surgical margin, as far away as possible from regions of BO or cancer. Post harvesting, two distinct regions were evident within the squamous xenografts. These included a cystic region and a germinal region (Figure 5-10). The 'cystic region' is lined by differentiated, non-keratinising squamous cells organized into four or five layers, with the cyst containing cellular debris and keratin. In contrast, the 'germinal region', is composed of a mass of cells that appear less well

differentiated and less well organised (Figure 5-10a). Within this region there is evidence of hyperkeratinisation with the formation of keratin islands. The outer layer of the xenograft represents the basal layer, whilst the inner layer represents the luminal surface. IHC analysis revealed that the xenografts were strongly positive for the squamous markers cytokeratin 5 and p63. Staining against cleaved caspase-3 revealed that there was only a scant amount of cell death (Figure 5-10).

In order to determine the levels of cellular proliferation within the model, a bromodeoxyuridine (BrdU) pulse-chase experiment was performed. As BrdU is an analogue of the DNA nucleoside thymidine, it becomes incorporated into cells as they replicate. By administering BrdU to mice harbouring xenografts over a certain timeframe (pulse phase), it is possible to determine the cells that have replicated over this period. Following administration, BrdU is then gradually lost with subsequent replications. The period between the cessation of administration and harvesting of tissue is denoted as the 'chase' phase. Cells that retain BrdU label at the end of an extended chase period are termed label retaining cells and represent slow cycling cells. Following a five-day BrdU pulse period in conjunction with a one-month chase period, BrdU positive cells were identified in the terminally differentiated layers of the stratified squamous epithelium (Figure 5-10f). It is most likely that these cells acquired the BrdU whilst in the basal layers before migrating towards the luminal surface.

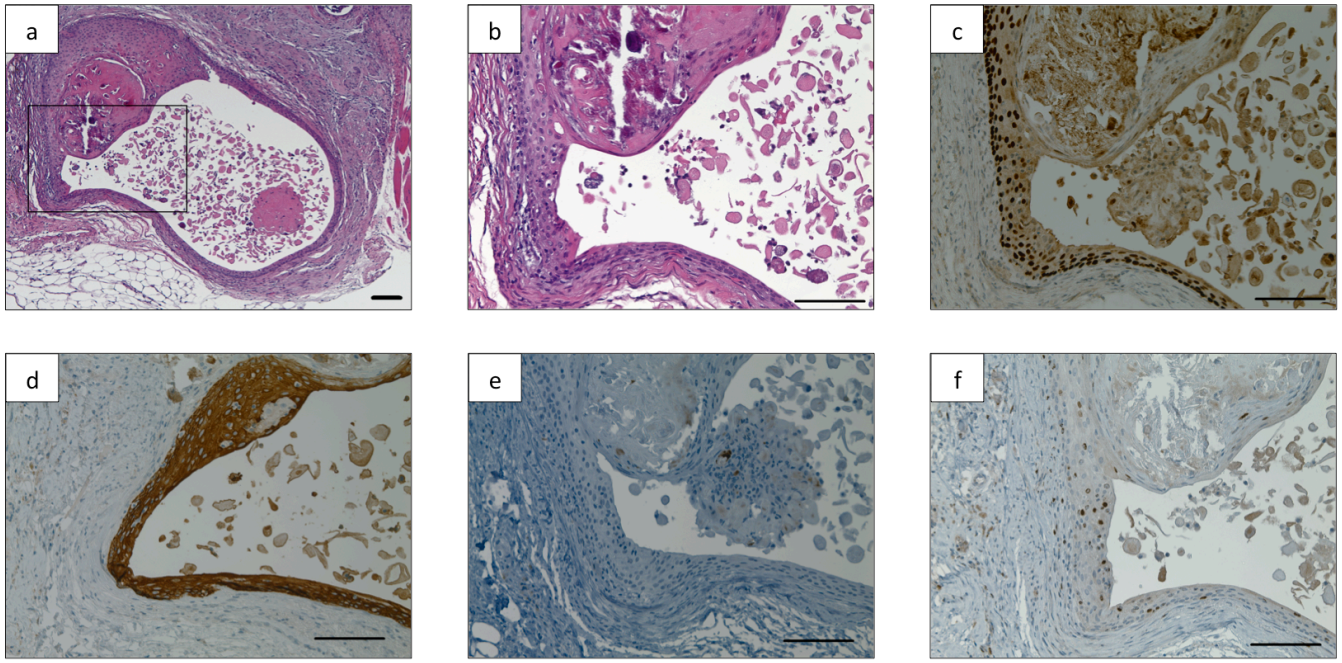

Figure 5-10 Validation and characterisation of the oesophageal squamous xenograft model

In this experiment, a five-day BrdU pulse period commenced two-weeks post the transplantation of normal oesophageal epithelium. Following this, the xenograft was serially passaged into another mouse and cultured for a further four weeks (chase phase). The xenograft was then harvested, fixed in formalin and embedded in paraffin for histological analysis. H&E staining demonstrates the formation of a stratified squamous epithelium (a). A magnified region of interest is shown (b). For the purpose of validation, IHC stains against p63 (c) and CK5 (d) are shown. In order to asses cellular viability and proliferation within the xenograft, staining against cleaved caspase-3 (e) and BrdU (f) is also shown. Counterstaining was performed using haematoxylin. Scale bars represent 100µm.

5.2.4 Development and validation of the Barrett's xenograft model

As per the squamous xenograft model, BO xenografts were established from tissue obtained from either endoscopic biopsy or surgical resection. In total, xenografts were successfully derived from eight out of 14 patient samples and were cultured for periods ranging from one to six months. Early xenografts typically contained both glandular and villous regions in addition to a more differentiated cystic structure lined by an intestinal type of epithelium (Figure 5-11). The xenograft lumen contained both cellular debris and secreted mucus that was produced by a functioning epithelium. Following extended culture, the columnar cells began to flatten and take on a cuboidal appearance. The number of glandular regions also diminished. Validation confirmed that the epithelium lining the xenograft is representative of the original human tissue (Figure 5-12). Staining against human mitochondria also confirms that the xenograft is of human origin. Further validation confirms that BO xenografts express markers of intestinal differentiation such as CDX2, MUC2, MUC5AC and Alcian blue. Ki67 positivity provides evidence of cellular proliferation within the xenograft, which, in mature structures, is predominantly confined to the glandular regions.

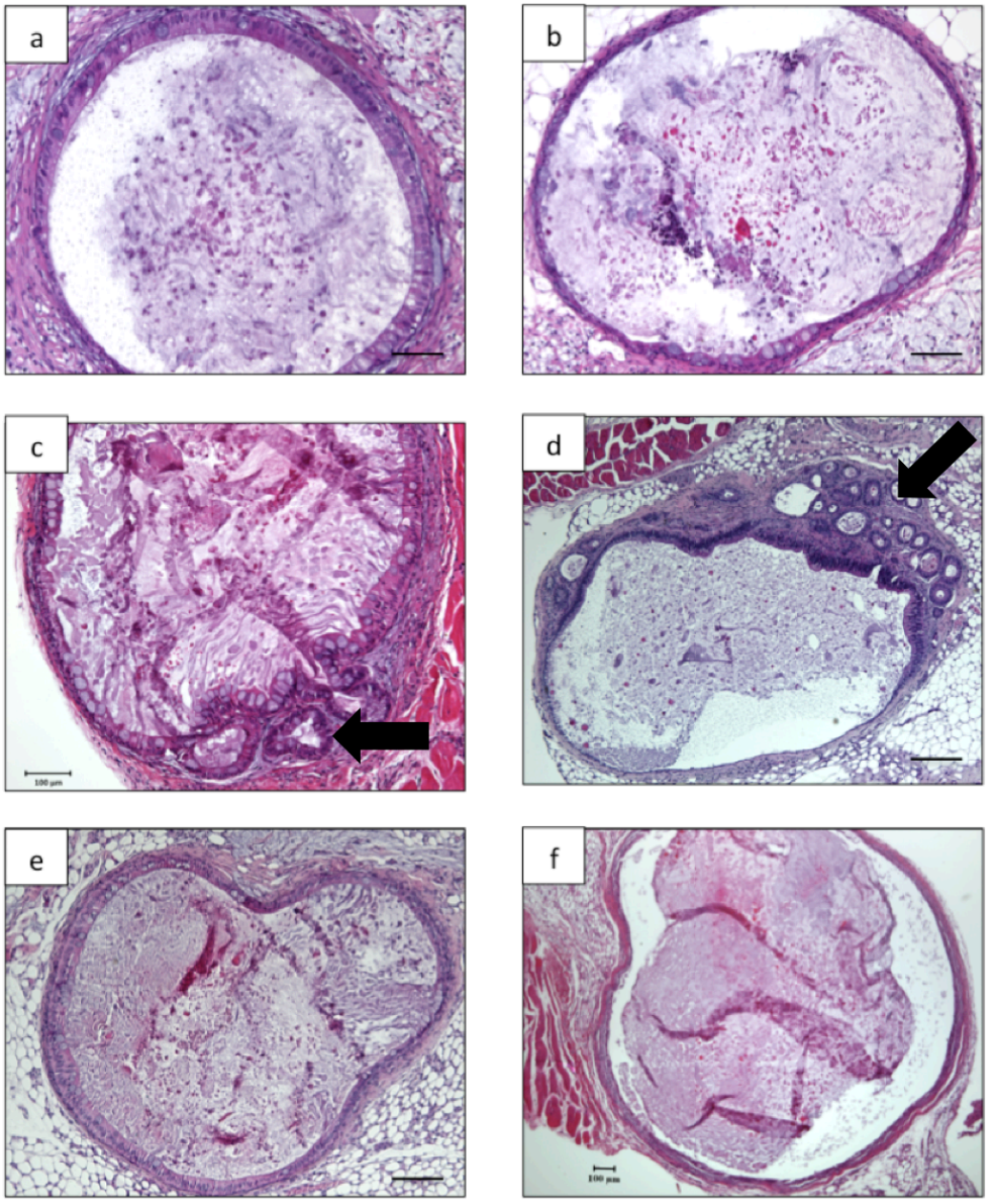

Figure 5-11 BO xenografts across a range of time points

H&E sections from a range of BO xenografts harvested at separate time points (a=42 days, b=42 days, c=92 days, d=97 days, e=104 and f=167 days). Xenografts are lined by a single layer of columnar epithelium and display varying amounts of goblet cells. The lumen consists of secreted mucin and cellular debris. Crypt and glandular regions are also evident within xenografts in c and d. Glandular regions are identified by arrows. Scale bars represent 100µm.

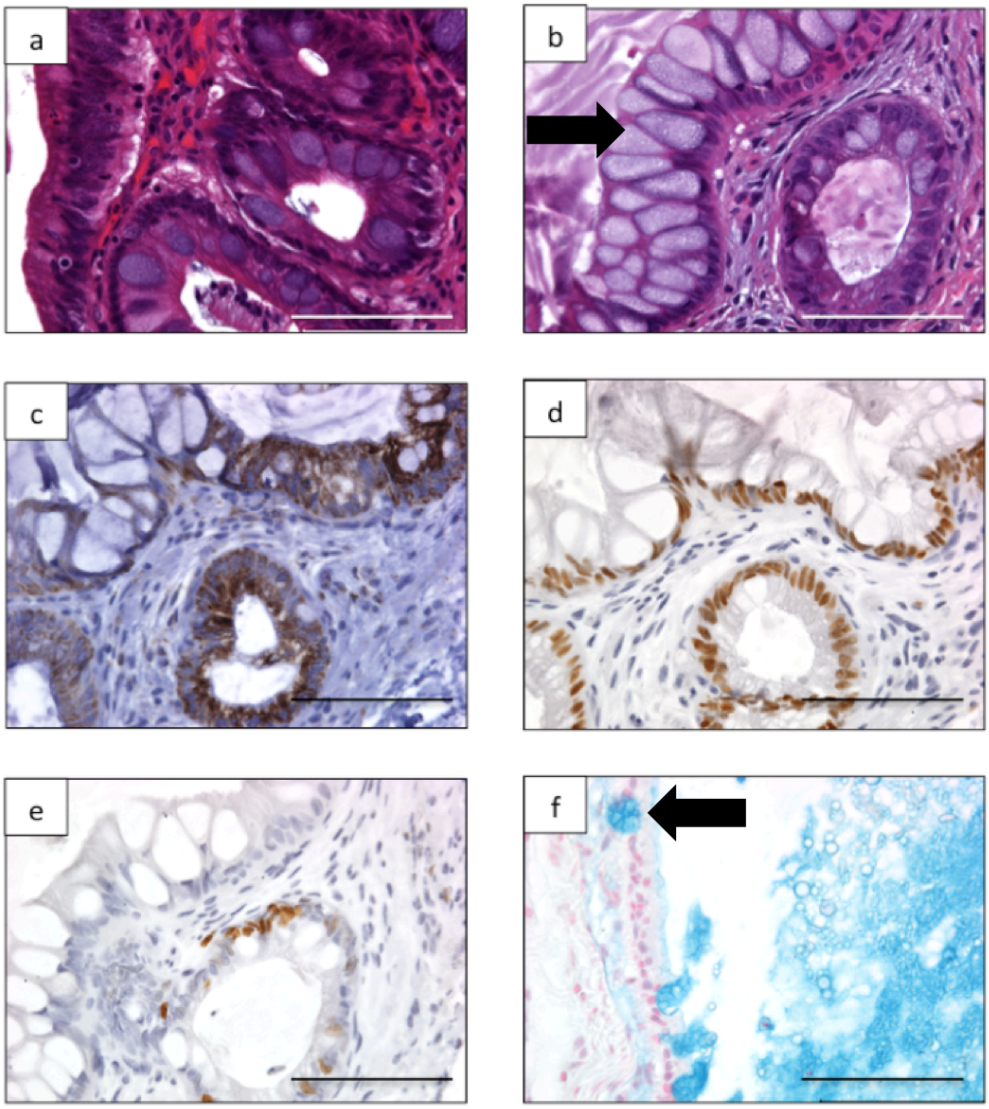

Figure 5-12 Validation and characterisation of the BO xenograft model

Barrett's xenografts recapitulate an intestinal phenotype, are of human origin and express markers of intestinal differentiation and proliferation. The above panels demonstrate H&E staining of a representative piece of original patient tissue prior to implantation (a) and the H&E staining of the corresponding xenograft following 92 days in culture (b). IHC staining against human mitochondria confirms that this xenograft is of human origin (c) and staining against the transcription factor CDX2 confirms an intestinal phenotype (d). Ki67 staining confirms ongoing evidence of cellular proliferation following 92 days in culture. Alcian blue staining was performed to assess for the presence of goblet cells and mucin production (f). This was performed on a separate xenograft that was derived from the same patient that had been in culture for 167 days. Goblet cells are indicated by arrows. Scale bars represent 100µm.

5.2.5 Attempted passaging of Barrett's xenografts

Two attempts were made at passaging Barrett's xenografts. The first attempt was unsuccessful, as the passaged xenograft (F2) had undergone lymphomagenic transformation. In the second attempt, a xenograft was passaged after only two weeks as part of a label retaining experiment. Following a five-day pulse period, the xenograft was passaged and cultured for one month (chase period). Unfortunately, the section of tissue that was collected at the time of passage lacked any evidence of an epithelial structure. It is most likely that this represented a sampling error as only murine tissue was evident in the sample. Following the chase period, the harvested tissue revealed evidence of a squamous epithelial structure (Figure 5-10). This most likely represents the misidentification of tissue at the time of collection, as it was thought that Barrett's tissue had been implanted.

5.2.6 Culturing the SCJ within the xenograft model

On two separate occasions xenografts were cultured that contained both stratified squamous and columnar epithelium (Figure 5-14). Within these xenografts a clearly defined SCJ separated both squamous and columnar regions. It is possible that these xenografts represent the ongoing culture of both squamous and columnar tissue collected from the native SCJ in the patient. Alternatively, it may have formed *de novo* from resident progenitor cells. On the first occasion, the xenograft was harvested from the same first-generation cohort that was used as part of the passaging experiment that was previously described in section 5.2.5 (Figure 5-13). As previously stated, this passaged xenograft contained only squamous features. This transition zone was extensively characterized by means of IHC analysis, as seen in the second example (Figure 5-14). Results indicated that columnar cells exclusively expressed CDX2, a marker of intestinal differentiation. The columnar epithelium also contained the occasional cell expressing MUC5AC. Within squamous regions, p63 was expressed in both basal and suprabasal regions. In contrast, staining against cytokeratin 5 demonstrated a more even distribution throughout the squamous regions. Interestingly, a layer of cells expressing both CK5 and p63 were evident below the layer of columnar epithelium immediately adjacent to the SCJ. Such an arrangement is consistent with the transitional epithelium recently identified by Jiang et al. (2017). Label retaining cells are also identified following a 32-day chase period, also residing below the columnar epithelium immediately adjacent to the SCJ (Figure 5-14h).

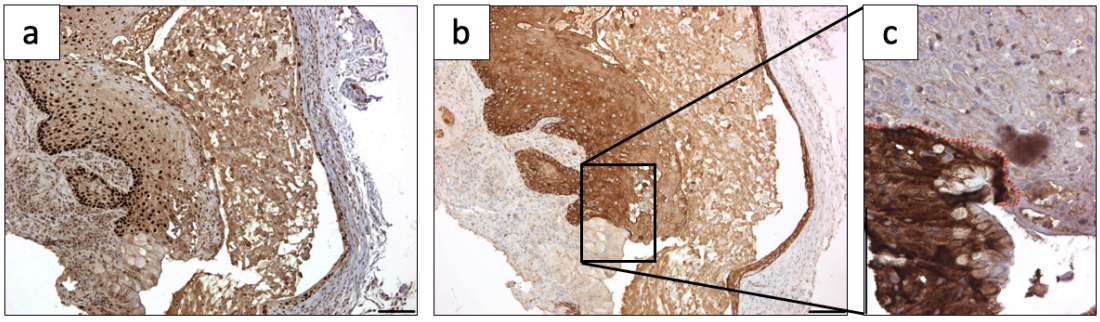

Figure 5-13 Evidence of a SCJ within the xenograft model

IHC staining against p63 (panel a) and CK5 (panel b) highlights the squamous regions that have been cultured within the xenograft. Staining against the columnar marker, MUC5AC, is shown in panel c. Within the magnified region of interest (panel c), the SCJ has been highlighted with a dotted red line. Scale bars represent 100µm.

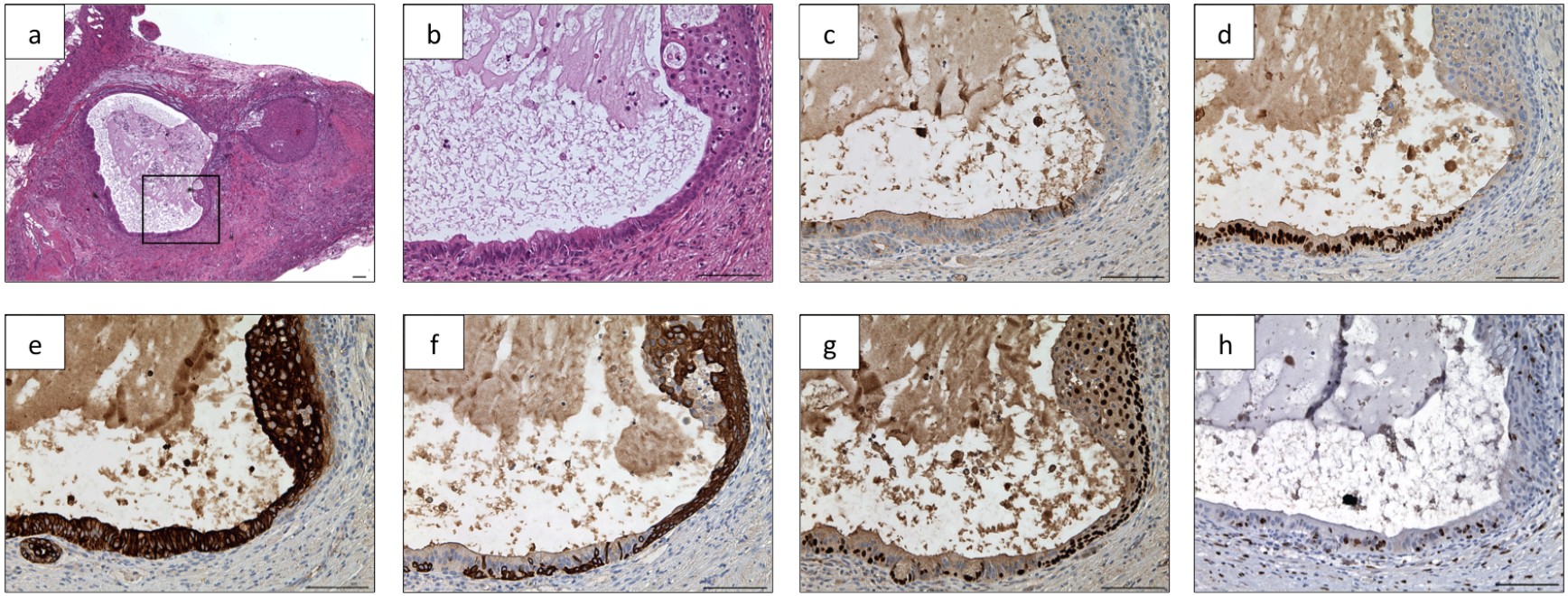

Figure 5-14 IHC characterisation of the SCJ within the xenograft model

Individual xenografts have the ability to support both stratified squamous and columnar epithelium simultaneously, as seen in panel a (H&E staining). The marked region of interest, demonstrating the junction between stratified squamous and columnar epithelium is shown in panel b (H&E staining). A panel of IHC stains have been performed to further characterise this region. These include MUC5AC (c), CDX2 (d), CK7 (e), CK5 (f) and p63(g). In addition, this xenograft has also been labelled with BrdU over period of five days. This was then followed by 32-day chase period. Staining against BrdU can be seen in panel h. Scale bars represent 100µm.

5.2.7 Evidence of lymphomagenic transformation within the Barrett's xenograft model

Just like the oesophageal cancer xenograft model (Section 3.5), the Barrett's xenograft model was also prone to lymphomagenic transformation. In keeping with the cancer xenograft model, these mice also developed splenomegaly with associated tumour formation. In total, this occurred on two separate occasions. Both of these cases occurred when the original tissue had been collected from patients with concurrent adenocarcinomas, resulting in a conversion rate of 2/8 (25%). In contrast, none of the six Barrett's xenografts that were implanted from patients without cancer developed lymphomas.

5.2.8 Characterisation of the xenograft model at early versus late time points

In an attempt to understand how the xenografts form, xenografts were harvested and analysed at both early (Figure 5-15) and late (Figure 5-16) time points. By analysing xenografts harvested at an early time point (day 19) by means of IHC staining against cleaved caspase-3, a marker of cell death, it is evident that the transplanted tissue maintains its viability (Figure 5-15). The only evidence of cellular death is from within the xenograft lumen (which is expected as it is filled with cellular debris) as well as the occasional differentiated cell from the luminal surface of the xenograft. Rudimentary structures, identified by the absence of a lumen, contain minimal evidence of cell death. In addition, results from a label-retaining assay performed on these same xenografts demonstrate that the rudimentary structures, when compared to the more differentiated structures, contain many more cells with BrdU incorporation. As BrdU becomes incorporated during DNA replication, this implies that the cells in these regions are cycling more actively. In this experiment, a five-day pulse period of BrdU was performed commencing one-week post implantation. A one-week chase period then followed leaving a total culture period of 19 days.

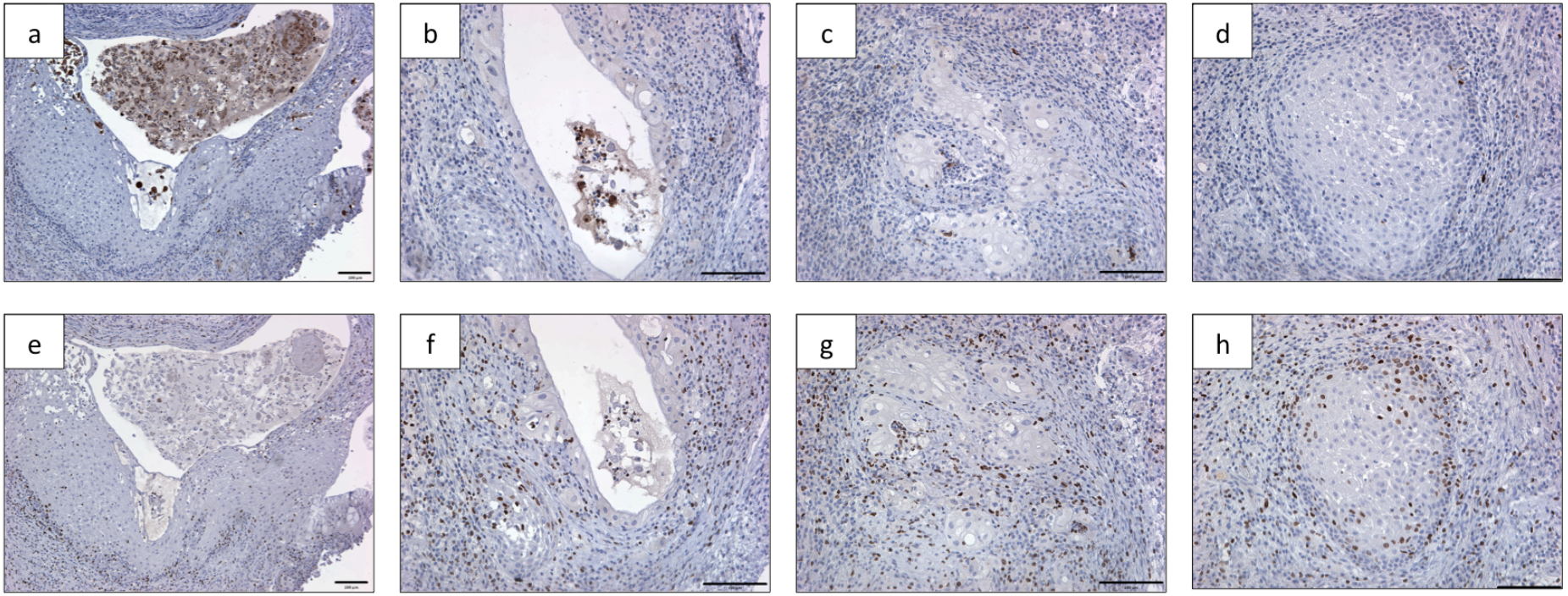

Figure 5-15 Assessment of cellular viability and proliferation within the early xenografts

A five-day BrdU pulse period commenced one week after the implantation of Barrett's tissue taken from a surgical resection specimen. This was followed by a seven-day chase period. All images represent different regions from within a single xenograft. IHC staining for cleaved caspase-3 (a, b, c and d) and BrdU (e, f, g and h) is shown. Top and bottom panels are matched. Scale bars represent 100µm.

In order to assess the proliferative regions of more mature xenografts, a five-day BrdU pulse was performed on BO xenografts that had been in culture for up to 3.5 months (Figure 5-16). Results from this experiment revealed that the majority of cellular replication within more mature xenografts takes place within the glandular regions. However, an area of cellular proliferation was also identified within a more differentiated region of the same xenograft. In the centre of this region was a single cell without any evidence of BrdU uptake, suggesting that this cell is cycling more slowly than the surrounding cells. Further flanking this region were more differentiated mucus producing cells (Figure 5-16b).

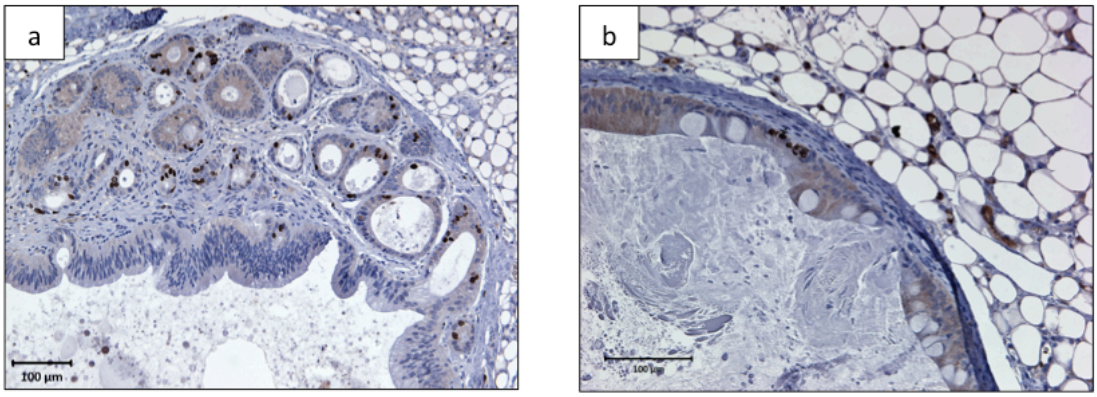

Figure 5-16 Labelling of cells within BO xenografts

Xenografts derived from endoscopic biopsies of two separate patients were cultured for 3 (a) and 3.5 months (b). Mice were then administered BrdU daily for 5 days. Both xenografts were harvested 12-hours following the last dose of BrdU. IHC staining against BrdU is shown. Scale bars represent 100µm.

From these results there is evidence that xenografts harvested at early time points contain many more 'rudimentary' structures that lack a lumen. It is highly probable that the more differentiated xenografts, characterized by cystic structures lined by a functional epithelium, derive themselves from these rudimentary structures.

5.2.9 Analysis of cell cycling within the Barrett's xenograft model

In order to analyse cell cycling within the xenograft model over an extended period of time, a series of label retaining experiments were performed on a cohort of mice bearing Barrett's xenografts. In this experiment, a 5-day pulse period was followed by chase periods of varying durations (Figure 5-17). Following the 5-day pulse phase, the majority of cells from within the xenograft were labelled with BrdU, indicating that the majority of the cells replicate within a 5-day period. Over the varying chase periods the proportion of BrdU positive cells gradually decreases. This is because the cells gradually lose their BrdU label with subsequent divisions. Within regions of stratified squamous epithelium, the migration of cells from the basal region to the luminal surface can be observed. Following an extended chase period of 42 days, only two label retaining cells can be identified residing immediately below the columnar epithelial layer. It is possible that these slowly cycling cells could represent stem-like cells.

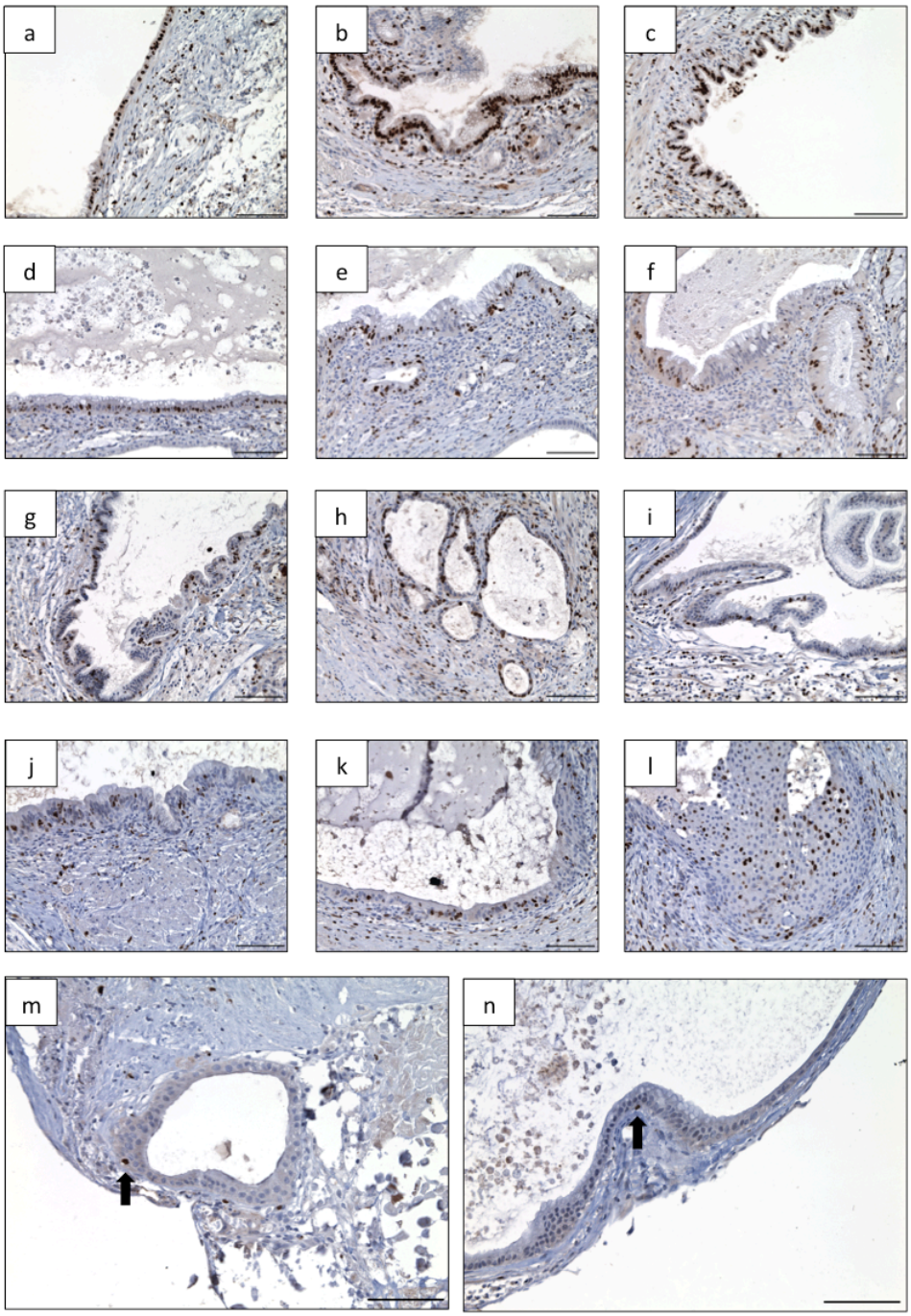

Figure 5-17 Label retention assay of BO xenografts across a range of time points

Endoscopic biopsies of BO were obtained from one individual patient and implanted into five separate mice in order to generate a cohort harbouring xenografts derived from the same patient. After a two-week period to allow for engraftment, host mice were administered BrdU daily for five days (pulse phase) in order to label the majority of cells. Following this, mice were then harvested at separate time points (chase period) in order to identify label retaining (slower cycling) cells. The following chase periods were used; two days (panels a, b and c), six days (panels d, e and f), 22 days (panels g, h and i), 32 days (panels j, k and l) and 42 days (panels m & n). IHC staining is shown against BrdU. Scale bars represent 100µm.

5.2.10 In vivo culturing of SMGs

Given the importance of the oesophageal submucosal gland as a potential stem cell niche, an attempt was made to both harvest and culture these structures using the IM xenograft technique. The aim of this pilot experiment was to firstly assess the feasibility of this approach and, secondly, to determine the type of epithelium that is able to be produced by the SMG. In order to do this, submucosal tissue was dissected from the proximal margin of a surgical resection specimen. The dissected region was from a region of normal squamous epithelium and clear of any BO and cancer. A representative piece of tissue was taken in order to confirm the presence of SMGs from within the specimen (Figure 5-18a). Results revealed the successful formation of xenografts following 53 days of in vivo culture. However, unlike the xenografts of both normal human oesophagus and BO, these xenografts failed to form a spherical or cyst-like structure (Figure 5-18b). Instead, they were predominantly composed of solid tissue containing multiple small, incompletely formed structures (Figure 5-18c). Rudimentary structures, lacking any noticeable lumen, were also present. The cultured tissue stained positively for the squamous markers cytokeratin 5 and p63 as well as cytokeratin 7 (a marker of ductal or transitional epithelium (Mohammed, Streutker, & Riddell, 2002) and lacked expression of the intestinal makers MUC5AC and MUC2 (Figure 5-18). Given that this experiment only yielded rudimentary structures, future experiments should be performed over longer culture periods to determine if the xenografts become more differentiated. Attempts should also be made to both passage these xenografts and perform pulse-chase analyses in an attempt to identify the location of potential stem cell populations.

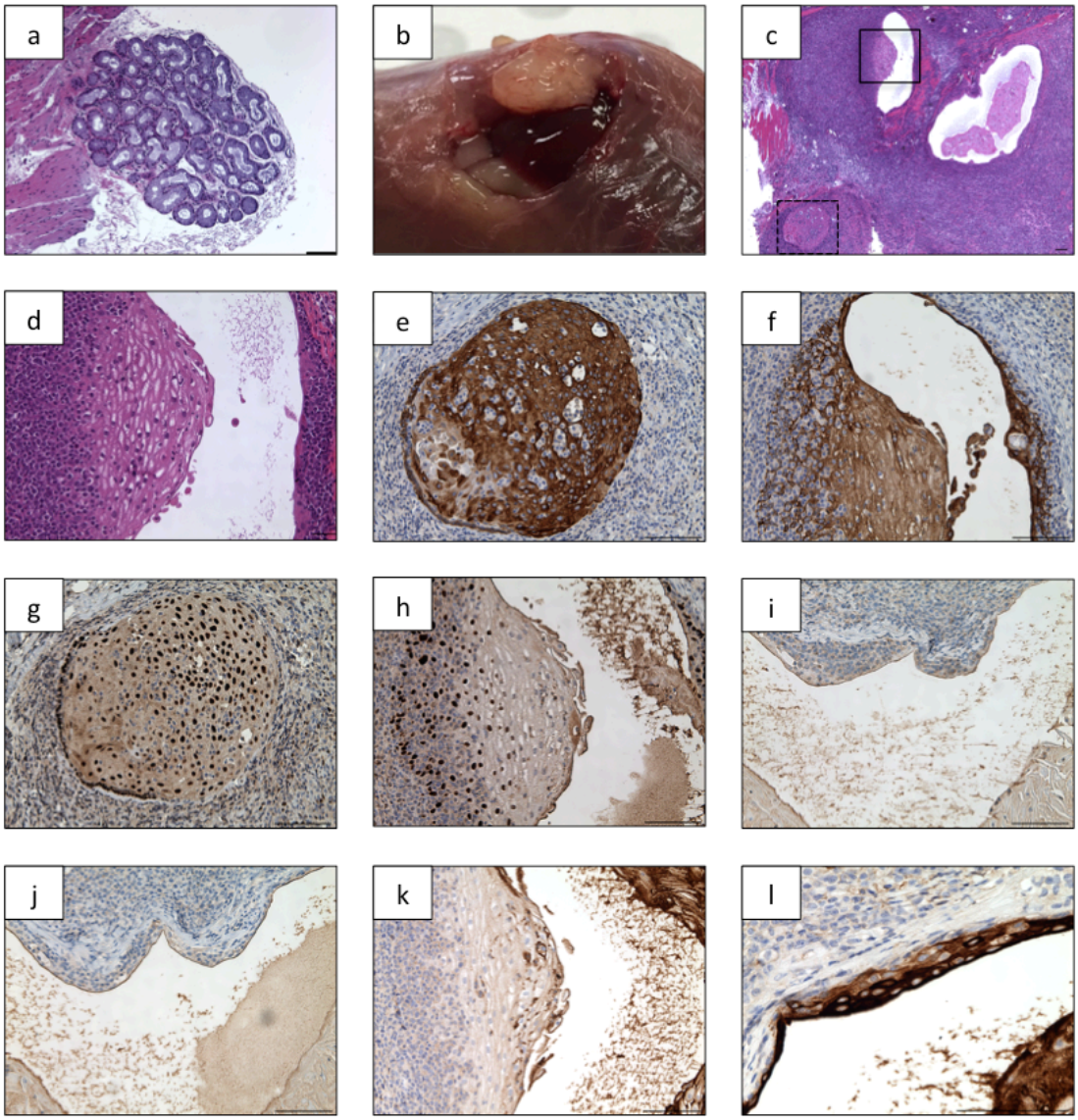

Figure 5-18 Generation of xenografts from oesophageal SMGs

SMGs were harvested from fresh surgical resection specimens. A representative piece of tissue was formalin fixed and paraffin embedded and stained with H&E in order to confirm that SMGs were present (a). Xenografts were harvested at 53 days post implantation (b). H&E staining revealed multiple epithelial structures (c). Two areas of interest have been marked. The solid square is shown in panels d, f, h and k whilst the dashed square is shown in panels e and g. IHC staining against CK5 (e and f), p63 (g and h), MUC5AC (i), MUC2 (j) and CK7 (k and l) was performed for further characterisation. Scale bars represent 100µm.

5.3 Discussion

This chapter highlights the successful generation of an improved preclinical model capable of culturing both normal human oesophageal epithelium and BO. This was achieved by adapting the IM xenograft technique in order to generate xenografts of both normal human oesophageal mucosa and BO, as the initial objective of 'optimising the hat chamber culture system' ultimately proved to be unsuccessful.

Although initial efforts focusing on improving both hat chamber fixation and cell containment within the model were successful, an epithelial layer was unable to be cultured. This is in contrast to the previous successful results published by Croagh (2006) and may be due to the fact that immortalised cell lines were used (rather than freshly derived cells) . In this series of experiments, It is most likely that the tissue cultured within the chamber simply represents a reaction to the growth factors contained within the Matrigel, as has previously been reported (Kawaguchi, Toriyama, Nicodemou-Lena, Inou, Torii et al., 1998). In the study by Kawaguchi et al. (1998) fat pads developed following the subcutaneous injection of Matrigel, supplemented with growth factors, into 6-week old mice. This was shown to be due to a process of neovascularisation followed by the migration of adipose precursor cells.

In order to further optimise the hat chamber culture system, numerous variables needed to be considered. Examples of these variables include cell type (fresh vs cultured), tissue digestion technique, both the timing and number of cells seeded, presence of feeder cells and the addition of Matrigel. Given the number of potential variables to be tested and the limited availability of fresh normal oesophageal and Barrett's tissue, further optimisation of this model was deemed to be both resource intensive and low yield. As a result, efforts shifted to the second objective, which was to adapt the IM xenograft technique in order to generate xenografts of both normal human oesophageal mucosa and BO.

Fortunately, the IM xenograft technique led to the successful generation of xenografts from both normal human oesophageal tissue and BO, representing the first known in vivo model of human oesophageal epithelium and BO. Through a series of pulse chase experiments and IHC analysis assessing for evidence of apoptosis, results have revealed that the xenograft model permits the ongoing culture of tissue over an extended period. However, unlike cancer xenografts which continue to increase in size, xenografts formed from normal tissue seem to

be limited to a diameter of only two to three millimetres. The xenografts cultured using the IM technique also share a striking resemblance to the 'organoid' model (Sato et al., 2011). In fact, when *in vitro* derived organoids are transplanted *in vivo*, they also have the ability to form 3-dimensional structures that recapitulate the cellular organization of the original tissue, much like the Barrett's xenografts in this chapter (Figure 5-19) (Watson, Mahe, Munera, Howell, Sundaram et al., 2014).

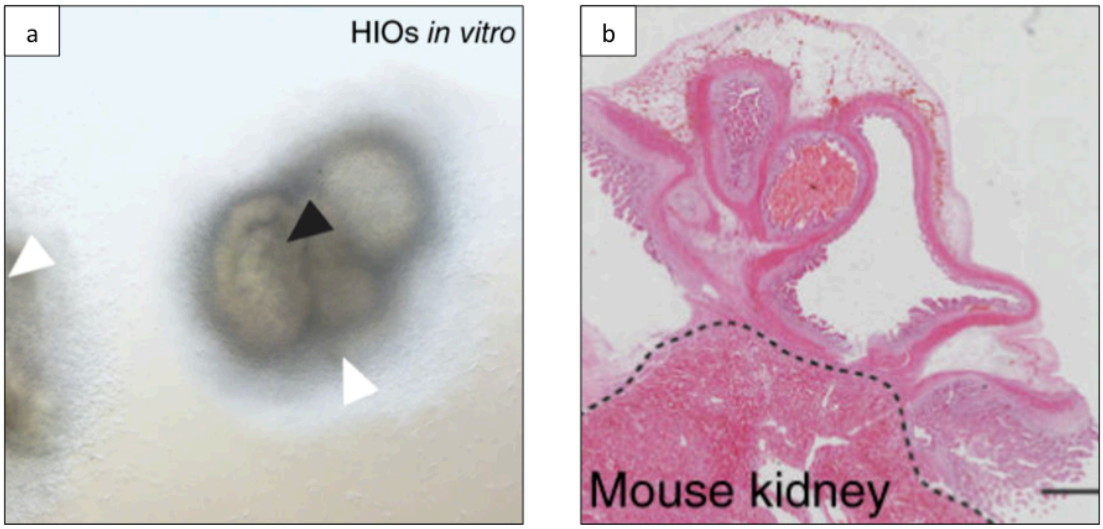

Figure 5-19 The *in vitro* and *in vivo* appearance of human intestinal organoids

A human intestinal organoid following both in vitro culture (a) and renal capsule xenografting (b) (Watson et al., 2014. Image reproduced with permission).

The implantation of normal oesophageal tissue led to successful xenograft formation in six out of the nine implantations. Interestingly, xenografts were only established following the implantation of tissue from surgical resection specimens and not endoscopic biopsies. This is likely due to the fact that the resection specimen contains cells from deeper within the epithelium, including the basal layer, whereas the endoscopic biopsies tend to be more superficial and contain a greater proportion of terminally differentiated cells. This is in keeping with the observation that squamous progenitor cells reside in the basal regions (Croagh, Phillips, Redvers, Thomas, & Kaur, 2007).

The implantation of Barrett's tissue led to successful xenograft formation from eight out of the 14 patients from which samples were obtained. Unlike the squamous xenografts, it was possible to derive Barrett's xenografts from both endoscopic biopsy and tissue pieces

obtained from surgical resection specimens. This is likely due to the fact that the luminal surface of BO contains cells that maintain the ability to proliferate, in contrast to the luminal surface of stratified squamous epithelium that only contains terminally differentiated cells. The results of validation confirmed that the xenografts are representative of the original human tissue and that the cells not only maintain viability but continue to proliferate. Using this technique, it was even possible to culture both squamous and columnar epithelium within individual xenografts. This property increases the power of the model, as it enables the study of the transition zone at the SCJ, one of the proposed locations of the Barrett's cell of origin.

As with the PDTX model (Section 3.5), validation also confirmed that two of the xenografts derived from Barrett's tissue had also undergone lymphomagenic transformation. In both of these occasions, the patients from whom the tissues were harvested had an undergone neoadjuvant therapy prior to surgery for their OAC. This phenomenon is in keeping with the theory that EBV infected B cells become activated following culture in an immunodeficient state, such as during chemotherapy and when tissue is cultured *in vivo* using immunodeficient hosts. Such a process has also been reported with the xenografting of non-cancerous gastric mucosa with associated gastritis into NOD SCID mice, with a transformation rate of 50% (2/4) (Zhang, Liu, Wang, Tang, Li et al., 2015).

Given that the xenograft model enables the ongoing culture of human tissue for extended periods, it has the potential to be used for a number of different applications. These could include the testing of novel drug therapies or investigating different aspects of the disease biology, such as the role of the SMG and the identification of potential stem cells. Such issues have proven to be difficult to investigate and have been the source of great controversy.

In an recently published attempt to identify a Barrett's stem cell, Pan et al (2013) conducted a series of label retaining assays on patients undergoing treatment for Barrett's adenocarcinomas as part of the stem cell assessment in neoplastic tissue (SAINT) trial. Subsequent analysis of the tissue revealed the location of the slowest cycling cells to be in the base of the SMGs (Figure 5-20) (Pan et al., 2013).

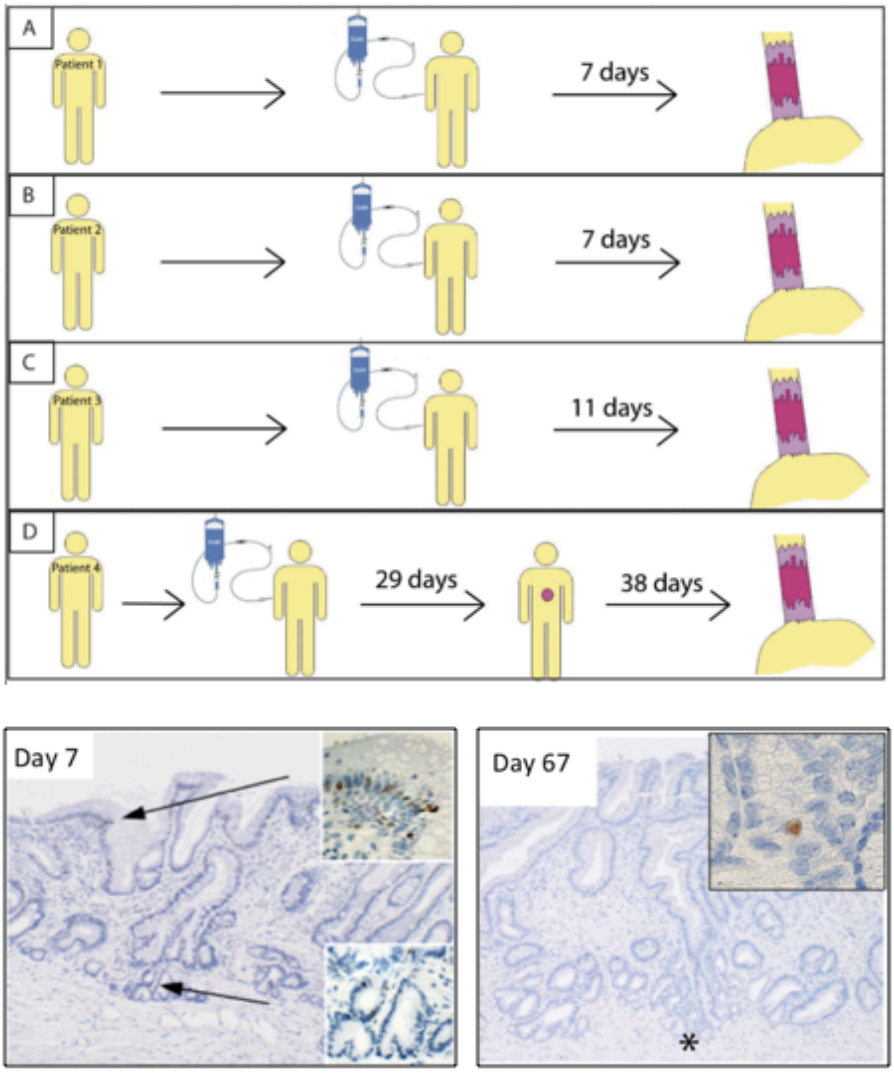

Figure 5-20 Overview and results from the Stem Cell Assessment In Neoplastic Tissue (SAINT) Trial

*Four patients undergoing treatment for oesophageal cancer received a single intravenous infusion of IdU followed by either oesophagectomy alone (patients a to c) or endoscopic mucosal resection followed by oesophagectomy (patient d). This created five separate chase points for analysis. IHC staining against IdU reveals the presence of label retaining cells (LRC). Arrows indicate the location of LRCs at day 7. * indicates the location of a single LRC at day 67, which is located within the base of the SMG (Pan et al., 2013. Image reproduced with permission).*

Unfortunately, further conclusions could not be drawn from this study as it was never repeated and there was only limited tissue available for analysis. However, using the xenograft model, a similar analysis of human tissue has been performed. Results from this assay revealed that the bulk of cellular activity within Barrett's tissue occurs within the crypt and glandular regions and that a population of label retaining cells reside below the columnar cells at the SCJ junction (Figure 5-14). IHC analysis revealed that the label retaining cells share the same location as p63 positive squamous cells.

Coincidentally, a similar population of p63 positive cells have also been identified from within human Barrett's tissue from a group led by Prof Krishnadath from the AMC in Amsterdam (Figure 5-21). This group were attempting to therapeutically target these potential stem cells through the use of a novel inhibitor of both BMP2 and BMP4 that they had developed (Calpe et al., 2015). Such inhibition is thought to be required for squamous differentiation to occur (Jiang, Ku, Zhou, Dellon, Falk et al., 2015). This led to a collaborative effort in which mice harbouring Barrett's xenografts were treated with this novel inhibitor. Results revealed that treated organoids tended to produce a more squamous-like phenotype and had fewer goblet cells (Appendix 4).

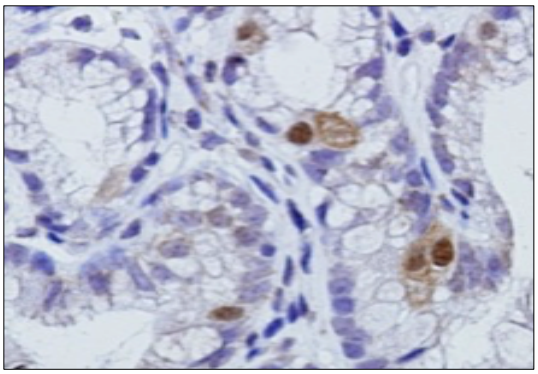

Figure 5-21 Presence of p63 cells within biopsies of BO

IHC staining against p63 reveals the presence of isolated p63 positive cells within a piece of BO tissue obtained at endoscopic biopsy. Image courtesy of Prof K. K. Krishnadath, AMC, Amsterdam).

In summary, the Barrett's xenograft model represents a significant improvement in the field of preclinical models for the study of BO. As already highlighted, it has great potential to be used as a tool to investigate different aspects disease biology such as the identification of stem cells and the role of the SMG. It has also proven to be a robust model and transferable to other laboratories where it has been used as a tool to investigate the effect of a novel molecular inhibitor. As such, it has proven to be a valuable resource.

Chapter 6 Summary and future directions

6.1 Introduction

Oesophageal cancer is the eighth most common cause of cancer death worldwide (Ferlay et al., 2010). In developing countries, this is largely driven by oesophageal SCC. However, in developed countries, the incidence of adenocarcinoma has now surpassed that of SCC (Pohl et al., 2005). This change has been linked to the rising obesity epidemic (Thrift, Pandeya, et al., 2012). Unfortunately, the majority of patients that present with OAC have advanced disease and cannot be cured. However, even in those patients who present with local disease and are treated with curative intent, the 5-year survival is only 45% (Howlader et al., 2015). This is despite a number of recent advances over the last two decades such as the introduction of neoadjuvant chemotherapy and radiotherapy, the development of improved endoscopic techniques for both the detection and management of early cancers, the development of minimally invasive surgical techniques and the improved management of post-operative complications (Thursfield et al., 2012). These measures have only led to an incremental improvement of 6% in the 5-year survival for all patients, over this time period (Thursfield et al., 2012).

It is clear that novel therapies are needed if we are to make any additional impact to the current 5-year survival. Given that the majority of OAC related death are due to the development of metastatic disease, research efforts aimed at improving patient survival need to focus on the treatment of systemic disease. Unfortunately, continued advances in this field have been limited by a lack of suitable preclinical models (Contino et al., 2016). For example, there are only six bona fide OAC cell lines that are widely available. This has been attributed to the limited availability of treatment naïve tissue and the difficulties associated with establishing OAC cell lines (Liu, Duong, et al., 2016). Another frequently used model, the PDTX, is also associated with low engraftment rates (Read et al., 2016). There is also no preclinical model for BO, the only known precursor lesion for OAC (Read et al., 2018). The aim of this thesis, therefore, was to develop improved preclinical models for the study of both Barrett's and OAC.

6.2 Summary of major findings

Central to this thesis is the development of an improved technique for the establishment of oesophageal PDTXs. Through the use of an IM transplantation technique, rather than the standard subcutaneous approach, the engraftment rate has more than doubled (Read et al., 2016). Validation has also confirmed that the PDTX model recapitulates the original tumour with respect to degree of differentiation, molecular and genetic profile and tumour biology. However, validation also confirmed that 20% of successfully engrafted PDTXs had undergone lymphomagenic transformation. Evidence suggests that this is due to the presence of EBV infected B cells within the transplanted tissue being cultured in an immunodeficient environment. This was an extremely important discovery to make as it has significant implications for the ongoing use of PDTX models, both in oesophageal and other cancers. Prior to these results being published, very few papers had recognised this phenomenon. By publishing these findings, researchers are now becoming cognisant of the potential for lymphomagenic transformation in PDTXs (e.g. Choi et al., 2016; Dieter et al., 2017; Kalavska et al., 2018). This will hopefully prevent the mistaken identification of PDTXs in the future and, with it, the publication of incorrect results.

Traditionally, the PDTX model has been used as a preclinical tool for drug discovery. As each PDTX line has its own unique mutational profile, the range of potential therapeutic targets increases with each additional PDTX line. Therefore, to fully harness the power of the model in this role, repositories, or biobanks, need to be established. Cohorts of specific PDTX lines can then be generated based upon the drug target being tested. However, for this approach to be feasible, PDTXs need to be able to be re-established following cryopreservation. In another major finding of this thesis, a robust and reliable technique for the successful cryopreservation and re-establishment of PDTXs was also reported. Surprisingly, such a technique had not previously been reported for oesophageal PDTXs. The study by Liu et al. highlights how an OAC PDTX line from the biobank was successfully re-established following cryopreservation and used as a preclinical model for drug development (D. S. Liu et al., 2015). Using the same cryopreservation and transplantation techniques, biobanks have been successfully established in other cancers, including both melanoma and anal SCC (Alsop et al., 2016; Bernardi, 2017). In the case of anal SCC, this represents the first reported biobank.

Drawing on the success of the PDTX model, xenografts were used as a perpetual source of tumour tissue in order to generate additional cell lines. In combination with the explant technique (Giard et al., 1973), whereby small tissue pieces (explants) were cultured for extended periods, a robust technique was established for the generation of xenograft-derived cell lines. In this technique, an extended period of culture of up to six months ensured that cells had ample time to adapt to in vitro culture. During this period, cancer cells were also supported by a bed of fibroblasts. This technique led to the formation of two additional OAC cell lines, each with matched PDTX, one of which having both metastatic and non-metastatic clones. Validation confirmed that these xenograft-derived cell lines were tumorigenic and shared the same mutational profile as the original patient tumour. Cell injection xenografts also recapitulated the original patient tumour with respect to degree of differentiation and molecular profile.

Having matched PDTX and xenograft-derived cell lines creates an extremely powerful preclinical tool, as it harnesses the advantages of both models. Such advantages include the presence of human stroma and tumour heterogeneity, as seen within the PDTX model, and the ability to perform high throughput in vitro studies, as seen with the cell line model. This power is further enhanced through the development of both metastatic and non-metastatic clones, providing a unique opportunity to investigate mechanisms associated with metastasis formation as well as potential therapeutic interventions. This is extremely important for research into OAC, as metastasis formation signals treatment failure and is the major cause of death in this patient population. Until now, models to study clinically relevant processes such as metastasis formation in OAC have been limited (Liu, Hoefnagel, et al., 2016).

The IM transplantation technique was also successfully used to form xenografts of both normal human oesophageal mucosa and BO. As these xenografts allow the extended *in vivo* culture of both normal and metaplastic oesophageal tissue they have many potential applications in the study of Barrett's carcinogenesis. The technique has also proven to be robust and transferable to other laboratories. In one of the main applications of the model, a series of experiments were performed at the AMC in Amsterdam, in which a novel molecular inhibitor was tested as a potential treatment for BO. The results from a series of repeated experiments revealed that inhibition of both BMP2 and 4 led to the formation of a squamous phenotype within the xenograft model, compared to vehicle treated xenografts which

maintained a Barrett's-like phenotype. In addition, the xenograft model has also been used to investigate the dynamics of cellular proliferation in BO, revealing that the bulk of cellular proliferation occurs within both crypt and glandular regions. Results also revealed the presence of slower cycling cells residing below the columnar epithelium at the SCJ.

The table below summarises the main advantages, disadvantages and potential applications of each of these newly established models.

Table 6-1 Summary table of the advantages, disadvantages and potential application of each of newly developed model

Model	Advantages	Disadvantages	Potential Applications
Cell Line	• Reproducible • Manipulable • Matched metastatic / non-metastatic clones • Robust • Able to be cryopreserved in order to form a biobank • Lowest cost	• Two-dimensional • Lack heterogeneity • Not completely representative of human tumours	• Testing of novel therapies • Investigate metastatic process
PDTX	• Contains human stroma • Maintains heterogeneity • Recapitulates the original patient tumour • Able to be cryopreserved → biobank	• Time required to establish • Resources required • Potential for lymphomagenic transformation • Unable to test responsiveness to immunotherapies	• Testing of novel therapies • Investigate metastatic process • Investigate model of cancer cell propagation • Investigate novel imaging modalities
Xenograft model of normal oesophageal tissue and BO	• Contain stromal elements • Forms 3-D structures. • Permits labelling of cells • Permits the ongoing culture for extended periods	• Difficult to manipulate • Limited ability to passage • Lacks environmental exposure • Tissue does not expand	• Investigation of stem cell biology • Investigating the role of the SMG • Testing of novel therapies

6.3 Future Directions

Future directions stemming from this thesis can be divided into two key areas. The first involves identifying additional experiments that are required in order to complete the validation of these newly developed models. The second involves the application of the models to clinically relevant areas.

Whilst the PDTX model has already undergone complete validation, both the cell lines and xenograft models of normal human oesophagus and BO require further characterisation. In regard to the cell lines, the majority of the validation already performed has focused on characterising both the in vitro and in vivo phenotype. In contrast, aside from the results from the targeted sequencing of known oncogenes and a STR analysis, little is known about the genotype of the cell lines. In order to better understand this, I would like to perform whole genome sequencing on the newly established lines. In order to do this, I have donated the cell lines to Professor Rebecca Fitzgerald, who is a key researcher in the field. Professor Fitzgerald has previously performed a large sequencing study on the range of OAC cell lines that were previously available (Contino et al., 2016). As part of a follow up study that is soon to be published, newly developed cell lines are also being sequenced. Included in this study are the cell lines IS076-A, IS076-P and TB471. This will ensure a more thorough validation of the cell lines and provide researchers with additional information to help with experimental design. Following publication, it is also intended that these newly derived cell lines will be placed into a cell line repository, in order to share this valuable resource.

In order to fully characterise the phenotype of the metastatic model, I would like to repeat both the migration assays and western blot analysis for the known markers of EMT. In addition, I have also submitted the matched metastatic and non-metastatic cell lines to a larger RNA sequencing study that is being conducted by Professor Krishnadath. This may provide greater insights into the metastatic pathways involved in OAC. It also has the potential to identify new therapeutic targets, which is clinically significant given that metastasis formation is the main cause of death in this patient population.

With respect to the Barrett's xenograft model, I would like to perform two additional experiments. Firstly, I would like to have additional attempts at passaging the xenografts, as I have only had limited success with this to date. If successful, this will increase the power of

the model by making it more accessible and, potentially, more manipulable. Secondly, I would like to perform a further analysis of the p63 positive cells that were identified below the columnar epithelium at the SCJ in the xenograft model. I believe that this observation is an important discovery, and that these cells may represent squamous progenitor cells. In order to confirm this, I would like to co-stain FFPE sections from xenografts that have been labelled with BrdU to confirm if the LRC are also the p63 positive cells.

In regard to the potential applications of these models, my first preference would be to continue the work that was performed in chapter three, which looked at the role of BMP inhibition in OAC. The preliminary results assessing the effectiveness of a new class of BMP inhibitor in the treatment of OAC were extremely encouraging. Also of interest, is its potential role in image directed surgery, as PDTXs with high BMP expression were able to be imaged through the use of a labelled form of this drug. If successful, this could have a significant impact in the surgical treatment of OAC.

In conclusion, this thesis describes the development and validation of multiple novel preclinical models for the study of Barrett's carcinogenesis. These models include an improved PDTX model, multiple new cell lines with matched PDTXs, including a subclone that spontaneously metastasises and the first xenograft model of both normal human oesophageal mucosa and BO. Given the paucity of pre-existing models that are clinically relevant, the development and successful validation of these new models constitutes a significant advancement in the field of OAC. By harnessing the full potential of these models, it is hoped that researchers will be able to develop further insights into this devastating disease and be able to translate future discoveries into improved patient outcomes.

References

Al-Batran, S.-E., Hofheinz, R. D., Pauligk, C., Kopp, H.-G., Haag, G. M., Luley, K. B., . . . Tannapfel, A. (2016). Histopathological regression after neoadjuvant docetaxel, oxaliplatin, fluorouracil, and leucovorin versus epirubicin, cisplatin, and fluorouracil or capecitabine in patients with resectable gastric or gastro-oesophageal junction adenocarcinoma (FLOT4-AIO): results from the phase 2 part of a multicentre, open-label, randomised phase 2/3 trial. *The Lancet Oncology, 17*(12), 1697-1708. doi:10.1016/s1470-2045(16)30531-9

Alsop, K., Thorne, H., Sandhu, S., Hamilton, A., Mintoff, C., Christie, E., . . . Bowtell, D. D. (2016). A community-based model of rapid autopsy in end-stage cancer patients. *Nat Biotechnol, 34*(10), 1010-1014. doi:10.1038/nbt.3674

Altorki, N., Schwartz, G. K., Blundell, M., Davis, B. M., Kelsen, D. P., & Albino, A. P. (1993). Characterization of cell lines established from human gastric-esophageal adenocarcinomas. Biologic phenotype and invasion potential. *Cancer, 72*(3), 649-657.

Alvarez, H., Koorstra, J. B., Hong, S. M., Boonstra, J. J., Dinjens, W. N., Foratiere, A. A., . . . Maitra, A. (2008). Establishment and characterization of a bona fide Barrett esophagus-associated adenocarcinoma cell line. *Cancer Biol Ther, 7*(11), 1753-1755.

Apisarnthanarax, S., Alauddin, M. M., Mourtada, F., Ariga, H., Raju, U., Mawlawi, O., . . . Chao, K. S. (2006). Early detection of chemoradioresponse in esophageal carcinoma by 3'-deoxy-3'-3H-fluorothymidine using preclinical tumor models. *Clin Cancer Res, 12*(15), 4590-4597. doi:10.1158/1078-0432.CCR-05-2720

Barbiere, J. M., & Lyratzopoulos, G. (2009). Cost-effectiveness of endoscopic screening followed by surveillance for Barrett's esophagus: a review. *Gastroenterology, 137*(6), 1869-1876. doi:10.1053/j.gastro.2009.10.011

Becker, L., Huang, Q., & Mashimo, H. (2010). Lgr5, an intestinal stem cell marker, is abnormally expressed in Barrett's esophagus and esophageal adenocarcinoma. *Dis Esophagus, 23*(2), 168-174. doi:10.1111/j.1442-2050.2009.00979.x

Behrens, D., Walther, W., & Fichtner, I. (2017). Pancreatic cancer models for translational research. *Pharmacol Ther, 173*, 146-158. doi:10.1016/j.pharmthera.2017.02.013

Bernardi, M. P. (2017). *Prediction and Prognosis in Anal Cancer: Developing Models to Improve Patient Outcome.* (Doctor of Medical Science), The University of Melbourne, Melbourne.

Bobryshev, Y. V., Freeman, A. K., Botelho, N. K., Tran, D., Levert-Mignon, A. J., & Lord, R. V. (2010). Expression of the putative stem cell marker Musashi-1 in Barrett's esophagus and esophageal adenocarcinoma. *Dis Esophagus, 23*(7), 580-589. doi:10.1111/j.1442-2050.2010.01061.x

Boeckxstaens, G. E., & Rohof, W. O. (2014). Pathophysiology of gastroesophageal reflux disease. *Gastroenterol Clin North Am, 43*(1), 15-25. doi:10.1016/j.gtc.2013.11.001

Boonstra, J. J., Tilanus, H. W., & Dinjens, W. N. (2015). Translational research on esophageal adenocarcinoma: from cell line to clinic. *Dis Esophagus, 28*(1), 90-96. doi:10.1111/dote.12095

Boonstra, J. J., van der Velden, A. W., Beerens, E. C. W., van Marion, R., Morita-Fujimura, Y., Matsui, Y., . . . Dinjens, W. N. M. (2007). Mistaken identity of widely used esophageal adenocarcinoma cell line TE-7. *Cancer Res, 67*(17), 7996-8001.

Boonstra, J. J., van Marion, R., Beer, D. G., Lin, L., Chaves, P., Ribeiro, C., . . . Dinjens, W. N. M. (2010). Verification and unmasking of widely used human esophageal adenocarcinoma cell lines. *J Natl Cancer Inst, 102*(4), 271-274.

Boonstra, J. J., van Marion, R., Douben, H. J., Lanchbury, J. S., Timms, K. M., Abkevich, V., . . . Dinjens, W. N. (2012). Mapping of homozygous deletions in verified esophageal adenocarcinoma cell lines and xenografts. *Genes Chromosomes Cancer, 51*(3), 272-282. doi:10.1002/gcc.20952

Boonstra, J. J., van Marion, R., Douben, H. J. C. W., Lanchbury, J. S., Timms, K. M., Abkevich, V., . . . Dinjens, W. N. M. (2012). Mapping of homozygous deletions in verified esophageal adenocarcinoma cell lines and xenografts. *Genes, chromosomes & cancer, 51*(3), 272-282. doi:10.1002/gcc.20952

Butler, K. A., Hou, X., Becker, M. A., Zanfagnin, V., Enderica-Gonzalez, S., Visscher, D., . . . Weroha, S. J. (2017). Prevention of Human Lymphoproliferative Tumor Formation in Ovarian Cancer Patient-Derived Xenografts. *Neoplasia, 19*(8), 628-636. doi:10.1016/j.neo.2017.04.007

Calpe, S., Correia, A. C., Sancho-Serra Mdel, C., & Krishnadath, K. K. (2016). Comparison of newly developed anti-bone morphogenetic protein 4 llama-derived antibodies with commercially available BMP4 inhibitors. *MAbs, 8*(4), 678-688. doi:10.1080/19420862.2016.1158380

Calpe, S., Wagner, K., El Khattabi, M., Rutten, L., Zimberlin, C., Dolk, E., . . . Krishnadath, K. K. (2015). Effective Inhibition of Bone Morphogenetic Protein Function by Highly Specific Llama-Derived Antibodies. *Mol Cancer Ther, 14*(11), 2527-2540. doi:10.1158/1535-7163.MCT-14-0956

Cancer Council Victoria. (2011). *Cancer in Victoria Statistics & Trends 2010*.

Chen, K., Ahmed, S., Adeyi, O., Dick, J. E., & Ghanekar, A. (2012). Human solid tumor xenografts in immunodeficient mice are vulnerable to lymphomagenesis associated with Epstein-Barr virus. *PLoS One, 7*(6), e39294. doi:10.1371/journal.pone.0039294

Chen, Z., Cheng, K., Walton, Z., Wang, Y., Ebi, H., Shimamura, T., . . . Wong, K. K. (2012). A murine lung cancer co-clinical trial identifies genetic modifiers of therapeutic response. *Nature, 483*(7391), 613-617. doi:10.1038/nature10937

Chiu, P. W. Y., Uedo, N., Singh, R., Gotoda, T., Ng, E. K. W., Yao, K., . . . Inoue, H. (2019). An Asian consensus on standards of diagnostic upper endoscopy for neoplasia. *Gut, 68*(2), 186-197. doi:10.1136/gutjnl-2018-317111

Cho, S. S., Jeon, J., Buch, L., Nag, S., Nasrallah, M., Low, P. S., . . . Lee, J. Y. K. (2018). Intraoperative near-infrared imaging with receptor-specific versus passive delivery of fluorescent agents in pituitary adenomas. *J Neurosurg*, 1-11. doi:10.3171/2018.7.JNS181642

Choi, Y. Y., Lee, J. E., Kim, H., Sim, M. H., Kim, K. K., Lee, G., . . . Cheong, J. H. (2016). Establishment and characterisation of patient-derived xenografts as paraclinical models for gastric cancer. *Sci Rep, 6*, 22172. doi:10.1038/srep22172

Civenni, G., Walter, A., Kobert, N., Mihic-Probst, D., Zipser, M., Belloni, B., . . . Sommer, L. (2011). Human CD271-positive melanoma stem cells associated with metastasis establish tumor heterogeneity and long-term growth. *Cancer Res, 71*(8), 3098-3109. doi:10.1158/0008-5472.can-10-3997

Clemons, N. J., Do, H., Fennell, C., Deb, S., Fellowes, A., Dobrovic, A., & Phillips, W. A. (2014). Characterization of a novel tumorigenic esophageal adenocarcinoma cell line: OANC1. *Dig Dis Sci, 59*(1), 78-88. doi:10.1007/s10620-013-2882-8

Clemons, N. J., Koh, S. Y., & Phillips, W. A. (2014). Advances in understanding the pathogenesis of Barrett's esophagus. *Discov Med, 17*(91), 7-14.

Clemons, N. J., Phillips, W. A., & Lord, R. V. (2013). Signaling pathways in the molecular pathogenesis of adenocarcinomas of the esophagus and gastroesophageal junction. *Cancer Biol Ther, 14*(9), 782-795. doi:10.4161/cbt.25362

Coad, R. A., Woodman, A. C., Warner, P. J., Barr, H., Wright, N. A., & Shepherd, N. A. (2005). On the histogenesis of Barrett's oesophagus and its associated squamous islands: a three-dimensional study of their morphological relationship with native oesophageal gland ducts. *J Pathol, 206*(4), 388-394. doi:10.1002/path.1804

Contino, G., Eldridge, M. D., Secrier, M., Bower, L., Fels Elliott, R., Weaver, J., . . . Fitzgerald, R. C. (2016). Whole-genome sequencing of nine esophageal adenocarcinoma cell lines. *F1000Res, 5*, 1336. doi:10.12688/f1000research.7033.1

Cooper, G. S., Kou, T. D., & Chak, A. (2009). Receipt of previous diagnoses and endoscopy and outcome from esophageal adenocarcinoma: a population-based study with temporal trends. *Am J Gastroenterol, 104*(6), 1356-1362. doi:10.1038/ajg.2009.159

Cowie, A., Garcia, E., Hayden, A. L., & Underwood, T. (2015). *Developing model systems to understand the functional and clinical significance of somatic genetic variations in oesophageal cancer*. Paper presented at the Association of Surgeons of Great Britain and Ireland Annual Congress, Manchester.

Craig, F. E., & Foon, K. A. (2008). Flow cytometric immunophenotyping for hematologic neoplasms. *Blood, 111*(8), 3941-3967. doi:10.1182/blood-2007-11-120535

Croagh, D. (2006). *Identification and characterization of mouse oesophageal stem cells and the development of an in vivo model to investigate the pathogenesis of Barrett's oesophagus.* (Doctor of Philosophy), The University of Melbourne, Melbourne.

Croagh, D., Phillips, W. A., Redvers, R., Thomas, R. J. S., & Kaur, P. (2007). Identification of candidate murine esophageal stem cells using a combination of cell kinetic studies and cell surface markers. *Stem Cells, 25*(2), 313-318.

Cunningham, D., Allum, W. H., Stenning, S. P., Thompson, J. N., Van de Velde, C. J., Nicolson, M., . . . Participants, M. T. (2006). Perioperative chemotherapy versus surgery alone for resectable gastroesophageal cancer. *N Engl J Med, 355*(1), 11-20. doi:10.1056/NEJMoa055531

Cunningham, D., & You, Z. (2015). In vitro and in vivo model systems used in prostate cancer research. *J Biol Methods, 2*(1). doi:10.14440/jbm.2015.63

Dangles-Marie, V., Pocard, M., Richon, S., Weiswald, L. B., Assayag, F., Saulnier, P., . . . Poupon, M. F. (2007). Establishment of human colon cancer cell lines from

fresh tumors versus xenografts: comparison of success rate and cell line features. *Cancer Res, 67*(1), 398-407. doi:10.1158/0008-5472.CAN-06-0594

de Both, N. J., Wijnhoven, B. P., Sleddens, H. F., Tilanus, H. W., & Dinjens, W. N. (2001). Establishment of cell lines from adenocarcinomas of the esophagus and gastric cardia growing in vivo and in vitro. *Virchows Arch, 438*(5), 451-456. doi:10.1007/s004280000358

Dean, M., Fojo, T., & Bates, S. (2005). Tumour stem cells and drug resistance. *Nat Rev Cancer, 5*(4), 275-284.

Decaudin, D. (2011). Primary human tumor xenografted models ('tumorgrafts') for good management of patients with cancer. *Anticancer Drugs, 22*(9), 827-841. doi:10.1097/CAD.0b013e3283475f70

Dieter, S. M., Giessler, K. M., Kriegsmann, M., Dubash, T. D., Mohrmann, L., Schulz, E. R., . . . Ball, C. R. (2017). Patient-derived xenografts of gastrointestinal cancers are susceptible to rapid and delayed B-lymphoproliferation. *Int J Cancer, 140*(6), 1356-1363. doi:10.1002/ijc.30561

Dodbiba, L., Teichman, J., Fleet, A., Thai, H., Starmans, M. H., Navab, R., . . . Liu, G. (2015). Appropriateness of using patient-derived xenograft models for pharmacologic evaluation of novel therapies for esophageal/gastro-esophageal junction cancers. *PLoS One, 10*(3), e0121872. doi:10.1371/journal.pone.0121872

Dodbiba, L., Teichman, J., Fleet, A., Thai, H., Sun, B., Panchal, D., . . . Liu, G. (2013a). Primary esophageal and gastro-esophageal junction cancer xenograft models: clinicopathological features and engraftment. *Lab Invest*. doi:10.1038/labinvest.2013.8

Dodbiba, L., Teichman, J., Fleet, A., Thai, H., Sun, B., Panchal, D., . . . Liu, G. (2013b). Primary esophageal and gastro-esophageal junction cancer xenograft models: clinicopathological features and engraftment. *Lab Invest, 93*(4), 397-407. doi:10.1038/labinvest.2013.8

El-Rifai, W., Harper, J. C., Cummings, O. W., Hyytinen, E. R., Frierson, H. F., Jr., Knuutila, S., & Powell, S. M. (1998). Consistent genetic alterations in xenografts of proximal stomach and gastro-esophageal junction adenocarcinomas. *Cancer Res, 58*(1), 34-37.

Evans, J. A., & McDonald, S. A. (2016). The Complex, Clonal, and Controversial Nature of Barrett's Esophagus. *Adv Exp Med Biol, 908*, 27-40. doi:10.1007/978-3-319-41388-4_3

Ferlay, J., Shin, H. R., Bray, F., Forman, D., Mathers, C., & Parkin, D. M. (2010). Estimates of worldwide burden of cancer in 2008: GLOBOCAN 2008. *Int J Cancer, 127*(12), 2893-2917. doi:10.1002/ijc.25516

Findlay, J. M., & Maynard, N. D. (2019). Pathophysiology and investigation of gastro-oesophageal reflux disease. In M. S. Griffin (Ed.), *Oesophagogastric Surgery: A Companion to Specialist Surgical Practice,* : Elsevier.

Frankell, A. M., Jammula, S., Li, X., Contino, G., Killcoyne, S., Abbas, S., . . . Fitzgerald, R. C. (2019). The landscape of selection in 551 esophageal adenocarcinomas defines genomic biomarkers for the clinic. *Nat Genet, 51*(3), 506-516. doi:10.1038/s41588-018-0331-5

Garcia, E., Hayden, A., Cowie, A., Mellone, M., Derouet, M., Duriez, P., . . . Underwood, T. J. (2015). AUTHENTICATION AND CHARACTERISATION OF A NEW OESOPHAGEAL ADENOCARCINOMA CELL LINE: MFD-1. *Gut, 64*(Suppl 1), A125-126.

Gazdar, A. F., Girard, L., Lockwood, W. W., Lam, W. L., & Minna, J. D. (2010). Lung cancer cell lines as tools for biomedical discovery and research. *J Natl Cancer Inst, 102*(17), 1310-1321. doi:10.1093/jnci/djq279

Giard, D. J., Aaronson, S. A., Todaro, G. J., Arnstein, P., Kersey, J. H., Dosik, H., & Parks, W. P. (1973). In vitro cultivation of human tumors: establishment of cell lines derived from a series of solid tumors. *J Natl Cancer Inst, 51*(5), 1417-1423.

Gillen, P., Keeling, P., Byrne, P. J., West, A. B., & Hennessy, T. P. (1988). Experimental columnar metaplasia in the canine oesophagus. *Br J Surg, 75*(2), 113-115.

Gregson, E. M., Bornschein, J., & Fitzgerald, R. C. (2016). Genetic progression of Barrett's oesophagus to oesophageal adenocarcinoma. *Br J Cancer, 115*(4), 403-410. doi:10.1038/bjc.2016.219

Gros, S. J., Kurschat, N., Dohrmann, T., Reichelt, U., Dancau, A. M., Peldschus, K., . . . Kaifi, J. T. (2010). Effective therapeutic targeting of the overexpressed HER-2 receptor in a highly metastatic orthotopic model of esophageal carcinoma. *Mol Cancer Ther, 9*(7), 2037-2045. doi:10.1158/1535-7163.MCT-10-0209

Grotenhuis, B. A., Dinjens, W. N., Wijnhoven, B. P., Sonneveld, P., Sacchetti, A., Franken, P. F., . . . Fodde, R. (2010). Barrett's oesophageal adenocarcinoma encompasses tumour-initiating cells that do not express common cancer stem cell markers. *J Pathol, 221*(4), 379-389. doi:10.1002/path.2733

Grotenhuis, B. A., Wijnhoven, B. P., & van Lanschot, J. J. (2012). Cancer stem cells and their potential implications for the treatment of solid tumors. *J Surg Oncol, 106*(2), 209-215. doi:10.1002/jso.23069

Guerreschi, P., Scalbert, C., Qassemyar, A., Kluza, J., Ravasi, L., Huglo, D., . . . Mortier, L. (2013). Patient-derived tumor xenograft model to guide the use of BRAF inhibitors in metastatic melanoma. *Melanoma Res, 23*(5), 373-380. doi:10.1097/CMR.0b013e328363ed92

Hidalgo, M., Amant, F., Biankin, A. V., Budinska, E., Byrne, A. T., Caldas, C., . . . Villanueva, A. (2014). Patient-derived xenograft models: an emerging platform for translational cancer research. *Cancer Discov, 4*(9), 998-1013. doi:10.1158/2159-8290.CD-14-0001

Howlader, Noone, Krapcho, Garshell, Miller, Altekruse, . . . Cronin. (2015). SEER Cancer Statistics Review, 1975-2012, National Cancer Institute. *J Natl Cancer Inst*.

Hughes, S. J., Nambu, Y., Soldes, O. S., Hamstra, D., Rehemtulla, A., Iannettoni, M. D., . . . Beer, D. G. (1997). Fas/APO-1 (CD95) is not translocated to the cell membrane in esophageal adenocarcinoma. *Cancer Res, 57*(24), 5571-5578.

Jadvar, H., Alavi, A., & Gambhir, S. S. (2009). 18F-FDG uptake in lung, breast, and colon cancers: molecular biology correlates and disease characterization. *J Nucl Med, 50*(11), 1820-1827. doi:10.2967/jnumed.108.054098

Jaiswal, K. R., Morales, C. P., Feagins, L. A., Gandia, K. G., Zhang, X., Zhang, H. Y., . . . Souza, R. F. (2007). Characterization of telomerase-immortalized, non-neoplastic, human Barrett's cell line (BAR-T). *Diseases Of The Esophagus: Official Journal Of The International Society For Diseases Of The Esophagus / I.S.D.E, 20*(3), 256-264.

Jiang, M., Ku, W. Y., Zhou, Z., Dellon, E. S., Falk, G. W., Nakagawa, H., . . . Que, J. (2015). BMP-driven NRF2 activation in esophageal basal cell differentiation and eosinophilic esophagitis. *J Clin Invest, 125*(4), 1557-1568. doi:10.1172/JCI78850

Jiang, M., Li, H., Zhang, Y., Yang, Y., Lu, R., Liu, K., . . . Que, J. (2017). Transitional basal cells at the squamous-columnar junction generate Barrett's oesophagus. *Nature, 550*(7677), 529-533. doi:10.1038/nature24269

John, T., Yanagawa, N., Kohler, D., Craddock, K. J., Bandarchi-Chamkhaleh, B., Pintilie, M., . . . Tsao, M. S. (2012). Characterization of lymphomas developing in immunodeficient mice implanted with primary human non-small cell lung cancer. *J Thorac Oncol, 7*(7), 1101-1108. doi:10.1097/JTO.0b013e3182519d4d

Kalavska, K., Kucerova, L., Schmidtova, S., Toro, L., Kozovska, Z., Plank, L., . . . Mego, M. (2018). Lymphoma transformation of tumor infiltrating lymphocytes observed in testicular patientderived xenograft models. *Oncol Rep, 40*(6), 3593-3602. doi:10.3892/or.2018.6769

Kan, T., Shimada, Y., Sato, F., Maeda, M., Kawabe, A., Kaganoi, J., . . . Imamura, M. (2001). Gene expression profiling in human esophageal cancers using cDNA microarray. *Biochem Biophys Res Commun, 286*(4), 792-801. doi:10.1006/bbrc.2001.5400

Kapoor, H., Agrawal, D. K., & Mittal, S. K. (2015). Barrett's esophagus: recent insights into pathogenesis and cellular ontogeny. *Transl Res, 166*(1), 28-40. doi:10.1016/j.trsl.2015.01.009

Kawaguchi, N., Toriyama, K., Nicodemou-Lena, E., Inou, K., Torii, S., & Kitagawa, Y. (1998). De novo adipogenesis in mice at the site of injection of basement membrane and basic fibroblast growth factor. *Proc Natl Acad Sci U S A, 95*(3), 1062-1066.

Keld, R. R., & Ang, Y. S. (2011). Targeting key signalling pathways in oesophageal adenocarcinoma: a reality for personalised medicine? *World J Gastroenterol, 17*(23), 2781-2790. doi:10.3748/wjg.v17.i23.2781

Kelloff, G. J., Hoffman, J. M., Johnson, B., Scher, H. I., Siegel, B. A., Cheng, E. Y., . . . Sullivan, D. C. (2005). Progress and Promise of FDG-PET Imaging for Cancer Patient Management and Oncologic Drug Development. *Clin Cancer Res, 11*(8), 2785-2808.

Kemper, K., Prasetyanti, P. R., De Lau, W., Rodermond, H., Clevers, H., & Medema, J. P. (2012). Monoclonal antibodies against Lgr5 identify human colorectal cancer stem cells. *Stem Cells, 30*(11), 2378-2386. doi:10.1002/stem.1233

Kleinberg, L. (2013). Therapy for locally advanced adenocarcinoma of the gastroesophageal junction: optimizing outcome. *Semin Radiat Oncol, 23*(1), 38-50. doi:10.1016/j.semradonc.2012.10.001

Kong, J., Crissey, M. A., Funakoshi, S., Kreindler, J. L., & Lynch, J. P. (2011). Ectopic Cdx2 expression in murine esophagus models an intermediate stage in the emergence of Barrett's esophagus. *PLoS One, 6*(4), e18280. doi:10.1371/journal.pone.0018280

Krishnadath, K. K. (2007). Novel findings in the pathogenesis of esophageal columnar metaplasia or Barrett's esophagus. *Curr Opin Gastroenterol, 23*(4), 440-445. doi:10.1097/MOG.0b013e32814e6b4f

Krishnadath, K. K., & Wang, K. K. (2015). Molecular pathogenesis of Barrett esophagus: current evidence. *Gastroenterol Clin North Am, 44*(2), 233-247. doi:10.1016/j.gtc.2015.02.002

Krishnan, B., & Morgan, G. J. (2007). Non-Hodgkin lymphoma secondary to cancer chemotherapy. *Cancer Epidemiol Biomarkers Prev, 16*(3), 377-380. doi:10.1158/1055-9965.EPI-06-1069

Kuo, B., & Urma, D. (2006). Esophagus - anatomy and development. *GI Motility Online.*

Kuriya, Y., Kitamura, M., Akaishi, T., Hirayama, K., Sekine, Y., Nishihira, T., & Kasai, M. (1983). A new cell line (TE-3) derived from human squamous cell carcinoma of the esophagus. *Tohoku J Exp Med, 139*(4), 377-387.

Landais, E., Saulquin, X., & Houssaint, E. (2005). The human T cell immune response to Epstein-Barr virus. *Int J Dev Biol, 49*(2-3), 285-292. doi:10.1387/ijdb.041947el

Lengyel, E., Burdette, J. E., Kenny, H. A., Matei, D., Pilrose, J., Haluska, P., . . . Stack, M. S. (2014). Epithelial ovarian cancer experimental models. *Oncogene, 33*(28), 3619-3633. doi:10.1038/onc.2013.321

Li, X. F., Du, Y., Ma, Y., Postel, G. C., & Civelek, A. C. (2014). (18)F-fluorodeoxyglucose uptake and tumor hypoxia: revisit (18)f-fluorodeoxyglucose in oncology application. *Transl Oncol, 7*(2), 240-247. doi:10.1016/j.tranon.2014.02.010

Liu, Yuan, X., Zeng, Z., Tunici, P., Ng, H., Abdulkadir, I. R., . . . Yu, J. S. (2006). Analysis of gene expression and chemoresistance of CD133+ cancer stem cells in glioblastoma. *Mol Cancer, 5*, 67. doi:10.1186/1476-4598-5-67

Liu, C. Y., Lin, H. H., Tang, M. J., & Wang, Y. K. (2015). Vimentin contributes to epithelial-mesenchymal transition cancer cell mechanics by mediating cytoskeletal organization and focal adhesion maturation. *Oncotarget, 6*(18), 15966-15983. doi:10.18632/oncotarget.3862

Liu, D. S., Duong, C. P., Phillips, W. A., & Clemons, N. J. (2016). Preclinical models of esophageal adenocarcinoma for drug development. *Discov Med, 22*(123), 371-379.

Liu, D. S., Hoefnagel, S. J., Fisher, O. M., Krishnadath, K. K., Montgomery, K. G., Busuttil, R. A., . . . Clemons, N. J. (2016). Novel metastatic models of esophageal adenocarcinoma derived from FLO-1 cells highlight the importance of E-cadherin in cancer metastasis. *Oncotarget, 7*(50), 83342-83358. doi:10.18632/oncotarget.13391

Liu, D. S., Read, M., Cullinane, C., Azar, W. J., Fennell, C. M., Montgomery, K. G., . . . Phillips, W. A. (2015). APR-246 potently inhibits tumour growth and overcomes chemoresistance in preclinical models of oesophageal adenocarcinoma. *Gut, 64*(10), 1506-1516. doi:10.1136/gutjnl-2015-309770

Maas-Szabowski, N., Fusenig, N. E., & Stark, H. J. (2005). Experimental models to analyze differentiation functions of cultured keratinocytes in vitro and in vivo. *Methods Mol Biol, 289*, 47-60.

Mahajan, A., & Cook, G. (2016). Clinical Applications of PET/CT in Oncology. In M. Khalil (Ed.), *Basic Science of PET Imaging*: Springer, Cham.

Mandard, A. M., Dalibard, F., Mandard, J. C., Marnay, J., Henry-Amar, M., Petiot, J. F., . . . et al. (1994). Pathologic assessment of tumor regression after preoperative chemoradiotherapy of esophageal carcinoma. Clinicopathologic correlations. *Cancer, 73*(11), 2680-2686.

Mari, L., Milano, F., Parikh, K., Straub, D., Everts, V., Hoeben, K. K., . . . Krishnadath, K. K. (2014). A pSMAD/CDX2 complex is essential for the intestinalization of epithelial metaplasia. *Cell Rep, 7*(4), 1197-1210. doi:10.1016/j.celrep.2014.03.074

Milano, F., van Baal, J. W., Buttar, N. S., Rygiel, A. M., de Kort, F., DeMars, C. J., . . . Krishnadath, K. K. (2007). Bone morphogenetic protein 4 expressed in

esophagitis induces a columnar phenotype in esophageal squamous cells. *Gastroenterology, 132*(7), 2412-2421. doi:10.1053/j.gastro.2007.03.026
Mohammed, I. A., Streutker, C. J., & Riddell, R. H. (2002). Utilization of Cytokeratins 7 and 20 Does Not Differentiate between Barrett's Esophagus and Gastric Cardiac Intestinal Metaplasia. *Modern Pathology, 15*(6), 611.
Moroz, M. A., Kochetkov, T., Cai, S., Wu, J., Shamis, M., Nair, J., . . . Blasberg, R. G. (2011). Imaging colon cancer response following treatment with AZD1152: a preclinical analysis of [18F]fluoro-2-deoxyglucose and 3'-deoxy-3'-[18F]fluorothymidine imaging. *Clin Cancer Res, 17*(5), 1099-1110. doi:10.1158/1078-0432.CCR-10-1430
Mullard, A. (2018). Can you trust your cancer cell lines? *Nat Rev Drug Discov, 17*(9), 613. doi:10.1038/nrd.2018.154
Munk Jensen, M., Erichsen, K. D., Bjorkling, F., Madsen, J., Jensen, P. B., Sehested, M., . . . Kjaer, A. (2013). Imaging of treatment response to the combination of carboplatin and paclitaxel in human ovarian cancer xenograft tumors in mice using FDG and FLT PET. *PLoS One, 8*(12), e85126. doi:10.1371/journal.pone.0085126
Nakagawa, H., Whelan, K., & Lynch, J. P. (2015). Mechanisms of Barrett's oesophagus: intestinal differentiation, stem cells, and tissue models. *Best Pract Res Clin Gastroenterol, 29*(1), 3-16. doi:10.1016/j.bpg.2014.11.001
Neuman, B. P., Eifler, J. B., Castanares, M., Chowdhury, W. H., Chen, Y., Mease, R. C., . . . Rodriguez, R. (2015). Real-time, near-infrared fluorescence imaging with an optimized dye/light source/camera combination for surgical guidance of prostate cancer. *Clin Cancer Res, 21*(4), 771-780. doi:10.1158/1078-0432.CCR-14-0891
Nicholson, A. M., Graham, T. A., Simpson, A., Humphries, A., Burch, N., Rodriguez-Justo, M., . . . Jankowski, J. A. (2012). Barrett's metaplasia glands are clonal, contain multiple stem cells and share a common squamous progenitor. *Gut, 61*(10), 1380-1389. doi:10.1136/gutjnl-2011-301174
Nishihira, T., Hashimoto, Y., Katayama, M., Mori, S., & Kuroki, T. (1993). Molecular and cellular features of esophageal cancer cells. *J Cancer Res Clin Oncol, 119*(8), 441-449.
Nishihira, T., Kasai, M., Mori, S., Watanabe, T., Kuriya, Y., Suda, M., . . . Sasaki, T. (1979). Characteristics of two cell lines (TE-1 and TE-2) derived from human squamous cell carcinoma of the esophagus. *Gan, 70*(5), 575-584.
Nones, K., Waddell, N., Wayte, N., Patch, A. M., Bailey, P., Newell, F., . . . Barbour, A. P. (2014). Genomic catastrophes frequently arise in esophageal adenocarcinoma and drive tumorigenesis. *Nat Commun, 5*, 5224. doi:10.1038/ncomms6224
Offman, J., & Fitzgerald, R. C. (2017). Alternatives to Traditional Per-Oral Endoscopy for Screening. *Gastrointest Endosc Clin N Am, 27*(3), 379-396. doi:10.1016/j.giec.2017.02.002
Ong, C.-A. J., Lao-Sirieix, P., & Fitzgerald, R. C. (2010). Biomarkers in Barrett's esophagus and esophageal adenocarcinoma: predictors of progression and prognosis. *World Journal Of Gastroenterology: WJG, 16*(45), 5669-5681.
Orlando, R. C. (1998). Review article: oesophageal mucosal resistance. *Aliment Pharmacol Ther, 12*(3), 191-197.
Pan, Q., Nicholson, A. M., Barr, H., Harrison, L. A., Wilson, G. D., Burkert, J., . . . Jankowski, J. A. (2013). Identification of lineage-uncommitted, long-lived, label-

retaining cells in healthy human esophagus and stomach, and in metaplastic esophagus. *Gastroenterology, 144*(4), 761-770. doi:10.1053/j.gastro.2012.12.022
Paterson, W. G. (2006). Esophageal peristalsis. *GI Motility Online.*
Pohl, H., & Welch, H. G. (2005). The role of overdiagnosis and reclassification in the marked increase of esophageal adenocarcinoma incidence. *J Natl Cancer Inst, 97*(2), 142-146. doi:10.1093/jnci/dji024
Public Health England. (2019). *The European Collection of Authenticated Cell Cultures*. United Kingdom: Public Health England Retrieved from www.phe-culturecollections.org.uk/aboutus/index.aspx
Quante, M., Bhagat, G., Abrams, J. A., Marache, F., Good, P., Lee, M. D., . . . Wang, T. C. (2012). Bile acid and inflammation activate gastric cardia stem cells in a mouse model of Barrett-like metaplasia. *Cancer Cell, 21*(1), 36-51. doi:10.1016/j.ccr.2011.12.004
Read, M., Liu, D., Duong, C. P., Cullinane, C., Murray, W. K., Fennell, C. M., . . . Phillips, W. A. (2016). Intramuscular Transplantation Improves Engraftment Rates for Esophageal Patient-Derived Tumor Xenografts. *Ann Surg Oncol, 23*(1), 305-311. doi:10.1245/s10434-015-4425-3
Read, M. D., Krishnadath, K. K., Clemons, N. J., & Phillips, W. A. (2018). Preclinical models for the study of Barrett's carcinogenesis. *Ann N Y Acad Sci, 1434*(1), 139-148. doi:10.1111/nyas.13916
Rhee, H., & Wang, D. H. (2018). Cellular Origins of Barrett's Esophagus: the Search Continues. *Curr Gastroenterol Rep, 20*(11), 51. doi:10.1007/s11894-018-0657-2
Rich, J. N. (2016). Cancer stem cells: understanding tumor hierarchy and heterogeneity. *Medicine (Baltimore), 95*(1 Suppl 1), S2-7. doi:10.1097/MD.0000000000004764
Rockett, J. C., Larkin, K., Darnton, S. J., Morris, A. G., & Matthews, H. R. (1997). Five newly established oesophageal carcinoma cell lines: phenotypic and immunological characterization. *Br J Cancer, 75*(2), 258-263.
Rouvelas, I., & Lagergren, J. (2010). The impact of volume on outcomes after oesophageal cancer surgery. *ANZ J Surg, 80*(9), 634-641. doi:10.1111/j.1445-2197.2010.05406.x
Rubenstein, J. H., & Shaheen, N. J. (2015). Epidemiology, Diagnosis, and Management of Esophageal Adenocarcinoma. *Gastroenterology, 149*(2), 302-317 e301. doi:10.1053/j.gastro.2015.04.053
Rumpel, C. A., Powell, S. M., & Moskaluk, C. A. (1999). Mapping of Genetic Deletions on the Long Arm of Chromosome 4 in Human Esophageal Adenocarcinomas. *The American Journal of Pathology, 154*(5), 1329-1334. doi:10.1016/s0002-9440(10)65386-2
Sarosi, G., Brown, G., Jaiswal, K., Feagins, L. A., Lee, E., Crook, T. W., . . . Spechler, S. J. (2008). Bone marrow progenitor cells contribute to esophageal regeneration and metaplasia in a rat model of Barrett's esophagus. *Dis Esophagus, 21*(1), 43-50. doi:10.1111/j.1442-2050.2007.00744.x
Sato, T., Stange, D. E., Ferrante, M., Vries, R. G., Van Es, J. H., Van den Brink, S., . . . Clevers, H. (2011). Long-term expansion of epithelial organoids from human colon, adenoma, adenocarcinoma, and Barrett's epithelium. *Gastroenterology, 141*(5), 1762-1772. doi:10.1053/j.gastro.2011.07.050

Secrier, M., Li, X., de Silva, N., Eldridge, M. D., Contino, G., Bornschein, J., . . . Fitzgerald, R. C. (2016). Mutational signatures in esophageal adenocarcinoma define etiologically distinct subgroups with therapeutic relevance. *Nat Genet, 48*(10), 1131-1141. doi:10.1038/ng.3659

Seery, J. P., & Watt, F. M. (2000). Asymmetric stem-cell divisions define the architecture of human oesophageal epithelium. *Curr Biol, 10*(22), 1447-1450.

Shackleton, M. (2010). Normal stem cells and cancer stem cells: similar and different. *Semin Cancer Biol, 20*(2), 85-92. doi:10.1016/j.semcancer.2010.04.002

Shimada, Y., Imamura, M., Wagata, T., Yamaguchi, N., & Tobe, T. (1992). Characterization of 21 newly established esophageal cancer cell lines. *Cancer, 69*(2), 277-284.

Sinnatamby, C. S. (2011). *Last's Anatomy Regional and Applied* (12th ed.): Elsevier.

Stoner, G. D., Kaighn, M. E., Reddel, R. R., Resau, J. H., Bowman, D., Naito, Z., . . . Harris, C. C. (1991). Establishment and characterization of SV40 T-antigen immortalized human esophageal epithelial cells. *Cancer Res, 51*(1), 365-371.

Streitz, J. M., Jr. (1994). Barrett's esophagus and esophageal cancer. *Chest surgery clinics of North America, 4*(2).

Sun, D., Wang, X., Gai, Z., Song, X., Jia, X., & Tian, H. (2015). Bile acids but not acidic acids induce Barrett's esophagus. *Int J Clin Exp Pathol, 8*(2), 1384-1392.

Tan, W. K., di Pietro, M., & Fitzgerald, R. C. (2017). Past, present and future of Barrett's oesophagus. *Eur J Surg Oncol, 43*(7), 1148-1160. doi:10.1016/j.ejso.2017.02.004

Tejani, M., & Burtness, B. (2012). Multi-Modality Therapy for Cancer of the Esophagus and GE Junction. *Gastrointestinal Cancers, 13*, 390-402. doi:10.1007/s11864-012-0193-5

Tentler, J. J., Tan, A. C., Weekes, C. D., Jimeno, A., Leong, S., Pitts, T. M., . . . Eckhardt, S. G. (2012). Patient-derived tumour xenografts as models for oncology drug development. *Nat Rev Clin Oncol, 9*(6), 338-350. doi:10.1038/nrclinonc.2012.61

Terada, T. (2013). Epstein-Barr virus associated lymphoepithelial carcinoma of the esophagus. *Int J Clin Exp Med, 6*(3), 219-226.

Thrift, A. P., Kendall, B. J., Pandeya, N., Vaughan, T. L., Whiteman, D. C., & Study of Digestive, H. (2012). A clinical risk prediction model for Barrett esophagus. *Cancer Prev Res (Phila), 5*(9), 1115-1123. doi:10.1158/1940-6207.CAPR-12-0010

Thrift, A. P., Pandeya, N., & Whiteman, D. C. (2012). Current status and future perspectives on the etiology of esophageal adenocarcinoma. *Front Oncol, 2*, 11. doi:10.3389/fonc.2012.00011

Thursfield, V., Farrugia, H., Karahalios, E., & Giles, G. (2012). *Cancer in Survival Victoria 2012: Estimates of survival for 2006-2010 (and comparisons with earlier periods)*. Melbourne: Thursfield V, Farrugia H, Karahalios E, Giles G. Cancer in Survival Victoria 2012: Estimates of survival for 2006-2010 (and comparisons with earlier periods). Cancer Council Victoria, Melbourne 2012 Retrieved from http://vcrdata.cancervic.org.au:8082/ccv/

Tosh, D., & Slack, J. M. (2002). How cells change their phenotype. *Nat Rev Mol Cell Biol, 3*(3), 187-194. doi:10.1038/nrm761

Tummers, W. S., Miller, S. E., Teraphongphom, N. T., van den Berg, N. S., Hasan, A., Longacre, T. A., . . . Poultsides, G. A. (2019). Detection of visually occult

metastatic lymph nodes using molecularly targeted fluorescent imaging during surgical resection of pancreatic cancer. *HPB (Oxford)*. doi:10.1016/j.hpb.2018.11.008

van Baal, J. W., Milana, F., Rygiel, A. M., Sondermeijer, C. M., Spek, C. A., Bergman, J. J., . . . Krishnadath, K. K. (2008). A comparative analysis by SAGE of gene expression profiles of esophageal adenocarcinoma and esophageal squamous cell carcinoma. *Cell Oncol, 30*(1), 63-75.

van Baal, J. W., Rygiel, A. M., Milano, F., Anderson, M., Bergman, J. J., Spek, C. A., . . . Krishnadath, K. K. (2008). Gene expression profile comparison of Barrett's esophagus epithelial cell cultures and biopsies. *Dis Esophagus, 21*(7), 628-633. doi:10.1111/j.1442-2050.2008.00810.x

van Hagen, P., Hulshof, M. C., van Lanschot, J. J., Steyerberg, E. W., van Berge Henegouwen, M. I., Wijnhoven, B. P., . . . Group, C. (2012). Preoperative chemoradiotherapy for esophageal or junctional cancer. *N Engl J Med, 366*(22), 2074-2084. doi:10.1056/NEJMoa1112088

Verstijnen, C. P., Kate, J. T., Arends, J. W., Schutte, B., & Bosman, F. T. (1988). Xenografting of normal colonic mucosa in athymic mice. *J Pathol, 155*(1), 77-85. doi:10.1002/path.1711550112

Visvader, J. E., & Lindeman, G. J. (2012). Cancer stem cells: current status and evolving complexities. *Cell Stem Cell, 10*(6), 717-728. doi:10.1016/j.stem.2012.05.007

Vockerodt, M., Yap, L. F., Shannon-Lowe, C., Curley, H., Wei, W., Vrzalikova, K., & Murray, P. G. (2015). The Epstein-Barr virus and the pathogenesis of lymphoma. *J Pathol, 235*(2), 312-322. doi:10.1002/path.4459

von Furstenberg, R. J., Li, J., Stolarchuk, C., Feder, R., Campbell, A., Kruger, L., . . . Garman, K. S. (2017). Porcine Esophageal Submucosal Gland Culture Model Shows Capacity for Proliferation and Differentiation. *Cell Mol Gastroenterol Hepatol, 4*(3), 385-404. doi:10.1016/j.jcmgh.2017.07.005

Wang, D. H., Clemons, N. J., Miyashita, T., Dupuy, A. J., Zhang, W., Szczepny, A., . . . Watkins, D. N. (2010). Aberrant epithelial-mesenchymal Hedgehog signaling characterizes Barrett's metaplasia. *Gastroenterology, 138*(5), 1810-1822. doi:10.1053/j.gastro.2010.01.048

Wang, D. H., & Souza, R. F. (2011). Biology of Barrett's esophagus and esophageal adenocarcinoma. *Gastrointest Endosc Clin N Am, 21*(1), 25-38. doi:10.1016/j.giec.2010.09.011

Wang, X., Ouyang, H., Yamamoto, Y., Kumar, P. A., Wei, T. S., Dagher, R., . . . McKeon, F. (2011). Residual embryonic cells as precursors of a Barrett's-like metaplasia. *Cell, 145*(7), 1023-1035. doi:10.1016/j.cell.2011.05.026

Wang, Z., Da Silva, T. G., Jin, K., Han, X., Ranganathan, P., Zhu, X., . . . Capobianco, A. J. (2014). Notch signaling drives stemness and tumorigenicity of esophageal adenocarcinoma. *Cancer Res, 74*(21), 6364-6374. doi:10.1158/0008-5472.CAN-14-2051

Watson, C. L., Mahe, M. M., Munera, J., Howell, J. C., Sundaram, N., Poling, H. M., . . . Helmrath, M. A. (2014). An in vivo model of human small intestine using pluripotent stem cells. *Nat Med, 20*(11), 1310-1314. doi:10.1038/nm.3737

Weaver, J. M., Ross-Innes, C. S., & Fitzgerald, R. C. (2014). The '-omics' revolution and oesophageal adenocarcinoma. *Nat Rev Gastroenterol Hepatol, 11*(1), 19-27. doi:10.1038/nrgastro.2013.150

Weaver, J. M., Ross-Innes, C. S., Shannon, N., Lynch, A. G., Forshew, T., Barbera, M., . . . Consortium, O. (2014). Ordering of mutations in preinvasive disease stages of esophageal carcinogenesis. *Nat Genet, 46*(8), 837-843. doi:10.1038/ng.3013

Wetterauer, C., Vlajnic, T., Schuler, J., Gsponer, J. R., Thalmann, G. N., Cecchini, M., . . . Rentsch, C. A. (2015). Early development of human lymphomas in a prostate cancer xenograft program using triple knock-out immunocompromised mice. *Prostate, 75*(6), 585-592. doi:10.1002/pros.22939

Whiteman, D. C., Appleyard, M., Bahin, F. F., Bobryshev, Y. V., Bourke, M. J., Brown, I., . . . Yusoff, I. F. (2015). Australian clinical practice guidelines for the diagnosis and management of Barrett's esophagus and early esophageal adenocarcinoma. *J Gastroenterol Hepatol, 30*(5), 804-820. doi:10.1111/jgh.12913

Whiteman, D. C., & Kendall, B. J. (2016). Barrett's oesophagus: epidemiology, diagnosis and clinical management. *Med J Aust, 205*(7), 317-324.

Williams, S. A., Anderson, W. C., Santaguida, M. T., & Dylla, S. J. (2013). Patient-derived xenografts, the cancer stem cell paradigm, and cancer pathobiology in the 21st century. *Lab Invest, 93*(9), 970-982. doi:10.1038/labinvest.2013.92

Worst, P. K., Mackenzie, I. C., & Fusenig, N. E. (1982). Reformation of organized epidermal structure by transplantation of suspensions and cultures of epidermal and dermal cells. *Cell Tissue Res, 225*(1), 65-77.

Yachimski, P. (2016). Complications of Gastroesophageal Reflux Disease. In M. Vaezi (Ed.), *Diagnosis and Treatment of Gastroesophageal Reflux Disease*: Springer, Cham.

Zehetner, J., DeMeester, S. R., Hagen, J. A., Ayazi, S., Augustin, F., Lipham, J. C., & DeMeester, T. R. (2011). Endoscopic resection and ablation versus esophagectomy for high-grade dysplasia and intramucosal adenocarcinoma. *J Thorac Cardiovasc Surg, 141*(1), 39-47. doi:10.1016/j.jtcvs.2010.08.058

Zhang, C. Z., Spektor, A., Cornils, H., Francis, J. M., Jackson, E. K., Liu, S., . . . Pellman, D. (2015). Chromothripsis from DNA damage in micronuclei. *Nature, 522*(7555), 179-184.

Zhang, L., Liu, Y., Wang, X., Tang, Z., Li, S., Hu, Y., . . . Ji, J. (2015). The extent of inflammatory infiltration in primary cancer tissues is associated with lymphomagenesis in immunodeficient mice. *Sci Rep, 5*, 9447. doi:10.1038/srep09447

Zhao, R., Quaroni, L., & Casson, A. G. (2012). Identification and characterization of stemlike cells in human esophageal adenocarcinoma and normal epithelial cell lines. *J Thorac Cardiovasc Surg, 144*(5), 1192-1199. doi:10.1016/j.jtcvs.2012.08.008

Zhou, G., Sun, Y. G., Wang, H. B., Wang, W. Q., Wang, X. W., & Fang, D. C. (2009). Acid and bile salt up-regulate BMP4 expression in human esophageal epithelium cells. *Scand J Gastroenterol, 44*(8), 926-932. doi:10.1080/00365520902998661

Appendices

1. PICF

PARTICIPANT INFORMATION AND CONSENT FORM

Full Project Title

Understanding the development and progression of Barrett's oesophagus and oesophageal adenocarcinoma.

Principal Investigator: Prof Wayne Phillips
Project Number: 10/108
Version: 3 dated 2nd February 2015

This Participant Information and Consent Form is 7 pages long. Please ensure that you have all the pages of this document.

1. **INTRODUCTION**

You are invited to take part in this research project because you are having an endoscopy. This Participant Information form contains detailed information about the research study. Knowing what is involved will help you decide if you want to take part in the research. Please read this information carefully. Ask questions about anything that you don't understand or want to know more about. Before deciding whether or not to take part, you might want to talk about it with a relative, friend or your local doctor. If English is not your first language and you require an interpreter, one will be provided for you.

Participation in this research is voluntary. If you don't wish to take part, you don't have to. You will receive the best possible care whether you take part or not.

If you decide you want to take part in the research project, you will be asked to sign the consent section. By signing it you are telling us that you:

- understand what you have read;
- consent to take part in the research project;
- consent to the use of your personal and health information.

You will be given a copy of the Participant Information and Consent form to keep as a record.

2. WHAT IS THE PURPOSE OF THIS STUDY?

We are conducting a medical research study to investigate the development of cancer of the oesophagus (the oesophagus is the 'food-pipe' that joins the throat to the stomach) and its response to treatment. You have been invited to take part in this study because you are having an endoscopy, a procedure in which your doctor will look at the lining of the oesophagus and take biopsies (small samples) for diagnostic purposes. If you agree to take part in the study we will ask you to allow us to collect up to four extra biopsies and provide a sample of blood for research purposes.

3. WHO IS CONDUCTING THE STUDY?

The study is being conducted by clinicians at St Vincent's Hospital in conjunction with researchers from the Surgical Oncology Research Laboratory at The Peter MacCallum Cancer Centre and has been approved by the Peter MacCallum Cancer Centre Research Ethics Committee in accordance with the guidelines of the National Health and Medical Research Council of Australia.

4. WHY DO YOU WANT ME TO TAKE PART?

In our laboratory we are trying to understand how oesophageal cancer forms, how it spreads throughout the body, and how it responds to anti-cancer therapies. We are also interested in testing new treatments in the laboratory setting using models that we have established. In order to conduct this research we need to look at a large number of blood and tissue samples. We also need samples of normal, pre-cancerous and cancerous tissue. Therefore, even if you don't have cancer, your samples will be valuable for our research. It is hoped that the results generated from this research will lead to improved treatment options for people with oesophageal cancer.

5. WHAT WILL BEING IN THE STUDY MEAN FOR ME?

Being in the study will involve giving permission for your doctor to take up to four extra biopsies and a sample of blood (10-20 ml) for our research at the time of your endoscopy. There will be no direct benefit to you from taking part in the study. However, the results of the study may help people with problems of the oesophagus in the future. There will be no cost to you and if you do not want to take part this will not affect your future medical care in any way.

6. **HOW ARE THE BIOPSIES COLLECTED?**

During endoscopy procedures we often collect small samples (biopsies) of tissue from the lining of the oesophagus. These are tested under the microscope for the diagnosis of various conditions. These results are given to you by your doctor and are used to plan your care.

We are seeking your permission to collect up to four extra biopsies at the time of your endoscopy. These biopsies are each about the size of a quarter of a grain of rice. Taking these extra biopsies does not cause any pain, and it is unlikely to cause any harm either. This process takes less than 5 minutes.

7. **WHAT WILL THE BIOPSY SAMPLES BE USED FOR?**

Qualified medical researchers will use the collected biopsies and blood samples in order to investigate the changes that occur within the cells lining the oesophagus. In the case of cancer samples, we wish to know how the cancer cells grow and how they respond to anti-cancer therapies.

We aim to identify those factors associated with more severe changes in the oesophagus and those factors associated with only mild changes. We also want to develop new tests that will help to identify those lesions that are at highest risk of progressing to cancer, and to develop new treatments that will prevent cancers from developing. We may also use your biopsy for experiments in which we will grow some of the tissue in the laboratory, so that we can study how the cells grow and respond to potential therapeutic agents. This could include the development of long-lived cell lines.

In some cases collaborators outside of The Peter MacCallum Cancer Centre may perform these studies. These studies have to be approved by the Human Research Ethics Committees at each institution and have to abide by the ethical and scientific principles set out by the National Health and Medical Research Council of Australia.

8. **ARE THERE ANY RISKS ASSOCIATED WITH THIS STUDY?**

One of the more serious complications associated with having an upper gastrointestinal endoscopy is perforation of the oesophagus. Depending on the case, the risk of such a complication occurring is between 1 in 500 to 1 in 5,000 cases. We are asking that your doctor take up to four extra biopsies at the time of your procedure. This in itself adds minimal risk, as the biopsy itself is very small. However, taking the biopsies means that your endoscopy will take a few minutes longer. When a blood sample is taken there is a chance that you might experience slight bleeding, minor bruising or pain. Trained personnel who are qualified to manage any such problems will take all blood samples.

9. **HOW IS MY PRIVACY PROTECTED?**

When you donate a sample of blood or tissue to this study we will make every effort to protect your privacy. All samples will be labelled with a unique number and stored securely. Only a small number of senior members of the study team will have access to identifiable information. Finally, no information that could be used to identify you will be used in any report or publication that originates from this project.

10. **CAN I WITHDRAW FROM THE STUDY?**

You are under no obligation to participate in the study. If you agree now and later change your mind, you can withdraw from the study by filling out the attached withdrawal of consent form and sending it to one of the investigators listed on this form. However you should be aware that, due to the nature of the research being conducted, should you elect to withdraw from the study, we cannot guarantee that all of your samples will be destroyed.

11. **WHAT IF I DO NOT WISH TO DONATE BLOOD OR TISSUE?**

Participation in research is entirely voluntary and you are under no obligation to donate blood or tissue. No matter what you decide to do about donating your tissue, it will not affect your relationship with your doctors, the institution, or your care, either now or in the future.

12. **WILL I FIND OUT THE RESULTS OF THE RESEARCH USING MY TISSUE?**

You will not be given the results from this research. This is because research can take a long time and must use tissue samples from many people before the results are known. As this kind of research by its very nature is experimental, any new discoveries may take considerable time before they can be translated into clinically relevant results.

CONSENT FOR RESEARCH

10/108: Understanding the development and progression of Barrett's oesophagus and oesophageal adenocarcinoma.

I _____ (*please print name*)

have read the information brochure	YES ☐
The consequences involved in participation in this research study have been explained to me and I understand these	YES ☐
I have had an opportunity to ask questions and am satisfied with the answers given	YES ☐

I hereby voluntarily consent to:

(1) Participate in the research study as described in the information brochure	YES ☐ NO ☐
(2) Have the following samples being collected and used for laboratory analysis as described in the information brochure:	
a. Extra biopsies to be taken during my endoscopy	YES ☐ NO ☐
b. A small (10-20mL) blood sample	YES ☐ NO ☐
(3) Allow the researchers access to my de-identified medical, oncology and pathology records (including material such as tissue blocks and slides if applicable)	YES ☐ NO ☐
(4) Allow my tissues to be used for genetic research	YES ☐ NO ☐
(5) Allow my tissues to be used for the generation of long-lived cell lines	YES ☐ NO ☐

In making my donations I understand that:

- The tissue (including its constituents and anything derived from it) will be stored indefinitely at PMCC and will be used for this and future research.
- The samples will be stored in a coded system to maintain confidentiality.
- There will be no cost, nor any financial benefit, to me for participating in the study. If my samples lead to the development of a commercial product in the future I will not receive payment for this.
- The samples will remain the property of The Peter MacCallum Cancer Centre. They will be stored in good faith, but their suitability for future use cannot be guaranteed. Samples will not be used for purposes other than those agreed to in this consent form.
- All studies using my samples will have to conform to the ethical and scientific principles set out by the National Health and Medical Research Council of Australia, the *Privacy Act 1988* and the Guidelines approved under section 95A of the *Privacy Act* (2001). I will not be notified about future use of my samples.

SIGNATURE: ..... **Date:** .....

I, the supervising physician confirm that I have fully explained the nature and purpose of the study to the patient taking part in the study. I confirm that he/she has read and kept a copy of the Patient Information Sheet and freely agrees to participate in the study.

Physician's name..... (Please print)

Physician's signature ..... Date.....

Form for Withdrawal of Participation

Title	**Understanding the development and progression of Barrett's oesophagus and oesophageal adenocarcinoma.**
Protocol Number	10/108
Principal Investigator	Prof Wayne Phillips
Location	Peter MacCallum Cancer Centre, East Melbourne

Declaration by Participant

I wish to withdraw from participation in the above research project and understand that such withdrawal will not affect my routine treatment, my relationship with those treating me or my relationship with The Peter MacCallum Cancer Centre

Name of Participant _____

Signature _____ Date _____

In the event that the participant's decision to withdraw is communicated verbally, the Study Doctor/Senior Researcher will need to provide a description of the circumstances below.

Who can I contact?

Reviewing HREC:
The reviewing HREC approving this research and contact details of the Executive Officer are:
Reviewing HREC name: The Peter MacCallum Cancer Centre
Position: Ethics Coordinator
Telephone: (03) 9656 1699
Email: ethics.department@petermac.org
The person you may need to contact will depend on the nature of your query. Therefore, please note the following:

For further information:
If you want any further information concerning this project, you can contact the principal researcher Prof Wayne Phillips on (03) 9656 1842, or Dr. Matthew Read on (03) 9656 1289.

For complaints:
If you have any complaints about any aspect of the project, the way it is being conducted or any questions about being a research participant in general, then you may contact:

Dr Tam C. Nguyen
Executive Officer of Research
St Vincent's Hospital Melbourne PO Box 2900
27 Victoria Parade, Fitzroy VIC 3065
Phone (03) 9231 3930 Fax (03) 9288
E-mail: Tam.NGUYEN@svha.org.au

You will need to tell the person you contact the name of one of the researchers responsible for the project.

2. The generation of a TMA from the PDTX biobank

In total, twelve separate oesophageal PDTX lines were selected for the TMA. These included seven adenocarcinoma lines and five squamous cell carcinoma lines. PDTX lines were selected that were easy to establish and grew rapidly once implanted. Once the PDTX lines were selected, representative H&E sections were analysed by a pathologist and regions of malignant tissue identified and marked. A TMA was then established from these marked regions by staff from the Victorian Cancer Biobank at the Peter MacCallum Cancer Centre. Normal human tissue was also included in the TMA for control purposes.

The layout of the TMA including the identification of individual FFPE histology blocks is shown in the following table.

PDTX Tissue Microarray Map

A

ID 1	ID 1	ID 8	ID 8		ID 13	ID 13	ID 15	ID 15		ID 10	ID 10	ID 18	ID 18		ID 22	ID 22	ID 22	ID 22		ID 22	ID 22
F0	F0	F0	F0		F0	F0	F0	F0		F0	F0	F0	F0		F0	F0	MET PDTX	MET PDTX		METS	METS
F1	F1	F2	F2		F1	F1	F1	F1		F2	F2	F2	F2		F1	F1	F1	F1		GOJ	GOJ
F2	F2	F3	F3		F3	F3	F3	F3		F3	F3	F2	F2		F2	F2	F2	F2		Liver	Liver
F2	F2	F4	F4		F3	F3	F4	F4				F3	F3		F3	F3				Peritoneum	Peritoneum
F3	F3				F4	F4						F4	F4								
F5	F5																				
ID 12	**ID 12**	**ID 11**	**ID 11**		**ID 23**	**ID 23**	**ID 24**	**ID 24**		**JH097**	**JH097**	**ID 22**	**ID 22**		**Control**	**Control**	**Control**	**Control**			
F0	F0	F0	F0		F0	F0	F0	F0		F0	F0	Cell line	Cell line		colon	colon	colon	colon			
F1	F1	F1	F1		F1	F1	F1	F1		F1	F1	EpCAM +	EpCAM +		small bow	small bow	small bow	small bow			
F2	F2	F2	F2		F2	F2	F2	F2		F2	F2	+NAFs	+NAFs		stomach	stomach	stomach	stomach			
							F3	F3		F3	F3	+CAFs	+CAFs								
												IS076-P	IS076-P								
												Is076-A	Is076-A								

B

6318/12	6318/12	2989/13	2989/13		4766/13	4766/13	5545/13	5545/13		3797/13	3797/13	419/13	419/13		4213/14	4213/14					
5225/12	5225/12	2254/14	2254/14		54/14	54/14	6587/13	6587/13		5279/13	5279/13	4214/14	4214/14		6136/14	6136/14	5654/14	5654/14		522/15	522/15
7019/12	7019/12	3225/14	3225/14		1514/14	1514/14	1338/14	1338/14		2168/14	2168/14	6138/14	6138/14		90/15	90/15	520/15	520/15		523/15	523/15
8927/12	8927/12	6137/14	6137/14		2619/14	2619/14	2162/14	2162/14				6140/14	6140/14		483/15	483/15				525/15	525/15
1749/13	1749/13				2165/14	2165/14						1326/15	1326/15							528/15	528/15
3497/13	3497/13											1321/15	1321/15								
4368/13	4368/13	4498/13	4498/13		5652/14	5652/14	5652/14	5652/14		5653/14	5653/14										
6243/13	6243/13	5621/13	5621/13		003/15	003/15	481/15	481/15		1857/15	1857/15	1724/15	1724/15		I	I	I	I			
1809/14	1809/14	6239/13	6239/13		1323/15	1323/15	736/15	736/15		2308/15	2308/15	1726/15	1726/15		II	II	II	II			
							1325/15	1325/15				1728/15	1728/15		III	III	III	III			
												1730/15	1730/15								
												1732/15	1732/15								

A, A map of the TMA outlining the location of each PDTX line. B, A matched map of the TMA containing the corresponding histopathology block numbers. ID, Original patient identification number (as detailed in Table 4-5). F0, original patient tumour. Fx, derived PDTX. NAF, normal associated fibroblasts. CAF, cancer associated fibroblasts. METS, metastatic deposits. GOJ, gastro-oesophageal junction. Red coloured box, oesophageal adenocarcinoma. Blue coloured box, oesophageal SCC. Yellow coloured box, control tissue.

3. Clinical details of the patients whose PDTXs underwent lymphomagenic transformation

GB975 (ID 4)

GB975 was a 69-year-old man who had a history of hypertension and was a past smoker. He initially presented with dysphagia and 8kg loss of weight that had occurred over a six-week period. Gastroscopy revealed a circumferential tumour of the distal oesophagus that was 5cm in length. There was no extension into the stomach. Histology revealed a moderately differentiated adenocarcinoma with mild chronic lymphoplasmacytic infiltrate. The tumour was HER2 positive as determined by both silver in-situ hybridisation and immunohistochemistry. Staging CT revealed thickening of the distal oesophagus with several enlarged mediastinal lymph nodes. There was no evidence of distant metastases. PET demonstrated extensive avidity within the primary tumour in addition to the mediastinal lymph nodes. The mediastinal lymph nodes were subsequently sampled via a mediastinoscopic approach. Histology confirmed the presence of metastatic carcinoma within these lymph nodes. Interestingly, the deposit was predominantly a high-grade neuroendocrine carcinoma, positive for the somatostatin receptor type 2 on immunohistochemistry, and only contained focal moderately differentiated adenocarcinoma. The Ki67 level within this tumour was reported as 80%. It was not clear whether this represented a form of divergent differentiation from a primary oesophageal carcinoma. The patient was subsequently treated with neoadjuvant chemoradiotherapy in the form of carboplatin and etoposide in addition to 50.4Gy radiotherapy over 28 fractions. A repeat PET demonstrated a complete metabolic response. Unfortunately, multiple medical problems prevented surgery and a re-staging PET/CT revealed evidence of both brain and bone metastases. The patient was subsequently managed palliatively by means of oesophageal stent and additional radiotherapy for bleeding.

AN959 (ID 9)

AN959 was a 63-year-old man with a history of heavy alcohol use and a 50-pack year smoking history. He presented with a three-month history of odynophagia and dysphagia on a background of 25kg of weight loss over the preceding year. He was initially investigated with a gastroscopy which revealed a non-obstructing tumour of the lower oesophagus, 6cm in length, which extended into the gastric cardia. Histology revealed that this was a moderately differentiated adenocarcinoma. Staging PET / CT revealed high avidity within the primary tumour but no evidence of either nodal or distant metastatic disease. There was, however, evidence of pulmonary tuberculosis. Unfortunately, a repeat CT performed during his work up six weeks later revealed new lung and liver lesions. The patient was subsequently treated with palliative chemoradiotherapy in the form of cisplatin and 5-FU in addition to 50Gy of radiotherapy.

RF226 (ID 14)

RF226 was a previously well 66-year-old man who presented with a poorly differentiated adenocarcinoma at the gastro-oesophageal junction. This was on a background of having had loss of weight and progressive dysphagia over a period of five months. He also had an episode of haematemesis requiring admission to hospital. Endoscopy confirmed a near obstructing tumour extending from 35cm from the incisors to 40cm. Subsequent staging PET / CT confirmed a large para-oesophageal nodal mass posterior to the pericardium in addition to an avid left gastric nodal mass. There was no evidence of distant metastases. He commenced neoadjuvant chemotherapy in the form of epirubicin, cisplatin and 5-FU as per the MAGIC protocol (Cunningham et al., 2006). Restaging PET confirmed a complete metabolic response with respect to the nodal disease. RF subsequently went on to have surgery in the form of a totally minimally invasive Ivor Lewis oesophagectomy followed by adjuvant treatment in the form of chemoradiotherapy. Histology confirmed residual poorly differentiated adenocarcinoma with 10/15 lymph nodes containing metastatic disease and a close proximal margin. Unfortunately, he developed locoregional recurrence six months post-operatively and underwent palliative therapy.

JA227 (ID 16)

JA227 was a previously well 78-year-old man with a known history of Barrett's oesophagus who was found to have an oesophageal adenocarcinoma on surveillance gastroscopy. Endoscopic ultrasound confirmed this to be an early tumour (T1b). Given that the subsequent staging PET / CT failed to demonstrate any evidence of either nodal or metastatic disease the patient proceeded directly to have an Ivor Lewis oesophagectomy. Histology revealed this to be a moderate to poorly differentiated adenocarcinoma with invasion into the submucosa and 1/10 lymph nodes involved with tumour. His post-operative course was complicated by an anastomotic leak.

JB259 (ID 19)

JB259 was a previously well 63-year-old man who presented with a mid to distal oesophageal adenocarcinoma. Endoscopy revealed this to be originating from a segment of Barrett's oesophagus. Staging FDG PET revealed an avid tumour that was 12cm in length with associated avid lymph nodes in the mediastinum and upper abdomen. The SUVmax of the primary tumour was 16.2. The patient subsequently underwent neoadjuvant chemotherapy in the form of three cycles of epirubicin, cisplatin and capecitabine. Unfortunately, this was tolerated poorly, and the patient lost significant weight and became deconditioned. Restaging CT revealed a marked response to the treatment with a significant reduction in tumour size. This was confirmed endoscopically and the patient proceeded to have an Ivor Lewis oesophagectomy. Unfortunately, histopathological assessment graded the response to treatment as poor (TRG of 3) with viable tumour cells invading the muscularis propria. The pathological stage post neoadjuvant treatment was T2N2M0.

4. Inhibition of BMP2 and BMP4 eradicates Barrett's esophagus and enhances the regeneration of squamous epithelium

Correia, A. P., Straub, D., Read, M., Hoefnagel, S., Westra, W., Mari, L., . . . Krishnadath, K. K. (2018). Inhibition of BMP2 and BMP4 eradicates Barrett's esophagus and enhances the regeneration of squamous epithelium. *Nature (under review)*.

Inhibition of BMP2 and BMP4 eradicates Barrett's esophagus and enhances the regeneration of squamous epithelium

*Ana Pacheco Correia, PhD student, a.c.pachecocorreia@amc.uva.nl
Center for Experimental and Molecular Medicine, Amsterdam University Medical Centers, The Netherlands.

*Danielle Straub, PhD student, d.straub@amc.uva.nl
Center for Experimental and Molecular Medicine, Amsterdam University Medical Centers, The Netherlands.

Matthew Read, m.read@mgos.com.au
Peter MacCallum Cancer Centre, Melbourne, Victoria, Australia and The Sir Peter MacCallum Department of Oncology, University of Melbourne, Parkville, Victoria, Australia

Sanne Hoefnagel, PhD student, s.j.hoefnagel@amc.uva.nl
Center for Experimental and Molecular Medicine (CEMM), Amsterdam University Medical Centers, The Netherlands.

Wytske Westra, W.M.Westra@amc.uva.nl
Center for Experimental and Molecular Medicine (CEMM), Amsterdam University Medical Centers, The Netherlands

Luigi Mari, PhD, Luigi.Mari@STJUDE.ORG
Department of Immunology, St. Jude Children's Research Hospital, Memphis, TN 38105, USA

Salvador Romero Pinedo, PhD Student, romeropinedo@gmail.com
Dpto. de Bioquímica y Biología Molecular e Inmunología. Instituto de Biopatología y Medicina Regenerativa. Centro de Investigaciones Biomédicas, Universidad de Granada, Spain.

Ana Abadia Molina, PhD, acbadia@ugr.es
Dpto. de Bioquímica y Biología Molecular e Inmunología. Instituto de Biopatología y Medicina Regenerativa. Centro de Investigaciones Biomédicas, Universidad de Granada, Spain.

Nicholas J. Clemons, PhD, nicholas.clemons@petermac.org
Peter MacCallum Cancer Centre, Melbourne, Victoria, Australia and The Sir Peter MacCallum Department of Oncology, University of Melbourne, Parkville, Victoria, Australia

Kenneth Wang, Prof, wang.kenneth@mayo.edu
Division of Gastroenterology and Hepatology, Mayo Foundation, Rochester, Minnesota, USA

Kaushal Parikh, PhD, kaushal.parikh@ndm.ox.ac.uk
MRC Human Immunology Unit, Weatherall Institute of Molecular Medicine, University of Oxford, John Radcliffe Hospital, Oxford, UK

Silvia Calpe, PhD, s.calpe@amc.uva.nl
Center for Experimental and Molecular Medicine (CEMM), Amsterdam University Medical Centers, The Netherlands.

Wayne A. Phillips, Prof, PhD, wayne.phillips@petermac.org
Peter MacCallum Cancer Centre, Melbourne, Victoria, Australia and The Sir Peter MacCallum Department of Oncology, University of Melbourne, Parkville, Victoria, Australia

Kausilia K. Krishnadath, Prof, PhD, MD, k.k.krishnadath@amc.uva.nl
Center for Experimental and Molecular Medicine (CEMM), Amsterdam University Medical Centers, The Netherlands

*shared first author

Correspondence: K.K.Krishnadath@amc.uva.nl, Department of Gastroenterology and Hepatology, Academic Medical Center, Meibergdreef 9 1105AZ, Amsterdam, the Netherlands

List of Abbreviations

AMC	Academic Medical Center
ANOVA	Analysis of Variance
ARIA	Animal Research Institute of the AMC
BA	Bile and Acids
BCA	Bicinchoninic Acid
BMP	Bone Morphogenetic Protein
BPE	Bovine Pituitary Extract
$CaCl_2$	Calcium Chloride
CDX2	Caudal type homeobox 2
CP-A	Human Cell Line of non-dysplastic Barrett's esophagus
Cre	Cyclization Recombinase
DAPI	4',6-Diamidino-2-Phenylindole
DGERD	Duodeno-gastro-esophageal reflux disease
ECL	Electrogenerated Chemiluminescent
EDTA	Ethylenediaminetetraacetic Acid
EPC2	Esophageal Epithelial Cells 2
GAPDH	Glyceraldehyde-3-Phosphate Dehydrogenase
GFP	Green Fluorescent Protein
H_2O_2	Hydrogen Peroxide
H&E	Hematoxylin & Eosin
HPRT1	Hypoxanthine-Guanine Phosphoribosyltransferase 1
hTERT	Human Telomerase Reverse Transcriptase
ID1	Inhibitor of DNA Binding 1
ID2	Inhibitor of DNA Binding 2
IF	Immunofluorescence
IHC	Immunohistochemistry
IL1-β	Interleukin 1 beta
IL2	Interleukin 2
i.p.	Intraperitoneal
IPA	Ingenuity Pathway Analysis
IVC	Individually Ventilated Cage
IvD	Instantie voor Dierenwelzijn (Animal Welfare Body)
K5	Cytokeratin 5
K7	Cytokeratin 7
K14	Cytokeratin 14
K19	Cytokeratin 19
KSFM	Keratinocyte Serum-Free Medium
LoxP	Locus of X-over P1
$MgCl_2$	Magnesium Chloride
mRNA	Messenger RNA
NSG	NOD scid gamma
p63	Protein 63
PBS	Phosphate-buffered saline
PPI	Proton Pump Inhibitor
pSMAD1/5/8	phospho-SMAD1/5/8
PVDF	Polyvinylidene Difluoride
qPCR	Quantitative Polymerase Chain Reaction
RNA	Ribonucleic Acid

SCJ	Squamo-Columnar Junction
SEM	Standard Error of the Mean
SHH	Sonic Hedgehog
Sox2	Sex Determining Region Y-Box 2
SQ	Squamous
TBS	Tris-Buffered Saline
TGF-β	Tumor Growth Factor Beta
VHH	Highly Specific Llama derived antigen binding fragments
WNT	Wingless-type MMTV integration site family
WT	Wild Type

ABSTRACT

Barrett's esophagus is an irreversible metaplasia of the lower esophagus and the only known precursor of esophageal adenocarcinoma, a highly malignant cancer. Development of Barrett's metaplasia is driven by increased Sonic hedgehog (SHH) and Bone Morphogenetic Protein 4 (BMP4) signaling (Milano 2007, Clemons 2009, Mari 2014). Here, we provide evidence that the selective inhibition of BMP2 and BMP4 effectively eradicates Barrett's epithelium. The activity of BMP2 and BMP4 signaling was high in Barrett's biopsies, whereas BMP7 and TGF-β pathways were higher in esophageal squamous mucosa. Selective inhibition of BMP2 and BMP4 within an *in vivo* organoid model of Barrett's esophagus, favored the development of squamous cells, rather than the columnar Barrett cells. In a mouse model, conditional knockout of *Noggin*, a natural antagonist of BMP2, BMP4 and BMP7, induced expansion of Barrett's like neo-columnar epithelium from multi-lineage glands. Conversely, inhibition of BMP2 and BMP4 led to the development of a neo-squamous lineage. Similarly, in wild type mice, inhibition of BMP2 and BMP4 resulted in the regeneration of neo-squamous epithelium after the cryo-ablation of columnar epithelium at the squamo-columnar junction. Through lineage tracing it was evident that the neo-squamous mucosa originated from $K5^{+}$ progenitor squamous cells. Together, this work demonstrates that specific inhibition of BMP2 and BMP4 inhibits the development of columnar metaplasia, providing a novel potential strategy for the treatment of Barrett's esophagus and prevention of progression to esophageal adenocarcinoma.

MAIN

Barrett´s esophagus is an epithelial type of metaplasia which results from inflammatory signals caused by chronic duodeno-gastro-esophageal reflux disease (DGERD)[1,2]. Barrett's esophagus patients require measures to reduce reflux such as acid suppression or fundoplication and periodic surveillance to prevent chronic inflammation and reduce cancer risk[3,4]. The incidence of Barrett's esophagus and esophageal adenocarcinoma are increasing[5]. At present, molecular therapies to cure Barrett's esophagus or other metaplastic lesions are lacking. In this study, our aim was to investigate if targeting key homeostatic pathways would be effective to eradicate Barrett's esophagus.

BMP signaling is essential for the homeostasis and differentiation of intestinal cell lineages[6]. The embryonic development of the esophagus is regulated by BMP4 and one of its natural inhibitors *Noggin*[7]. *Noggin* binds to the BMP2, BMP4 and to a lesser extent to the BMP7 protein[8], preventing them from binding to their cognate receptors and activating downstream canonical signaling[9]. The normal adult esophagus is characterized by low levels of BMP2 and BMP4, and high levels of BMP7, especially within the upper basal layer, the latter required for the physiological differentiation of the stratified squamous epithelium[10,11]. Upregulation of the SHH mediated canonical BMP4-pSMAD pathway has been identified as a key determinant in the shift from the normal squamous cells to the columnar and intestinal type of cells characteristic of Barrett's metaplasia[10,12,13]. Increased levels of BMP4 are seen in squamous mucosal biopsies following exposure to bile acids alone and in the setting of active inflammation caused by DGERD[10,14]. In murine models with induced inflammation of the esophagus through bile reflux, IL1-β or BMP4 overexpression, activation of the BMP pathway leads to proliferation of neo-columnar epithelium at the squamo-columnar junction (SCJ) in the stomach, resembling Barrett's metaplasia[12,15].

A more comprehensive analysis and validation in a Gene Expression Omnibus dataset (accession number GSE26886)[16] reveals upregulation of SHH-TGF-β/BMP signaling in Barrett's mucosal biopsies compared to normal squamous mucosa (Fig1A, Extended data Fig1A, B). Ingenuity pathway analysis indicates higher BMP signaling, driven by both BMP2 and BMP4 in Barrett's esophagus compared to normal squamous mucosa, the latter having more active TGF-β pathways and BMP7 signaling (Fig1B). IHC analysis of Barrett's derived patient biopsies confirms increased protein expression of BMP2 and BMP4, and their downstream targets pSMAD1/5/8, ID1 and ID2 (Fig1C). pSMAD1/5/8 expression in squamous biopsies is the highest in the basal layers (Fig1C). By Western blot we confirm higher expression of BMP2, BMP4, BMP5 and BMP6 in human Barrett's biopsies (Extended data Fig1C).

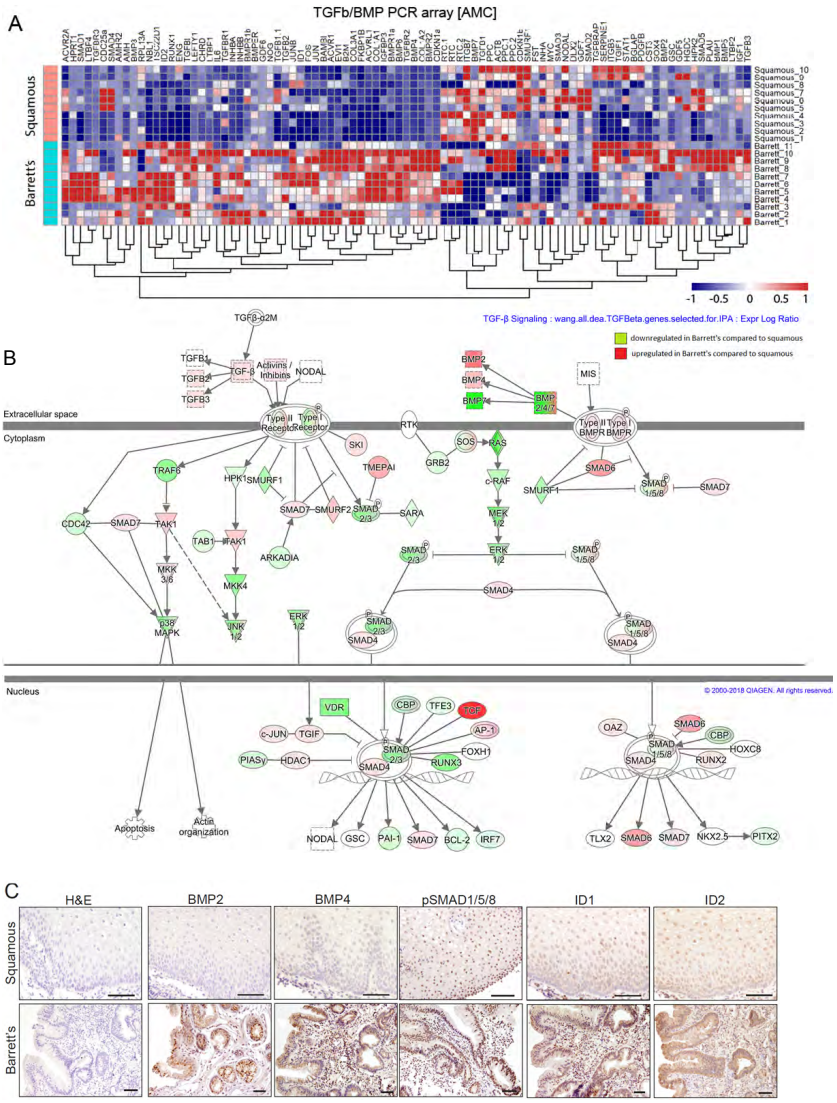
A
TGFb/BMP PCR array [AMC]
Squamous
Barrett's
-1
-0.5
0
0.5
1
B
TGF-β Signaling : wang.all.dea.TGFBeta.genes.selected.for.IPA : Expr Log Ratio
downregulated in Barrett's compared to squamous
upregulated in Barrett's compared to squamous
Extracellular space
Cytoplasm
Nucleus
© 2000-2018 QIAGEN. All rights reserved.
C
H&E
BMP2
BMP4
pSMAD1/5/8
ID1
ID2
Squamous
Barrett's

Figure 1: SHH-TGF-β/BMP signaling in Barrett's esophagus and esophageal squamous epithelium. Gene expression analysis of human squamous and Barrett's biopsies and effect of conjugated bile acids on epithelial cells. [A] Clustering of expression values of TGF-β/BMP pathway genes in patients derived biopsies of Barrett's esophagus and normal esophageal squamous mucosa. [B] Ingenuity Pathway Analysis of TGF-β/BMP signaling in Barrett's esophagus compared to normal squamous tissue (SQ)[16]. [C] Representative IHC for BMP2 and BMP4, and their downstream targets pSMAD1/5/8, ID1 and ID2, in normal squamous and Barrett's biopsies. Hematoxylin is used as a counterstain. (Scale bars: 100μm).

To test the effects of BMP inhibition on human Barrett's epithelium, we developed a novel *in vivo* organoid model by intramuscular implantation of endoscopic biopsies in NSG mice. This model is able to sustain both normal human squamous and Barrett's epithelia (Fig2, Extended data Fig2A). Expression of the human mitochondrial antigen confirmed the human origin of the organoids (not shown). The squamous biopsies and corresponding *in vivo* organoids show multi-layered lining of Alcian Blue$^-$, CDX2$^-$, p63$^+$ and K5$^+$ squamous cells with a papillary-resembling region (Fig2B, C). The Barrett's biopsies and corresponding *in vivo* organoids are lined with a secretory CDX2$^+$ columnar epithelial layer, containing Alcian Blue$^+$ mucus producing goblet cells (Fig2D). At the basal side of the mucous cells, a few p63$^+$, K5$^+$ squamous cells can be observed.
Most of the currently available BMP inhibitors and antagonists are not selective for targeting single family members such as BMP2 or BMP4[8]. Recently, we isolated highly specific Llama derived antigen binding fragments (VHHs), which selectively inhibit BMP4 (anti-BMP4) or BMP2 and 4 (anti-BMP2/4)[17,18]. Intraperitoneal (i.p.) injections of NSG mice with anti-BMP4 for at least eight weeks, starting one week after implantation of the human Barrett's biopsies (Fig2E), results in an organoid with a mixed epithelial layer characterized by a multi-layered squamous epithelium with p63$^+$, K5$^+$ cells and a reduced number of mucous-producing cells (Fig2F). Treatment with anti-BMP2/4 results in p63$^+$/K5$^+$ multilayered epithelium, weakly expressing K19, but with Involucrin$^+$ and Sox2 expressing cells (Fig2F, Extended data Fig3). Mucous producing Alcian Blue$^+$ and CDX2$^+$ cells are absent (Fig2F). Compared to the control mice, the number of Ki67$^+$ proliferative cells is reduced in the treated Barrett's organoids (Extended data Fig3). Of interest is that a population of remnant p63$^+$ and K5$^+$ squamous cells is also observed in the original Barrett's biopsy that corresponds with the treated Barrett's implant (Fig2D, Extended data Fig2B). Analysis of patient biopsies already indicated that based on expression profiles, Barrett's esophagus has similarities to both, normal squamous and stomach cardia epithelia[19]. BMP2/4 inhibition also results in a transient loss of goblet cells in the colon, which recovers 4 weeks after the end of treatment (Extended data Fig4). All mice presented normal weights, stools and behavior during the treatments. Thus, in a novel organoid model that sustains Barrett's and squamous epithelia, inhibition of both BMP2 and BMP4 is required for a selective reduction of

all Barrett's mucous producing goblet cells and favors the proliferation and establishment of squamous epithelium (Fig2F).

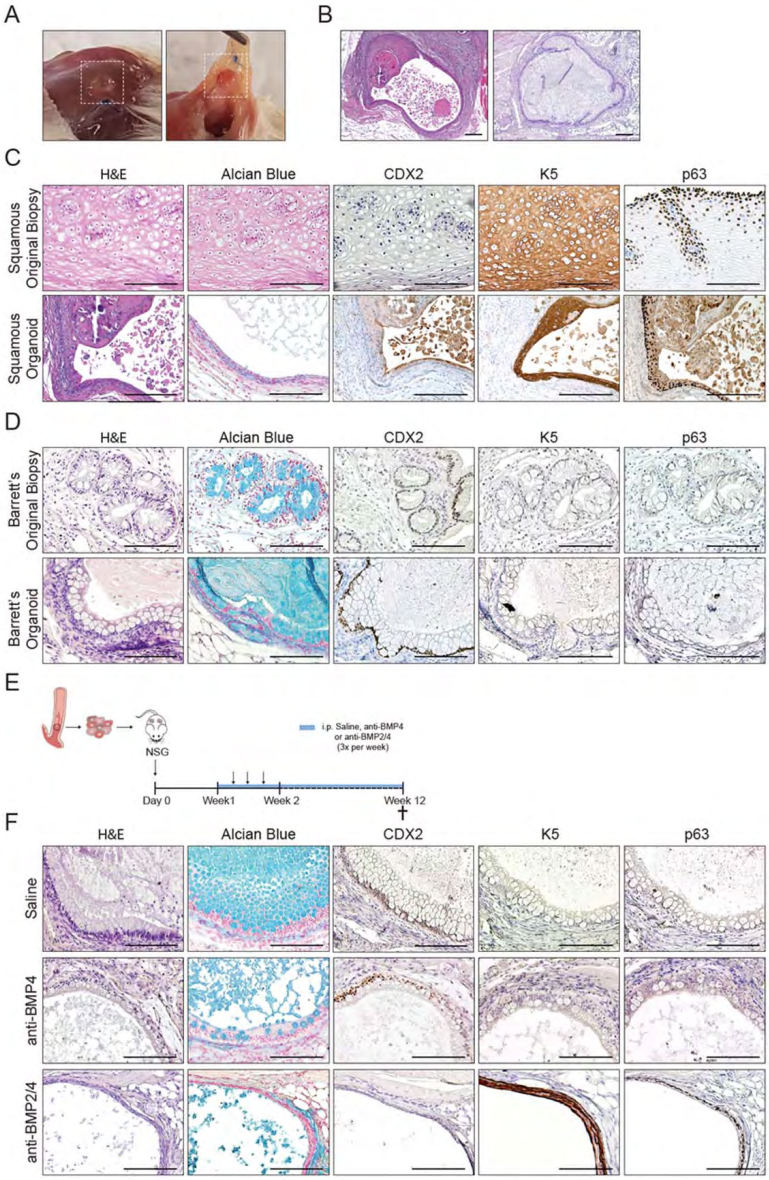
A
B
C
H&E
Alcian Blue
CDX2
K5
p63
Squamous Original Biopsy
Squamous Organoid
D
H&E
Alcian Blue
CDX2
K5
p63
Barrett's Original Biopsy
Barrett's Organoid
E
NSG
i.p. Saline, anti-BMP4 or anti-BMP2/4 (3x per week)
Day 0
Week1
Week 2
Week 12
F
H&E
Alcian Blue
CDX2
K5
p63
Saline
anti-BMP4
anti-BMP2/4

Figure 2: Effects of BMP2 and BMP2/4 inhibition on Barrett's esophagus biopsies in an *in vivo* organoid model. [A] A dissected *in vivo* organoid from the dorsal musculature of an NSG mouse. [B] H&E staining of a complete squamous (left side) and Barrett's (right side) *in vivo* organoid. [C] H&E, Alcian blue staining and IHC for CDX2, K5 and p63 of a squamous biopsy and corresponding organoid, and [D] and of a Barrett's biopsy and corresponding organoid. [E] Experimental set-up of intramuscular implantation of human biopsies to obtain *in vivo* organoids and treatment schemes with the inhibitors. [F] H&E, Alcian blue staining and IHC of CDX2, K5 and p63 of Barrett's *in vivo* organoids treated with saline, anti-BMP4 or antiBMP2/4. Hematoxylin is used as a counterstain. (Scale Bar 200 µm).

In a *K14-Bmp4* transgenic model, we have previously observed the development of columnar metaplastic glands at the SCJ. The expected effects were modest due to concomitant upregulation of the BMP antagonist, *Noggin*[12]. Conversely, a *Noggin* knockout was embryonically lethal, however analysis of the fetal tissue showed aberrant columnar cells lining the esophagus[20].

Here, by crossing Rosa26-CreERT2 mice with loxP [*Noggin*] loxP mice (Fig3A), a novel *Noggin* knockout model representative of columnar metaplasia has been established. Tamoxifen injection at eight weeks results in absence of *Noggin* in the esophagus, forestomach, stomach body, antrum, intestine and colon in adult mice (Extended data Fig 5A). After 24 weeks, in line with previous observations[20], the *Noggin*$^{-/-}$ mice have maintained expression of BMP4 and pSMAD1/5/8 comparable to the wild type controls (Extended data Fig 5B). Also, there are no major differences in morphology and histology of the esophagus, intestine and colon (Extended data Fig 5C). However, 4 weeks after deletion of *Noggin*, we observe expanded multi-lineage glands at the SCJ of the stomach, characterized by abundant neo-columnar epithelium resembling Barrett's columnar metaplasia[12,21](Fig3A). To investigate if BMP2/4 inhibition can inhibit the expansion of the neo-columnar epithelium from the multi-lineage glands, or divert the expansion towards neo-squamous epithelium, the *Noggin*$^{-/-}$ mice have been treated with the BMP2/4 inhibitor (Fig3B). Eight weeks of systemic treatment with anti-BMP2/4 results in decreased BMP signaling as can be observed by a reduction in pSMAD1/5/8 expression (Fig3C). Inhibition of BMP2 and BMP4 results in increased proliferative activity of the squamous layer, which seems to originate from the outer layer of the multi-lineage glands. Additionally, there is expansion of the multi-layered neo-squamous epithelium and development of papillae-like structures (Fig3B). Thus, conditional deletion of *Noggin* results in the development of a Barrett's like neo-columnar epithelium at the SCJ of the stomach of this murine model. Inhibition of BMP2 and BMP4 inhibits the neo-columnar lineage and enhances development of a neo-squamous epithelium. Both the neo-columnar and neo-squamous lineages seem to be derived from the multi-lineage glands residing at the SCJ in mice.

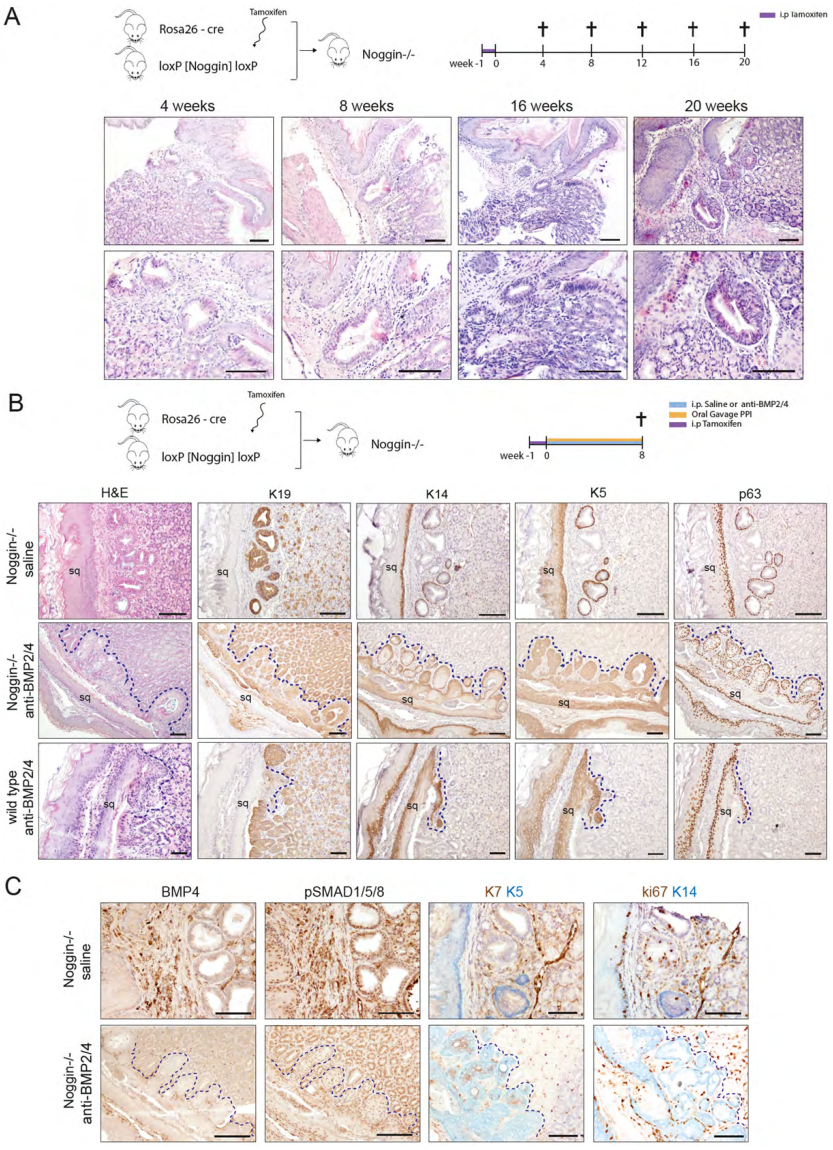
A
Rosa26 - cre
loxP [Noggin] loxP
Tamoxifen
Noggin-/-
i.p Tamoxifen
week -1 0 4 8 12 16 20
4 weeks
8 weeks
16 weeks
20 weeks
B
Rosa26 - cre
loxP [Noggin] loxP
Tamoxifen
Noggin-/-
i.p. Saline or anti-BMP2/4
Oral Gavage PPI
i.p Tamoxifen
week -1 0 8
H&E
K19
K14
K5
p63
Noggin-/- saline
Noggin-/- anti-BMP2/4
wild type anti-BMP2/4
sq
C
BMP4
pSMAD1/5/8
K7 K5
ki67 K14
Noggin-/- saline
Noggin-/- anti-BMP2/4

Figure 3: Effects of BMP2/4 inhibition on neo-columnar epithelium development in a conditional *Noggin* knockout Barrett's model. [A] Rosa26-creERT2 mice have been crossed with loxP [*Noggin*] loxP mice and injected with tamoxifen for 3 days to obtain *Noggin*$^{-/-}$ mice. H&E of SCJ in the stomach of the *Noggin*$^{-/-}$ mice at 4, 8, 16 and 20 weeks. [B] Creation of *Noggin*$^{-/-}$ mice and scheme for treatment by saline or anti-BMP2/4. All mice received proton pump inhibitors (PPIs). H&E and IHC staining for K19, K14, K5 and p63 of multi-lineage glands at the SCJ in the stomach of WT and *Noggin*$^{-/-}$ mice treated with anti-BMP2/4 or saline. [C] IHC for BMP4, pSMAD1/5/8, K7/K5, Ki67/K14 of multi-lineage glands at the SCJ in *Noggin*$^{-/-}$ mice treated with saline or anti-BMP2/4. Hematoxylin was used as a counterstain. (Scale Bar 100 µm) (broken line indicates the border of the neo-squamous epithelium).

In wild type CB6F1/Crl mice, cryo-ablation of the columnar mucosa in the forestomach just distal to the SCJ, results in the regeneration of normal stomach columnar epithelium and restored architecture of the crypts after 21 days (Fig4A-C). In cryo-ablated mice treated with the BMP2/4 inhibitor for 21 days, the ablated columnar stomach epithelium has been replaced by a multilayered K5^{+}, p63^{+} neo-squamous epithelium that poorly expresses the columnar marker K19 (Fig4D).

The repopulation of the esophageal mucosa is further investigated by using a K5-GFP lineage tracing model. Using K5-CreERT2 crossed with Rosa26-Tomato-*loxP [stop] loxP*-GFP mice, tamoxifen injection activates the GFP reporter gene in K5^{+} cells, permanently marking these cells and their progeny as they repopulate the mucosa (Fig4E). After cryo-ablation of the columnar epithelium, the re-epithelization of the stomach in the K5-GFP mice is comparable to that of the wild type CB6F1/Crl mice (Fig4D, F). Treatment of the K5-GFP mice with the BMP2/4 inhibitor for 21 days results in the appearance of a GFP^{+} neo-squamous epithelium replacing the ablated columnar epithelium (Fig 4F). The GFP expression indicates the origin of the neo-squamous cells from K5^{+} progenitors (Fig4F).

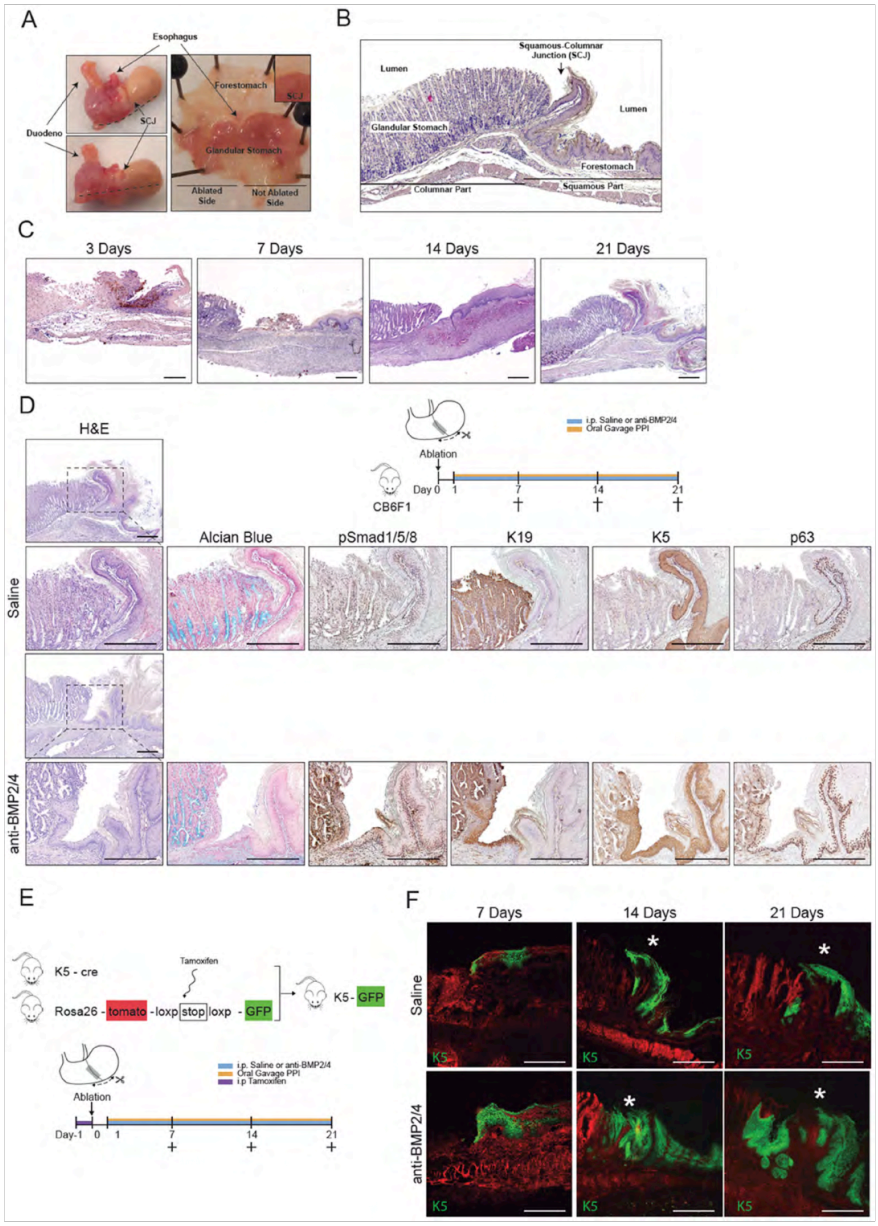
A
Esophagus
Duodeno
SCJ
Forestomach
Glandular Stomach
Ablated Side
Not Ablated Side
B
Squamous-Columnar Junction (SCJ)
Lumen
Glandular Stomach
Forestomach
Columnar Part
Squamous Part
C
3 Days
7 Days
14 Days
21 Days
D
H&E
Ablation
i.p. Saline or anti-BMP2/4
Oral Gavage PPI
Day 0
CB6F1
Alcian Blue
pSmad1/5/8
K19
K5
p63
Saline
anti-BMP2/4
E
K5 - cre
Rosa26 - tomato - loxp stop loxp - GFP
Tamoxifen
K5 - GFP
Ablation
i.p. Saline or anti-BMP2/4
Oral Gavage PPI
i.p Tamoxifen
Day-1
F
7 Days
14 Days
21 Days
Saline
anti-BMP2/4
K5

Figure 4: Anti-BMP2/4 treatment and lineage tracing of K5$^+$ progenitor cells in a cryo-ablation model. [A] Macroscopic view of a dissected WT CB6F1/Crl mouse stomach, 21 days after ablation of a glandular part of the stomach. [B] H&E staining of a normal SCJ including both the forestomach and glandular stomach of WT mice. [C] H&E of the SCJ of WT mice after 3, 7, 14 or 21 days of cryo-ablation of the glandular stomach epithelium. [D] Cryo-ablation and scheme for treatment with saline or anti-BMP2/4. All mice received PPIs. H&E, Alcian blue stainings and IHC for pSMAD1/5/8, K19, K5 and p63, of the SCJ in CB6F1/Crl mice, 21 days after cryo-ablation and treatment with saline or anti-BMP2/4. Hematoxylin was used as a counterstain. [E] Crossing of K5-cre mice with Rosa26-Tomato-*lox-stop-lox*GFP mice and injection with Tamoxifen to generate K5-GFP lineage tracing mice. Cryo-ablation and scheme for treatment with saline or anti-BMP2/4. [F] GFP expressing squamous cells traced in K5-GFP mice after cryo-ablation of the columnar epithelium in the proximal stomach at the SCJ (*) in mice treated with saline or anti-BMP2/4. (Scale Bar 200 µm).

In general, metaplastic changes are associated with altered signaling of pathways which are involved in embryonic development. Critical are the SHH, TGF-β and BMP pathways[22]. BMPs seem to be highly homologous molecules that signal via their receptors BMPR I and II. Yet, due to interactions with diverse transcription and regulatory factors, and through non-canonical signaling, their effects are highly pleotropic[12]. Apart from BMP4, we found that BMP2 was also highly expressed in Barrett's biopsies[10,12], while in addition to BMP7 there is high TGF-β activity in the squamous mucosa[11]. Consistent with these findings, the inhibition of both BMP2 and BMP4 within our novel human *in vivo* organoid model prevented the formation of a Barrett's phenotype. Both, BMP2 and BMP4 are known for their homeostatic functions within columnar epithelia. The specific inhibition of BMP4 alone, or in combination with BMP2, was made possible using our recently developed BMP inhibitors[17,18]. Remarkably, in the anti-BMP2/4 treated *in vivo* Barrett's organoids there was efficient regeneration of stratified squamous epithelium. We presume that the remnant K5$^+$, p63$^+$ squamous progenitor cells observed in the corresponding Barrett's biopsies developed into the neo-squamous epithelium. This was most likely possible because the function of BMP7, essential for squamous differentiation[10], was left intact. In a second model, we were able to develop columnar metaplasia resembling Barrett's by knocking out the natural BMP2,4,7 inhibitor *Noggin*. In line with the recent model developed by Jiang[21], the neo-columnar epithelium arose from multi-lineage glands. Within this same model, the inhibition of BMP2 and BMP4 decreased the proliferation of columnar cells, whilst the development of a neo-squamous epithelium originating from the outer layer of the multi-lineage epithelium was enhanced. To further interrogate the effect of BMP2/4 inhibition on the homeostasis of normal columnar tissue and to understand the origin of the neo-squamous epithelium at the SCJ, we developed a third model in which the columnar epithelium was ablated at the SCJ. Following ablation, anti-BMP2/4 treatment inhibited the regeneration of normal columnar stomach epithelium. Instead, the ablated epithelium was replaced by neo-

squamous epithelium. Lineage tracing demonstrated that the origin of this neo-squamous epithelium originates from $K5^+$ squamous progenitor cells.

In summary, we found that BMP2 and BMP4 signaling are highly active in Barrett's esophagus, whilst in normal squamous mucosa TGF-β pathways and BMP7 are higher. We demonstrated that specific inhibition of BMP2 and BMP4 effectively constrained regeneration of stomach columnar epithelium and Barrett's esophagus in multiple models. Because our novel inhibitor is highly specific for BMP2 and BMP4 and has no effect on BMP7, the regeneration of normal stratified squamous epithelium was not affected. To our knowledge this is the first targeted therapy that can potentially be applied for treatment of a metaplastic lesion. In the future such therapy might be implemented as a novel chemo-preventive strategy. If successful, this could prevent cancer progression and reduce the burden of costly surveillance programs.

MATERIAL AND METHODS:

Ethics

Use of all human patient material was approved by the institutional Medical Ethical Committee of the Academic Medical Center of Amsterdam (AMC). All patients gave informed consent to participate in the study before sample collection. Samples were collected during the routine surveillance program at the Gastroenterology and Hepatology Department of the AMC. All patients were on long-term proton pump inhibition (PPI) therapy. After a confirmed diagnosis of intestinal metaplasia without dysplasia by endoscopy and histology, samples were used in our study. All animal research was conducted under protocols approved by the Animal Experimental Committee of the AMC in compliance with the Animal Welfare Body (IvD) (*in vivo* organoids model protocol 103046, *Noggin* -/- model protocol LEX102613 and ablation model protocol LEX159). All animals were kept in the Animal Research Institute of the AMC (ARIA), and experiments were performed under ARIA standard operating procedures.

RNA extraction and PCR array of human biopsies

Tissue samples from human specimens from the normal squamous epithelium and Barrett's epithelium were placed in RNAlater® (ThermoFisher Scientific) overnight at 4°C and then stored at -80°C. RNA was isolated using the Qiagen RNeasy isolation kit (Qiagen), following the manufacturer's protocol. Purified human tissue RNA was analyzed using RT² Profiler PCR Arrays for human TGF-β BMP Signaling Pathway and human Hedgehog Signaling pathway (Qiagen), according to manufacturer's protocol. In short, cDNA was synthesized with 1µg of purified RNA using RT2 First Strand Kit (Qiagen). cDNA templates were mixed with the PCR master mix, samples were aliquoted in equal volumes to the plates, and real-time PCR cycling programs were run. For the Hedgehog Signaling array, the online RT² Profiler PCR Array Data Analysis tool from Qiagen was used for normalization and calculation of fold changes and p-values when comparing the two subgroups of samples, Barrett's and squamous tissue. For the BMP/TGF-β array, RNA starting concentrations per sample were calculated using the linregPCR tool, and visualized in a heatmap.

Bioinformatics analysis

Gene expression profiles of Barrett's esophagus and esophageal squamous epithelium[16] were downloaded from the Gene Expression Omnibus (accession number GSE26886). Data were generated using Affymetrix Human Genome U133 Plus 2.0 Array and already pre-processed by use of the GC-RMA algorithm. In this set, gene expression was compared between 20 specimens containing cells from Barrett's biopsies obtained through laser capture microdissection and 19 specimens of squamous epithelium from healthy individuals.

Chip annotation file GPL570-55999 was used for annotation of the probe sets. First, data was filtered using the nsFilter function from the genefilter package[25]. 62 control probesets and 27307 probesets with low

variance were removed. Thereafter, differential expression analysis was performed using the Limma package[27]. Probesets with multiple-test corrected p-value < 0.05, were considered significantly differentially expressed. Unannotated and promiscuous probes (probes associated with more than one gene) were excluded from further analysis. For genes associated with more than one probeset, we used the arithmetic mean of log2 fold changes from these probesets for further analysis in Ingenuity Pathway Analysis (IPA). Genes and log2 fold changes were uploaded in IPA, and gene set enrichment analysis for the TGF-β/BMP/SHH pathways was performed. Overviews of these pathways are shown in figure 1. The TGF-β Signaling pathways were visualized using Path Designer.

A gene-clustered heatmap was drawn for qPCR data from the AMC dataset using the heatmap package, after log transformation and calculation of z-scores for all samples per gene.

A similar gene-clustered heatmap was drawn for the validation (Wang) dataset, displaying those genes that were analyzed in the AMC dataset, after calculating z-scores for all samples per gene. In case of multiple significantly differentially expressed probesets coding for the same gene, mean expression of these probesets was used as expression value of that particular gene.

Western Blot of human biopsies

After dissecting, tissue biopsies were briefly washed with cold phosphate-buffered saline (PBS) and cut into smaller pieces while on ice. Minced tissue was transferred to a homogenizer, and 500 µl of RIPA buffer (ThermoFisher Scientific) supplemented with protease inhibitors (ThermoFisher Scientific) was added per 10 mg of tissue. Samples were carefully homogenized and kept on ice for 30 min while mixing occasionally. Subsequently, samples were sonicated for 2-5 minutes and centrifuged at 10,000 x g for 20 minutes at 4°C. The supernatant was transferred to a new tube and stored at -20°C until future use.

Protein concentrations were determined using the Pierce™ BCA Protein Assay Kit (Pierce Biotechnology), following the manufacturer's protocol. Lysates were combined with sample buffer (125 mM Tris-HCl, pH 6.8; 4% SDS; 2% β-mercaptoethanol; 20% glycerol; 1 mg bromophenol blue) and loaded with the equal amount of protein (15 µg/lane) on a 12% SDS-polyacrylamide gel and subsequently blotted onto polyvinylidene difluoride (PVDF) transfer membranes (Millipore). The membranes were blocked with blocking solution (5% Nonfat milk in Tris-buffered saline (TBS) with 1% Tween®20 and afterwards incubated with the appropriate primary antibody solution anti-BMP2, Peprotech (#500-P195); anti-BMP4, R&D (#mab757); anti-BMP5, Abcam (#ab10858) and anti-BMP6, R&D (#AF507) at a 1:500 dilution in blocking solution overnight at 4ºC. Subsequently, membranes were washed and incubated with secondary antibodies, HRP-anti-Goat (Dako (#P0160), HRP-anti-rabbit (Dako (#P0448)) and HRP-anti-mouse (Dako (#P0447)), diluted 1:2000 in blocking solution for 1 hour at room temperature. Membranes were incubated with Pierce™ enhanced chemiluminescent (ECL) substrate (Pierce Biotechnology, Rockford, IL USA) and proteins visualized using

ImageQuant LAS 4000 (GE Healthcare Life Science). Densitometry analysis was performed using Image J 1.45s (Wayne Rasband, National Institutes of Health, USA).

In vivo organoid model

NOD-scid interleukin-2 (IL2) receptor gamma chain knockout (NSG) mice were purchased from The Jackson Laboratory and bred in-house at the Animal Research Institute of the Academic Medical Center of Amsterdam (AMC). All mice were maintained in specific pathogen free conditions, given autoclaved standard pellet feed and water *ad libitum*, and housed in ventilated racks.

Fresh samples were collected endoscopically from the squamous epithelium and Barrett's segment of four different patients. Samples were placed in chilled PBS without Mg^{2+} and Ca^{2+} and supplemented with 200 U/ml of penicillin and 200µg/ml of streptomycin and kept on ice. Each biopsy was divided into approximately 1 to 2mm^3-sized pieces discarding any necrotic areas and blood clots. Representative samples were fixed in 10% buffered formalin for histological evaluation and the remaining pieces for implantation were placed in Matrigel (Corning) and kept on ice until implantation. All biopsies were implanted within 2h of collection.

A total of 16 NSG mice were used. Mice were anesthetized via an i.p. injection of ketamine (100mg/ml) and xylazine (20mg/ml) solution. After weighing, mice were injected with 10µl of the anesthetic solution per gram of body weight. The dorsum of each mouse was shaved and prepared with a 2% chlorhexidine gluconate/70 % isopropyl alcohol solution. Under aseptic conditions, a 15-mm midline incision was made immediately caudal to the dorsal hump at the level of the renal angle. Using blunt dissection, a skin flap was raised and the skin retracted laterally in order to expose the implantation site. A superficial stay suture was placed in the dorsal musculature immediately caudal to the lowest rib using a 4/0 braided absorbable suture. After tenting the muscle fibers, an intramuscular pocket was created using a combination of sharp and blunt dissection until it was just large enough to accommodate the Barrett's biopsy. The Barrett's biopsy was then coated in matrigel and placed in the intramuscular pocket prior to suture closing. One or two separate transplantation sites were used per mouse. A 4/0 non-absorbable suture was used to mark the site of implantation. The skin was closed using 3/0 braided absorbable suture. Implants were cultured for a maximum period of 12 weeks in order to form the *in vivo* organoid structures. Commencing one-week post implantation and continuing for a total of 12 weeks, mice were treated with either saline (control group), anti-BMP4 or anti-BMP2/4 (treatment group) via i.p. injections[17]. Mice were closely monitored for any sign of discomfort and/or stress throughout the experiment.

At the end of the 12-week treatment period mice were culled using CO_2 inhalation. Immediately following culling, mice were shaved and their skin was prepared. After identifying the non-absorbable marking suture, the muscle was incised around the site of xenograft leaving a 2mm wide margin. Following this, the muscle

was retracted medially and the *in vivo* organoid harvested. Samples were fixed in 10% buffered formalin to be assessed both histologically and immunohistochemically.

Noggin knockout (*Noggin-/-*) mouse model

Nog$^{tm1.1Rmh}$/J mice (JAX stock #016117) were crossed with Rosa26-creERT2 mice (JAX stock #008463) (Jackson, USA). Tamoxifen (1mg, i.p.) was administrated for three consecutive days to delete *Noggin* in all cells expressing Rosa26-creERT2. Stomach tissues were formalin fixed and paraffin embedded for H&E staining and for IHC.

Ablation mouse model

CB6F1 mice were purchased from Charles River (CB6F1/Crl strain code 176) and housed in the ARIA. Experiments were performed using 8 to 10-week-old male mice, with an initial weight above 20g. Before and after the procedure, animals received liquid food for three days. Afterwards, normal pellet food and tap water were available *ad libitum*.

Mice were subjected to inhalation of 2% isoflurane for induction and maintenance of anesthesia. The animals were gently fixed to a heating pad (37 °C) and after weighing, the abdomen was shaved and prepared with a 2% chlorhexidine gluconate/70 % isopropyl alcohol solution. A single injection of pain-killer (5mg/kg, Melovem) was administrated subcutaneously. A 1.5 to 2cm midline laparotomy was then made. With the help of atraumatic forceps, the stomach was exteriorized. A small gastrotomy was then made along the anterior border of the stomach and crossing the SCJ. Gastric contents were emptied as much as possible using atraumatic forceps and cotton swaps. Using a cryo-pen (Cryoalfa LUX), liquid nitrogen was applied to the posterior wall of the stomach at the SCJ in order to ablate the epithelium. Liquid nitrogen was applied twice in the same location for 10 seconds each time. The stomach was closed with continuous stitches using an 8/0 non-absorbable suture. The sutured stomach was placed back inside the peritoneal cavity and the abdominal wall and skin were closed separately using a 5/0 vicryl absorbable suture.

Postoperatively and after recovering from anesthesia, mice received liquid food for three consecutive days, wherein on the third day they had available both liquid and normal pellet food. Antibiotic water (400g/ml, Baytril 2.5%, Bayer) was also present for the first five days after surgery. Afterwards, autoclaved tap water was available *ad libitum*. The animal cages were kept on a warming blanket for the first 24 postoperative hours. Animals were euthanized if they displayed signs of suffering, such as >15% weight loss after surgery. Throughout the experiment, mice received daily oral gavage of omeprazole (400mol/kg, Teva) and i.p. injection of either saline (control group) or anti-BMP2/4 (500µg/ml; treatment group)[17].

K5^{+} lineage tracing mouse model

K5-GFP mice were generated by crossing Rosa26-Tomato-*loxP [stop] loxP*-GFP (JAX stock #007576) purchased from the Jackson Lab, with K5-creERT2 mice, kindly donated by Dr. Chen[28]. Genotyped positive K5-GFP mice were housed in +/+ IVC cages in ventilated racks in the ARIA. Experiments were performed on 12 weeks old mice, both female and male. To induce lineage tracing of K5 cells, mice received i.p. injection of tamoxifen (0.25mg/kg) one day before the ablation procedure. The K5-GFP mice stomach was ablated as described above. For 14 days, the mice received daily oral gavage of omeprazole (400mol/kg, Teva) and i.p. injection of either saline (control group) or anti-BMP2/4(500µg/ml; treatment group)[17].

Immunohistochemistry

Formalin-fixed, paraffin-embedded tissue samples were used for IHC. Slides with 5µm thick sections from the paraffin blocks were cut and deparaffinized in xylene and rehydrated in a graded series of ethanol. Antigen retrieval was performed in citrate buffer saline (0.01mol/L, pH 6.0) for 20 min at 98 degrees. Endogenous peroxidase activity was blocked by incubation of slides in 3% H_2O_2 for 30 minutes, followed by 10% normal goat serum for 30 min to block nonspecific bindings. Slides were incubated at room temperature for 2h or overnight at 4°C, with primary antibodies as listed in Table S2. Slides were washed in TBS + 1%Tween® 20 and incubated with the respective biotin linked secondary reagents from the LSAB™2 Kits (Dako) following the manufacturer's protocol. Peroxidase activity was visualized using DAB^+ (Dako). Finally, sections were counterstained with Mayer's hematoxylin, dehydrated and mounted.

Table S2: List of the antibodies used in Immunohistochemistry.

Antibody	Clone	Dilution	Company
BMP2	-	1:100	Biosciences
BMP4	-	1:400	Abcam
CDX2	CDX2-88	1:200	Biogenex
Human mitochondria	-	1:1000	Abcam
Involucrin	SY5	1:100	Covalab
K5	EP1601Y	1:200	Epitomics
K14	LL002	1:200	Abcam
K19	-	1:200	Epitomics
Ki67	-	1:200	Thermo Scientific
p63	4A4	1:100	Santa cruz
pSMAD1/5/8	-	1:100	Millipore
SOX2	-	1:200	Epitomics
MUC5AC	-	1:100	ThermoFisher Scientific

Noggin	-	1:100	Epitomics

Immunofluorescence

Tissue slides were de-paraffinized and antigen retrieval was performed in citrate buffer pH 6. Slides were blocked in 10% goat serum for 10 min and treated with the avidin/biotin blocking kit (Vector lab). Slides were incubated with primary antibodies *Noggin* (1:100 epitomics) and Ki67 (1:100 Thermo Scientific), washed with TBS + 1%Tween® 20 and incubated with goat-anti-rabbit-fluor488. Glass slides were mounted with DAPI (Roche, Mannheim, Germany)/vectashield (Vector laboratories Inc, Burlingame, CA, USA). Images were acquired on an Olympus BX51 fluorescent microscope using cell^F software (Olympus Optical, Tokyo, Japan).

Statistics

qPCR data was tested for a normal distribution using the Shapiro test. The Mann-Whitney U test was performed to investigate differences in expression of each gene between Barrett's esophagus and normal squamous tissue. Genes with a $p < 0.05$ were considered differentially expressed.

Statistical differences in protein level were determined using Kruskal-Wallis test in a multiple comparison 1-way ANOVA.

Paired t-tests were performed to test statistical differences in mRNA expression of BMP2,4,5,6 and 7 and SHH in cells treated with bile acids at different timepoints. Statistical significance was set at $p < 0.05$. Unpaired t-test: *p<0.05, **p<0.01, ***p<0.001, ****p<0.0001.

REFERENCES

1 Spechler SJ. Barrett's esophagus and esophageal adenocarcinoma: pathogenesis, diagnosis, and therapy. Med Clin North Am. 2002;86(6):1423–45.

2 Souza RF. From Reflux Esophagitis to Esophageal Adenocarcinoma. Dig Dis. 2016;34(5):483-90.

3 American Gastroenterological Association, Spechler SJ, Sharma P, Souza RF et al. AGS medical position statement on the management of BE. Gastroenterology. 2011;140(3):1084-91.

4 DeMeester TR. Antireflux surgery in the management of Barrett's esophagus. J Gastrointest Surg. 2000;4(2):124-8.

5 Coleman HG, Xie SH, Lagergren J. The Epidemiology of Esophageal Adenocarcinoma. Gastroenterology. 2018;154(2):390-405.

6 Auclair BA, Benoit YD, Rivard N, Mishina Y, Perreault N. BMP signaling is essential for terminal differentiation of the intestinal secretory cell lineage. Gastroenterology. 2007;133(3):887-96.

7 Que J, Choi M, Ziel JW, Klingensmith J, Hogan BL. Morphogenesis of the trachea and esophagus: current players and new roles for noggin and Bmps. Differentiation. 2006;74(7):422-37.

8 Zimmerman LB, De Jesus-Escobar JM, Harland RM 1996 The Spemann organizer signal noggin binds and inactivates BMP-4. Cell 1996;86:599–606.

9 Piccolo S, Sasai Y, Lu B, De Robertis EM. Dorsoventral patterning in Xenopus: inhibition of ventral signals by direct binding of chordin to BMP-4. Cell. 1996;86(4):589-98.

10 Milano F, van Baal JW, Buttar NS, Rygiel AM, de Kort F, et al. Bone morphogenetic protein 4 expressed in esophagitis induces a columnar phenotype in esophageal squamous cells. Gastroenterology. 2007;132(7):2412-21.

11 Jiang M, Ku WY, Zhou Z, Dellon ES, Falk GW et al. BMP-driven NRF2 activation in esophageal basal cell differentiation and eosinophilic esophagitis. J Clin Invest. 2015;125(4):1557-68.

12 Mari L, Milano F, Parikh K, Straub D, Everts V et al. A pSMAD/CDX2 complex is essential for the intestinalization of epithelial metaplasia. Cell Rep. 2014;7(4):1197-210.

13 Clemons NJ, Wang DH, Croagh D, Tikoo A, Fennell CM, et al. Sox9 drives columnar differentiation of esophageal squamous epithelium: a possible role in the pathogenesis of BE. Am J Physiol Gastrointest Liver Physiol. 2012;303(12):G1335-46.

14 Zhou G, Sun YG, Wang HB et al. Acid and bile salt up-regulate BMP4 expression in human esophageal epithelium cells. Scand J Gastroenterol. 2009;44(8):926-32.

15 Quante M, Bhagat G, Abrams JA, Marache F, Good P, et al. Bile acid and inflammation activate gastric cardia stem cells in a mouse model of Barrett-like metaplasia. Cancer Cell. 2012;21(1):36-51.

16 Wang Q, Ma C, Kemner W. Wdr66 is a novel marker for risk stratification and involved in epithelial-mesenchymal transition of esophageal squamous cell carcinoma. BMC Cancer 2013;13:137.

17 Calpe S, Wagner K, El Khattabi M, Rutten L, Zimberlin C et al. Effective Inhibition of Bone Morphogenetic Protein Function by Highly Specific Llama-Derived Antibodies. Mol Cancer Ther. 2015;14(11):2527-40.

18 Calpe S, Correia AC, Sancho-Serra MD, Krishnadath KK. Comparison of newly developed anti-bone morpho-genetic protein 4 llama-derived antibodies with commercially available BMP4 inhibitors. MAbs 2016;8(4):678-88

19 van Baal JW, Milano F, Rygiel AM, Bergman JJ, Rosmolen WD et al. A comparative analysis by SAGE of gene expression profiles of Barrett's esophagus, normal squamous esophagus, and gastric cardia. Gastroenterology. 2005;129(4):1274-81.

20 Brunet LJ, McMahon JA, McMahon AP, Harland RM. Noggin, cartilage morphogenesis, and joint formation in the mammalian skeleton. Science. 1998;280(5368):1455-7.

21 Jiang M, Li H, Zhang Y, Yang Y, Lu R et al. Transitional basal cells at the squamous-columnar junction generate Barrett's oesophagus. Nature. 2017;550(7677):529-533.

22 Pavlov K, Meijer C, van den Berg A, Peters FT, Kruyt FA, Kleibeuker JH. Embryological signaling pathways in Barrett's metaplasia development and malignant transformation; mechanisms and therapeutic opportunities. Crit Rev Oncol Hematol. 2014;92(1):25-37.

23 Harada H, Nakagawa H, Oyama K et al. Telomerase induces immortalization of human esophageal keratinocytes without p16INK4a inactivation. *Mol Cancer Res*. 2003;1(10):729-38.

24 Kalabis J, Wong GS, Vega ME et al. Isolation and characterization of mouse and human esophageal epithelial cells in 3D organotypic culture. *Nat Protoc.* 2012;7(2):235-46.

25 Palanca-Wessels MCA, Klingelhutz A, Reid BJ et al. Extended lifespan of BE epithelium transduced with the human telomerase catalytic subunit: a useful in vitro model. *Carcinogenesis.* 2003;24(7): 1183–1190.

26 Gentleman R, Carey V, Huber W and Hahne F (2017). genefilter: genefilter: methods for filtering genes from high-throughput experiments. R package version 1.60.0.

27 Ritchie ME, Phipson B, Wu D, Hu Y, Law CW, Shi W and Smyth GK. "limma powers differential expression analyses for RNA-sequencing and microarray studies." Nucleic Acids Research 2015, 43(7), e47.

28 Liang CC, You LR, Chang JL et al. Transgenic mice exhibiting inducible and spontaneous Cre activities driven by a bovine K5 promoter that can be used for the conditional analysis of basal epithelial cells in multiple organs. *J Biomed Sci.* 2009;16:2.

EXTENDED DATA AND FIGURES:

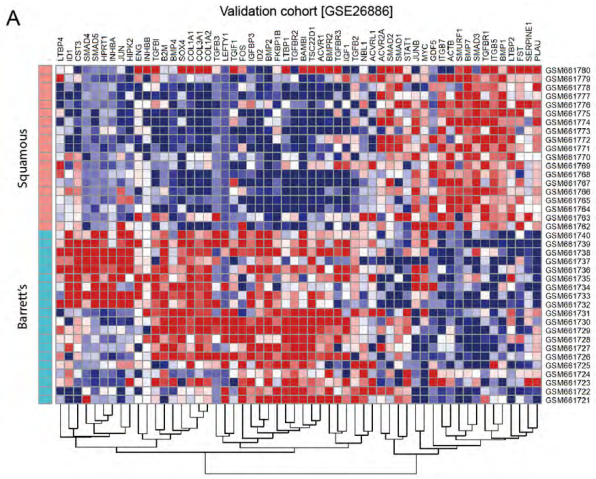

B

	SHH/WNT PCR array [AMC]		Validation cohort [Wang 2013]	
	log2FC	p value	log2FC	p value
HHIP	6,39	0	3,87	0
SHH	6,29	0	2,79	0
BMP5	6,11	0,01	NA	NA
IHH	4,87	0	2,37	0
FGF9	4,38	0	2,7	0
ZIC2	4,26	0,02	1,54	0,03
BMP2	3,64	0	4,33	0
BMP4	3,57	0	1,89	0
PTCH1	2,98	0	3,13	0
BMP6	2,5	0	NA	NA
PRKACB	2,25	0	4,11	0
GLI1	1,97	0,03	NA	NA
RAB23	1,95	0,03	1,7	0
PTCH2	1,51	0,04	NA	NA
CRIM1	1,48	0	1,14	0
DHH	1,44	0,04	NA	NA
CTNNB1	1,39	0	0,73	0
IFT52	0,94	0,02	-0,17	0,35
NUMB	0,93	0	NA	NA
SIAH1	0,88	0	-0,31	0,1
C18orf8	0,84	0	0,17	0,5
STK36	0,8	0	0,56	0,01
CSNK1D	0,67	0,04	-1,3	0
CSNK1G2	0,63	0,05	-0,6	0
OTX2	-0,61	0,04	NA	NA
CSNK1A1L	-1,06	0,01	NA	NA
PRKX	-1,14	0,03	-3,42	0
MTSS1	-1,28	0,05	-2,01	0
WNT4	-1,57	0,04	-4,95	0
FGFR3	-1,7	0,03	-3,86	0
BMP7	-1,75	0,02	-3,16	0
WNT5A	-2,15	0,01	-2,45	0
WNT10A	-2,7	0,03	-0,6	0,1
WNT7B	-5,53	0,03	NA	NA
FOXE1	-6,2	0,02	-4,75	0

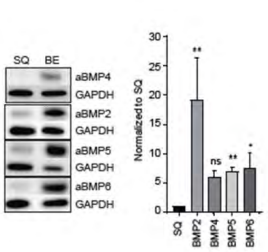

Figure 1: [A] Clustering of RNA expression in biopsies from Barrett's and squamous tissue (Squamous) and from a validation cohort (Wang 2013, GSE26886). [B] qPCR of SHH/WNT pathway genes in biopsies from Barrett's and squamous tissue from AMC patients (left), and from a validation cohort (right) (Wang 2013, GSE26886). Genes significantly differentially expressed in Barrett's compared to squamous in the AMC cohort ($p < 0.05$). [C] Western blot of BMP2, 4, 5 and 6 in Barrett patient's biopsies (left panel). Levels of BMPs in Barrett's biopsies were quantified and normalized to squamous tissue. Data are represented as mean (± SEM) of three independent experiments performed in triplicate. Multiple comparison 1 way-ANOVA *$p < 0.05$ and **: $p < 0.01$. SEM: Standard error of the mean; ns: not significant.

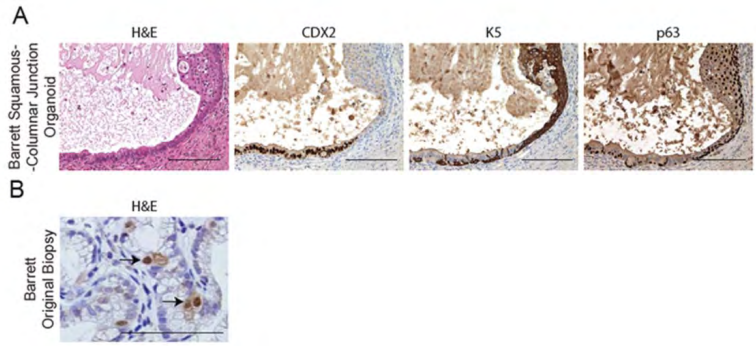

Figure 2: [A] H&E and IHC for CDX2, p63 and K5 of an organoid obtained from a biopsy taken at the SCJ from a Barrett's patient. [B] IHC staining of $p63^{+}$ remnant cells (arrows) in a Barrett's biopsy. Hematoxylin is used as a counterstain (Scale Bar 200 µm)

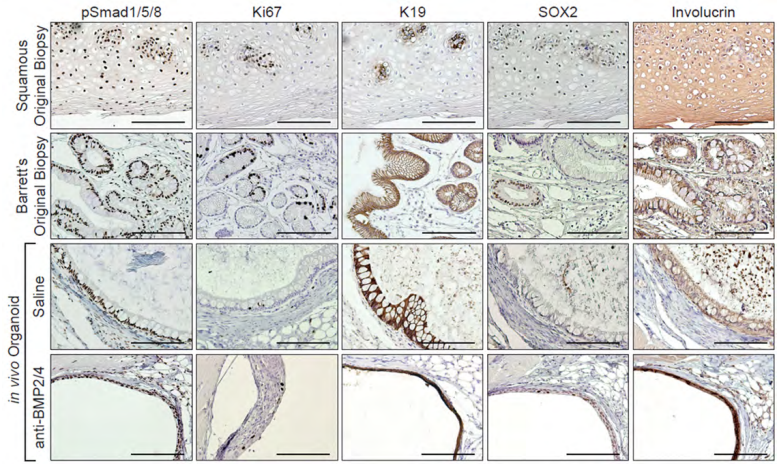

Figure S3: IHC staining of squamous and Barrett's biopsies in comparison with the corresponding *in vivo* Barrett's organoid treated with Saline or BMP2/4 inhibitor. IHC staining for pSMAD1/5/8, Ki67, K19, SOX2 and Involucrin. Hematoxylin was used as a counterstain. (Scale Bar 200 µm)

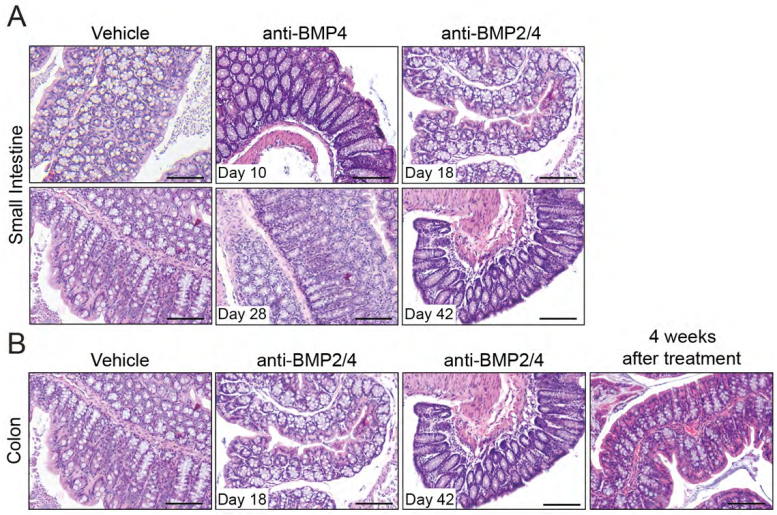

Figure S4: The effect of anti-BMP2/4 treatment on the intestine of WT mice. [A] H&E staining of the small intestine in mice at different time points of anti-BMP4 or anti-BMP2/4 treatment. [B] H&E of

the colon 18 and 42 days of treatment with antibmp2/4, and after stopping treatment for 4 weeks. (Scale Bar 200 µm).

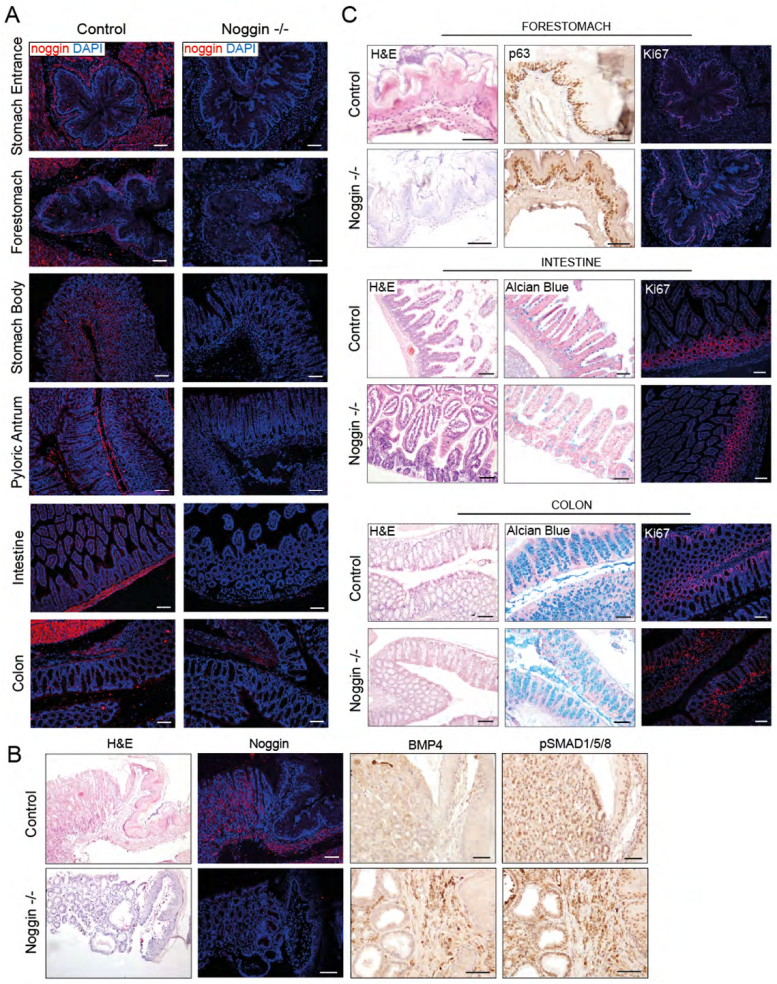

Figure S5: *Noggin-/-* mice injected with Tamoxifen for 3 days (i.p.) and compared to control mice (*Noggin-/-* without Tamoxifen injection) [A] The stomach entrance, forestomach, stomach body,

antrum, intestine and colon were stained for *Noggin* by immunofluorescence and counterstained with DAPI. [B] Immunofluorescence for BMP4 and *Noggin* of the SCJ, 24 weeks after tamoxifen injection. Hematoxylin and DAPI were used as counterstain. [C] IHC of p63 and ki67 of the forestomach. Alcian Blue staining and IHC for ki67. Hematoxylin or DAPI were used as counterstains. (Scale Bar 100 μm)

ACKNOWLEDGEMENTS

Funding: ERC-2011-StG-282079, ERC-2016-POC-737612, KWF-4745, NWO- AGIKO stipend

Scholarship support M. Read: Royal Australasian College of Surgeons and the Faculty of Medicine at the University of Melbourne.

AUTHOR CONTRIBUTIONS:

Ana C:	study design, acquisition of data and interpretation, drafting of manuscript, statistical analysis.
Danielle S:	study design, acquisition of data and interpretation, drafting of manuscript, statistical analysis.
Matthew R:	study design, acquisition of data and interpretation, drafting of manuscript, statistical analysis.
Sanne H:	study design, acquisition of data and interpretation, drafting of manuscript, statistical analysis.
Luigi M:	acquisition of data and interpretation.
Wytske W:	acquisition of data and interpretation.
Nicholas C:	acquisition of data and interpretation.
Salvador R:	study design, acquisition of data and interpretation, drafting of manuscript, statistical analysis.
Ana AM:	critical revision of the manuscript for important intellectual content
Kenneth W:	critical revision of the manuscript for important intellectual content, material support
Kaushal P.	critical revision of the manuscript for important intellectual content
Silvia C:	critical revision of the manuscript for important intellectual content
Wayne P:	critical revision of the manuscript for important intellectual content, material support
KK:	study concept and design, data interpretation, drafting and revision of the manuscript.